Technical Report 69-98 October 1969

COMPUTER ANALYSIS OF EVOKED POTENTIAL CORRELATES OF THE CRITICAL BAND

by

Charles Milroy Suter

UNIVERSITY OF MARYLAND
COMPUTER SCIENCE CENTER
COLLEGE PARK, MARYLAND

Technical Report 69-98 October 1969

COMPUTER ANALYSIS OF EVOKED POTENTIAL CORRELATES OF THE CRITICAL BAND

by

Charles Milroy Suter

This research was supported in part by National Institute of General Medical Sciences training grant 2T01GM01075 from the National Institutes of Health, U.S. Public Health Service research grant NB7773 from the National Institutes of Health, and the National Aeronautics and Space Administration grant ~~NsG~~ NGL-21-002-008 398.

PREFACE

One of the most challenging areas of computer science is artificial intelligence and one of the most important approaches to improving the technology of artificial intelligence is to study real intelligence in biological systems. An essential ingredient of intelligence, real or artificial, is the processing of sensory information. In biological systems, sensory information processing is most highly developed and complex in the mammal. While one would like to study in a quantitative fashion the problems of intelligence at all levels of the nervous system, a realistic assessment of the current state of neurophysiological science limits us to the more basic levels of the sensory pathways whether they be audition, touch, vision or other. Even at these levels an understanding of the parallel and serial processing of information can be of enormous value to computer science.

The auditory system is a particularly useful sensory system to study because acoustic stimuli are comparatively easy to quantify and control. Ignoring the problems of binaural hearing, a stimulus consists of only a single variable, sound pressure level, varying with time. Consequently the stimuli and responses lend themselves quite naturally to analysis by existing methods developed in communication and information theory. Ultimate accurate simulation of the auditory information channel with all it implies is a distinct possibility in the not distant future. There is, however, a significant obstacle to progress in the understanding of biological sensory systems and that is the difficulty of interpreting the responses of the neural systems to the stimuli. The obstacle exists whether one is concerned with the responses of large populations of cells, as this study is, or those of individual cells observed simultaneously. With respect to the

slow wave response of large populations of cells, the electrical response of the nervous system is a continually varying mixture of components, physiological or mathematical, that depend upon both the stimulus and the state of the animal during the experiment. Any meaningful correlation of the response to the stimulus must be capable of separating the response attributes which are stimulus related to those which are not. To date, most of the efforts to do this have been rather primitive and unrewarding. More recently advantage has been taken of existing computer science technology to investigate the applicability of a variety of information theoretic, pattern recognition approaches to this significant biological problem. Thus far no single completely satisfying technique has emerged, nor is any likely to in view of the magnificent complexity of the nervous system and the bewildering variety of ways it chooses to exhibit its activity. What will probably emerge is an expanding group of analysis techniques tailored to fit particular types of nervous system problems.

This report, then, is concerned with two computer science related problems: (1) to elucidate methods of auditory sensory information processing and pattern recognition; (2) to investigate the applicability of an existing pattern recognition technique, that of the method of principal components, to the analysis of nervous system responses.

Edmund M. Glaser, D Sc

TABLE OF CONTENTS

Chapter	Page
INTRODUCTION	1
METHODS	33
RESULTS	58
DISCUSSION	156
SUMMARY AND CONCLUSIONS	168
APPENDIX A. Glossary of Terms	170
APPENDIX B. CAT Channel Selector and Noise Parameter Gate Amplifier	174
APPENDIX C. Pseudo-ramdon Trigger Interval Generator (PRTIG).	181
APPENDIX D. Bandwidth of the Masking Noise	189
APPENDIX E. Tone Burst Characteristics	192
APPENDIX F. Sound System Calibration	195
APPENDIX G. Principal Component Analysis	198
APPENDIX H. Electronically Controlled Switches	220
BIBLIOGRAPHY	224

LIST OF FIGURES

Figure		Page
1.	The masking of tones by wide-band noise.....	2
2.	The critical ratio versus frequency.....	4
3.	The critical band measured by loudness summation.....	6
4.	Frequency spectra for amplitude and frequency modulated signals.....	8
5.	Functions relating the width of the critical band to frequency, as determined by three experiment methods: masking, threshold, and phase.....	10
6.	The critical band, critical ratio, and difference limen as functions of frequency.....	11
7.	Masked audiograms as a function of increasing bandwidth of masking noise.....	12
8.	Volume change of cochlear canal per mm of its length and the maximum depth of bulge of the cochlear partition, both with a difference of pressure across the cochlear partition of 1 cm of water.....	17
9.	The spatial distribution of frequency along the cochlear partition of cat.....	19
10.	The critical band predictions, critical ratio, and 20 times the frequency DL in cats.....	21
11.	An idealized tuning curve for a neuron in the auditory system.....	24
12.	Average evoked responses to clicks obtained for six electrode placements over auditory cortex in five cats.....	29
13.	Diagram of evoked response recording equipment.....	34
14.	The stimulus paradigm.....	38
15.	Plotted evoked response data from two types of experiment sessions.....	46
16.	Block diagram of the auditory stimulus generating equipment used in constant noise experiment sessions.....	52

17. Block Diagram of the auditory stimulus generating equipment used in constant tone experiment sessions..... 55

18. Average evoked responses to clicks and tone bursts..... 59

19. Average evoked responses to constant noise experiment sessions..... 62

20. Average evoked responses to constant tone experiment sessions..... 64

21.-26. Masking curves for peak amplitude of evoked response.. 67

27.-32. Masking curves for peak-to-peak amplitude of evoked response..... 73

33.-38. The eigenvectors and mean of average evoked responses for six eigenvector sets from four cats..... 84

39.-46. Masking curves from constant noise experiment sessions 99

47.-53. Masking curves for constant tone experiment sessions.. 110

54.-61. Principal component masking curves corresponding to the amplitude measurement masking curves plotted in figures 21 to 32..... 123

62.-67. Masking curves for the principal component data shown in table 15..... 138

68.-73. Principal components from the tone intensity and signal-to-noise runs for the six eigenvectors listed in table 5 for one cat..... 145

74. Principal component corresponding to ER_2 versus tone intensity and signal-to-noise ratio for one cat..... 153

75. Principal component corresponding to ER_3 versus tone intensity and signal-to-noise ratio for one cat..... 154

B1. Equipment set-up for controlling the gating of the CAT input channels and the characteristics of the masker noise.. 175

B2. Schematic of the CAT circuitry involved in the gating of the CAT input channels..... 177

B3. The voltages present at various points in figure B1 and the condition of the count flip-flops and CAT channels.... 179

C1. Diagram of equipment used to produce trigger pulses with a random inter-trigger interval from a tape recording..... 182

C2. The voltages present at the various points in figure C1 indicated by the letters..... 183

C3. Diagram of equipment used to produce trigger pulses with a random inter-trigger interval on a magnetic tape recording..... 186

C4. The voltages present at the various lettered points in figure C3..... 187

E1. The onset envelope and spectrum of a tone burst..... 193

F1. Frequency response of the tone burst generator and audio system..... 197

G1. A principal component analysis in a 2-space..... 199

G2. A geometric interpretation of the transformation from the evoked response (x) variables to the principal component (y) variables..... 203

G3. The matricies used in a principal component analysis..... 207

G4. The first 4 eigenvectors from one experiment session..... 215

H1. Emitter follower circuit used to interface the Raytheon CK1114 Raysistor to the noise parameter gate amplifier and the alternate stimulus masker gate output..... 222

LIST OF TABLES

Table		Page
1.	Thresholds in dB for four cats at each of three tone burst frequencies	36
2.	The stimulus parameters for constant noise experiment sessions	41
3.	The stimulus parameters for constant tone experiment sessions	43
4.	Latencies of the evoked response components ER_1, ER_2 and ER_3 for the evoked responses to clicks and tone bursts	60
5.	The eigenvector latency ranges	91
6.	The percent variance accounted for by the first four principal components	92
7.	Correlation coefficients between the first four principal components from constant noise experiment sessions	94
8.	Correlation coefficients between the first four principal components from constant tone experiment sessions	95
9.	Frequency limits of masking curves for constant noise experiment sessions	108
10.-12.	Frequency limits of masking curves for constant tone experiment sessions	117
13.	Frequency limits of masking curves shown in figures 54 to 61	132
14.	Frequency limits of masking curves shown in figures 21 to 32	133
15.	Standard errors of principal components for three sets of stimulus parameters on one cat	136
16.	Standard errors of principal components for one set of stimulus parameters on two cats	137
D1.	Sample rates and measured noise bandwidths	190

INTRODUCTION

The critical band theory is a theory of hearing which attempts to predict the interaction of auditory stimuli from a knowledge of their spectra. A critical band is an interval in the frequency domain over which various psychophysical measurements such as masking and loudness remain constant, while others, such as phase sensitivity and auditory threshold, change as the bandwidth of an auditory stimulus is changed. The size of a critical band is a function of its center frequency and the physical properties of the inner ear.

Many of the early estimates of the critical bandwidth relied on masking experiments. The critical band theory predicts that a masking noise will diminish a listener's ability to hear a tone only when the noise contains frequency components which are within a band of frequencies (the critical band) centered geometrically about the frequency of the tone. Fletcher was the first to state the closeness of the masker and signal frequencies in terms of a critical band hypothesis (1). The bottom curve of figure 1 is the threshold of hearing in a quiet environment. The curve at the top of the crosshatched area is the spectrogram of a masking noise. The solid dots show the threshold of hearing in the presence of the masking noise. It can be seen from figure 1 that this noise causes 50 dB of masking at each frequency. Fletcher assumed that the intensity of a just-masked tone, I_m, was equal to the intensity of the noise within a critical band, $I_f \Delta f_{cr}$,

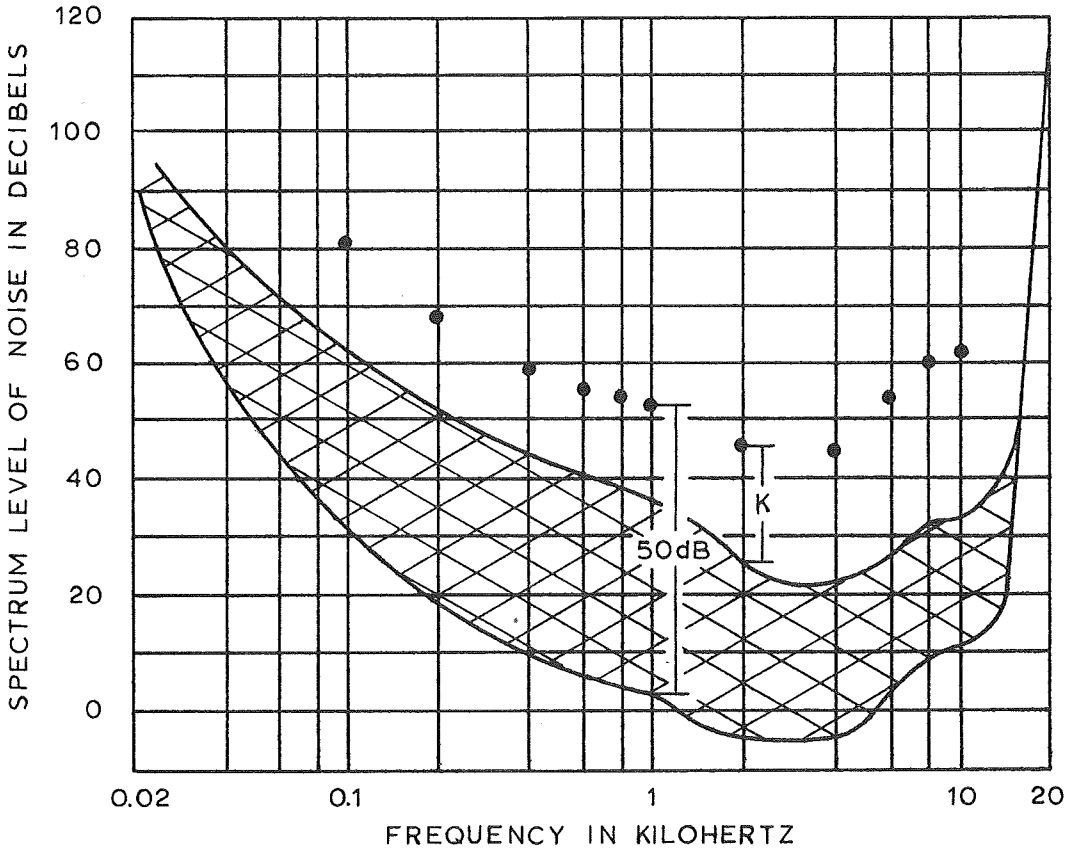

Fig. 1. A noise with the spectrogram shown by the curve at the top of the crosshatched area causes the threshold of hearing to be shifted from its level in a quiet environment, shown by the curve at the bottom of the crosshatched area, to a level 50 dB higher at each frequency, shown by the dots. The difference, K, between the masked threshold and the noise spectrogram is proportional to the critical band; and, assuming equal power in the masked tone and the portion of the noise which produces the masking,

$$K = 10 \text{ Log } \Delta f_{cr} \qquad (2)$$

Later experiments (4) indicate that K in equation 2 should be called the critical ratio, which results in a smaller estimate of the critical bandwidth than experiments which do not require a defined power ratio between noise and masked tone. After Fletcher (1).

where:

I_f is the spectral density of the noise, watts/cm^2/Hz

Δf_{cr} is the width of the critical band, Hz.

In terms of figure 1, which shows intensity levels, this relation becomes:

$$10 \text{ Log } (I_m/I_o) = 10 \text{ Log } (I_f \Delta f_{cr}/I_o) \quad (1)$$

Where I_o is the standard reference intensity, 10^{-16} watts/cm^2. If K is the difference in dB between the dots and the noise spectrogram, then

$$K = 10 \text{ Log } \Delta f_{cr} \quad (2)$$

It can be seen from figure 1 that K is not the same at all frequencies. The relation between K and frequency is shown in figure 2. At any frequency the critical bandwidth,

$$\Delta f_{cr} = \text{antilog } (K/10). \quad (3)$$

The critical bandwidths calculated by Fletcher are about 20 times the minimum perceptible change in frequency, as measured by Shower and Biddulph (2) for a tone of corresponding frequency. Hawkins and Stevens (3) noted that there is rather close agreement between the critical bandwidths calculated by Fletcher, and confirmed by them, and the width in Hertz of equal pitch intervals 50 mels wide.

It should be noted that the critical bandwidths measured by Fletcher and by Hawkins and Stevens depend upon the assumption of equal power in the just masked tone and the portion of the noise which is causing the masking. Zwicker, Flottorp, and Stevens (4) made measurements of the critical band which require no such assumption. Listeners adjusted the loudness of a reference tone until it was equal

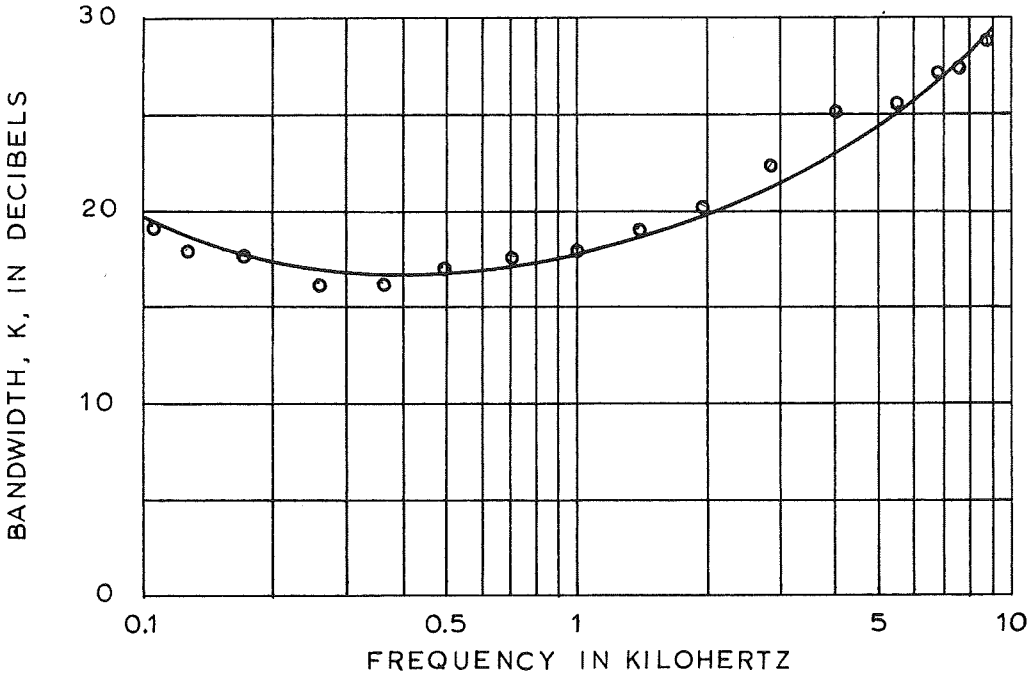

Fig. 2. Relation between K in figure 1 and frequency. K is the ratio between the monaural masked threshold of a pure tone and the level per cycle of the masking noise measured at the frequency of the pure tone. The circles show the values obtained by Hawkins and Stevens (3). The smooth curve is usually interpreted as defining the width of the band of frequencies that actually contributes to the masking of a tone located at the center of the band, assuming equal power in the masking band and the masked tone. From Hawkins and Stevens (3).

to that of a test stimulus having a constant power, and consisting of either a narrow band noise or a tone complex made up of four uniformly spaced, equally intense tones. The spectrum of the test stimulus was centered about the frequency of the reference tone. The loudness of the test stimulus remained constant as its bandwidth was increased from zero to the width of the critical band. Figure 3 shows loudness versus bandwidth for three center frequencies. The break in the curve occurs at the critical bandwidth. As the bandwidth was increased beyond the critical bandwidth, the test stimulus became louder. For a given intensity of tone complex the greatest loudness occurred for uniformally spaced tones. The greatest increase in loudness for test stimulus bandwidths greater than the critical bandwidth occurred at loudness levels in the vicinity of 50 to 60 phons. The bandwidth at which the test stimulus began to change in loudness, the critical band, was invariant with both the spacing of tones in the complex and the loudness level of the complex. These critical bandwidths are about two-and-a-half times as wide as those discussed above. Zwicker, et al suggest that the previous measurements be called critical ratios because of their dependence upon the ratio of masked tone intensity to noise spectral density.

Earlier work done by Zwicker and Gässler were reviewed in this paper (4). Zwicker (5) measured the sensitivity of the ear to phase differences in a stimulus as its bandwidth was increased. This was accomplished by comparing the detectability of amplitude modulation (AM) and frequency modulation (FM). If a tone at the carrier frequency f_c is amplitude modulated by a second tone f_m, the resulting frequency

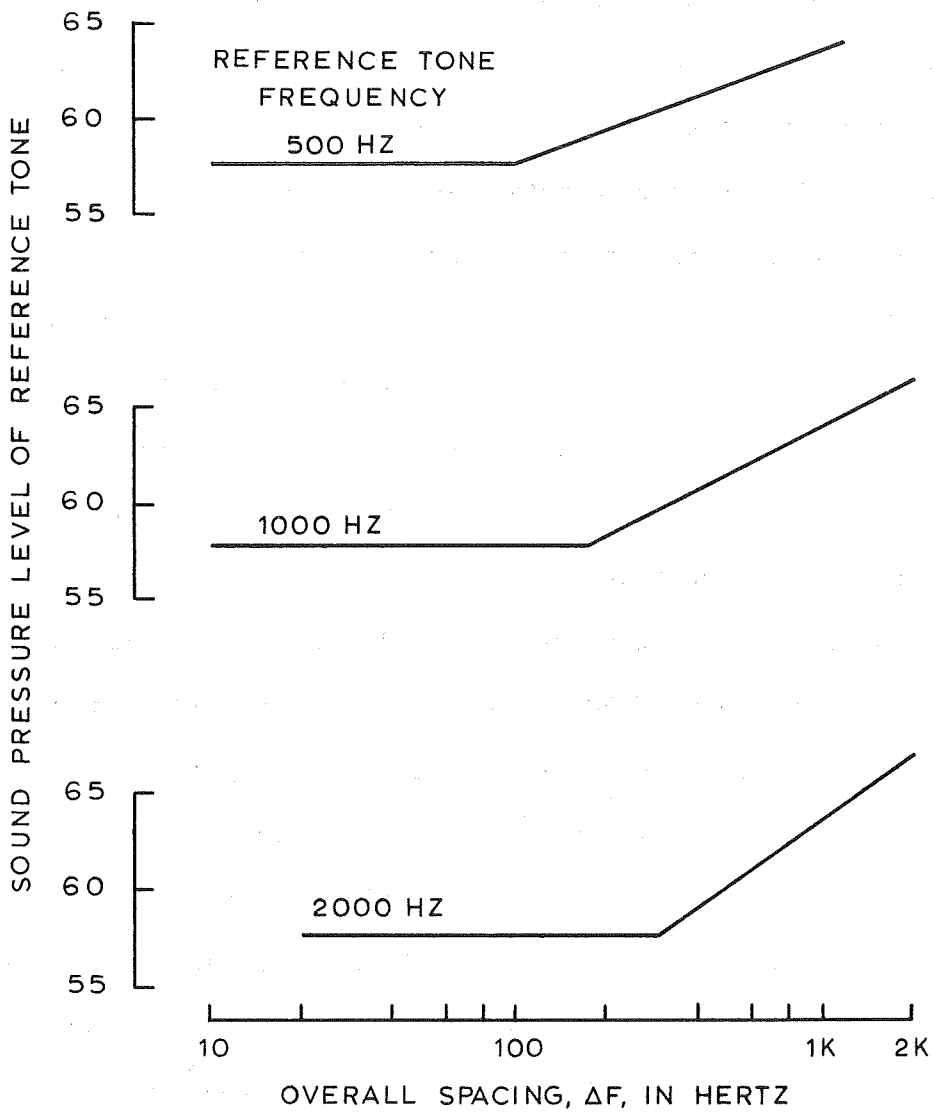

Fig. 3. The SPL of a reference tone required to make its loudness equal to the loudness of a test stimulus consisting of either a narrow band noise or tone complex, as a function of the bandwidth, ΔF, of the test stimulus. The total power in the test stimulus remained constant and its spectrum was centered about the frequency of the reference tone. The break in the curve defines the critical bandwidth for each reference tone frequency. From Zwicker (4).

spectrum is shown in figure 4. If the same carrier is frequency modulated by the same modulating tone, f_m, such that the range of frequency deviation of carrier is small compared to f_m the resulting frequency spectrum is identical to the AM frequency spectrum, except that the phase of one sideband is 180° out of phase with the other. Zwicker measured the amount of power required in the sidebands for a listener to be able to detect the presence of each kind of modulation as the bandwidth, 2 f_m, was increased. For bandwidths smaller than the critical band, less power was required in the sidebands for detection of the amplitude modulation than for detection of the frequency modulation. At and beyond the critical bandwidth the presence of modulation in the AM and FM signals were equally detectable. In other words the ear is sensitive to phase for detection of modulation only within the critical band. The critical bandwidths measured by this experiment are labeled "phase" in figure 5.

In another experiment, Zwicker (6) measured the threshold of a narrow band noise centered geometrically between two equally intense masking tones. The threshold of the noise remained constant as the frequency separation of the tones was increased up to the critical bandwidth, beyond which the masked threshold dropped rather abruptly. The critical bandwidths measured by this procedure are labeled "masking" in figure 5.

Gässler (7) measured the power of a stimulus at threshold as the bandwidth of the stimulus, a narrow band noise or a tone complex, was increased. For sub-critical bandwidths the power at threshold was constant. Beyond the critical bandwidth, additional power was required

$$f(t) = \cos(2\pi f_c t) + m \cdot \cos(2\pi f_m t) \cdot \cos(2\pi f_c t)$$

$0 \leq m \leq 1$ m is the degree of modulation

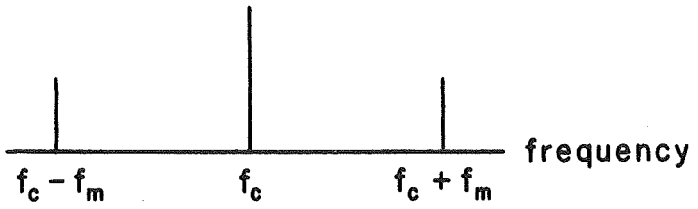

Amplitude Modulation

$$f(t) = \cos(2\pi f_c t) - \beta \cdot \sin(2\pi f_m t) \cdot \sin(2\pi f_c t)$$

$\beta = \Delta f / f_m << \pi/2$ β is the modulation index

Δf is the maximum frequency deviation of $f(t)$ from f_c

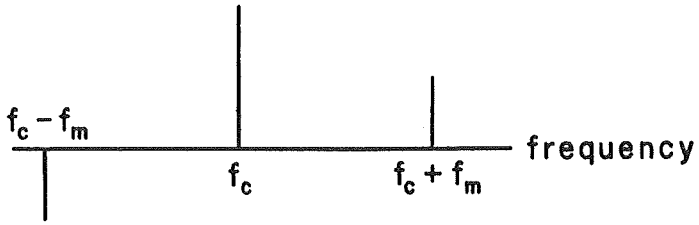

Frequency Modulation

Fig. 4. Frequency spectra for amplitude and frequency modulated signals. The frequency of the modulated carrier is f_c. The frequency of the modulating sinusoid is f_m, where $f_m << f_c$ and the frequency deviation of the FM carrier is small compared to f_m. The bandwidths of the two signals are equal to $2f_m$. The only difference between these two signals is the phase of the sidebands.

to reach threshold. The critical band was invariant with the addition of a wide band masking noise, which raised the thresholds to a greater intensity level, confirming the independence of the critical band from stimulus intensity level found in the other types of experiments. The critical bandwidths calculated from these experiments are labeled "threshold" in figure 5.

Figure 6 shows the critical band function obtained by the four types of experiments, loudness summation, phase, masking, and threshold, just discussed. The curve labeled "critical ratio" shows the critical band values found by Fletcher (1) and by Hawkins and Stevens (3). The bottom curve shows the just detectable change in frequency as measured by the range of frequency modulation for a modulating tone of 4 Hz. These values are in good agreement with those of Shower and Biddulph (2).

Greenwood (8) measured masked audiograms using noise which varied from subcritical to supracritical in bandwidth. He modulated a carrier frequency with low frequency noise which was flat from 10 Hz to a desired cut-off frequency, above which it was attenuated 30 to 50 dB per octave. The resulting masker was a narrow band noise, centered around the carrier frequency, with a very sharp cut-off, and a 20 Hz gap at the center of the spectrum. Figure 7 shows the masked audiograms for various bandwidths of noise. For bandwidths below the critical bandwidth the masking increased as the tone frequency was raised toward the center frequency of the noise. As the tone frequency was increased above the center frequency of the noise the masking decreased, giving a triangular shaped audiogram. The spectral level of the noise was

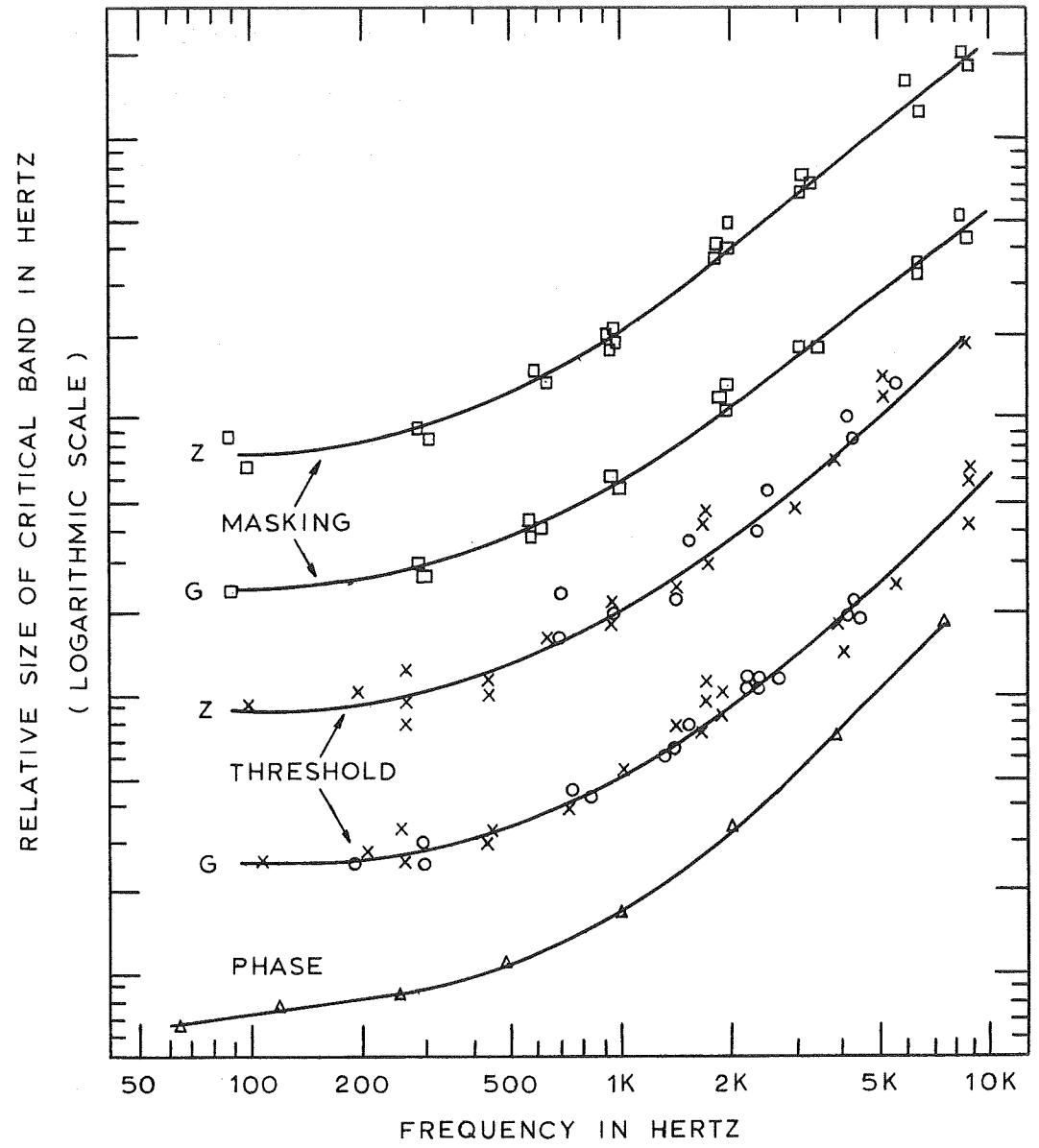

Fig. 5. Functions relating the width of the critical band to frequency, as determined by three experiment methods: masking, threshold, and phase. The letters Z and G refer to individual observers. On the curve derived from threshold measurements, the crosses represent studies with pure tones and the circles represent studies with bands of noise. The points on the lowest curve represent average values for four observers. For purposes of clarity the curves have been separated by one-half a logarithmic unit. (See figure 6 for the size of critical bandwidths). From Zwicker (4).

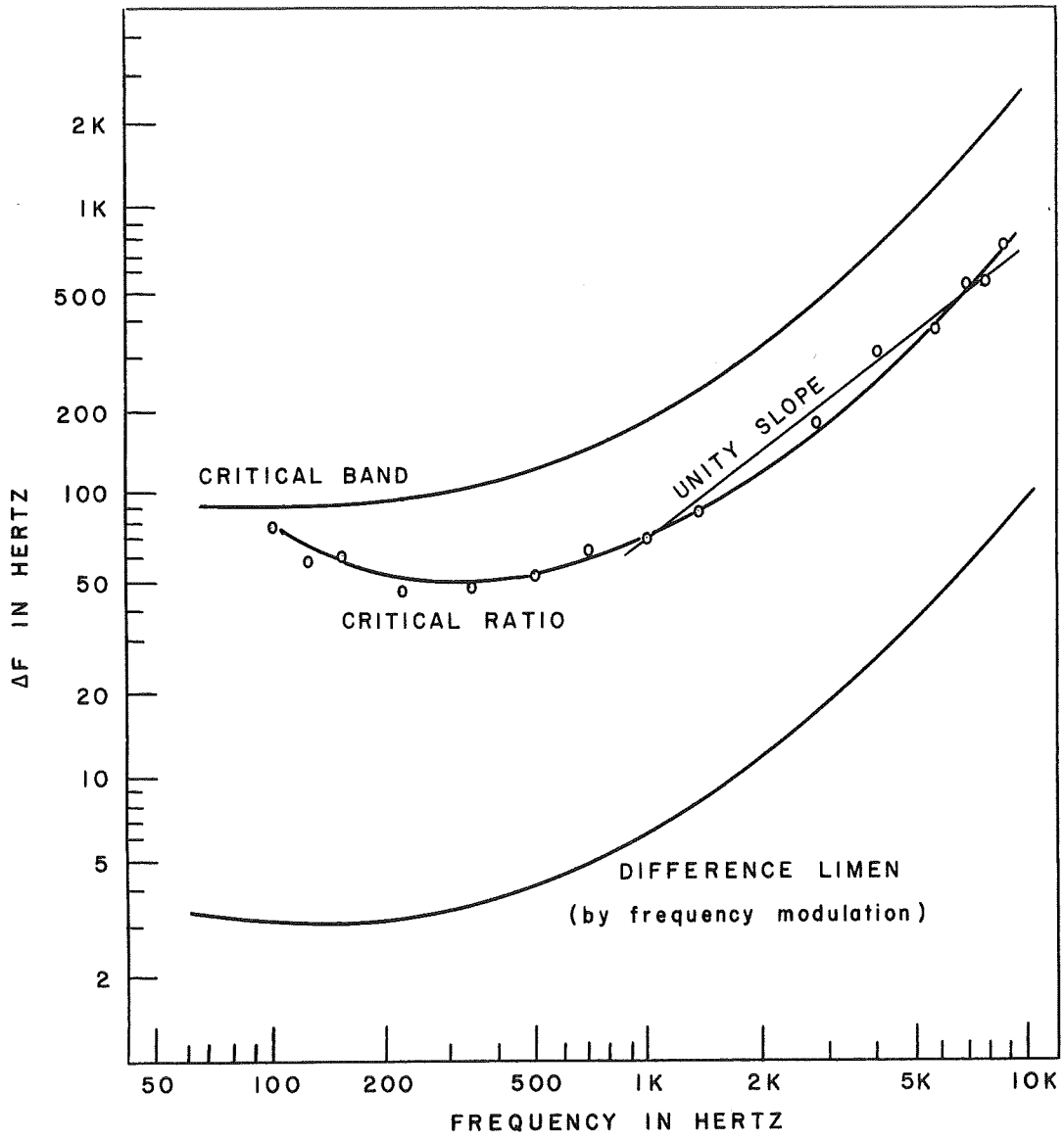

Fig. 6. The top curve, derived from four kinds of experiments, shows the width ΔF of the critical band as a function of the frequency of the center of the band. The middle curve shows the width of the band derived from the critical ratio, which is defined as the ratio between the intensity per cycle of a noise and the intensity of a pure tone that is just masked by the noise (points are from Hawkins and Stevens). The bottom curve shows the just noticeable range of frequency modulation. After Zwicker (4).

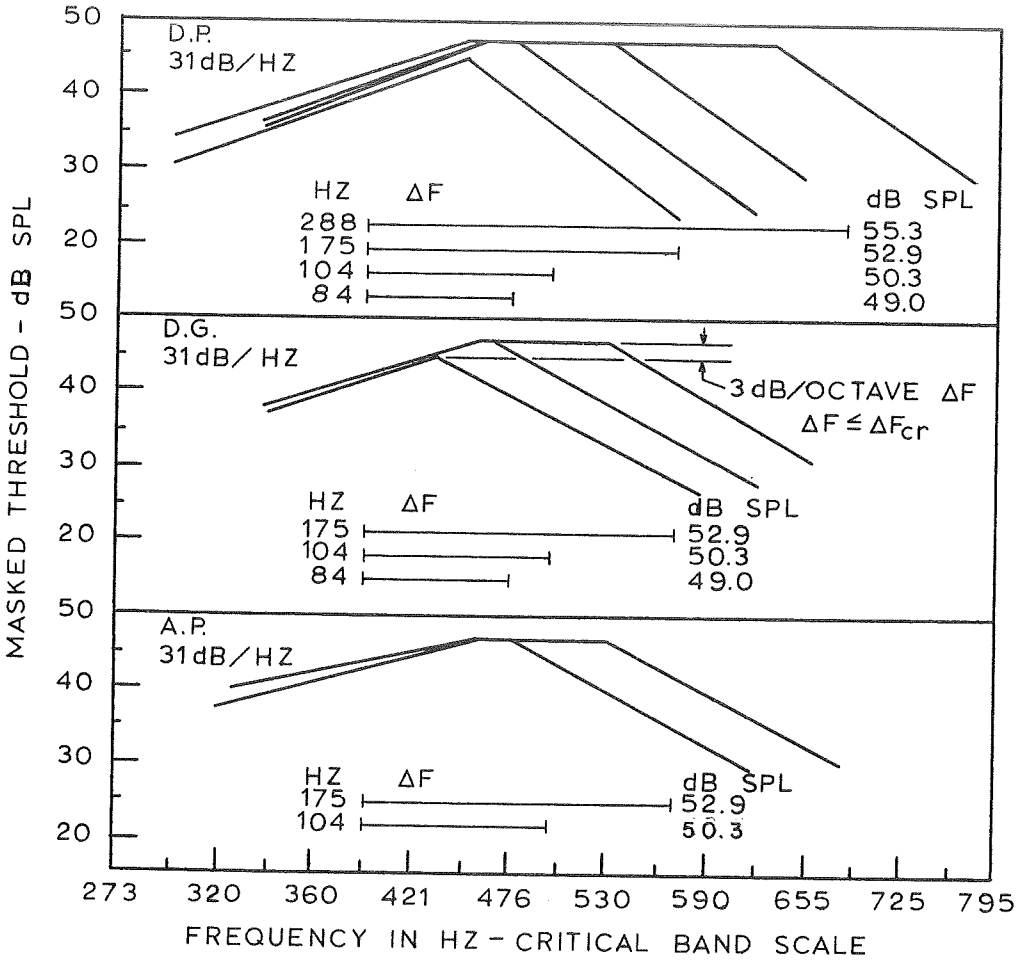

Fig. 7. Masked audiograms as a function of increasing bandwidth for subjects D. P., D. G., and A. P. The spectrum level and the lower frequency limit of the masking noise were held constant. The spectrum level appears at the upper left of each box. The lower limit of all bands was 395 Hz. Bandwidths are given in Hz and in the form of horizontal bars showing the position of the bands on the frequency scale. Four abscissa intervals represent a critical band; the scale was constructed from the table of values published by Zwicker et al (4). The level of each band of noise is given at the end of each bar. Noise level in SPL = spectrum level + 10 Log ($\Delta F - 20$) where 20 Hz is the width of the hole in the center of each band of noise. The heights of the audiograms are approximately proportional to the total power in the masking bands for bandwidths up to critical width. Critical bandwidth appears to be at least 84 Hz and perhaps less than 104 Hz at the frequency tested here. After Greenwood (8).

constant, thus doubling the bandwidth of the noise doubled its total power, neglecting the 20 Hertz gap, or raised its intensity level by 3 dB. The lower frequency limit of the noise was held constant while its bandwidth was increased. For bandwidths below the critical bandwidth the maximum amount of masking, the apex of the triangular audiogram, was increased by 3 dB per octave of added noise. At and beyond the critical bandwidth there was no increase in the level of masking with increased noise frequencies. The trapezoidal audiogram occurred at supracritical bandwidths because the spectrum of the masking noise was effectively composed of several overlapping critical bands. The critical bandwidths measured by Greenwood were in good agreement with those measured by Zwicker et al (4) for frequencies from 0.6 to 1.9 kHz. Above and below these frequencies the estimates of the critical band measured by Greenwood were smaller.

The major concern of Greenwood's paper was to show the functional (in the mathematical sense of the word) relation between the critical bandwidth and the mechanics of the inner ear. Earlier investigators (1, 4) had speculated that the critical bandwidth represented a constant distance along the cochlear partition, independent of position. To test this, Greenwood postulated an equation relating critical bandwidth to position along the cochlear partition, measured from the helicotrema, based on data (4, 9) showing the relations of both frequency to position and critical bandwidth to frequency. Inspection of figure 6 shows that the critical bandwidth is almost a linear function of frequency (indicated by a unity slope) for frequencies above 1 kHz. Greenwood's values of the critical bandwidth would tend to make the

plot straighter. From the data of Bekesy (9) relating frequency of maximum displacement to position along the basilar membrane of man, it can be shown that frequency is an exponential function of distance, for frequencies above 1 kHz. Hence, the abscissa in figure 6 can be considered a linear plot of basilar membrane position, and the logarithm of critical bandwidth versus distance along the basilar membrane measured from the helicotrema becomes

$$\text{Log } \Delta f_{cr} = ax + b \tag{4}$$

where

Δf_{cr} = critical bandwidth (Hz)

x = distance (mm) along the basilar membrane.

Greenwood plotted this relation from the available data (4, 9) and obtained the slope, a, and the intercept, b. For man

$$a = 0.06$$

$$b = 1.3592$$

and

$$\text{Log } \Delta f_{cr} = 0.06\ x + 1.3592 \tag{4a}$$

From equation 4

$$\Delta f_{cr} = B \cdot 10^{ax} \tag{5}$$

where

$$B = 10^{b}$$

For man,

$$\Delta f_{cr} = 22.9 \cdot 10^{0.06x} \tag{5a}$$

Greenwood postulated that if critical bands were laid end to end along the basilar membrane, the frequency of maximum membrane displacement could be determined for a given position on the cochlear partition

by summing up the values for the critical bandwidths from the helicotrema to the position x.

Stated mathematically:

$$f = \int_{o}^{x} \Delta f_{cr}\, dx = B \int_{o}^{x} 10^{ax}\, dx \qquad (6)$$

where f is the frequency of maximum stimulation at position x, and x is the distance along the basilar membrane measured from the helicotrema.

Let the variable x be measured in units which correspond to a length along the basilar membrane occupied by one critical band. Equation 6 then gives the width of a critical band when the upper and lower limits differ by unity.

Integrating equation 6

$$f = A\,(10^{ax} - 1) \qquad (7)$$

where

$$A = 10^{b}\,(a \ln 10)^{-1}$$

For man,

$$f = 165.4\,(10^{0.06x} - 1) \qquad (7a)$$

Assigning a value of 35 to x in equation 7a results in a frequency of 20 kHz which is approximately the upper limit of hearing in man. Because the length of the human basilar membrane is close to 35 millimeters, the unitage of x is approximately one millimeter. Hence one critical band occupies about one millimeter of cochlear partition.

Differentiating equation 7a with respect to x,

$$\frac{df}{dx} = 22.9 \cdot 10^{0.06x} = \Delta f_{cr} \qquad (8)$$

shows that the critical band is equal to the gradient of frequency along the basilar membrane. (This relation was implied by equation 6, and the fit of equation 7a to Bekesy's data supports its correctness.)

Another interesting aspect of these equations is evident from the compliance of the cochlear partition at different points along its length. The left ordinate of figure 8 is the compliance, C, of the cochlear partition. Let y be the distance along the cochlear partition, measured from the stapes. The slope of the plotted line is 0.06 and the equation for compliance is,

$$C = C_o \cdot 10^{0.06y} \tag{9}$$

From figure 8 and equation 9

$$E = E_o \cdot 10^{0.06x} \tag{10}$$

where,

E is the reciprocal of compliance, volume elasticity

x is the distance along the cochlear partition measured from the helicotrema.

The similarity of equations 8 and 10 suggests that functions relating critical bandwidth and frequency to position along the basilar membrane bear a close relation to cochlear mechanics.

Greenwood obtained values for the coefficient of x in equation 7 for several species from compliance versus position curves published by Bekesy (9). He noted that the value of this coefficient could be calculated for other species by multiplying the value of the coefficient for man, 0.06, by μ, where

$$\mu = \frac{\text{length of basilar membrane in man}}{\text{length of basilar membrane in other species}}$$

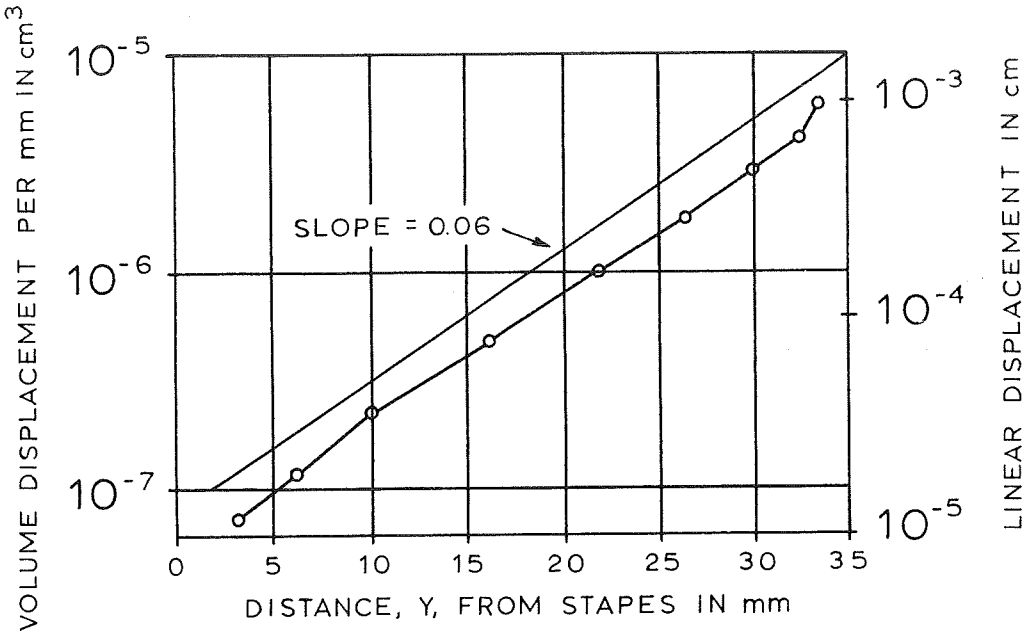

Fig. 8. Volume change of cochlear canal per mm of its length (left ordinate) and the maximum depth of bulge of the cochlear partition (right ordinate), both with a difference of pressure across the cochlear partition of 1 cm of water. Compliance is defined as the ratio of volume change to pressure change. The left ordinate is logarithmic and shows the compliance. The equation of the relation between compliance, C, and the distance, y, shown by the abscissa is

$$\text{Log } C = ay + \text{Log } C_o$$

from which

$$C = C_o \, 10^{ay}$$

The value of a is determined from the slope of the plotted relation and is equal to 0.06. After Bekesy (10) and Greenwood (8).

For cat

$$a_{(cat)} = \mu a_{(man)}$$
$$= (35/22) \cdot 0.06 \qquad (11)$$
$$= 0.095$$

The constant A in equation 7 for the other species is calculated by multiplying A for man by μ^2.

For cat

$$A_{(cat)} = \mu^2 A_{(man)}$$
$$= (35/22)^2 \cdot 165.4 \qquad (12)$$
$$= 418.6$$

and

$$f = 418.6\ (10^{0.095\ x} - 1) \qquad (7b)$$

The accuracy of this equation can be determined by comparing its predictions with experimental data. Schuknect (11) published data on the hearing losses resulting from selective lesions made in the cochlea of cats. These data demonstrate the spatial distribution of frequency along the cochlear partition. The fit of Greenwood's equation, 7b, to these data is shown in figure 9.

From equations 5 and 7,

$$\Delta f_{cr} = af \ln 10 + B \qquad (13)$$

Equation 13 gives the width of the critical band, Δf_{cr}, at any frequency, f. For man

$$\Delta f_{cr} = 0.138f + 22.9 \qquad (13a)$$

The bandwidths predicted by equation 13a are in good agreement with the critical bandwidths measured by Zwicker et al (4) between 0.6 and 1.9 kHz. The corresponding equation for cat is

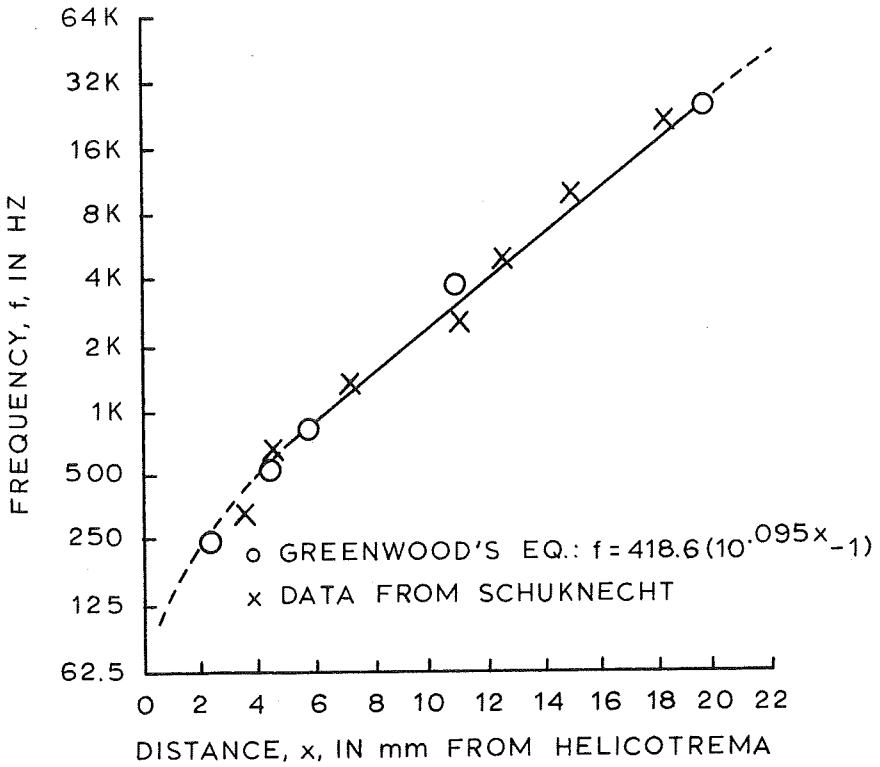

Fig. 9. The spatial distribution of frequency along the cochlear partition of cat as determined by hearing losses resulting from selective cochlear lesions. The crosses represent Schuknecht's data. The circles represent the calculations using equation 7b. After Greenwood (8) and Schuknecht (11).

$$\Delta f_{cr} = 0.218f + 91.5 \qquad (13b)$$

This equation can be tested using data published by Watson (12), who used supracritical bandwidth masking noise to measure the critical ratio for cats that were trained in a double-grill cage to make an avoidance response to tones. Figure 10 shows a plot of equation 13b and the values of Watson's critical ratios expressed in Hertz, assuming equal power in the effective masking noise and the just masked tone. Watson attempted to show that the critical ratios for cat were equal to 20 times the frequency difference limens for cat reported by Elliot (13).

It is generally accepted (14 - 16) that the signal-to-noise ratio for a critical bandwidth masking noise is not the same at each frequency. Using the signal-to-noise ratios at different frequencies found by Greenwood for man (14) on Watson's critical ratio data for cat would make the corresponding "critical bandwidths" for cat considerably larger than those predicted by equation 13b. No values of masked signal-to-noise ratio for critical bandwidth noise are yet available for cat, and the correctness of Greenwood's equation, 13b, is still uncertain, indicating the desirability of a more direct approach to its evaluation.

The critical band studies discussed above measured the width of the critical band by observing a transition in the behavior (constant or changing) of a psychophysical measurement (threshold, loudness, phase sensitivity, masked threshold) as the bandwidth of a stimulus or masker was increased from subcritical to supracritical. From the diversity of phenomena which show a critical band effect and the cochlear

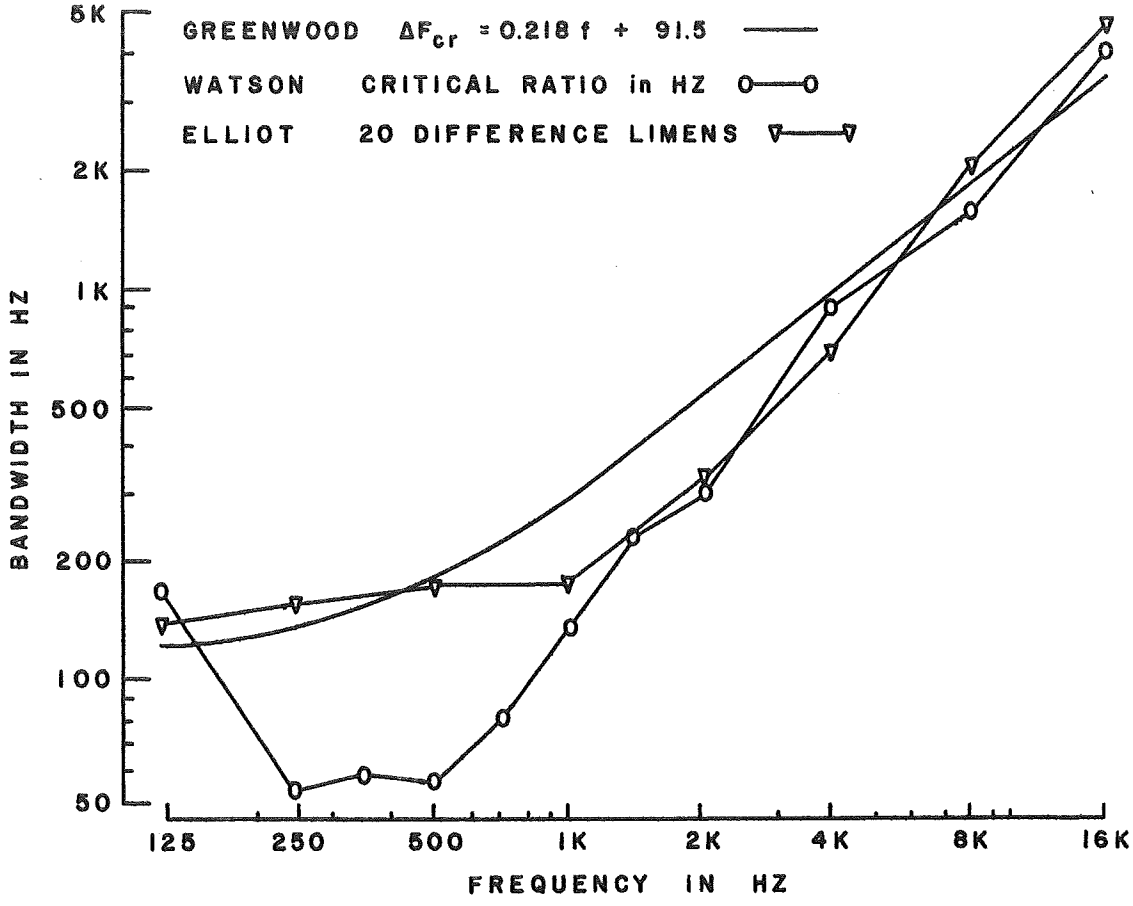

Fig. 10. Estimates of the critical band and critical ratio. The solid line shows the bandwidths predicted by Greenwood's equation (8). The circles are from Watson's data (12). The triangles represent 20 times the frequency difference limens for cat reported by Elliot (13).

mechanical-critical band relationship postulated by Greenwood, the critical band appears to be a fundamental property of the auditory system, and as such should possess observable neurophysiological correlates. Previous studies do not give any indication of where in the auditory system these critical band effects are produced. From Greenwood's equations it may seem reasonable to postulate a peripheral origin for the critical band effects. However, the tonotopic organization generated within the inner ear is retained to some extent at all levels of the auditory system, including auditory cortex (17, 18), and it seems possible that the critical band effects may have a neural origin as opposed to a mechanical origin on the basilar membrane. Supporting this notion is the study by Mulligan et al (19) which showed that a tonal signal masked by noise when signal and noise are presented to one ear, becomes audible, or unmasked, when the masker is also presented to the other ear if, and only if, the critical band frequencies remain in the noise being presented to the second ear. Unmasking is suggestive of a central neural basis for at least this critical band effect since it would be difficult to explain in terms of a peripheral mechanism.

Most studies of critical band phenomena have relied on psychophysical experiments for an assessment of critical band effects. The information concerning critical band effects within the auditory system may be limited because the measured phenomena are produced by complex systems responsible for perception and reaction. What, if any, influences these systems exert on the critical band is not known. Investigations of the critical band effects on neurophysiological phenomena

measured from structures within the auditory system should remove at least these restrictions as well as provide the possibility for revealing the underlying mechanisms. Although no neurophysiological investigations of the critical band, as such, are found in the literature, critical band effects may be manifest in the data from other types of neurophysiological experiments on the auditory system. Because neurons are the functional units in the nervous system, single unit studies are considered first. The discussion is largely restricted to cats since most of the relevant auditory research has been done on this species, including the research represented by this dissertation.

Many studies have been made on the sensitivity of neurons to tone stimuli of various frequencies and intensities in various centers of the auditory system of cat (20), including auditory nerve (21 - 26), cochlear nucleus (27 - 30), superior olivary nuclei (31, 32), inferior colliculus (33 - 35), medial geniculate body (36, 37), and auditory cortex (17, 38 - 42). From the data, tuning curves such as in figure 11 can be plotted where the ordinate and abscissa are intensity level and frequency, respectively, of the tonal stimuli. Most neurons studied responded to a tone of minimum intensity at one particular frequency, called the characteristic frequency, CF. Some neurons at the different centers appeared to have several dips in their tuning curves or to have a broad frequency range for maximum sensitivity (minimal intensity level of stimuli). Some units showed a decrease in their spontaneous firing rate when a tone was presented (27, 39, 40), or showed a diminution in the response to one tone when a second tone was presented (20, 26). Although these various effects are frequency

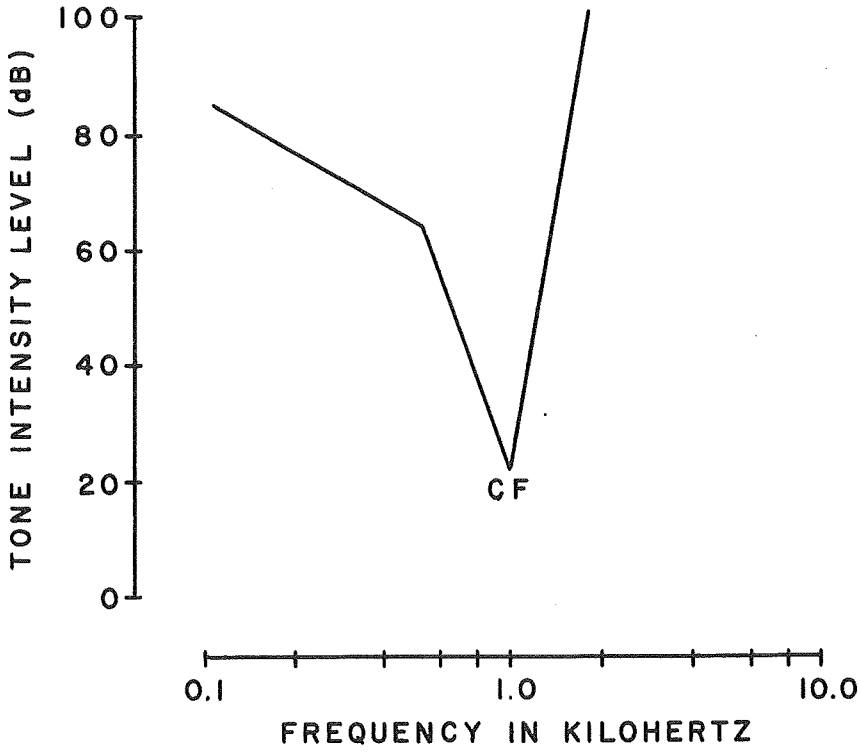

Fig. 11. An idealized tuning curve for a neuron in the auditory system. The curve shows the minimum intensity of a tone required to elicit a neuron response as a function of the frequency of the tone. The frequency of the tone requiring the least power to elicit a response is the characteristic frequency, CF, of the neuron. In general, the units in higher centers, up to the medial geniculate body, show sharper tuning properties (20). On either side of the tuning curve is an area of intensity-frequency of tone which inhibits the neuron's response to a second tone (20, 26).

dependent, no direct relationship to the critical band is evident. One of the features of the critical bandwidth is its invariance with intensity of stimulus; although this is not universally accepted (43). However, the bandwidth of the tuning curves broadens as the intensity level of stimulus is increased. Evans and Whitfield plotted for cortical neurons the bandwidth of the tuning curves at a level 15 dB above the threshold at CF versus CF (39). Using logarithmic coordinates for both bandwidth and CF in Hertz resulted in a straight line with a slope of about 0.18, indicating that the bandwidth at this level is an exponential function of frequency. The critical bandwidth it will be recalled, is presumed to be a linear function of frequency above 1 KHz. It may well be that the failure of single units to demonstrate critical band effects is a reflection of the theory (44, 45) that the central nervous system handles information in terms of neuron population or networks rather than on a single neuron basis, and therefore one must examine the statistical properties of the response of a population of neurons to study stimulus processing. One such statistic is most likely expressed in evoked macropotentials such as those recorded on the surface of the cortex.

The relation between cortical macropotentials and the discharge pattern of neurons has been the subject of several investigations (44 - 52). The macropotentials are probably generated from the sum of dendritic potentials, which in turn affect the probability that the involved neurons will discharge. One theory postulated for the positive phase of the macropotential recorded from the cortical surface is that dendritic depolarization occurring deep in the cortex acts as a current

sink. This concept is supported by the phase reversal of an evoked response as the recording electrode is moved deep into the cortex. This theory is also supported by the observation that the short latency portion of the response is positive and the endings of the specific thalamic afferents, presumably responsible for causing the dendritic depolarization of the early response, are located in the internal granular layer, layer IV. The intracortical synapses occur mostly in the external granular layer and are responsible for the later portions of the evoked cortical potential. Their superficial location, layer II, would act as current sink for deeper current sources, accounting for the late negative phase of the evoked surface macropotential. Another factor which can account for positive surface potentials is hyperpolarization of superficial dendrites. John (44) presents a good review of some of the theories of cortical macropotentials. An excellent model, replete with experimental data, is provided by Towe (51), which shows a possible mode of generating evoked potentials from sequentially activated neurons. His model values were obtained from time-depth studies on single cells and the model predictions compared very well with time-depth vertical current contour maps obtained experimentally. One important aspect of Towe's model is the independence of the various positive and negative phases of an evoked response. This is discussed below, in relation to macropotential studies done by Teas and Kiang (53).

The only work using evoked cortical macropotentials to measure critical band phenomena was reported by Tunturi (54) who worked with dogs. The large variance in his data makes any assessment of critical

band phenomena very difficult. Hind (55), using strychnine patches to enhance the evoked potentials over a restricted area of auditory cortex in anesthetized cat, was able to demonstrate tonotopic organization in the auditory cortex. The spread of frequencies eliciting a response at different areas did not show any specific critical band effect. More recent studies (17, 20, 56) of restricted areas of auditory cortex show organization of single units in columns normal to the surface of auditory cortex. Although the spread of CFs found in a given column of cortex is fairly restricted, no determination of critical bandwidths appears consistent from the data.

The apparent lack of critical band effects in previous neurophysiological experiments indicates a possible need for performing experiments which are designed specifically to measure critical band phenomena. The experiments reported here were designed for this purpose and were patterned in several respects after experiments performed by Teas and Kiang (53). The major similarities between these experiments and the earlier ones by Teas and Kiang are that awake cats with chronically implanted epidural electrodes over their primary auditory cortex are modestly restrained in a sound shielded room. Repeated auditory stimuli are presented in free field and the evoked cortical response is averaged over a series of stimulus presentations. In the present experiments, critical band effects are evident from changes in the various features of the primary evoked response to tone bursts imposed by narrow band masking noise. The experiments by Teas and Kiang are reviewed in order to establish a framework for a discussion of the features of average evoked responses from the auditory cortex of cat.

Average evoked responses to clicks obtained by Teas and Kiang from five cats are shown in figure 12. These responses are divided into 3 components: ER_1, with a peak latency between 12 and 14 msec; ER_2 with a peak latency between 22 and 29 msec; and ER_3 with a peak latency between 45 and 73 msec. The animals were located about 140 cm from the speaker; thus 4 msec of the latencies is caused by the time required for the auditory stimulus to travel from the speaker to the animal. The electrode locations are indicated to the right of each response. The reference electrode was always located in the frontal sinus. In addition to these electrodes, potentials were monitored from the posterior lateral gyrus and dorsal neck muscles. The failure of these locations to show any activity which was synchronized with the evoked responses from auditory cortex supports the claim that the recorded average evoked responses represent activity from only the auditory cortex. Average evoked responses obtained from one animal before and after surgical destruction of the left middle ear and cochlea did not differ substantially, indicating that the characteristic waveform of the responses was not dependent upon stimulation of both ears. Recordings of individual responses demonstrated that all three components were present and hence that the ER_1-ER_2 complex was not a bimodal probability curve for a single event.

As mentioned above, in connection with Towe's model for the generation of the evoked cortical potential, the various positive and negative phases were considered to be independent. Teas and Kiang demonstrated that the various components of the response could be altered independently of one another by changes in the state of the

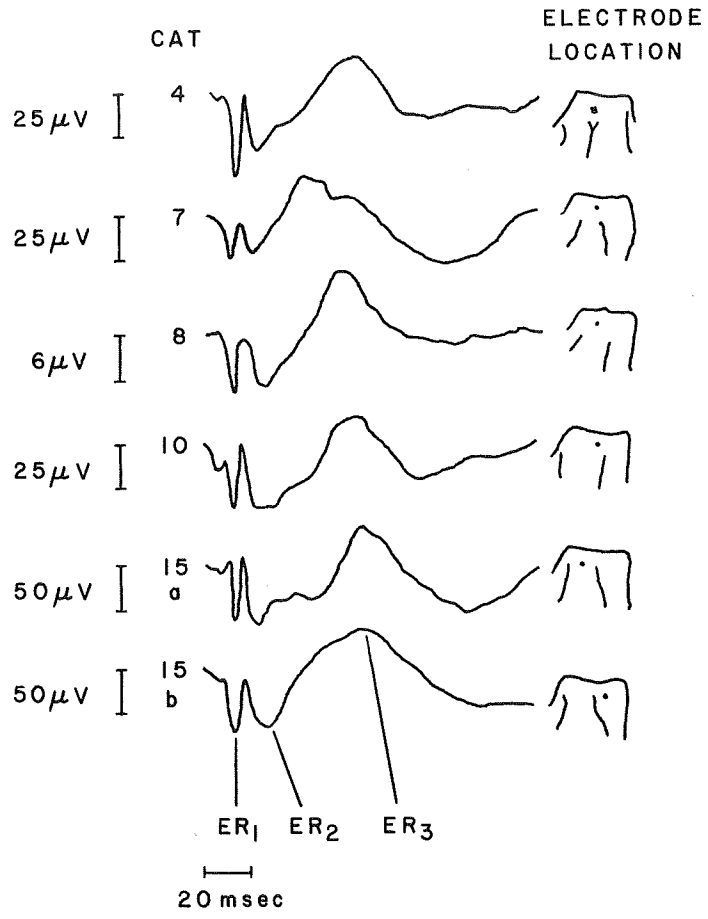

Fig. 12. Average evoked responses to clicks obtained for six electrode placements over auditory cortex in five cats. The responses were selected from the first recording session for each cat, in which the animal was awake. The waveforms are composed of three prominant peaks: ER_1, ER_2, and ER_3. Their latency ranges are: for ER_1, 12-14 msec; for ER_2, 22-29 msec; for ER_3, 45-73 msec. The insets show the electrode location in each cat. The reference electrode was always in the frontal sinus. The stimuli were 0.1 msec clicks delivered at a rate of 1 per sec, and at intensities approximately 50 dB above the level necessary for a just detectable average response. Downward deflections indicate positivity of the cortical electrode referred to the frontal sinus. From Teas and Kiang (53).

animal or differences in the auditory stimulus. In some of the animals, the dura was punctured during electrode implantation. This resulted in an evoked response with a normal ER_2 and ER_3, but no ER_1. When an animal with a normal response was anesthetized with surgical doses of barbiturates the ER_2 and ER_3 were abolished but ER_1 remained normal. When one of the cats with a punctured dura was anesthetized, the ER_1 component appeared in the response. The state of the animal was divided, roughly, into three classifications based on recorded dorsal neck muscle activity (EMG) and the background electrocorticogram (ECG) from auditory cortex. The animal was considered awake when the EMG was large and the ECG showed low voltage fast (LVF) activity. Under these conditions the average evoked responses were normal, as shown in figure 12. When the EMG was either medium or small and the ECG showed high voltage slow (HVS) activity, the animal was considered drowsy and ER_3 was found to be absent from the average evoked response. The animal was considered asleep when the EMG showed little activity and the ECG showed LVF activity. During this state the ER_3 component was absent from the average evoked response and the ER_2 component was drastically altered.

The three evoked response components were also differentially sensitive to changes in the stimulus parameters. As the click intensity was raised from threshold (defined as the intensity of stimulus at which an average evoked response could just be detected) to about 70 dB above threshold, the ER_1 amplitude increased and its latency decreased. A further increase in stimulus intensity resulted in a decrease in ER_1 amplitude, which was less apparent when the animal was anesthetized.

The ER_2 and ER_3 components generally became larger with increases in intensity, but their behavior varied between cats and between experiment sessions for the same cat. The evoked response to clicks could be abolished by presenting the clicks in a background of continuous wideband noise. As the intensity of the noise was increased from zero, the ER_1 amplitude decreased, and was almost abolished before the ER_2 and ER_3 components began to show a reduction. At this intensity of noise - ER_1 abolished but ER_2 and ER_3 still close to normal amplitude, with ER_2 having an increased latency - listeners who monitored the acoustic stimuli with earphones reported that they could easily hear the clicks. At noise intensities great enough to abolish ER_2 and ER_3, the listeners reported that they could not hear the clicks. It was possible to obtain a response in which ER_2 was present without either ER_1 or ER_3 by masking the ER_1 with noise when the animal was in a drowsy state (during which ER_3 was absent). ER_1 was present without ER_2 or ER_3 when the animal was anesthetized or sometimes when the animal was asleep. At no time was ER_3 reported without at least an ER_2 present.

Average evoked responses to tone bursts having a duration of 7 msec and rise-fall times of 1 msec were also obtained by Teas and Kiang. The responses were generally similar to those evoked by clicks. Although a sufficient number of records were not obtained to show tonotopic organization, the ER_1 in the responses reported displayed a sensitivity to tone frequency.

There are several advantages to using an experimental technique similar to that used by Teas and Kiang. The animals are awake, and are thus in a state which is similar to that of subjects participating in

psychophysical experiments. The surgical procedure is a relatively easy one to perform, and, once set-up, the animals can be used in a large number of experiments lasting over a period of years. The average evoked responses have at least two, and possible more, independent components, providing several possible chances to see critical band effects. One is thus not forced to place all his responsive eggs in one neuron population basket!! These advantages led to the choice of this technique as an approach to measuring neurophysiologic correlates to the critical band.

METHODS

Female cats weighing between 5 and 7 pounds were prepared under pentobarbital sodium, 15 mg per pound body weight, IP. A small hole, approximately 1/16 x 1/8 inch was made in the skull over the A1 area of auditory cortex (18), care being exercised not to puncture the dura. A teflon coated stainless steel wire, 0.007 inch in diameter was bared at the terminal 3/8 inch and doubled over 3/16 inch from the end, forming a blunt, bared end 3/16 inch in length. This end was inserted through the hole drilled in the skull and made to lie between the dura and the skull, over the primary auditory cortex. The other end of this epidural electrode wire terminated in a small connector, Amphenol Micromed, which was imbedded in the frontal sinus homolateral to the electrode location. Both the electrode wire and the connector were secured to the skull using dental plate cement. The reference electrode was a three inch length of uninsulated wire, the same size as the electrode wire and terminating in the Amphenol connector and was positioned under the skin surrounding the connector. At the termination of the surgical preparation 500,000 units of penicillin were administered IM. The animals were permitted at least three days to recover before auditory experiments were performed.

During each experiment session a set of auditory stimuli, consisting of tone bursts and masking noise, was presented to the animal and the average evoked response to the tone bursts, recorded from the implanted electrodes, was accumulated in a small on-line average response computer, CAT 1000. Figure 13 shows a diagram of the evoked response

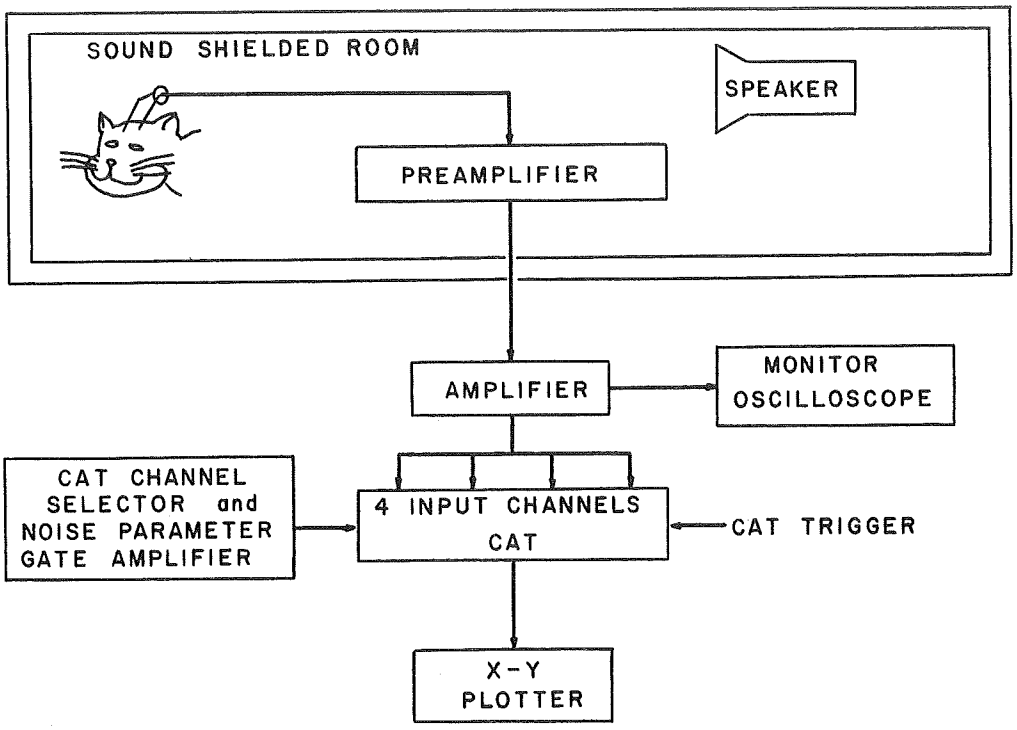

Fig. 13. Diagram of evoked response recording equipment. The electrocorticogram is recorded from an implanted epidural electrode and amplified by the preamplifier and amplifier which are constructed using Philbrick operational amplifiers. The overall gain is set at 20K. The cortical activity is monitored on an oscilloscope and can be recorded on a Grass Polygraph. The function of the CAT channel selector and noise parameter gate amplifier is discussed in Appendix B. The CAT is a small on-line, wired program computer with an analog output which is plotted using an X-Y plotter.

recording equipment. The output of an experiment session is a set of plotted average evoked responses. The cat was placed in a double walled acoustically shielded room, IAC 1202A, in which the sound stimuli were presented in free field from a Dukane Ionovac Duk 5 speaker. The animal was modestly restrained by a cloth sack from which its head protruded. The sack was secured to a moveable table in such a fashion that the cat's head remained in approximately the same position relative to the speaker. The state of the animal was determined by visual observation from a window in the sound shielded room and occasionally from the electrocorticogram which was recorded on a strip chart recorder for brief periods throughout the experiment session. The cat was maintained in an awake state by repeated arousal (puffs of air delivered from a tube positioned in front of the cat) when necessary. All equipment except the speaker and the first stage of the electrocorticogram amplifier was located external to the sound shielded room and the window was covered to reduce visual stimuli to the animal.

The intensity level of the tonal stimuli used during each experiment was adjusted relative to the animal's hearing threshold in a quiet environment. These thresholds were determined prior to running the experiments; the threshold being defined as that tone burst intensity level which evoked a visually detectable average evoked response in 50% of the trials. The tone burst intensity was changed in 5 dB steps in determining the threshold. The threshold sound pressure level (dB re 0.0002 dyne/cm^2) of threshold tone bursts are shown for four cats at three tone burst frequencies in table 1.

Table 1. Thresholds in dB re 0.0002 dyne/cm^2 for four cats at each of three tone burst frequencies. The tone bursts had Gaussian shaped onsets and 10 msec rise times. Threshold is defined as that tone burst intensity level which results in a visually detectable average evoked response in 50% of the trials. The tone burst intensity was changed in 5 dB steps.

Frequency of tone (KHz)	Cat			
	110	116	119	120
9	3	13	28	18
14	2	22	22	22
22	20	25	50	50

The effect of the noise on the evoked response was determined by comparing the average evoked response to the tone burst presented in a noise background with the average evoked response to the tone-burst presented without the noise. The state of the animal probably fluctuated during an experiment session and because such fluctuations could influence the difference between average evoked responses recorded at different times during an experiment session, it was advantageous to accumulate the average evoked responses to the tone-bursts presented alternately with and without the noise over the same time span.

Figure 14 shows the general stimulus paradigm used which permitted the accumulation of four average evoked responses over the same period of time. The first and third evoked responses were to tone bursts presented without noise. The second and fourth evoked responses were to tone bursts presented in a noise background, or, in the case of the fourth evoked response in some of the experiment sessions, to tone bursts of reduced intensity. Noise backgrounds which differed in spectra, intensity, or type of carrier modulation were used with the second and fourth tone bursts of the paradigm. The interval of time between the onsets of two successive tone bursts was a random variable, t_i, which had a minimum of 0.8 seconds, a maximum of about 2 seconds and a mode of approximately 1.2 seconds. The probability density function of t_i is shown at the top of figure 14. The random interval between tone bursts reduced the degree to which late components in the average evoked response to one tone burst were accumulated in the average evoked response to the next tone burst (57). The tone burst onset was delayed by t_d (either 150 or 300 msecs) from the trigger pulse in order

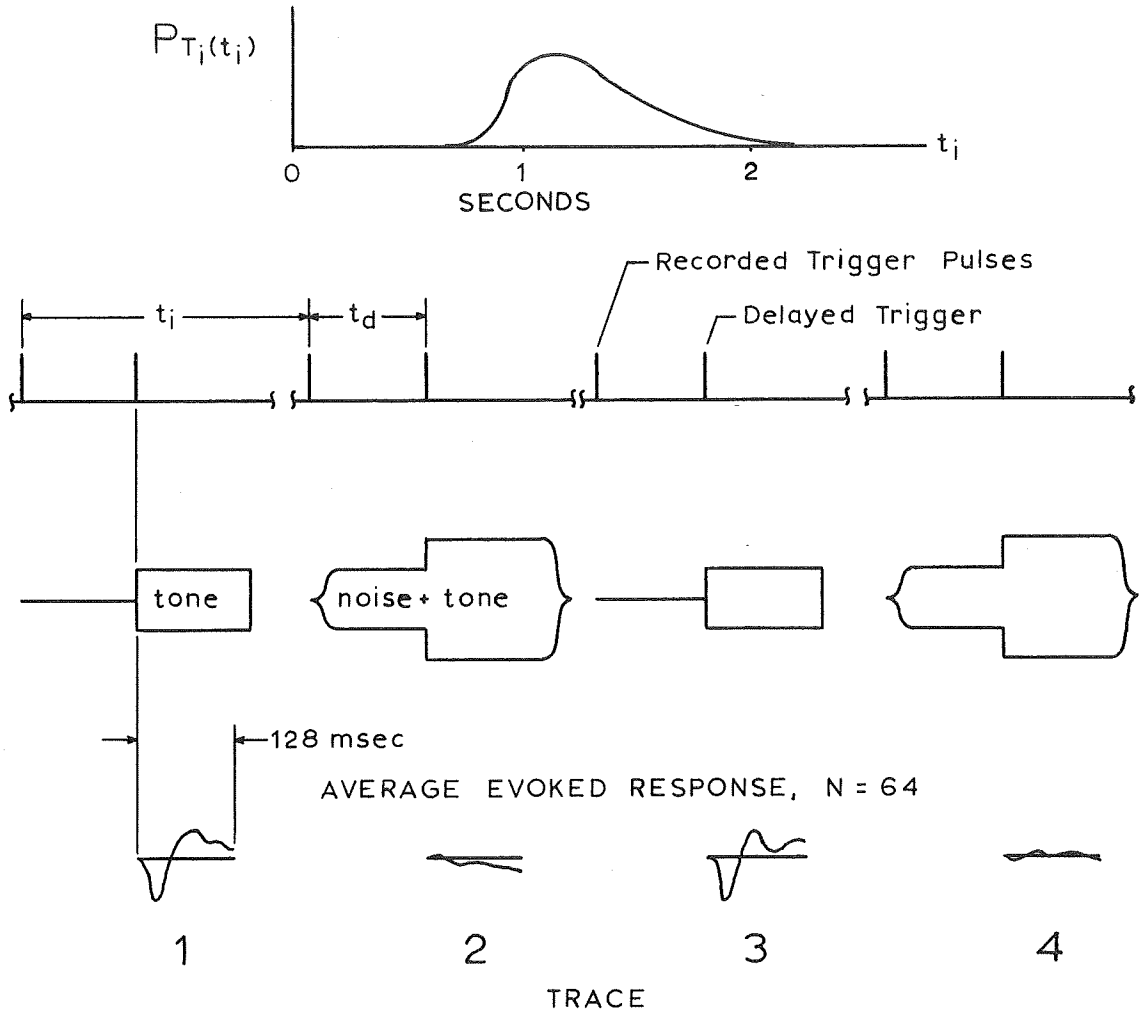

Fig. 14. The general stimulus paradigm consists of four tone bursts separated by a randomly varying interval of time. A masker noise is presented during the second and fourth tone bursts. The time interval separating tone bursts is determined by trigger pulses which are recorded on magnetic tape. The onset of the tone burst is delayed from the recorded trigger pulse by t_d msecs. The average evoked responses to the four tone bursts are accumulated over a 128 msec period following the onset of the tone burst. The stimulus paradigm is repeated 64 times to obtain the average evoked responses.

to allow most of the evoked response to the onset of the noise to terminate prior to the start of the evoked response to the second and fourth tone bursts. The average evoked responses to the four tone bursts were accumulated over a 128 millisecond period following the onset of the tone bursts, in four channels of a CAT (Technical Measurements Corporation Model 1000 Computer of Average Transients). The sound stimulus remained on until after the evoked response had been sampled, thus eliminating the "off" response from the average evoked response. The stimulus paradigm was presented sixty-four times during each run to obtain the four average evoked responses. The accumulation of the average evoked response was not begun until after the presentation of several stimuli in order to eliminate large changes in the rms level of the background ECG and the "first stimulus" effects which causes the evoked responses to the first of a series of stimuli to be larger than the evoked responses to subsequent stimuli (58).

The accumulation of four average evoked responses over the same time period is referred to as a run. The four average evoked responses for each run are referred to as traces.

The critical band effects of masking noise on the average evoked response were tested using two types of experiment sessions. The first, designated "constant noise", examined the critical band at 14 KHz using different structures (modulation voltage, bandwidth of modulating noise, and noise intensity level) of narrow band FM noise centered at 14 KHz as a background to tone bursts ranging in frequency from 7 to 28 KHz. These experiment sessions were conducted in order to obtain an approximation of the most suitable noise condition for the

second type of experiment session, designated "constant tone". The stimulus parameters used during the constant noise experiments are shown in table 2. Each set of stimulus parameters was used during at least four experiment sessions. Data from the experiment sessions grouped together in the Days Post-op column were usually pooled for purposes of data analysis. The tone bursts were delivered at an SPL which was approximately 50 dB above the animal's threshold at 14 KHz, for all sessions except on days post-op 188, 189, 190, and 191 when a level 30 dB above threshold was used. If the frequency response of the sound system were perfectly flat, the tone SPLs shown in table 2 would have applied to tones of all frequencies used. However, as can be seen in Appendix F, all tone SPLs were within 5 dB of the 14 KHz tone SPL. Four noise parameters are listed under the Trace 2 and Trace 4 headings. The first, BW, is the setting of the 10 position switch which determines the bandwidth of the modulating noise. EMFMOD is the rms voltage of the modulating noise at the input of the voltage controlled oscillator. The frequency of this oscillator changed 7 KHz per volt of input signal. The bandwidth of the FM noise spectrum at the 6 dB (1/2 maximum amplitude) points was measured for each combination of BW and EMFMOD, and is shown under the "6 - dB/bw" heading. It is interesting to note that at a given BW setting the bandwidth of the FM noise is a monotonically increasing function of EMFMOD. However, at a given value of EMFMOD, the bandwidth of the FM noise decreases as the BW is increased above a particular setting. For smaller values of EMFMOD the bandwidth of the FM noise reaches a maximum at lower settings of BW. It should be appreciated that behavior of this sort makes band-

Table 2. The stimulus parameters for constant noise experiment sessions. An * in a Days Post-op cell indicates 2 sessions on the same day. Only FM noise was used for these sessions. BW is the setting of a 10 position switch which determines the bandwidth of the modulating noise. EMFMOD is the rms voltage at the input of the voltage controlled oscillator. Both BW and EMFMOD determine the bandwidth of the FM noise. The 2 structures of noise used during each session are shown along with the measured bandwidth, in Hz, at the 6 dB points of the FM noise spectrum, 6-dB bw (Appendix D). S/N is the signal-to-noise ratio in dB. The SPLs shown were measured for a 14 KHz tone. The SPL of the other tones were within 5 dB of this level (Appendix F). Cat 110 was used for these experiment sessions.

Days Post-op	Tone SPL	Trace 2 BW	EMFMOD	6-dB bw	S/N	Trace 4 BW	EMFMOD	6-dB	S/N
118 * 121 122 *	52	5	0.10	1.8K	0	5	0.01	250	0
125 * 126 *	52	5	0.10	1.8K	10	5	0.10	250	10
142 143 146 147	52	5	0.01	250	10	5	0.01	250	0
149 150 154 155	52	7	0.01	200	10	7	0.01	200	0
171 172 175 176	52	10	0.01	130	10	10	0.01	130	0
178 182 183 184	52	10	0.10	1.4K	0	10	0.05	425	0
188 189 190 191	32	7	0.10	2.1K	0	7	0.05	1.0K	0

width estimates of the FM noise from mathematical computation extremely difficult (59, 60). The signal-to-noise ratio, S/N, refers to the rms level of the tone relative to the rms level of the noise. These measurements were made using a tone frequency of 14 KHz and were not corrected for the differences encountered using other tone frequencies, since these differences were less than 5 dB.

Constant tone experiment sessions used tone burst frequencies of 9, 14 and 22 KHz to examine critical band effects at these frequencies. Tone bursts were presented in a background of FM and AM noise (traces 2 and 4, respectively) in order to test for differences in the masking effectiveness of these types of noise.* Three sets of stimulus parameters differing only in the frequency of the tone burst and the set of 15 noise carrier frequencies were used during these experiments. Each of the 3 sets of stimulus parameters was used during 4 experiment sessions with each of 4 cats. Table 3 shows the days post-op each set of stimulus parameters was used on each cat.

The use of AM noise as a masker in these evoked response experiments imposed a restriction on the range of noise bandwidths available. It was believed, apriori, that a very narrow bandwidth noise would provide greater resolution of critical band phenomena. However, the AM noise, by its nature, possesses large amplitude fluctuations. If a very narrow bandwidth is used, the tone burst onset could occur during a period when the instantaneous noise level was near zero, and an

*The combination of FM noise and tone produces a stimulus which does, indeed, fluctuate in amplitude, although not to the extent which occurs with AM noise.

Table 3. The stimulus parameters for constant tone experiment sessions. During the first 17 runs of each session an FM noise was presented with the 2nd tone burst and an AM noise with the 4th tone burst in the stimulus paradigm. The BW setting for these noises was 7, and the EMFMOD was set at 0.035 volts rms in order to produce FM noise with the same bandwidth as the AM noise. The measured bandwidth at the 6 dB points of the noise spectrum was 720 Hz for both AM and FM noise. The signal-to-noise ratio was 0 dB. The SPLs of the tones were 30 dB above the corresponding values for animal and tone frequency shown in table 1. For runs 18 to 22 of each session the FM noise was presented with the 2nd tone burst at signal-to-noise ratios of 20, 10, 5, 0, and −10 dB, respectively. The 4th tone burst was presented without noise at SPLs of 20, 10, 5, 0, and −10 dB, relative to those shown in table 1, for runs 18 to 22, respectively. The days post-op are shown for each cat and tone frequency.

Frequency of tone (KHz)	Cat			
	110	116	119	120
9	422 428 430 431	3 9 12 15	33 41 43 46	3 11 17 21
14	421 427 429 433	5 8 13 15	34 36 44 49	4 15 19 22
22	424 429 430 433	7 8 10 14	35 42 45 48	8 16 20 23

evoked response would appear, despite the long term presence of the noise (61). At wider bandwidths of noise, the amplitude fluctuations appear similar to tone burst onsets and have the effect of evoking a large number of overlapping evoked responses. Using a supracritical bandwidth noise would reduce the masking since only a fraction of the noise power would be providing the masking. The bandwidth of the AM noise is determined by the setting of the BW switch. A setting of 7 appeared to represent a reasonable value and resulted in a bandwidth of the AM noise spectrum of 720 Hz at the 6 dB points. The BW setting was determined by the AM noise requirement and could not be switched between AM and FM noise presentations. The value of EMFMOD was set to 0.035 volts rms resulting in an FM noise bandwidth of 720 Hz for BW equal to 7.

The signal-to-noise ratio was measured for the situation of noise carrier frequency equal to tone frequency. For the first 17 runs the signal-to-noise ratio was 0 dB, except for control 1 and control 2 runs. Because the sound system had an essentially flat frequency response, no correction for signal-to-noise ratio was made for noise carrier frequencies not equal to the tone frequency. During experiment sessions using a tone frequency of 22 KHz noise center frequencies of 34 and 44 KHz were required. The range setting of the frequency dial on the voltage controlled oscillator was switched to a value for which the frequency sensitivity was increased from 7 KHz/volt to 23.3 KHz/volt. The EMFMOD was reduced to 0.0105 volts rms for these two noise conditions in order to maintain a bandwidth of 720 Hz. The AM noise required the use of an additional amplifier (see figure 17) and an

additional gain of 1 and 3 dB was provided to the AM noise at noise carrier frequencies of 34 and 44 KHz, respectively, in order to compensate for frequency distortion in this amplifier. The changes made in the noise generating equipment to compensate for conditions at 34 and 44 KHz are not shown in the data, since this would have caused possible confusion and computer programming problems.

The tone burst SPL was 30 dB above the values shown in table 1 for the corresponding animal and frequency. The 4th tone burst of the stimulus paradigm was presented at SPLs of 20, 10, 5, 0 and −10 dB relative to threshold in runs 18 to 22 respectively. No noise was presented with the fourth tone burst during these runs. The intensity level of the FM noise presented with the 2nd tone burst was set to give signal-to-noise ratios of 20, 10, 5, 0, and −10 dB for runs 18 to 22 respectively.

Data from the two types of experiment sessions are shown in figure 15. During constant noise experiments the spectra of the noises remained constant while the tone frequency (shown to the left of each run in figure 15a) was changed between runs. The tone burst frequency remained unchanged during constant tone experiments while the center frequency of the noise (shown to the left of each run in figure 15b) was changed between runs for fifteen runs. For the additional seven runs the center frequency of the noise and the frequency of the tone burst were the same. During constant noise experiments the onset of the tone burst was delayed 150 milliseconds from the onset of the noise. This delay was increased to 300 milliseconds for constant tone experiments because it appeared from a preliminary analysis of constant noise data

Fig. 15. The following three figures show computer plotted evoked response data from two types of experiment sessions. Figure 15a shows all of the data from a constant noise experiment session. Figure 15b shows 15 runs from a constant tone experiment session in which AM and FM noise were used. Figure 15c shows the remaining runs of this session, including two control runs and five runs in which the signal-to-noise ratio and tone burst intensity were changed for traces 2 and 4, respectively. The terms used in these figures are defined:

NOISE CARRIER FREQ	-	the center frequency of the noise
BW	-	one of ten positions of a switch which determines noise bandwidth
CAT	-	identifies the animal used
SIGNAL & NOISE ATTN	-	the settings in dB of these attenuators
DAY POST-OP	-	the number of days since the electrode was implanted
SIG/NOISE	-	the ratio in dB between the rms voltage of the tone burst and noise
EMFMOD	-	the rms voltage of the modulating noise at the input of the FM oscillator
TRACE	-	identifies each of the four average evoked responses in a run
RUN	-	shows the sequence in which the various stimuli were presented
FREQ KHZ	-	the frequency of the tone used for each run in constant noise sessions (figure 15a only)
NOISE CARRIER FREQ (KHZ)	-	the center frequency of the noises, AM and FM, used for each of 15 runs in constant tone sessions (figure 15b only)
CONTROL 1 & 2	-	two types of control runs performed during all experiment sessions. Runs 14 and 12 in figure 15a correspond to the two control runs shown in figure 15c
KHZF	-	a code number which identifies the stimulus characteristics used for each run

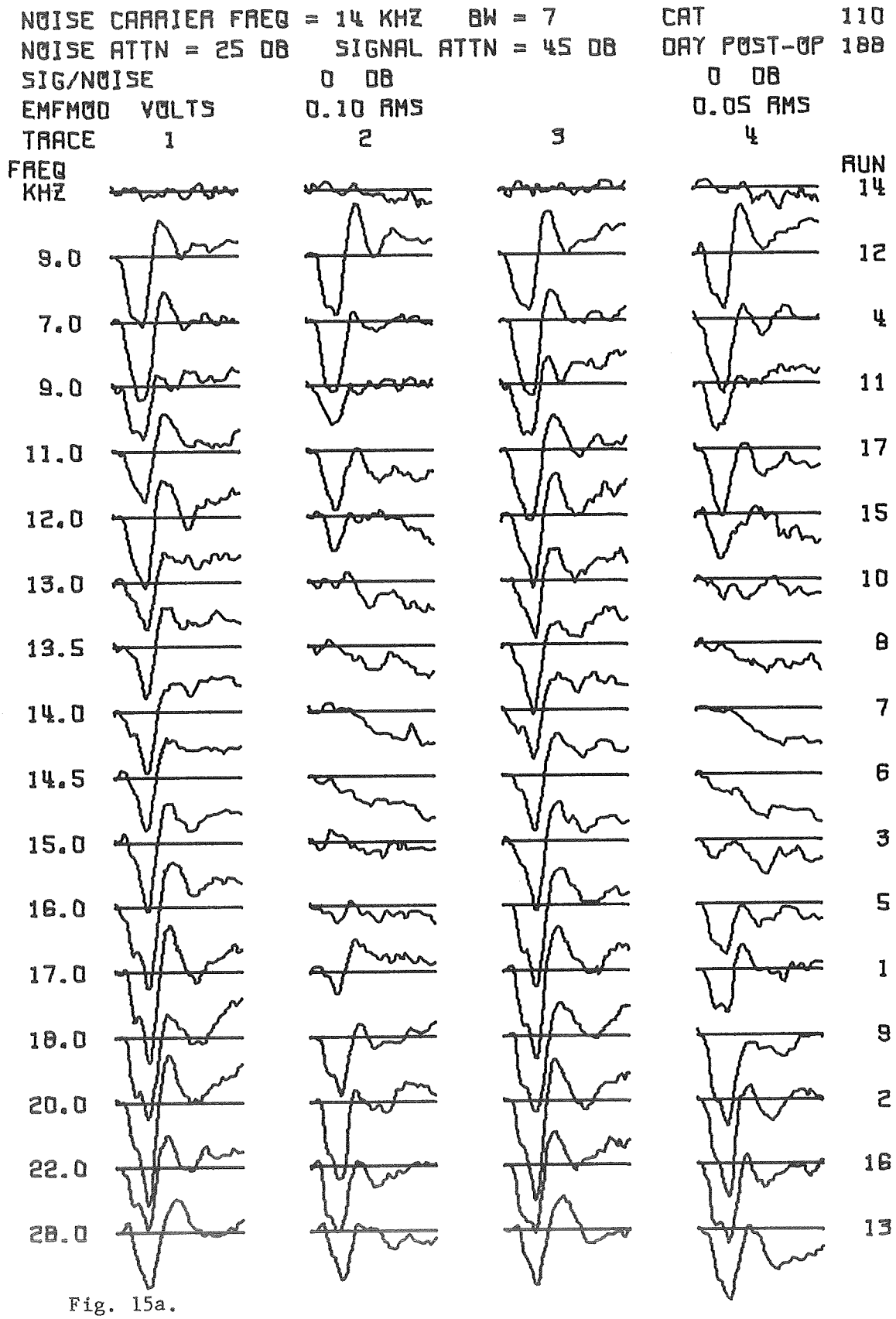
NOISE CARRIER FREQ = 14 KHZ BW = 7
CAT 110
NOISE ATTN = 25 DB SIGNAL ATTN = 45 DB
DAY POST-OP 188
SIG/NOISE 0 DB 0 DB
EMFMOD VOLTS 0.10 RMS 0.05 RMS
TRACE 1 2 3 4
FREQ KHZ
RUN
9.0
7.0
9.0
11.0
12.0
13.0
13.5
14.0
14.5
15.0
16.0
17.0
18.0
20.0
22.0
28.0
14
12
4
11
17
15
10
8
7
6
3
5
1
9
2
16
13

Fig. 15a.

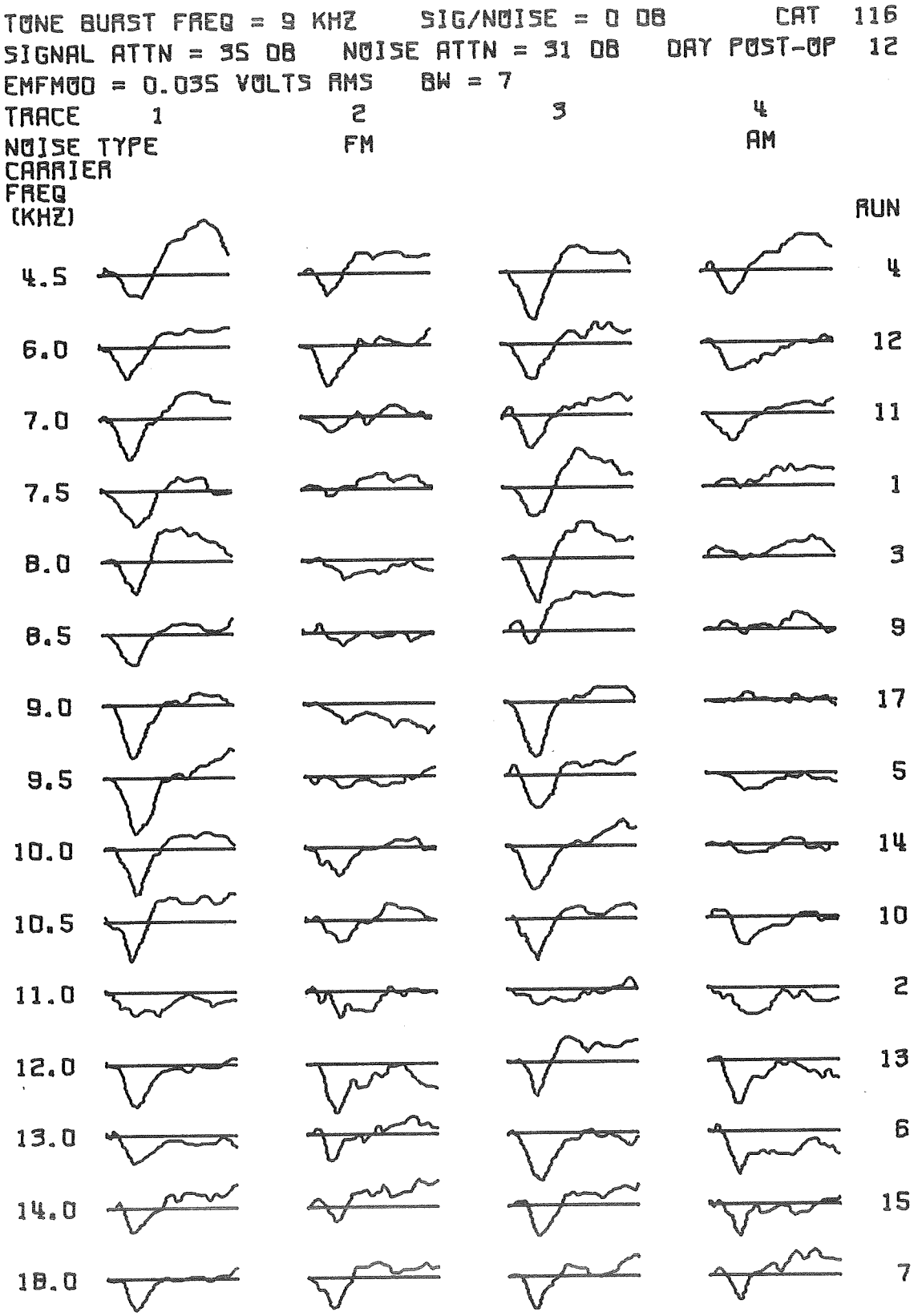
TONE BURST FREQ = 9 KHZ SIG/NOISE = 0 DB CAT 116
SIGNAL ATTN = 35 DB NOISE ATTN = 31 DB DAY POST-OP 12
EMFMOD = 0.035 VOLTS RMS BW = 7
TRACE 1 2 3 4
NOISE TYPE FM AM
CARRIER FREQ (KHZ)
RUN
4.5 4
6.0 12
7.0 11
7.5 1
8.0 3
8.5 9
9.0 17
9.5 5
10.0 14
10.5 10
11.0 2
12.0 13
13.0 6
14.0 15
18.0 7

Fig. 15b.

TONE BURST FREQ = 9 KHZ FM NOISE ON TRACE 2 CAT 116
NOISE CARRIER FREQ = 9 KHZ BW = 7 DAY POST-OP 12
EMFMOD = 0.035 VOLTS RMS SIGNAL ATTN = 35 DB

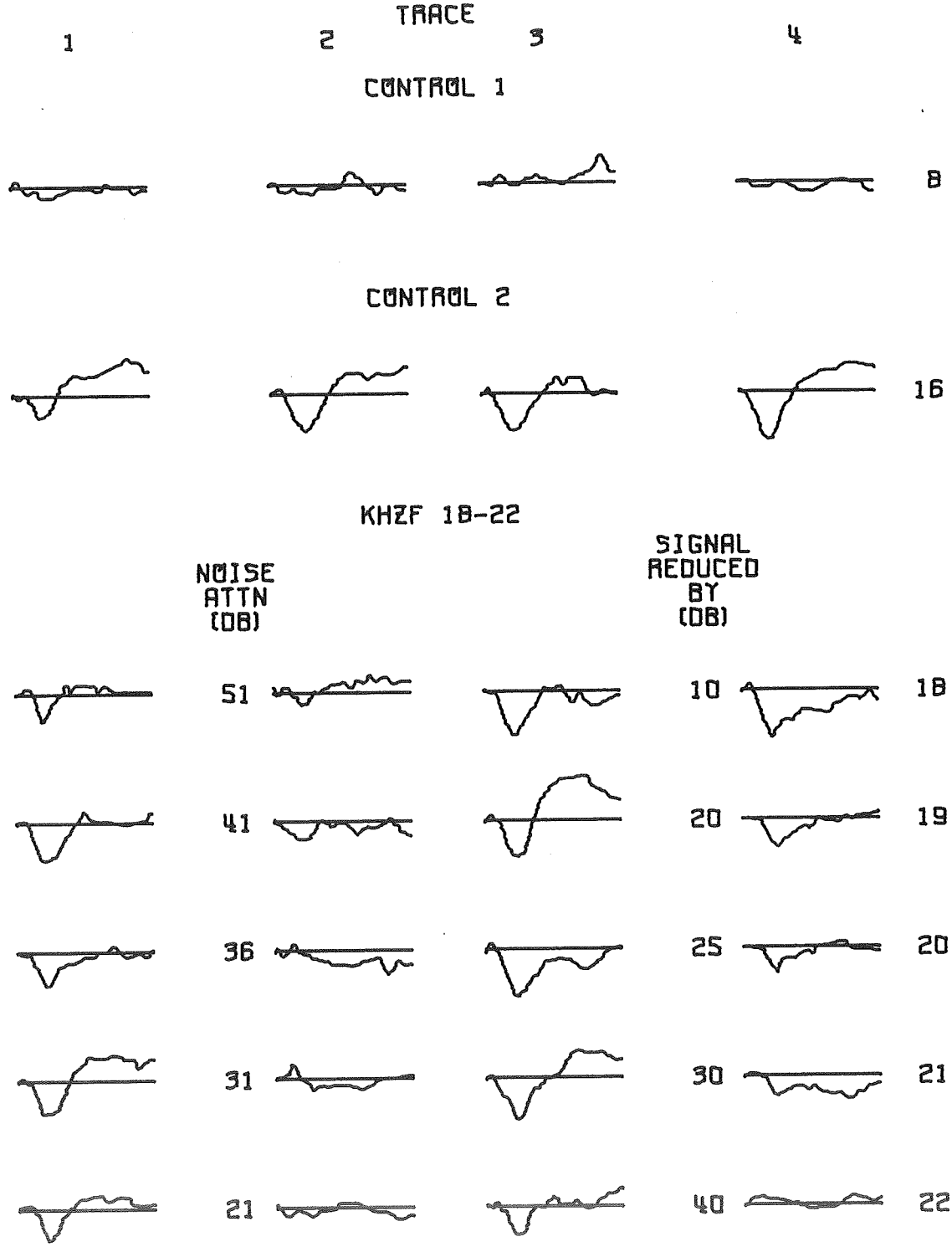

Fig. 15c.

that 150 milliseconds wasn't always sufficient time for completion of the evoked response to the noise.

During both types of experiments two types of control runs were made. The first (control 1) consisted of presenting the stimulus paradigm with the intensity of the tone bursts reduced below the animal's threshold of hearing (actually the tone burst was not presented to the animal). The first and third average "evoked responses" of this control provide an estimate of the distortion in an average evoked response to a tone burst caused by background electrocortical activity. The second and fourth average "evoked responses" provide an estimate of the distortion in an average evoked response to a tone burst presented in a noise background which is caused by the evoked response to the onset of the noise. The control 1 run appears at the top of the plotted data in a constant noise session (RUN 14 in figure 15a) or on the second page under the control 1 heading in plots of constant tone experiment data (figure 15c). The second type of control run (control 2) consisted of presenting the four tone bursts without masking noise. Theoretically, this should have resulted in four identical average evoked responses. The degree to which they differed provides an indication of the variability to be expected in an average evoked response, apart from that caused by masking. The control 2 run appears on the second line of data (RUN 12 in figure 15a) in plots for constant noise experiments and under the control 2 heading in plots of constant tone experiment data (figure 15c).

The order in which the different frequencies of noise or tone and control runs were used was determined by random drawing of 17 numbered

cards. The run numbers correspond to the order of the runs for each experiment session. Runs 18 to 22 (present only in constant tone experiment sessions) always had the same stimulus conditions and were conducted to provide a comparison of the evoked response to a tone burst which is reduced in loudness by either masking or reducing its intensity.

The tone bursts had a Gaussian shaped onset and offset, thereby minimizing spectral spreading for a given rise/fall time. The rise/fall time of the tone bursts was 2.5 milliseconds in constant noise experimental sessions and 10 milliseconds in constant tone experiment sessions.

Figure 16 shows a block diagram of the auditory stimulus generating equipment used in constant noise experiment sessions. Randomly occurring trigger pulses were played back from a magnetic tape and used to advance the stimulus counter a preset number of times. The stimulus counter, operating through the CAT channel selector and noise parameter gate amplifier, determined which of the four CAT channels accumulated a generated evoked potential and which of two noise conditions was available for masking. The duration of the masking noise presented during even numbered tone burst presentations was determined by the alternate stimulus masker gate. After a 150 millisecond delay the trigger pulse activated the signal zero level detector which sensed the next positive zero crossing of the tone oscillator, so as to eliminate acoustic transients, and generated a synchronization pulse for the CAT analysis sweep and the tone burst envelope generator. The output of the tone burst envelope generator was multiplied by the tone oscillator

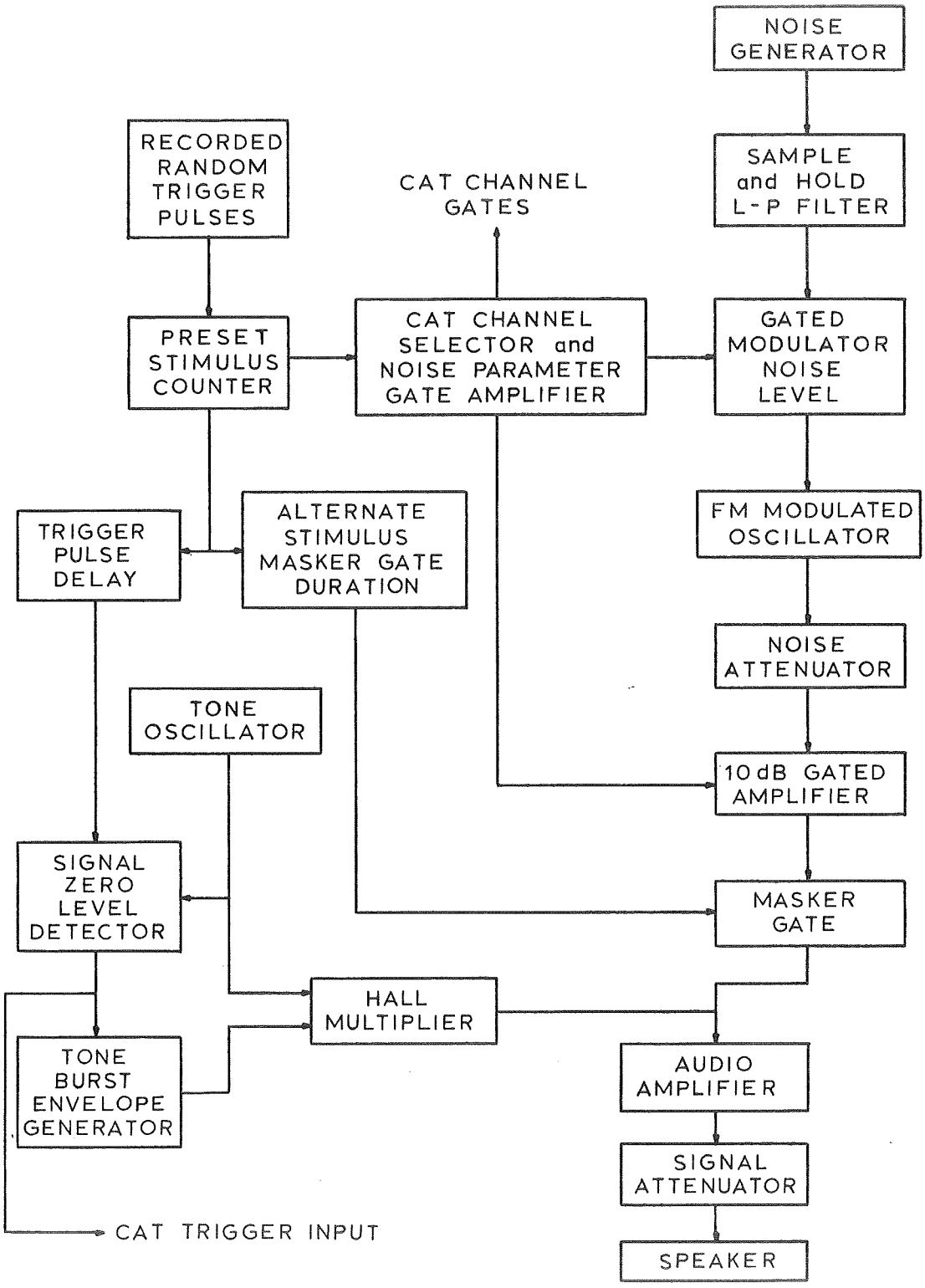

Fig. 16. Block diagram of the auditory stimulus generating equipment used in constant noise experiment sessions.

signal to produce the desired tone burst at the input of the audio power amplifier. The stimulus level was adjusted by the signal attenuator and presented to the animal in free field.

The masking noise consisted of a sinusoidal carrier which was frequency modulated by a random A.C. voltage having a Gaussian amplitude distribution and a spectrum which was flat from zero to one of ten switch selectable cut-off frequencies. The modulating noise source, an Allison Lab Model 655, had a flat spectrum from 5 Hz to 30 KHz. The sample-and-hold circuit sampled the noise source output at one of ten switch selectable rates, designated BW in the specification of stimulus parameters. The output of the sample-and-hold circuit was filtered by a four-stage active low-pass filter with a switch selectable cut-off frequency matched to the sample rate such that the power output of the modulating noise was constant at all bandwidths. The voltage level of the modulating noise, and hence the bandwidth of the FM masking noise, could be electronically switched by the CAT channel selector and noise parameter gate amplifier from one value for the second tone burst to another value for the fourth tone burst. The rms voltage used was labeled EMFMOD in the stimulus parameter specification and never exceeded 0.1 volts (see Appendix D). The modulating noise voltage modulated the frequency of a Wavtek Model 105 voltage controlled oscillator (FM modulated oscillator). The signal-to-noise ratio was determined by the setting of the noise attenuator, but could be electronically decreased 10 dB during the fourth tone burst by amplifying the noise in the 10 dB gated amplifier. During constant noise experiment sessions the CAT channel selector and noise parameter gate amplifier was

programmed to control either the bandwidth of the noise via the gated modulator level or the level of the noise via the 10 dB gated amplifier, but was not used to control both level and bandwidth during any one experiment session. The masker gate provided the desired masking noise, under control of the alternate stimulus masker gate duration circuit, to a summing junction at the input of the audio amplifier which combined masking noise with the second and fourth tone bursts of the stimulus paradigm. The onset and offset times of the noise burst were dependent upon the characteristics of the masker gate, a Raytheon CK 1114 raysistor, and were approximately 30 and 45 milliseconds respectively (see Appendix H). The long rise time was required to keep the evoked response to the noise burst relatively small.

The audio equipment used for constant tone experiment sessions was generally similar to that discussed above except for some of the noise generating equipment shown in figure 17. The CAT channel selector and noise parameter gate amplifier was programmed to turn off the modulating noise to the FM modulated oscillator during presentation of the fourth tone burst, when AM noise was required, and to control the selection of the AM/FM noise selector during the AM-FM runs. During runs 18 to 22 the AM noise was disconnected and no noise was presented with the fourth tone burst, which was decreased in intensity by the gated attenuator under control of the CAT channel selector and noise parameter gate amplifier. The noise generator and the sample-and-hold and low pass filter were the same as discussed above, except that the noise was connected to both the FM oscillator via the modulator noise gate and the AM modulator (Hall multiplier). The BW switch was set at 7 and the

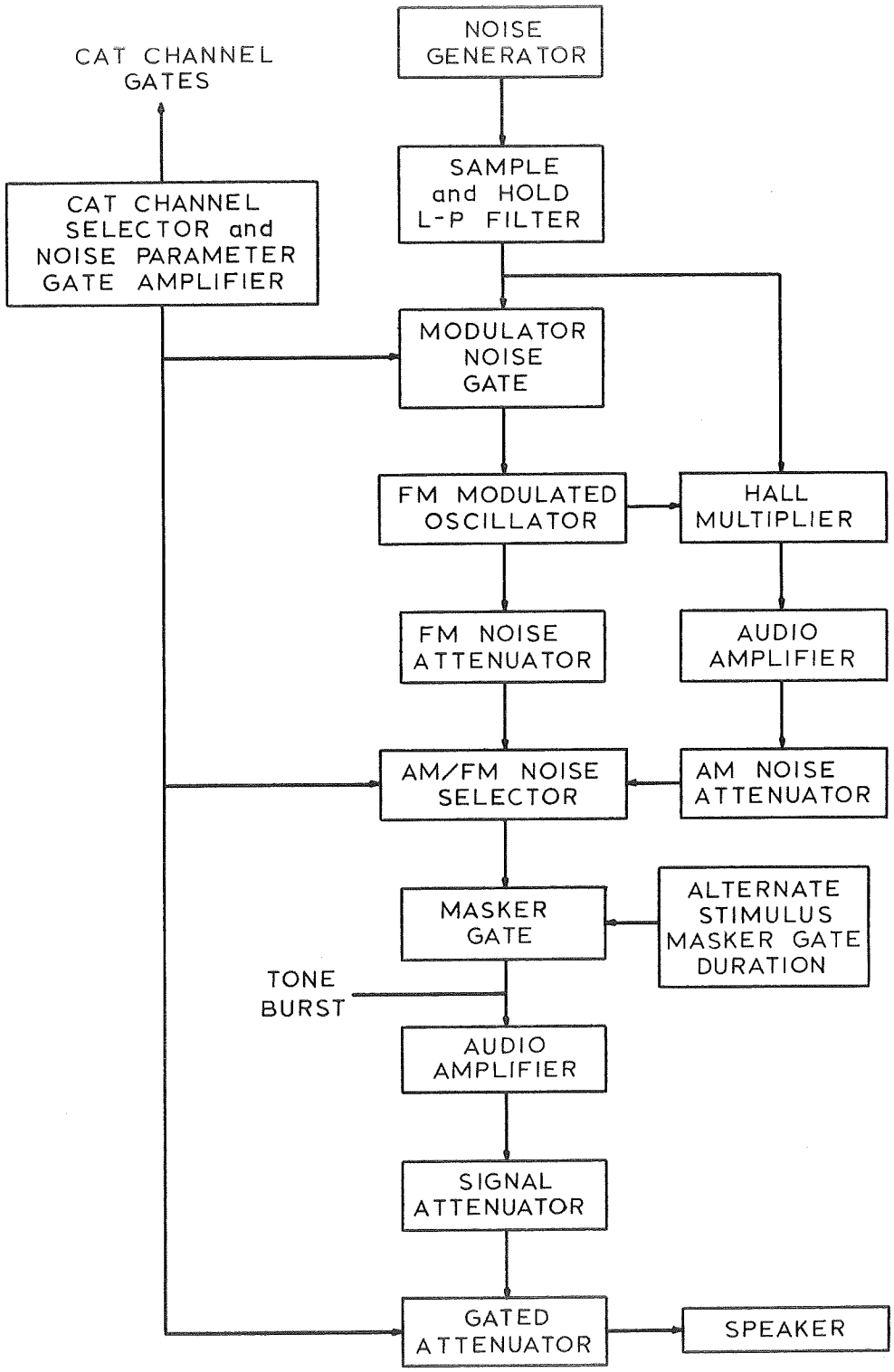

Fig. 17. Block diagram of the noise generating equipment used in constant tone experiment sessions.

noise voltage to the FM oscillator (EMFMOD) was set to 0.035 volts rms in order to produce AM and FM noises with the same bandwidth. During the second tone burst in the paradigm the AM/FM noise selector selected the FM noise. During the fourth tone burst the modulating noise to the FM oscillator was turned off, and this oscillator provided the carrier for the AM noise. The AM noise from the Hall multiplier was amplified by an audio amplifier so that the AM and FM attenuators would have identical settings at any signal-to-noise ratio. The alternate stimulus masker gate duration, masker gate, tone-noise summing junction, audio amplifier and signal attenuator operated in the same manner as in the constant noise experiment sessions. During the fourth tone burst in runs 18 to 22 an additional amount of stimulus attenuation was produced by the gated attenuator.

A more detailed discussion of the noise and tone burst characteristics and the stimulus generating equipment is contained in the appendices.

The end product of an experiment session was a set of average evoked responses plotted from the analog output of the CAT on 8-1/2 x 11 inch sheets of graph paper, one page for each run. The amplitude of each plotted average evoked response was measured at 128 equally spaced time points and punched on computer cards, using a D-MAC digitizer table. The amplitudes were measured from a baseline calculated from the first five milliseconds of the response on the assumption that this represented a baseline of EEG activity prior

to the time when peripheral auditory stimulation evoked a cortical response*. The limited size of the IBM 360 computer† used for subsequent analysis made necessary the use of only 64 of the 128 amplitude measurements on the evoked responses. The amplitudes at odd numbered time points (1, 3, 5, ... 127 msec) were selected, arbitrarily, for further analysis. The digitized traces from each experiment session were plotted on a Calcomp plotter, as shown in figure 15, and checked for any errors in digitization, and then subjected to a principal component analysis (see Appendix G).

*The evoked response sample began at the onset of the tone burst at the speaker. The cat was approximately 60 cm from the speaker and thus "heard" the tone burst about 2 msec later. Assuming a neural conduction path 50 mm long with a conduction velocity of 20 meters per second and 3 synapses consuming an additional 3 msec of time, the assumption of zero evoked response over the first 5 milliseconds of analysis appears reasonable.

† The programs were written for a 32K word memory. Since then, the size of storage has been increased to 64K, but the programs were not changed since 64 points appears more than adequate to specify the evoked response.

RESULTS

A set of average evoked responses from four cats to clicks and to tone bursts of different rise times and frequencies is shown in figure 18. The average evoked responses to tone bursts with rise times of 10 msec were obtained from a random sampling of the data from constant tone experiment sessions and do not represent any statistic of the data. The SPL of these tone bursts were 30 dB above the corresponding threshold values for the animal and frequency shown in table 1. The click was produced from a 0.1 msec pulse with a peak amplitude equal to the peak amplitude of the 14 KHz tone burst used for each animal. The three evoked response components, ER_1, ER_2 and ER_3, can be seen in the average evoked responses to clicks, but are not always obvious in the average evoked response to tone bursts. Changes in the average evoked response can be seen as the stimulus is changed from a click to a tone burst and as the rise time of the tone burst is increased. The greatest changes occur in the latencies of the evoked response components. Latency measurements of these evoked response components were made on the original records used to generate figure 18 and are shown in table 4. The range of latencies for the evoked response components from average evoked responses to clicks, reported by Teas and Kiang (53), are also shown in table 4. All of the latencies are in msec and have been corrected for the time required by the sound stimulus to reach the animal. The latencies of ER_1 found here for clicks appear to bracket the latency values for ER_1 reported by Teas and Kiang. The latencies of ER_2 and ER_3 appear close to the values reported by Teas and Kiang, except

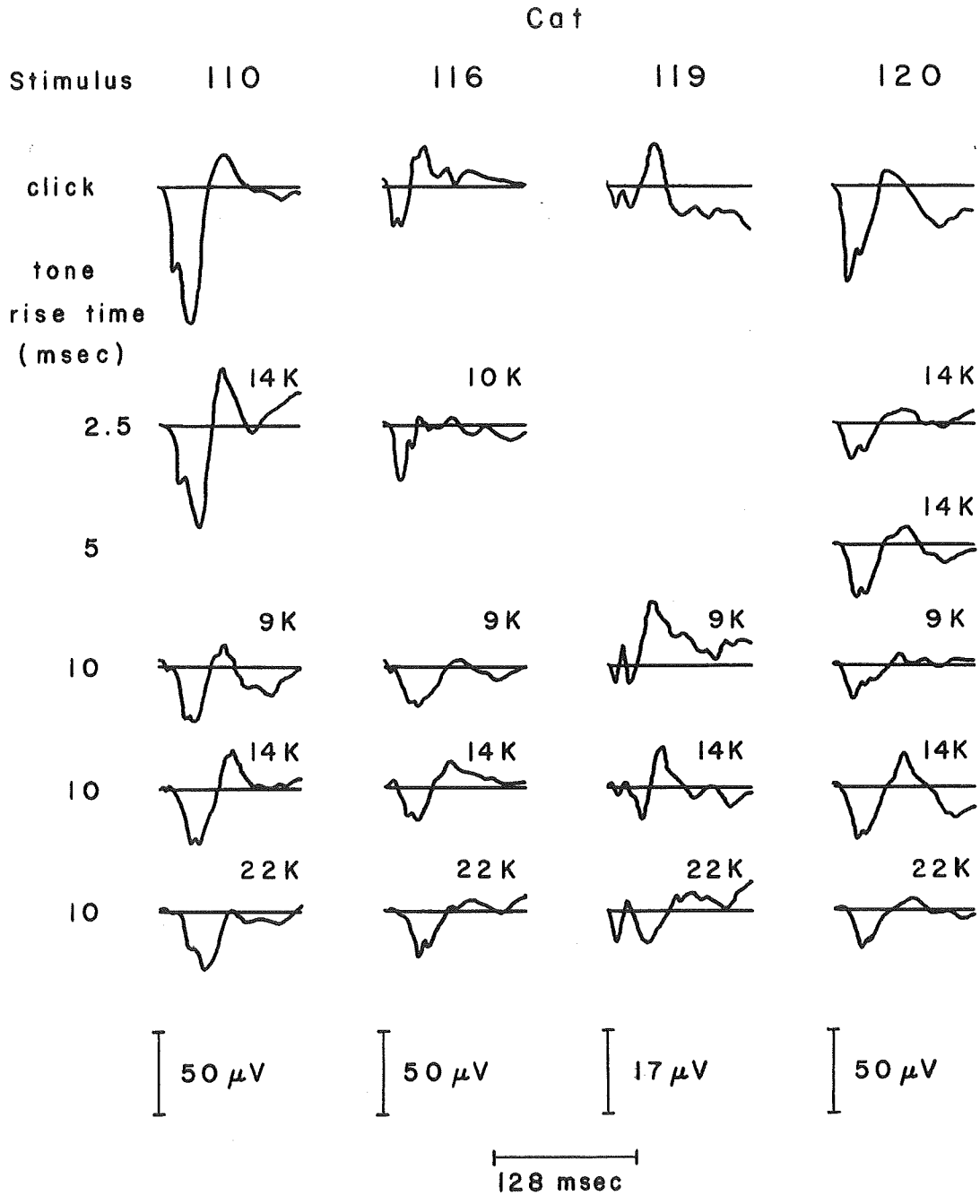

Fig. 18. Average evoked responses to clicks and tone bursts. The frequency of the tone is shown with the average evoked responses. The ordinate scale for each cat is shown below its column of evoked responses. The abscissa is 128 msec for all responses.

Table 4. Latencies of the evoked response components ER_1, ER_2 and ER_3 for the evoked responses to clicks and tone bursts, from four cats, and the corresponding latencies reported by Teas and Kiang (53). All latencies are in msec, and have been corrected for the time required by the sound stimulus to reach the animal. An * indicates that the component was not evident. These latencies were measured on the original records used to generate figure 18, and do not necessarily represent mean values. t_r is the rise time (msec) of the tone burst. f_o is the frequency (Hz) of the tone. The 3 numbers in each cell are latencies for ER_1, ER_2 and ER_3, respectively.

Stimulus	Cat 110	116	119	120	Range of latencies from Teas and Kiang
Click	13 24 56	5 12 33	6 19 39	12 25 45	8 - 10 18 - 25 41 - 69
Tone t_r 2.5 f_o	17 33 55	8 16 27		15 30 51	
5				22 31 63	
10 9K	23 32 57	20 28 68	7 20 39	18 30 57	
10 14K	27 37 62	18 26 56	8 26 47	21 30 62	
10 22K	* 35 55	25 35 68	9 28 58	20 * 59	

for cat 116 which shows shorter latencies. The greatest change in latency in going from click to tone burst with 10 msec rise time occurs for ER_1, causing ER_1 and ER_2 to be merged into a complex evoked response component. Taking into account the differences in the auditory stimuli (clicks versus long rise time tone bursts), the average evoked responses obtained in these experiments appear to correspond to those obtained by Teas and Kiang.

Electrode locations were checked in more than a dozen cats which had been surgically prepared by the same procedure as those used for these experiments, and were all found to be over the primary auditory cortex. Some of these animals had been used in previous experiments, not reported here, while others failed to show evoked responses to loud sounds. Middle ear infection was present in most of the "deaf" animals. The electrode location in one of the animals used in these experiments, cat 119, which had the smallest amplitude of evoked potential, was examined and found to be over the anterior, dorsal quadrant of the A1 area, almost adjacent to the suprasylvian sulcus. No reason for the smaller evoked potentials from this cat was evident from the examination of electrode placement. Cats 110, 116 and 120 are presently being used in other experiments and verification of electrode location in these cats has not been made. Because of the nature of the responses obtained, there is no reason to expect that the electrodes are not over the A1 area.

The average evoked responses from a typical constant noise experiment are shown in figure 19. Runs 13 and 7 were control 1 (no tones) and control 2 (no noise) runs, respectively. The frequency of the tone

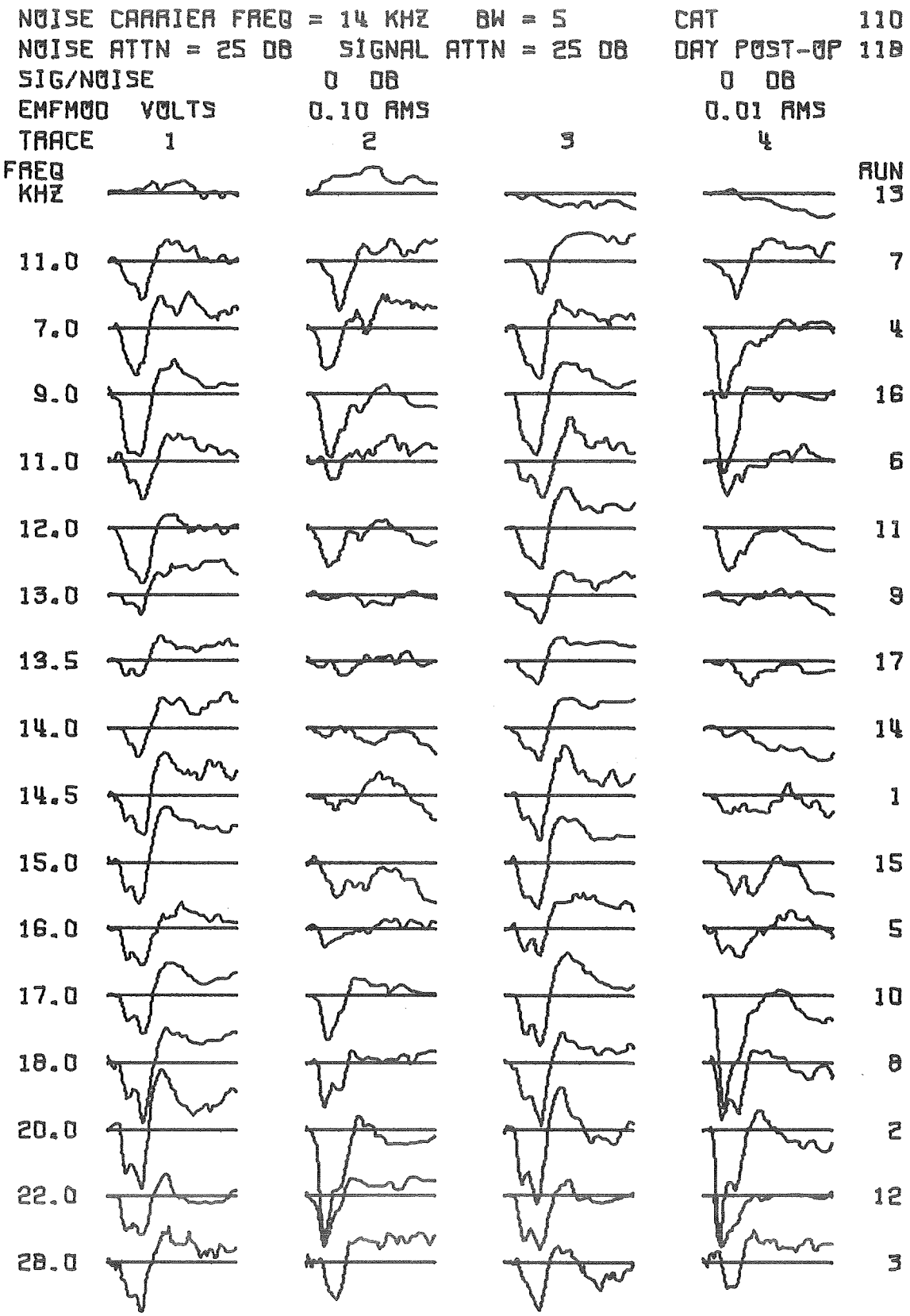

Fig. 19. Average evoked responses to constant noise experiment sessions.

for each run is shown to the left of the traces. As the tone frequency approaches the center frequency of the noise, 14 KHz, the degree of evoked response masking seen in traces 2 and 4 becomes more evident. Some of the variability seen in the evoked responses is caused by the differences in the tone burst frequency between runs, but most of the variability is probably due to physiologic variability. That part of the variability caused by using different tone burst frequencies was eliminated in the constant tone experiments.

The average evoked responses from a typical constant tone experiment are shown in figure 20. As in figure 19, the effect of the masking noise on traces 2 and 4 is more pronounced for noise carrier frequencies close to the tone frequency. For constant tone experiment sessions, a noise attenuator setting of 31 dB gives a signal-to-noise ratio of 0 dB. For trace 2 of runs 18 to 22 the reduction in noise level is shown as an equivalent noise attenuator setting. The signal level for trace 4 is shown as reduced from its level 30 dB above threshold. Hence, run 21 has the condition of signal-to-noise equal 0 dB for trace 2 and tone burst intensity at threshold SPL for trace 4.

Sets of average evoked responses such as those in figures 19 and 20 could, perhaps, be analyzed by visual inspection of the records. It is doubtful, however, that any two investigators would interpret the data in the same manner and a more quantitative approach to analyzing the data is desirable. One such approach would be to measure the evoked response components, ER_1, ER_2 and ER_3. Unfortunately these components are not evident in many of the average evoked responses to

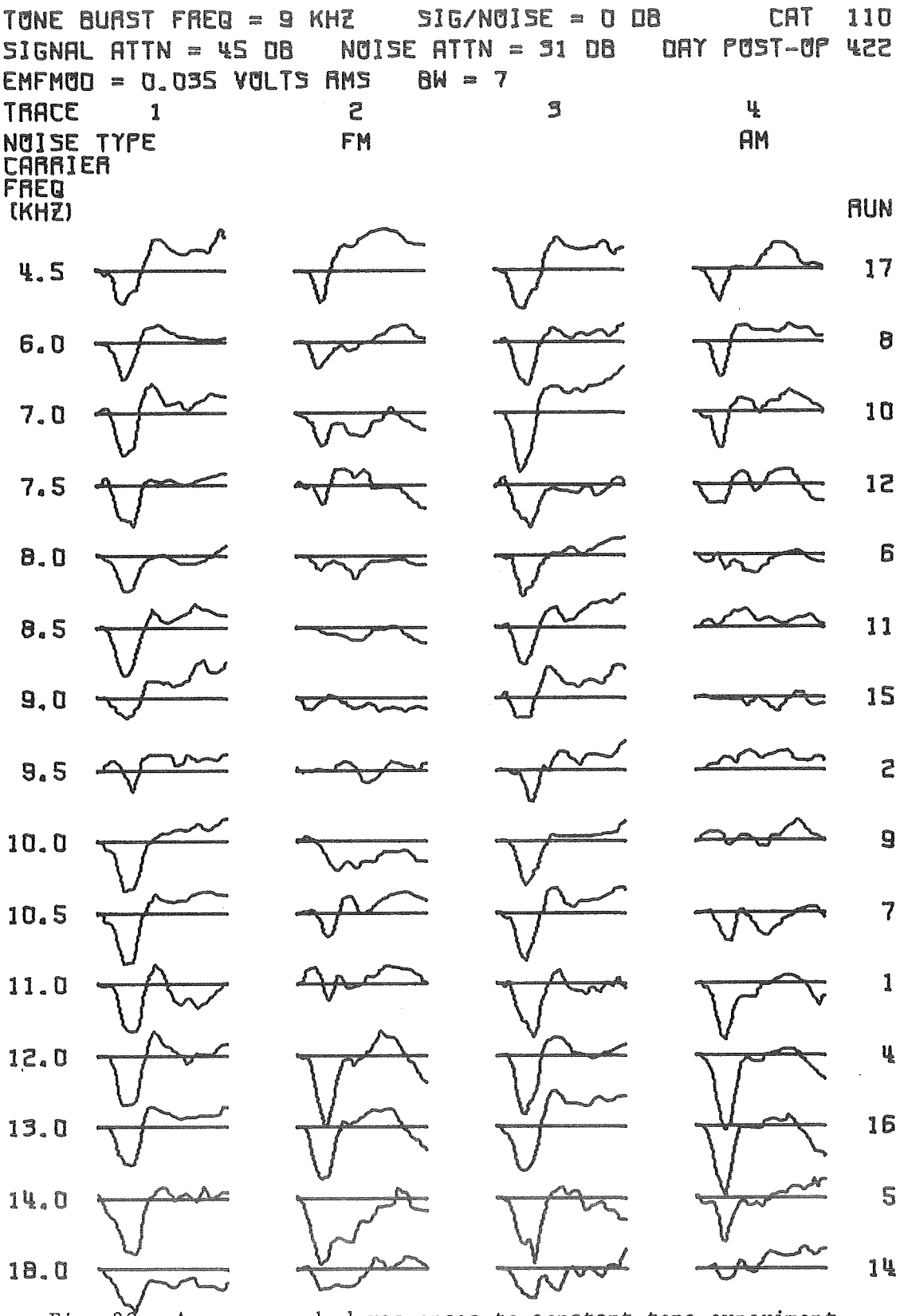

Fig. 20. Average evoked responses to constant tone experiment sessions.

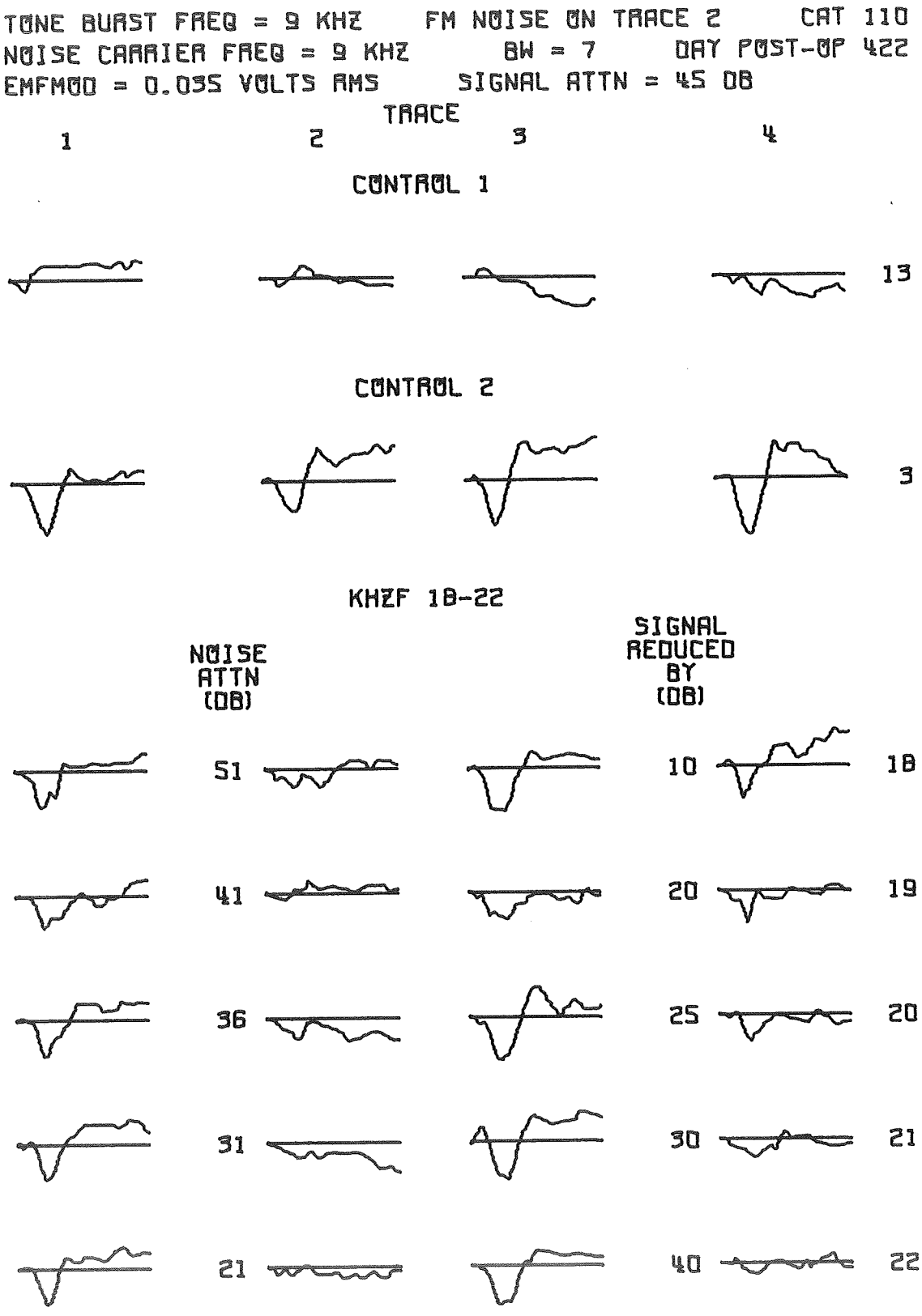
TONE BURST FREQ = 9 KHZ FM NOISE ON TRACE 2 CAT 110
NOISE CARRIER FREQ = 9 KHZ BW = 7 DAY POST-OP 422
EMFMOD = 0.035 VOLTS RMS SIGNAL ATTN = 45 DB
TRACE
1
2
3
4
CONTROL 1
13
CONTROL 2
3
KHZF 18-22
NOISE ATTN (DB)
SIGNAL REDUCED BY (DB)
51
10
18
41
20
19
36
25
20
31
30
21
21
40
22

Fig. 20. cont.

tone bursts; particularly when the tone burst is presented in a noise background.

Two other methods of measuring the average evoked responses were used initially. The first method measured the amplitude* of the average evoked responses, from a baseline, at some predetermined time point. This time point was selected as the most consistent latency for a large, early, positive voltage peak in the average evoked responses to unmasked tone bursts. This latency appeared to be 30 msec for cat 110 and 25 msec for cat 116 for constant tone experiment sessions using a tone frequency of 14 KHz. This method of measuring the average evoked responses is designated, "peak amplitude of evoked response," in figures 21 to 26. The second method of measuring the average evoked responses, used initially, measured the peak-to-peak amplitude of the average evoked responses. The measurement was made from the largest positive voltage peak, occurring prior to 50 msec, to the largest negative voltage peak, occurring prior to 70 msec. The measurements made by this method are designated, "peak-to-peak amplitude of evoked response," in figures 27 to 32. Some of the average evoked responses to masked tones failed to show even a small positive voltage peak within the first 40 milliseconds. These negative values for the positive voltage peak appear to result from the background electrocortical activity, as seen in the control 1 runs in figures 19 and 20. Rather than make a negative measurement, these peak amplitudes were given a value of 1 mm. This bias

*The voltage calibration of all original records was the same (50 μV/78 mm) and amplitude measurements could have been made in terms of either microvolts or millimeters of plot amplitude. The amplitudes reported in this dissertation are in millimeters of plot amplitude since this was less time consuming and easier to check for measurement errors.

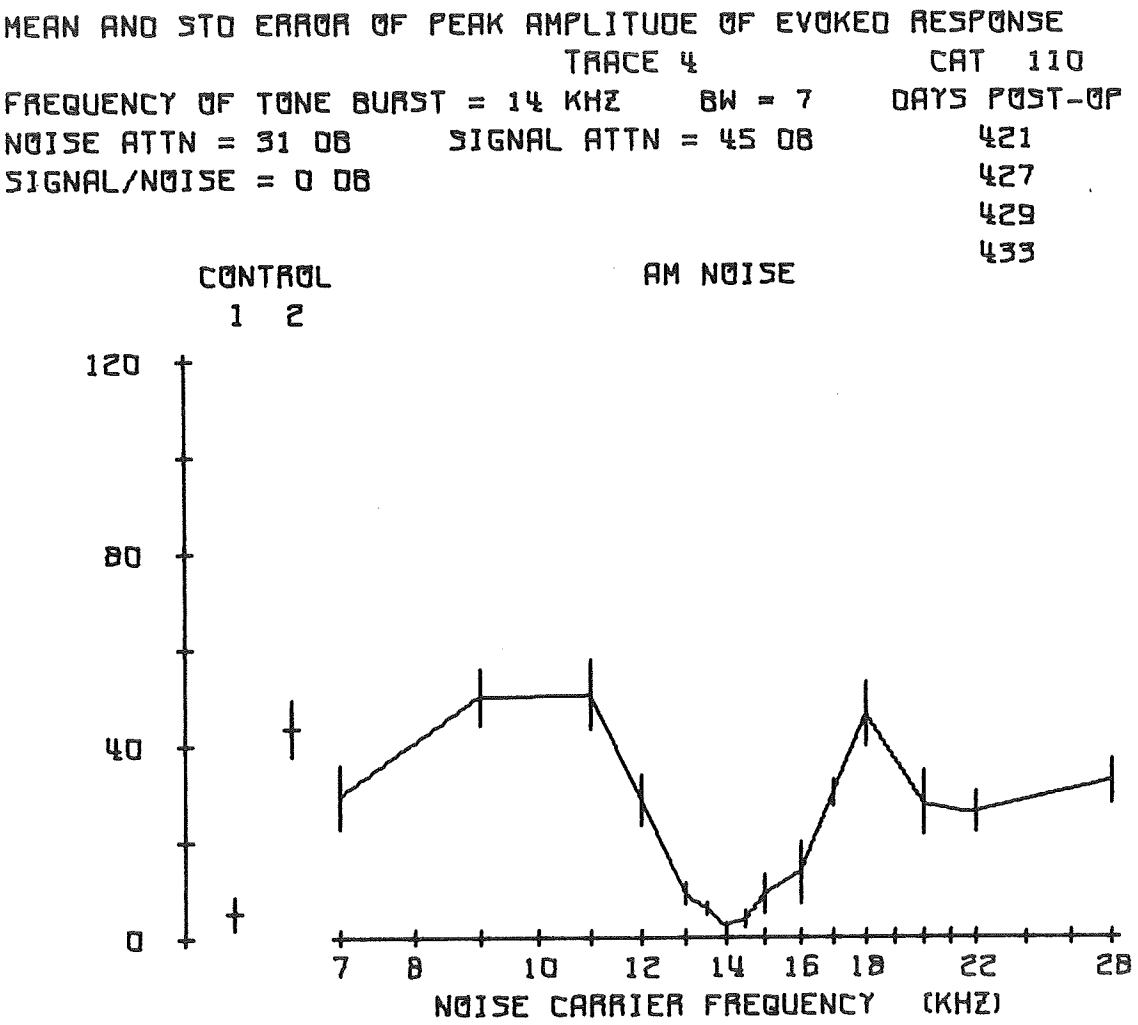

Fig. 21. Means and standard error of the means of peak amplitude of trace 4 evoked responses as a function of the center frequency of the masking noise. The vertical lines extend from the mean ±1 standard error. Data from control 1 and control 2 runs are plotted. Statistics are computed from data on cat 110 from four experiment sessions.

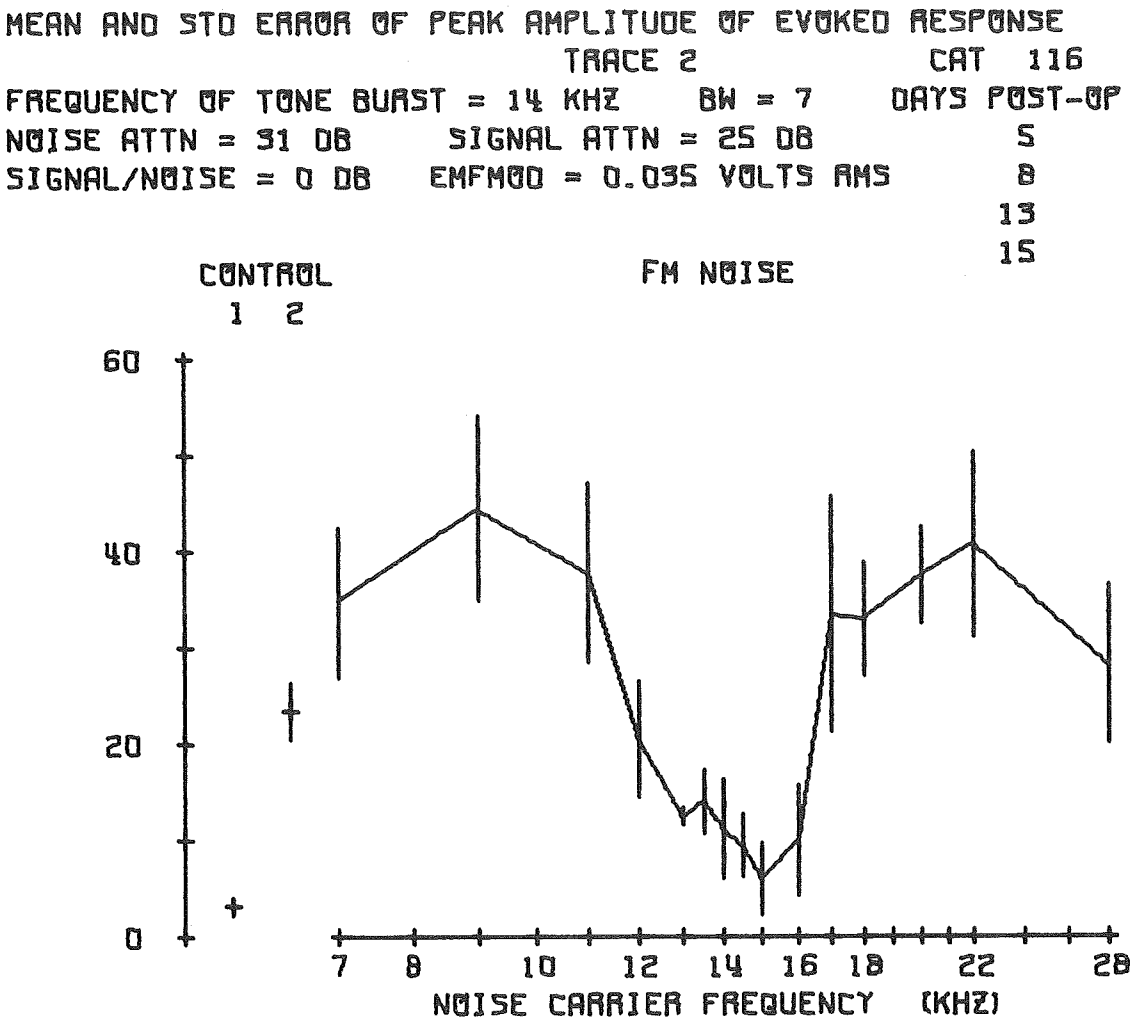

Fig. 22. Means and standard error of the means of peak amplitude of trace 2 evoked responses as a function of the center frequency of the masking noise. The vertical lines extend from the mean ±1 standard error. Data from control 1 and control 2 runs are plotted. Statistics are computed from data on cat 116 from four experiment sessions.

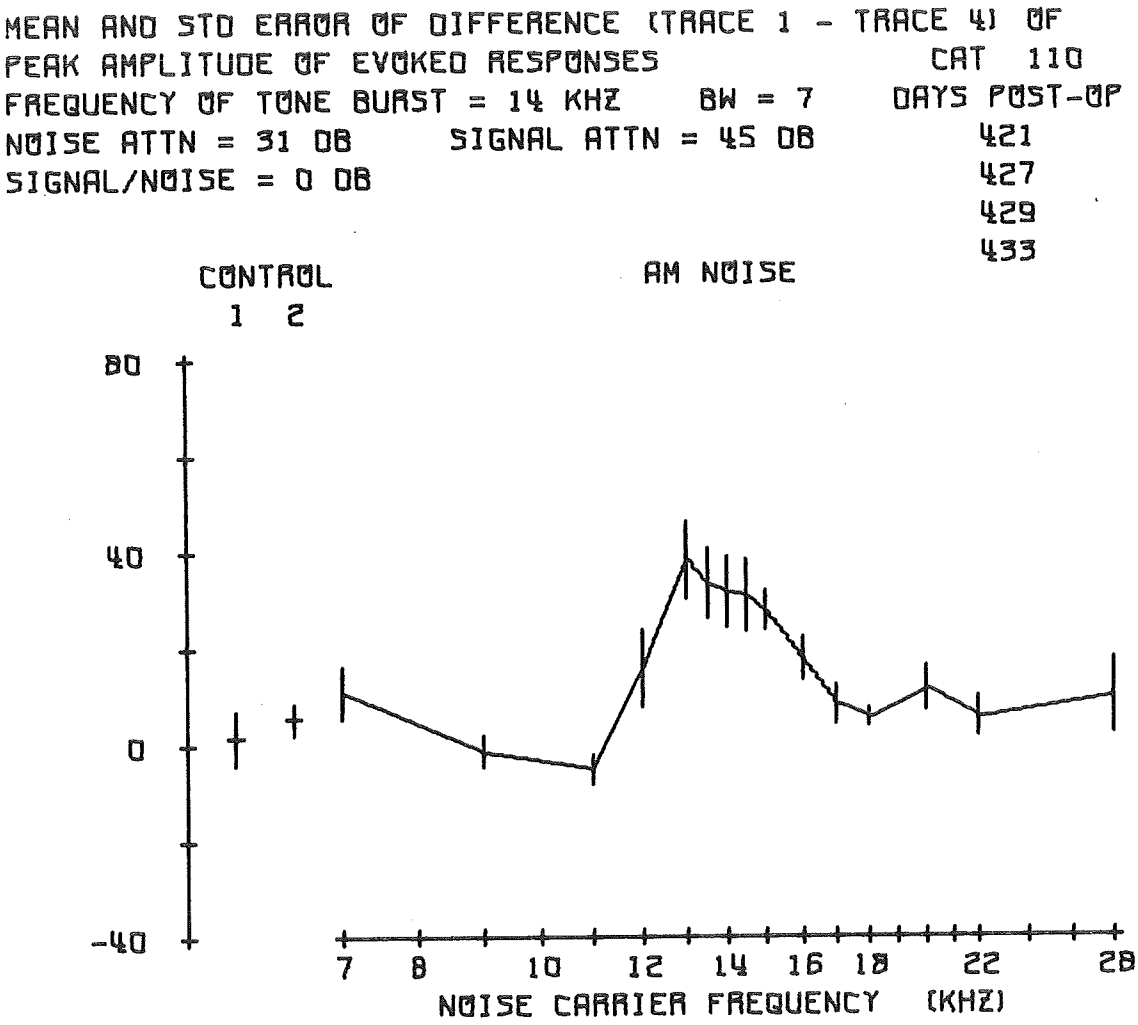

Fig. 23. Means and standard error of the means of the difference between the peak amplitudes of trace 1 and trace 4 evoked responses as a function of the center frequency of the masking noise. Data from the same experiments as in figure 21.

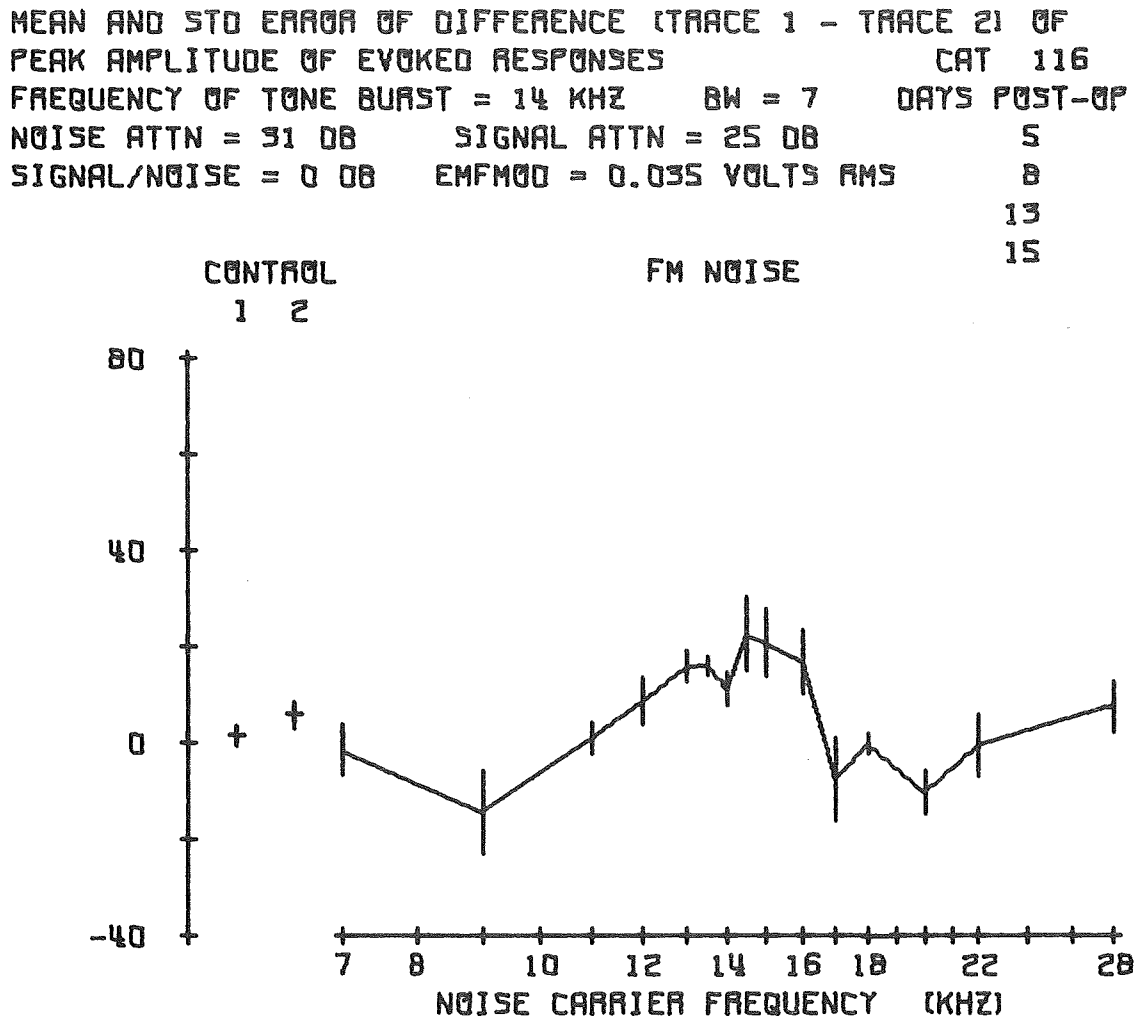

Fig. 24. Means and standard error of the means of the difference between the peak amplitudes of trace 1 and trace 2 evoked responses as a function of the center frequency of the masking noise. Data from the same experiments as in figure 22.

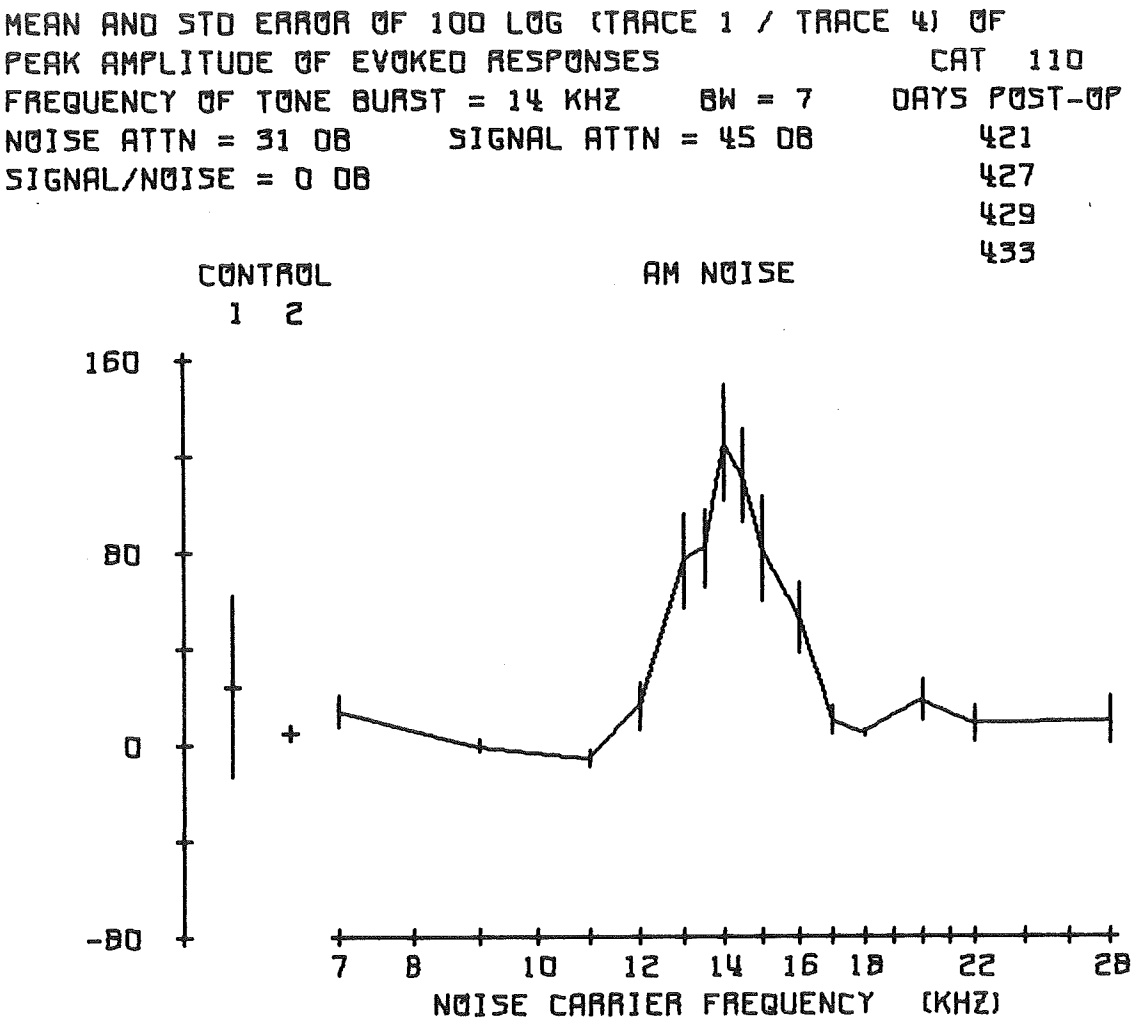

Fig. 25. Means and standard error of the means of the log of the ratio of the peak amplitudes, trace 1/trace 4, of the evoked responses as a function of the center frequency of the masking noise. Data from the same experiments as in figure 21.

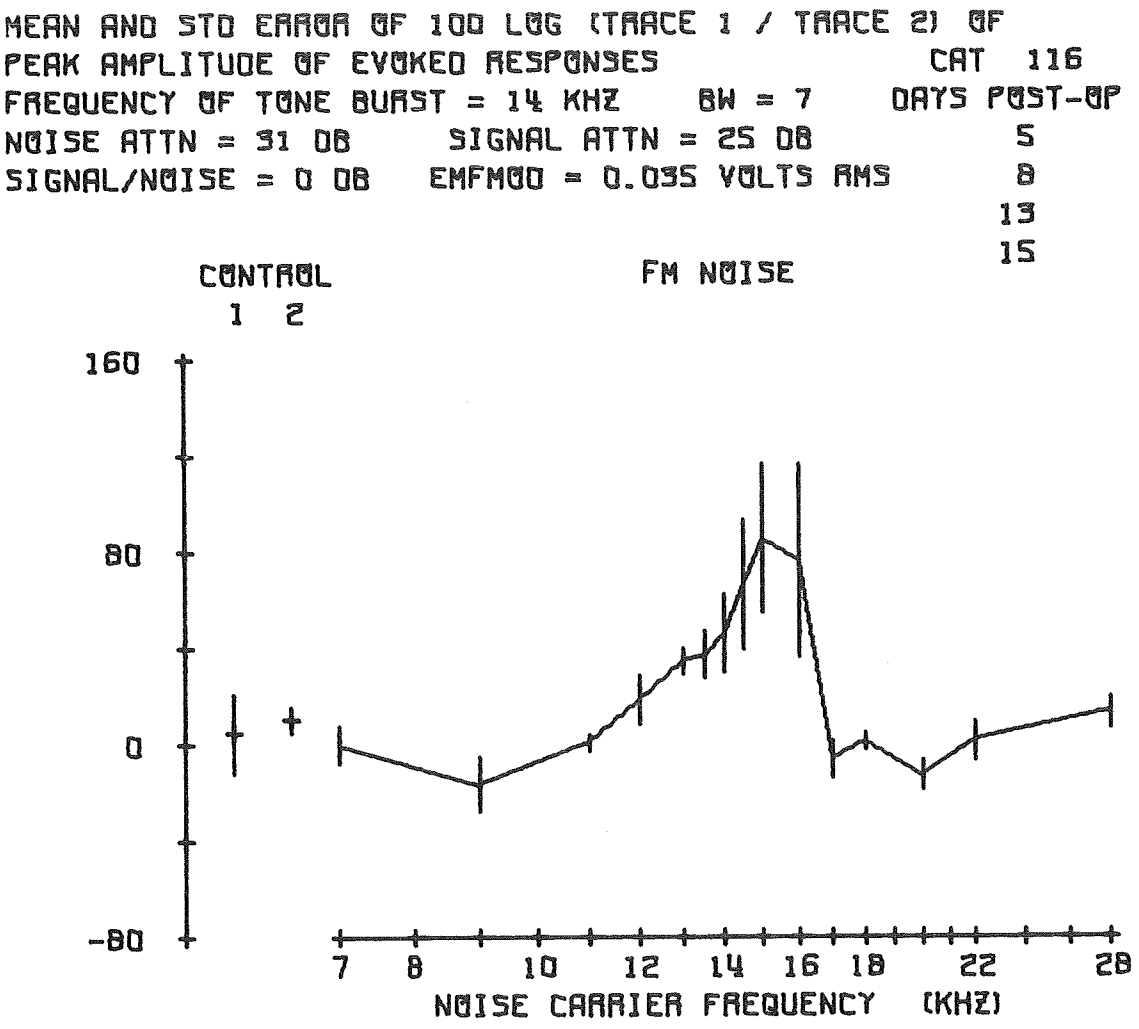

Fig. 26. Means and standard error of the means of the log of the ratio of the peak amplitudes, trace 1/trace 2, of the evoked responses as a function of the center frequency of the masking noise. Data from the same experiments as in figure 22.

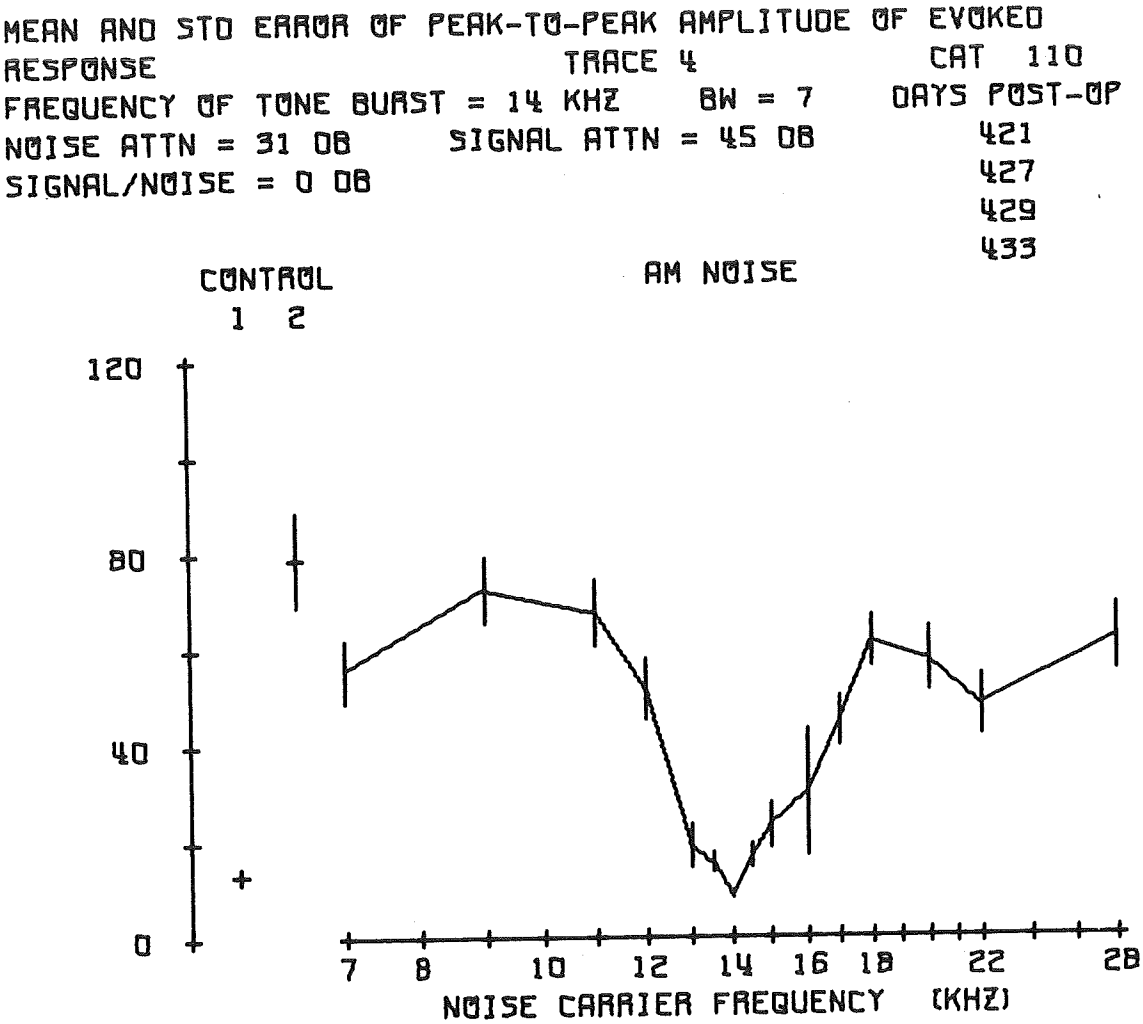

Fig. 27. Means and standard error of the means of peak-to-peak amplitude of trace 4 evoked responses as a function of the center frequency of the masking noise. Data from the same experiments as in figure 21.

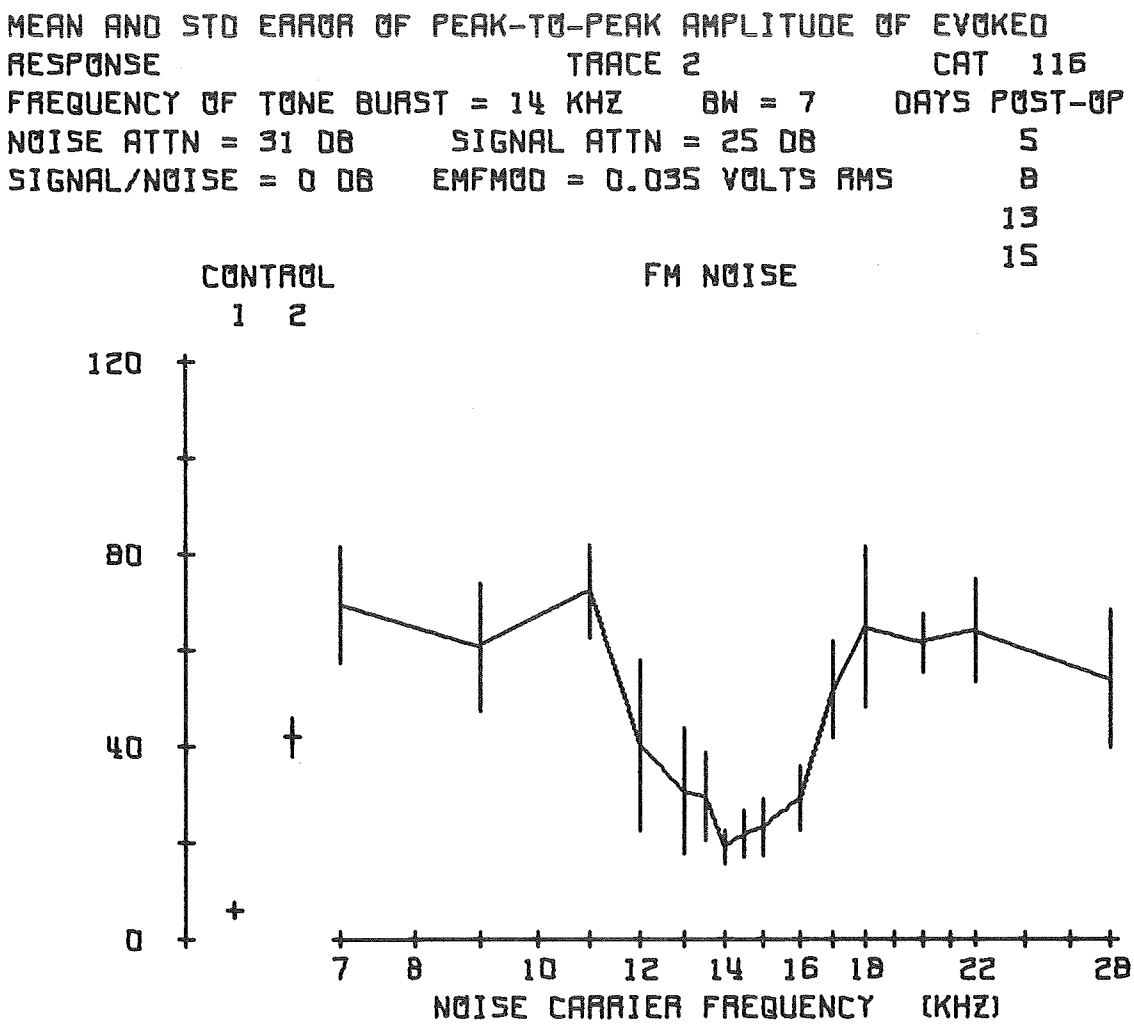

Fig. 28. Means and standard error of the means of peak-to-peak amplitude of trace 2 evoked responses as a function of the center frequency of the masking noise. Data from the same experiments as in figure 22.

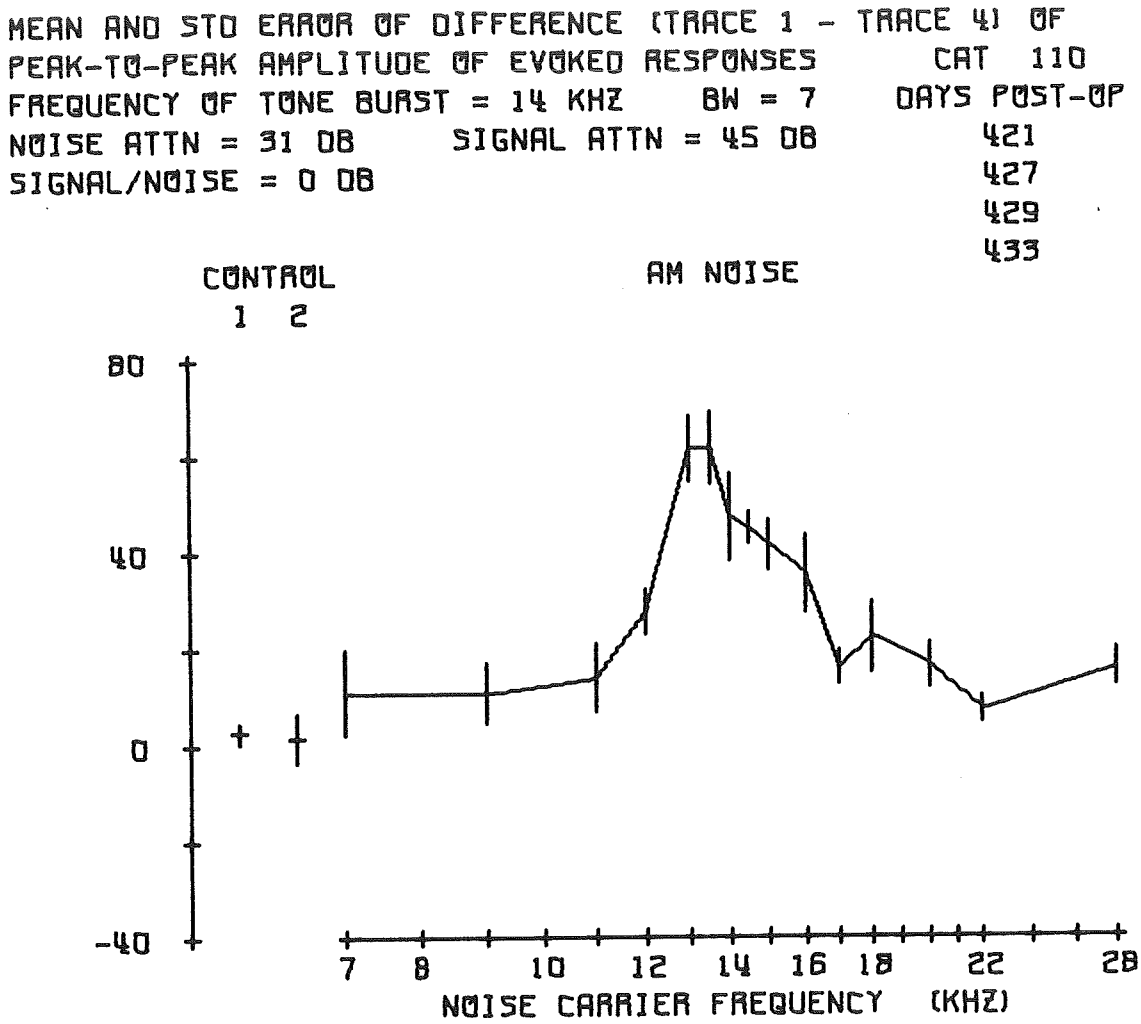

Fig. 29. Means and standard error of the means of the difference between the peak-to-peak amplitudes of trace 1 and trace 4 evoked responses as a function of the center frequency of the masking noise. Data from the same experiments as in figure 21.

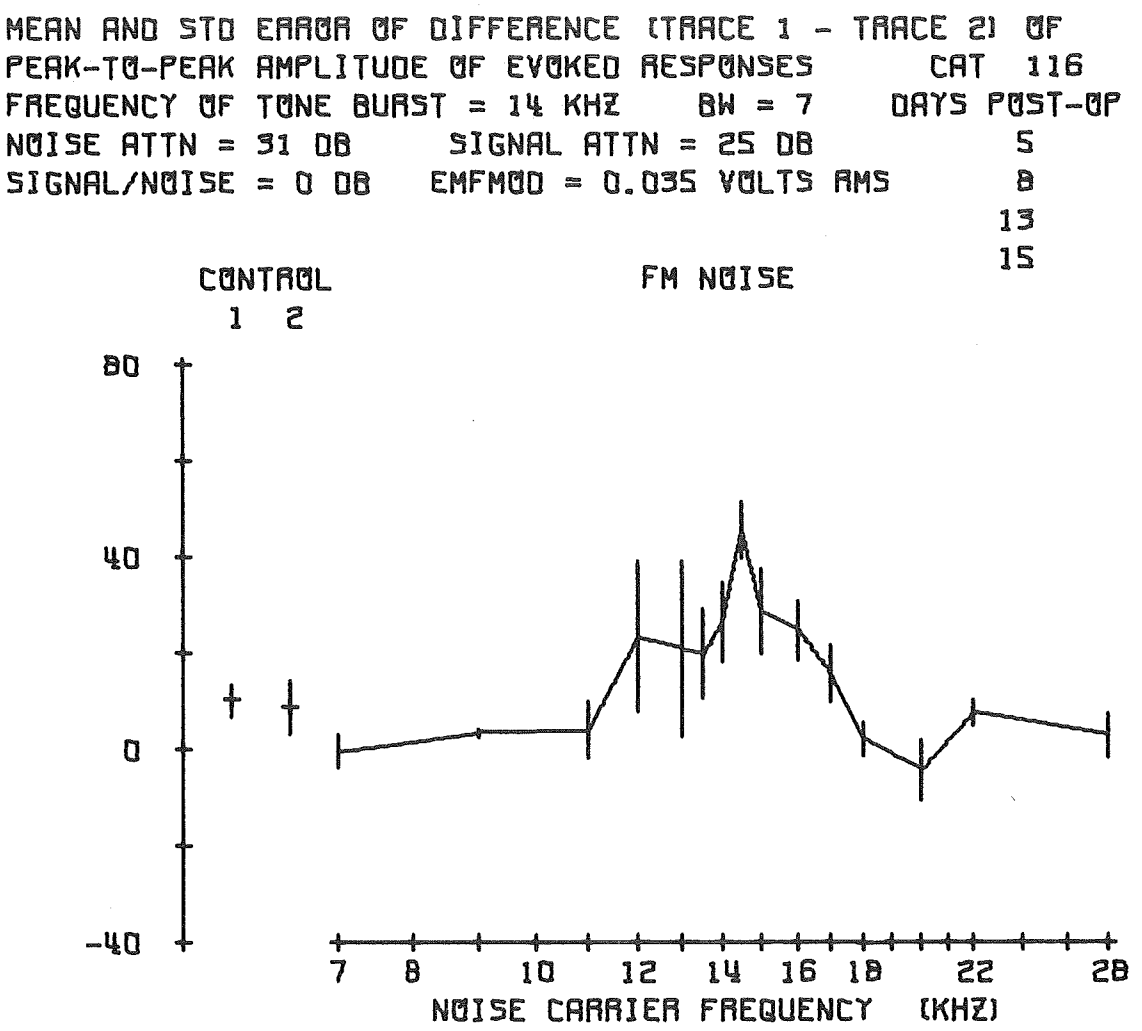

Fig. 30. Means and standard error of the means of the difference between the peak-to-peak amplitudes of trace 1 and trace 2 evoked responses as a function of the center frequency of the masking noise. Data from the same experiments as in figure 22.

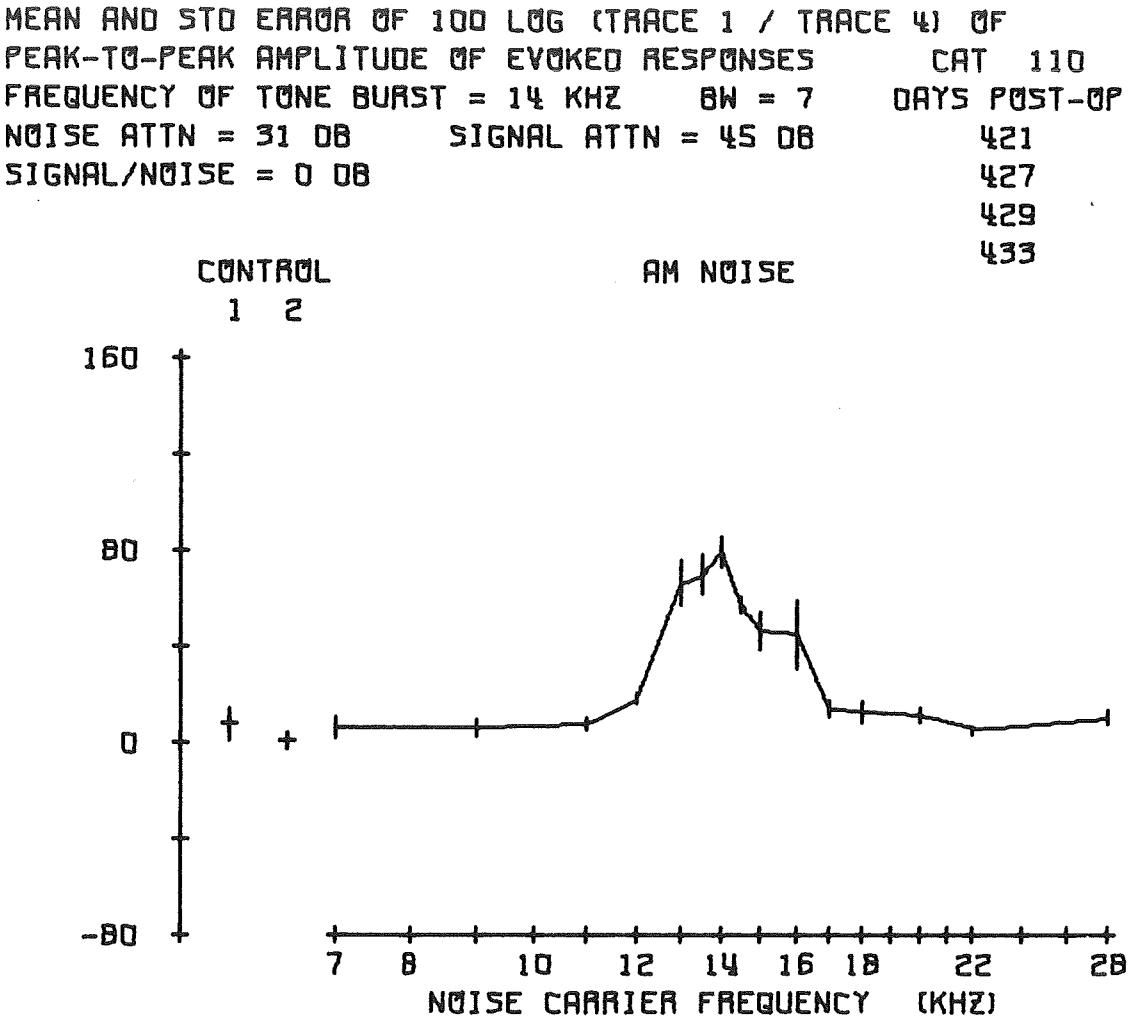

Fig. 31. Means and standard error of the means of the log of the ratio of the peak-to-peak amplitudes, trace 1/trace 4, of the evoked responses as a function of the center frequency of the masking noise. Data from the same experiments as in figure 21.

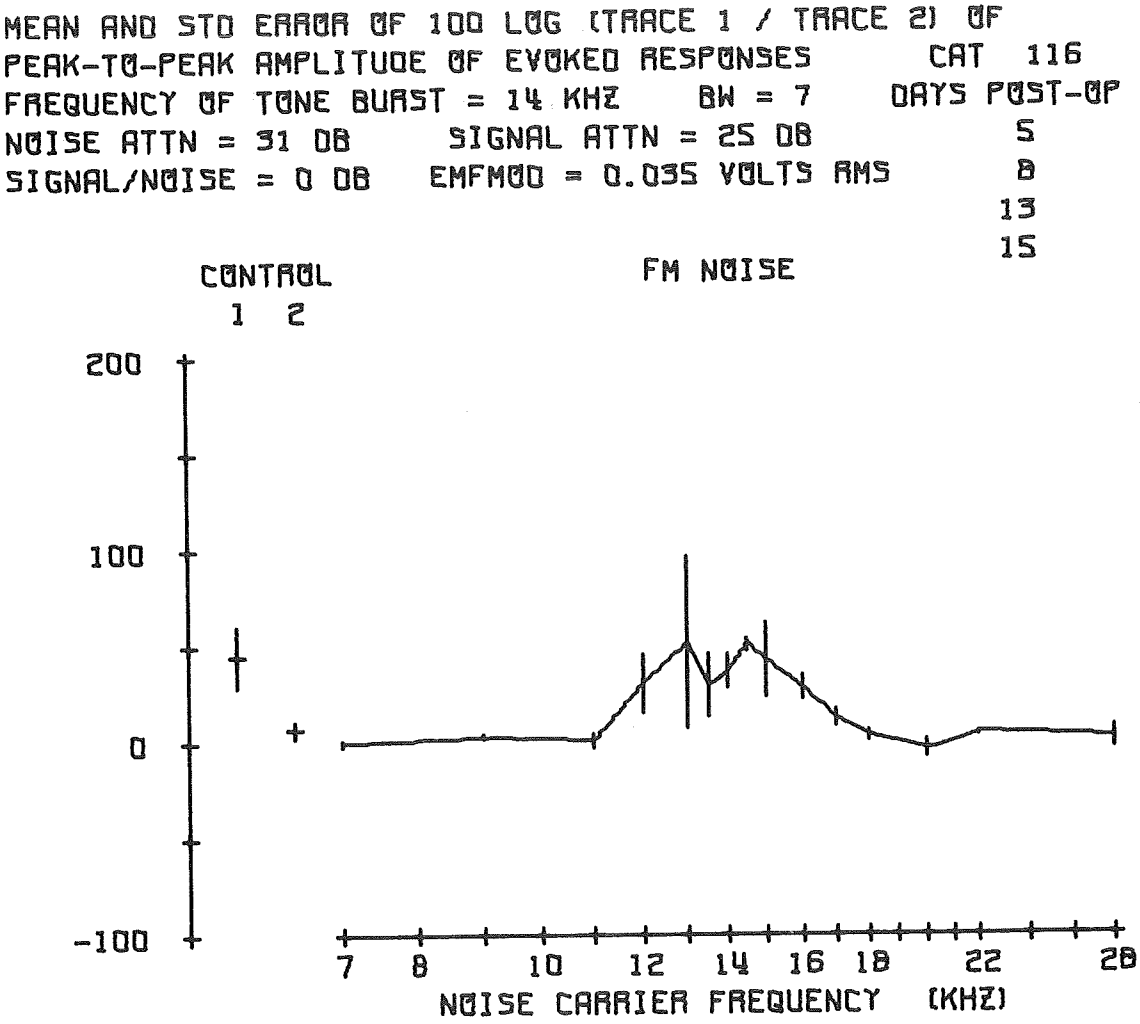

Fig. 32. Means and standard error of the means of the log of the ratio of the peak-to-peak amplitudes, trace 1/trace 2, of the evoked responses as a function of the center frequency of the masking noise. Data from the same experiments as in figure 22.

was necessary; otherwise negative ratios of amplitude measurements would have resulted and logarithms of the ratios* could not have been computed.

The amplitude measurements on the average evoked responses by the two methods just described were averaged for each cat over the four experiment sessions having the same stimulus parameters. The means and standard error of the means of the amplitudes from the four experiment sessions were plotted in three ways: 1) the measured amplitudes for either trace 2 or 4 were plotted against the noise carrier frequency as in figures 21, 22, 27 and 28; 2) the amplitude for either trace 2 or 4 was subtracted from the amplitude of trace 1 in the same run and the differences plotted against the noise carrier frequency, as in figures 23, 24, 29 and 30; 3) the amplitude for trace 1 was divided by the amplitude for either trace 2 or 4 of the same run. The logarithm of this ratio was multiplied by 100 (to avoid significant fractions) and plotted against noise center frequency as in figures 25, 26, 31 and 32. The interpretation of these plots will be deferred until after the corresponding principal component plots have been presented.

There are several disadvantages to the methods which have just been described for measuring the average evoked responses: 1) for the peak amplitude measurement, a large number of responses must be surveyed before selecting the time point to be used, and the time point chosen would probably vary with different investigators; 2) slight variations in measuring the latency can result in large variations in the amplitude

*The logarithm of the ratio of evoked response amplitudes was necessary because the ratio of masked to unmasked traces were computed for some of the data and the mean of ratios is not equal to the ratio of the means.

measured, since the selected latency doesn't correspond to a peak latency in all of the average evoked responses; 3) the peak amplitude measurement may reflect the amplitude of one evoked response component in one trace and, because of latency shifts, reflect the amplitude of another evoked response component in another trace; 4) the peak-to-peak amplitude may depend upon the amplitudes of two independent evoked response components, such as ER_1-ER_2 or ER_2-ER_3 or, in some traces, a combination of all three components; 5) for both methods, the measured parameter which is being used to represent the entire average evoked response is weighted heavily on one or two time points in the average evoked response and is prone to error caused by noise peaks on the trace; and 6) for a large number of records, these methods of measuring the average evoked responses are very time consuming, and are prone to errors in measuring, copying and analyzing the data.

After considering the intrinsic disadvantages of subjective manual evoked response measurements, it was decided to seek a more objective approach. One such approach, which has been used in one form or another in previous evoked response experiments (44, 62), is the principal component analysis (63, 64, 65). A more detailed discussion of principal component analysis is presented in Appendix G.

The principal component analysis of the evoked responses requires the use of a large digital computer. The average evoked response is represented in digital form by a series of 64 amplitude measurements* (evoked response variables), spaced 2 msec apart. In this form, the

*This number was chosen arbitrarily as indicated on page 57.

average evoked response can be considered as a vector in a 64-space; where each coordinate of the 64-space corresponds to one of the 64 time coordinates of the average evoked response. The principal component analysis provides an objective and parsimonious description of the average evoked response in terms of a few orthogonal vectors which effectively span the 64-space. These orthogonal vectors define the coordinates of the principal component space (which is contained within the original 64-space).

Two steps are involved in going from the evoked response coordinates to the principal component coordinates (eigenvectors). The first step is a rotation of the 64-space so as to diagonalize the variance-covariance matrix of the evoked response data. Each of the 64 rotated coordinate axes is an axis for a principal component and is specified by a set of 64 direction cosines called an eigenvector. The mth set of direction cosines contains the cosines of the angles between the mth rotated coordinate axis and the 64 original evoked response axes and is designated as the mth eigenvector. Programs for performing the eigenvector computations are available from several sources in many computer centers. The eigenvectors for the data reported here were obtained using the IBM 360 scientific subroutine EIGEN (66). After the rotation has been performed, the eigenvectors are sorted by the variance (eigenvalue) of their principal components and the minimum number of eigenvectors required to effectively span the average evoked response data space are retained. It was found that the first 4 principal components usually accounted for about 90% of the variance (information about the data), while the 5th principal component accounted for less than 3% of

the variance, of the data analyzed here. Hence, an average evoked response can be specified in terms of the principal components measured along the first 4 eigenvectors. This set of 4 eigenvectors has a unique orientation in the 64-space such that the covariances of the principal components is minimized and most of the variance is absorbed by the first principal component, most of the residual variance absorbed by the second principal component, and so on. There is no compelling reason why this represents the most desirable orientation of the eigenvectors. Consequently, these 4 eigenvectors are rotated by the varimax criterion (67) using the IBM 360 scientific subroutine VARMX. The varimax rotation has three consequences: 1) the number of time coordinates in the evoked response which contribute to each principal component is reduced; 2) the amount of variance accounted for by each principal is distributed more evenly across the principal components; and 3) the covariances of the principal components are no longer minimized.

The eigenvectors obtained from the program EIGEN and their corresponding principal components are designated "before varimax rotation" in the results to be discussed. The eigenvectors obtained from the program VARMX and their corresponding principal components are designated "after varimax rotation".

The average evoked responses obtained from the same cat for experiment sessions using tone bursts with the same rise time and sound level were pooled to calculate the variance-covariance matrix which was then used to compute eigenvectors for the pooled sessions. It can be seen from table 2 that average evoked responses from days post-op 118 to 184 were pooled and those from days post-op 188 to 191 were pooled. For

constant tone experiment sessions, the data for each cat were pooled. A total of six sets of eigenvectors were computed. Once the eigenvectors had been computed, the principal components from experiment sessions having the same stimulus parameters, shown blocked off in the days post-op column of table 2 and shown grouped by cat and frequency in table 3, were pooled and analyzed. The six sets of eigenvectors are shown in figures 33 to 38. The ordinates apply to both columns of plots. The ordinates for the eigenvectors have no units since they indicate the cosine of the angle between the eigenvector* and each of the 64 evoked response time coordinates. All of the average evoked responses which were pooled for calculating the data variance-covariance matrix were averaged to obtain the mean of the average evoked responses. This mean is plotted under both columns of eigenvectors to facilitate a comparison of the eigenvectors and the evoked response components. The abscissae for the eigenvectors and the mean of the average evoked responses are identical and show the 64 time coordinates measured in milliseconds from the start of the evoked response. The percent variances shown, apply only to the principal components from the days post-op in each figure.

*The term eigenvector is used two ways: 1) it is a unit vector in a n-space along which a principal component is measured; 2) it is the set of direction cosines of a unit vector. The set of direction cosines should, perhaps, be called an eigenfunction, but the term eigenvector is commonly used (64, 65).

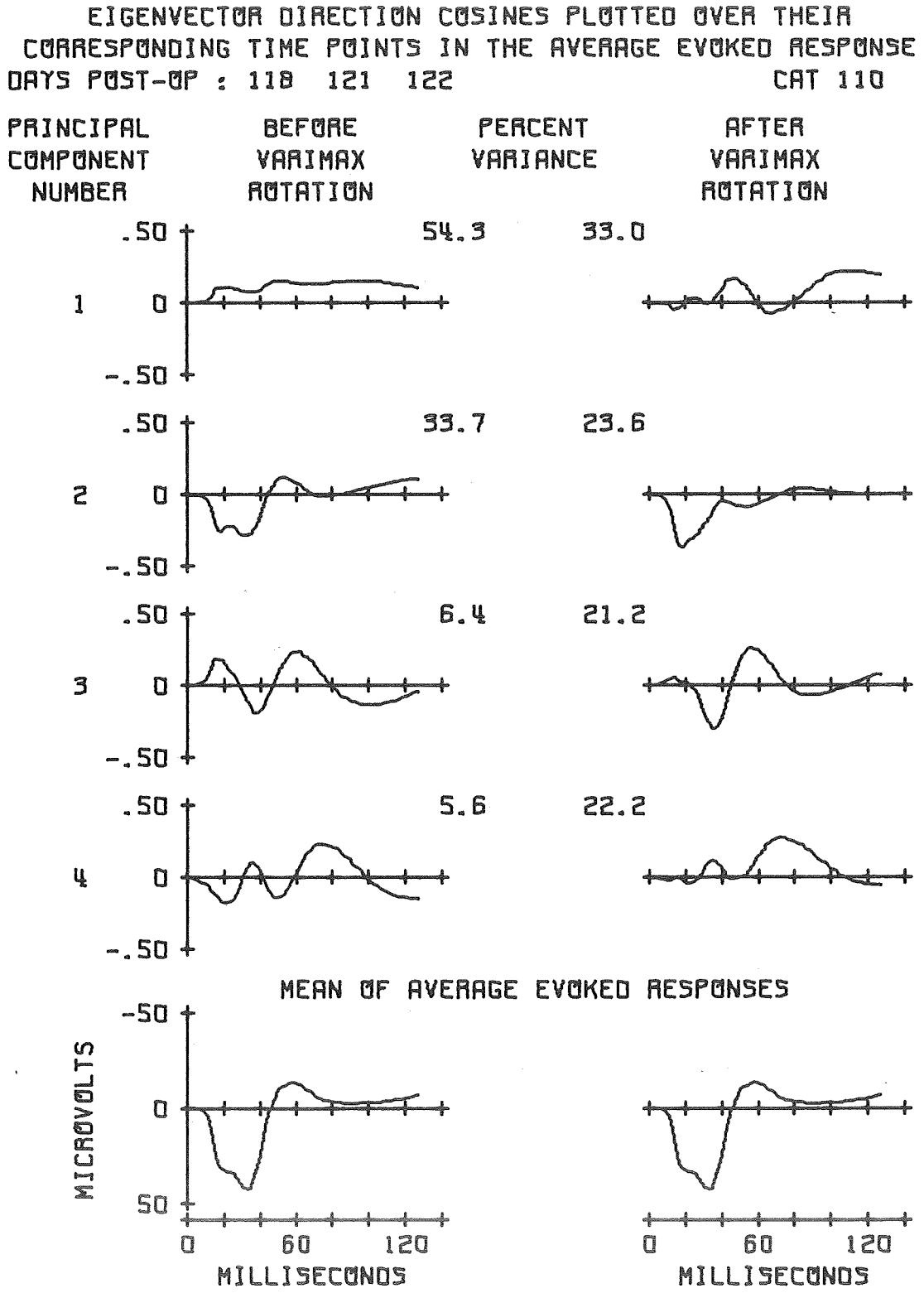

Fig. 33. The eigenvectors and mean of average evoked responses for cat 110, days post-op 118 to 184.

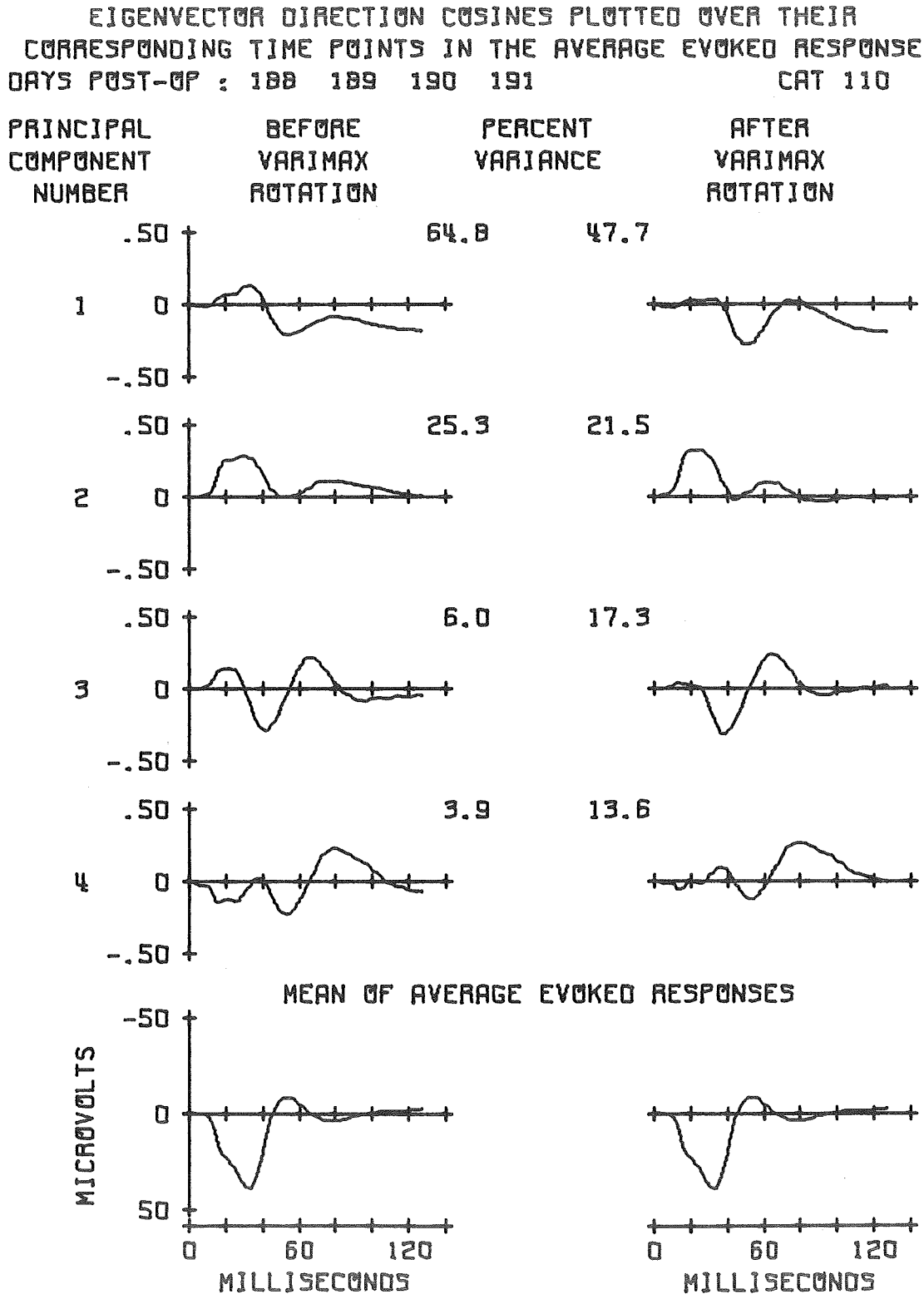

Fig. 34. The eigenvectors and mean of average evoked responses for cat 110, days post-op 188 to 191.

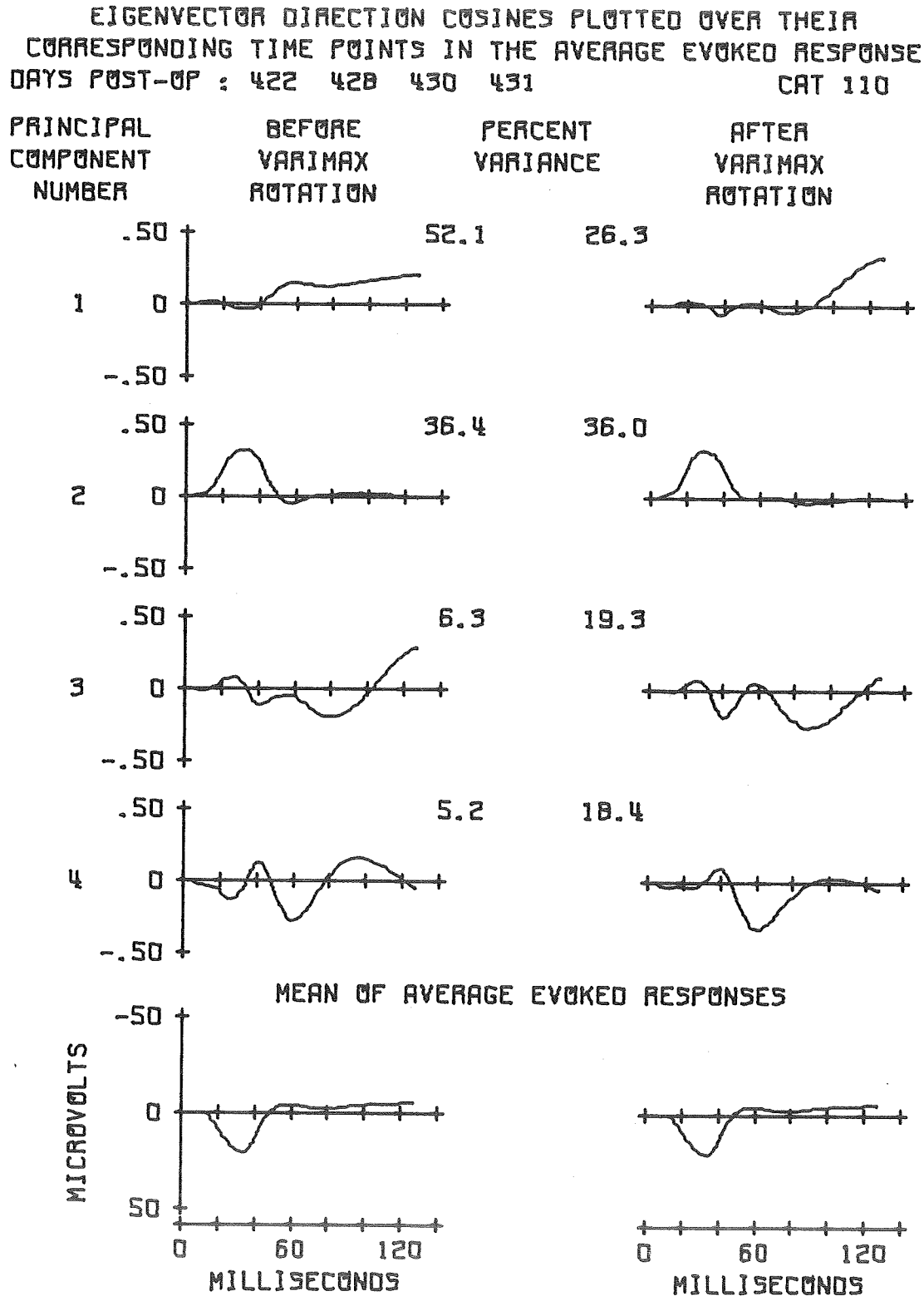

Fig. 35. The eigenvectors and mean of average evoked responses for cat 110, days post-op 421 to 433.

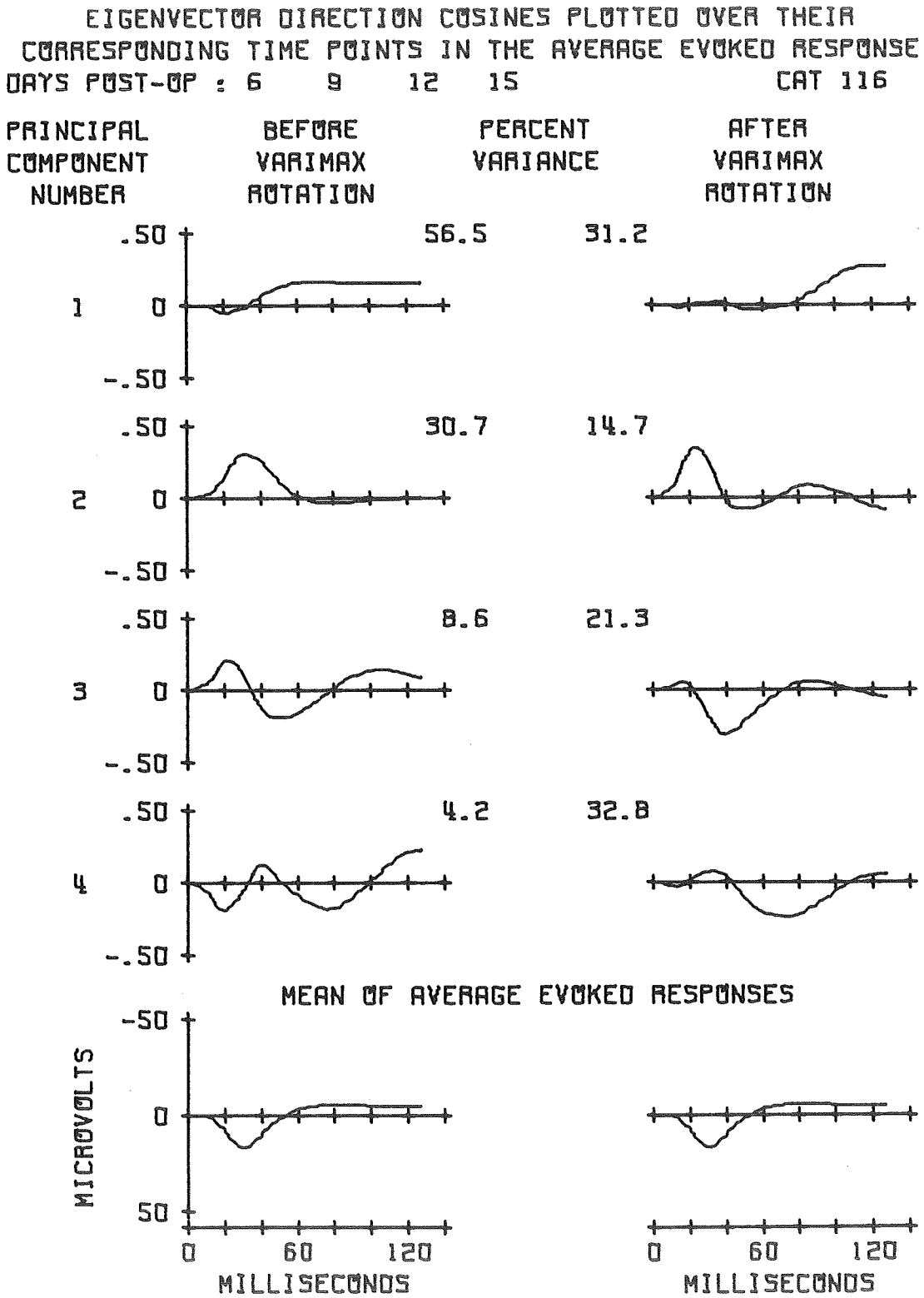

Fig. 36. The eigenvectors and mean of average evoked responses for cat 116, days post-op 5 to 15.

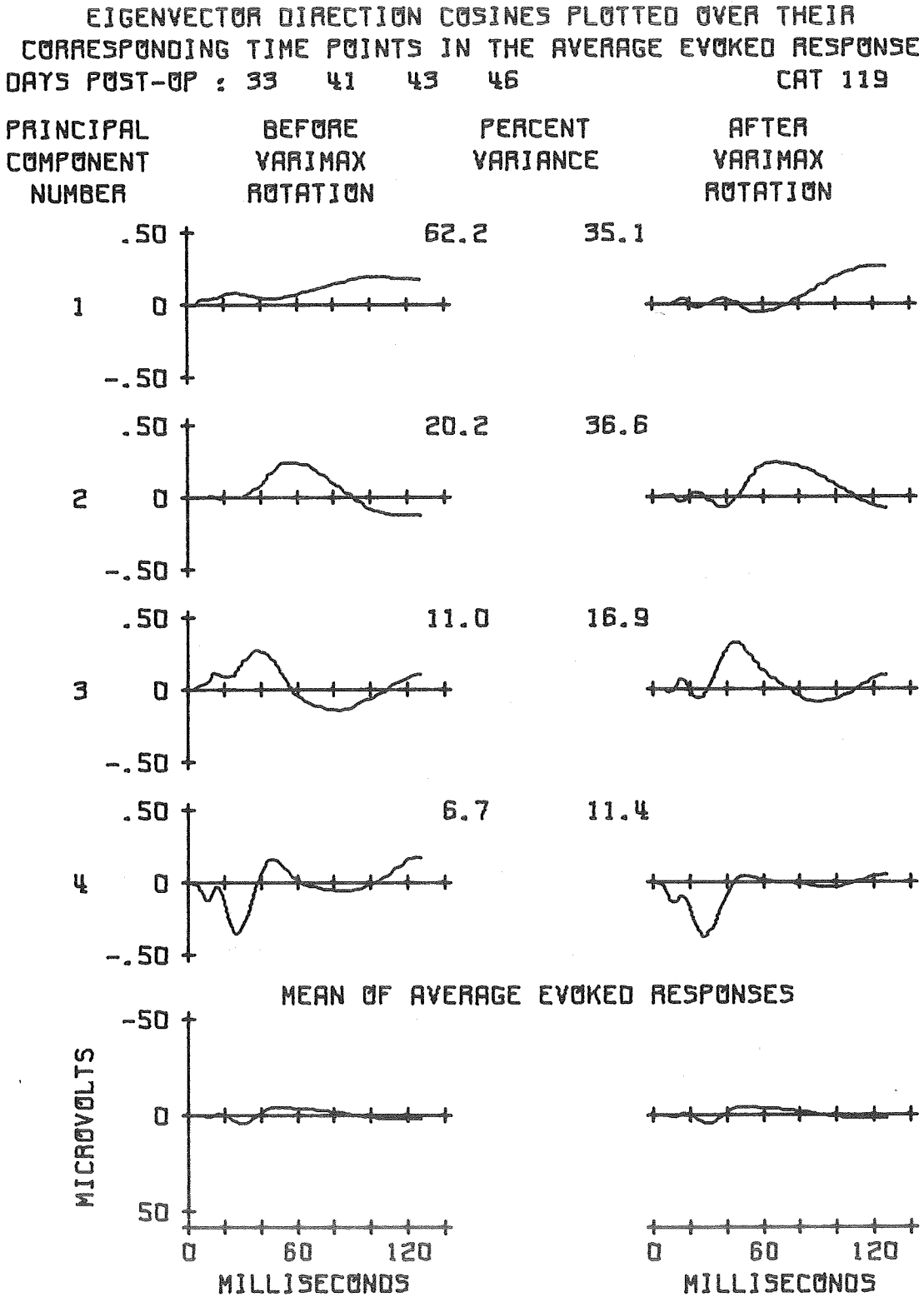

Fig. 37. The eigenvectors and mean of average evoked responses for cat 119, days post-op 33 to 49.

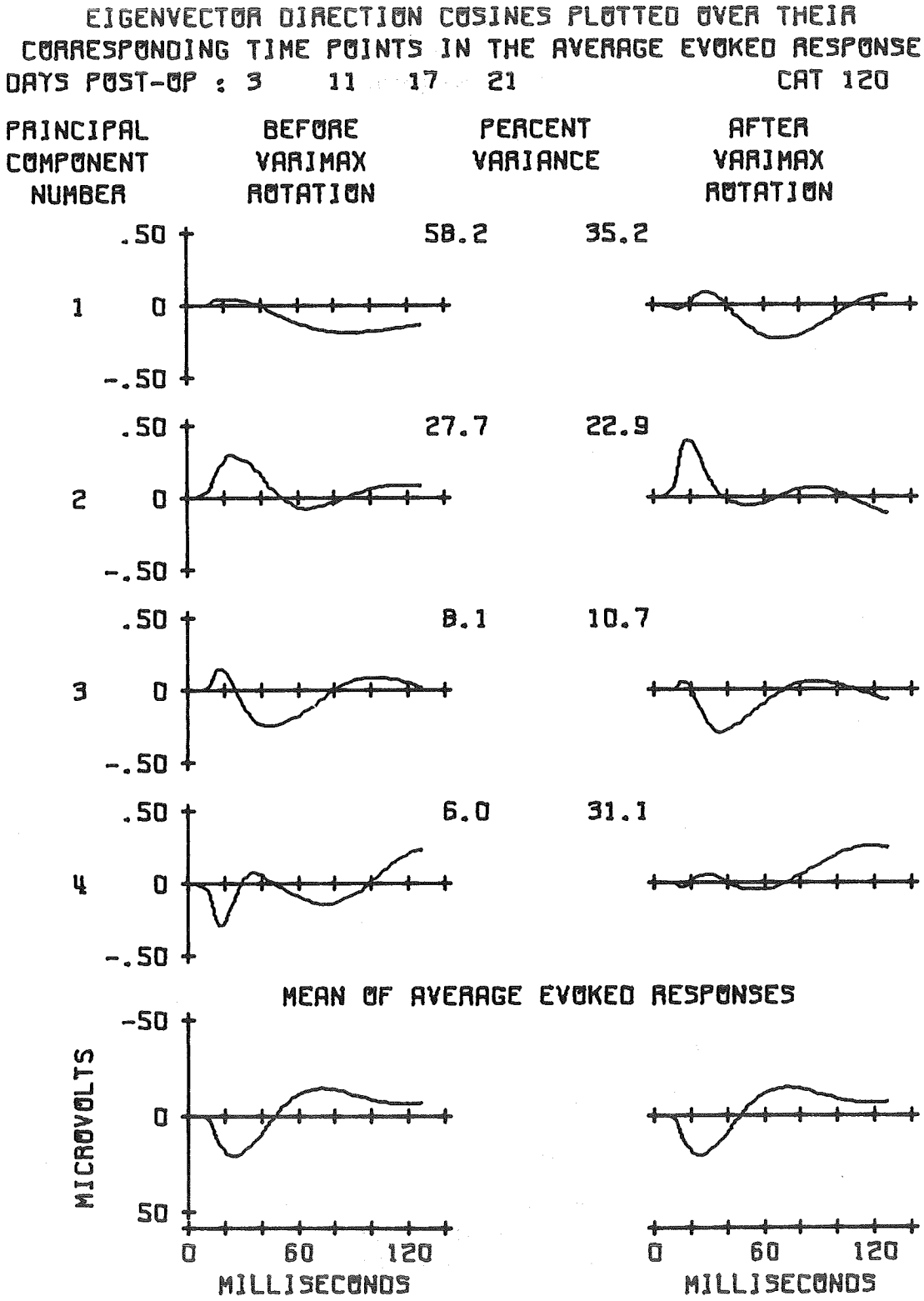

Fig. 38. The eigenvectors and mean of average evoked responses for cat 120, days post-op 3 to 23.

Comparison of eigenvectors from figures 33 to 38 reveals similarities* in the eigenvectors derived from different data pools. An eigenvector is largest over those time points in the evoked response which make the greatest contribution to its principal component. To quantify the similarities between sets of eigenvectors, the range of evoked response time points over which the absolute value of the amplitude of an eigenvector is equal to, or greater than, one-half of the absolute value of its largest peak amplitude is shown in table 5. It can be seen from this table that the order of similar eigenvectors was not the same in all sets. The effect of the varimax rotation is also demonstrated by this table.

The homogeneity of the eigenvector sets can also be demonstrated by a consideration of the information (variance) about the data provided by each eigenvector. Table 6 shows the percent of the variance accounted for by the first four principal components. Each entry in a principal component column shows the percent of the variance of just the first four principal components, before or after varimax rotation, for the particular set of experiment sessions, accounted for by that principal component. It can be seen that the percent variance and the distribution of the percent variances accounted for by the principal components is similar both between sets of eigenvectors and between experiment sessions within each set. The entries in the % Total Variance column show the percent of the variance of all of the data pooled for computing each set of eigenvectors accounted for by the first four principal

*The inversion of some of the eigenvectors, between sets, is not significant to the similarities since it is caused by the eigenvectors forming either a dextral or sinistral set of coordinates.

Table 5. The eigenvector latency ranges. Each column heading shows the cat and experiment sessions pooled for computing the variance-covariance matrix from which the eigenvectors were derived. The entries in the table show the principal component number, before (B) or after (A) varimax rotation, and the range of evoked response time points (msec) over which the amplitude of the eigenvector is equal to, or greater than one-half of its peak amplitude. The entries in each row of the table are blocked into groups containing similar eigenvectors.

110 118-184	110 188-191	110 421-433	116 5-15	119 33-49	120 3-23
1 B 15-128	1 B 47-72 97-128	1 B 50-128	1 B 42-128	1 B 67-128	1 B 58-128
1 A 41-53 90-128	1 A 42-61 110-128	1 A 104-128	1 A 95-128	1 A 92-128	4 A 91-128
2 B 12-40	2 B 15-41	2 B 19-43	2 B 21-48	4 B 20-32 122-128	2 B 15-41
2 A 12-32	2 A 13-36	2 A 19-42	2 A 13-33	4 A 20-37	2 A 13-28
4 A 60-92	4 A 69-101	4 A 51-75	4 A 51-95	2 A 51-96	1 A 51-93
3 A 29-42 49-67	3 A 31-47 59-72	3 A 37-46 72-106	3 A 30-56	3 B 28-50	3 A 26-55

Table 6. The percent variance accounted for by the first four principal components. The Days Post-op column shows the experiment sessions which were pooled for analysis, on the basis of cat and stimulus parameters (tables 3 and 4), after the eigenvectors had been computed. The entries in this column are blocked into groups which were pooled to compute the eigenvectors. The entries in the f_o column, listed only for constant tone experiment sessions, show the tone frequency used. The entries in a principal component column show the percent of the variance of the first four principal components, from the experiment sessions for each row, accounted for by that principal component. The entries in the % Total Variance column show the percent of the variance of all 64 principal components, from all of the data used to compute the eigenvectors, accounted for by the first four principal components.

Cat	Days Post-op	f_o KHz	Principal Component Before Varimax Rotation 1	2	3	4	After Varimax Rotation 1	2	3	4	% Total Variance
110	118-122		54	34	6	6	33	24	21	22	93
	125-126		58	33	5	3	29	24	21	26	
	142-147		55	34	7	4	33	30	18	19	
	149-155		58	30	8	4	39	26	16	17	
	171-176		61	30	6	3	38	29	13	20	
	178-184		57	29	7	7	31	20	17	32	
110	188-191		65	25	6	4	48	22	17	14	94
110	422-431	9	52	36	6	5	26	36	19	18	88
	421-433	14	59	31	5	5	29	31	19	21	
	424-433	22	38	41	13	8	28	38	20	15	
116	6-15	9	56	31	9	4	31	15	21	33	94
	5-15	14	72	18	6	4	32	13	14	41	
	7-14	22	47	41	7	4	24	14	32	29	
119	33-46	9	62	20	11	7	35	37	17	11	89
	34-49	14	69	14	9	8	39	33	14	13	
	35-48	22	53	32	11	4	46	28	17	9	
120	3-21	9	58	28	8	6	35	23	11	31	96
	4-22	14	76	16	5	3	42	11	11	36	
	8-23	22	63	17	15	5	32	9	16	42	

components of the set. The inclusion of the 5th eigenvector would have added less than 3% to these percentages, without adding to the meaningful information obtained from the data.

One property of principal components before varimax rotation is that they are uncorrelated. The correlation coefficients between the first four principal components, before and after varimax rotation, are shown in tables 7 and 8. The matrix of correlation coefficients between the first four principal components is a 4 x 4 array. The diagonal elements of this matrix represent the coefficient of correlation of each principal component with itself; which is 1.0. The matrix is symmetrical, meaning, for instance, that the coefficient of correlation of the first principal component with the second principal component is equal to the coefficient of correlation of the second with the first. To conserve space, only the upper triangular, off-diagonal, portion of the matrix of correlation coefficients is shown in tables 7 and 8. This includes the columns for the 2nd, 3rd and 4th principal component, and the rows for the 1st, 2nd and 3rd principal components.

An inspection of tables 7 and 8 reveals that the coefficients of correlation between principal components, before varimax rotation, is significantly greater than zero. There are at least two possible reasons for these non-zero coefficients. First to be considered is the round-off error in the computer. Diagonalizing a 64 by 64 variance-covariance matrix requires about 10 minutes of CPU time, on an IBM 360/44, which doesn't include input-output time. Using double precision would have increased the computer time required, and would probably not have reduced the covariances appreciably since the present program,

Table 7. Correlation coefficients between the first four principal components from constant noise experiment sessions. The upper triangular, off-diagonal, portion of the matrix of correlation coefficients between the first four principal components is shown for pooled experiment sessions in the Days Post-op column, before and after varimax rotation. The column and row headings for each triangle reference the principal components. Cat 110

Days Post-op	Before Varimax Rotation				After Varimax Rotation		
	2nd	3rd	4th		2nd	3rd	4th
	.27	.16	−.04	1st	−.17	.54	.81
118-122		.20	.47	2nd		.41	−.18
			.21	3rd			.60
	.21	.36	.17	1st	−.22	.61	.91
125-126		.28	.48	2nd		.39	−.32
			.00	3rd			.54
	.11	.20	−.25	1st	−.21	.52	.80
142-147		−.03	.36	2nd		.32	−.40
			.06	3rd			.51
	.12	.00	−.37	1st	−.25	.47	.76
149-155		−.08	.14	2nd		.32	−.48
			.25	3rd			.43
	.05	.05	−.33	1st	−.24	.54	.81
171-176		−.28	.10	2nd		.28	−.56
			.00	3rd			.37
	−.04	−.24	.40	1st	−.17	.27	.74
178-184		.05	−.29	2nd		.51	−.54
			−.21	3rd			−.09
	.08	.01	−.03	1st	.27	−.67	−.65
188-191		−.05	−.06	2nd		−.50	.24
			−.06	3rd			.27

Table 8. Correlation coefficients between the first four principal components from constant tone experiment sessions. The upper triangular, off-diagonal, portion of the matrix of correlation coefficients between the first four principal components is shown for pooled experiment sessions for each cat at each frequency, before and after varimax rotation. The column headings for each triangle are: 2nd, 3rd and 4th. The row headings are: 1st, 2nd and 3rd. f_o is frequency in Hz.

Varimax Rotation	f_o 9K			14K			22K		
				Cat 110					
Before	−.10	−.10	.02	−.34	−.11	.08	.25	.12	.03
		−.08	−.13		−.07	.03		.03	.04
			.01			.06			.01
After	−.18	−.69	−.74	−.41	.77	−.78	.22	−.44	−.44
		−.08	.21		.13	.47		−.36	.00
			.68			.68			.42
				Cat 116					
Before	−.10	.30	−.17	−.16	−.15	.07	−.02	.12	−.13
		.06	−.11		.19	−.13		−.09	.02
			.07			−.06			.13
After	−.02	−.08	−.80	−.36	−.37	−.87	−.07	−.11	−.76
		−.66	.21		−.29	.46		−.69	.26
			.05			.33			.04
				Cat 119					
Before	.45	.12	.06	.45	.07	.03	−.13	−.11	−.11
		.01	.12		.20	.03		.04	.09
			.03			−.11			.03
After	.62	.41	−.55	.76	.41	−.47	.30	−.26	−.58
		.54	−.38		.53	−.48		.37	−.25
			−.37			−.36			−.17
				Cat 120					
Before	−.11	.33	.10	.17	.13	−.10	−.08	−.15	−.08
		.15	−.53		−.36	−.27		.02	.29
			−.03			.16			−.08
After	.24	.25	−.76	.50	−.08	−.89	.34	−.10	−.68
		−.48	.18		−.59	−.32		−.07	.09
			−.40			−.05			.03

EIGEN, normally reduces the covariance terms to 10^{-6}. The greater portion of the round-off error is probably caused by using only 5 significant figures, two decimal places, in the output cards containing the principal components. Using a greater number of significant figures would have doubled the number of output cards required and, considering that the input evoked response variables were only to 4 significant figures, would not have been justified. The second possible reason for the non-zero correlation coefficients is the small portion of the data used to compute the correlation coefficients. The data from a large number of experiment sessions was used to create the variance-covariance matrix which was subsequently diagonalized. However, only a limited sample of the principal components (1/6 or 1/3 of the constant noise or tone experiments, respectively) were used at any one time to compute the correlation coefficients shown in tables 7 and 8. The only exception is for days post-op 188-191 in table 7. The data from these experiment sessions was the only data used for the variance-covariance matrix and the residual covariance present, before varimax rotation, is a reflection of only the round-off error. These correlation coefficients are generally much smaller than the corresponding coefficients from other experiment sessions, indicating that the limited size of the sample used to compute the other coefficients may be a significant factor, and possible indicating a slight nonhomogeneity in the different sets of experiment sessions. The range of stimulus parameters used resulted in both unmasked and completely masked average evoked responses and it appears likely that some degree of correlation exists between all segments of the 128 millisecond average evoked responses, although the work of Teas and Kiang (53) indicates that this response is not a unitary phenomenon.

Summarizing the previous results, it is evident from a casual inspection of the average evoked response records, such as those in figures 19 and 20, that a critical band effect is present; i.e. that the degree of masking is determined by the center frequency of a narrow band noise relative to the tone frequency. The critical band effect was shown more quantitatively by the various plots of amplitude measurements, figures 21 to 32, made on the average evoked responses. Because of the disadvantages inherent in manual average evoked response measurements, a more automated and objective approach was sought. The principal component analysis appears to fulfill these requirements and provides a set of orthogonal axes (eigenvectors) which have both error-minimizing and entropy-minimizing properties (68). Several of the eigenvectors were found to be consistent between eigenvector sets and between experiment sessions within the same set, as indicated by waveform and variance measurements shown in tables 5 and 6. Measuring the average evoked responses along each group (before and after varimax rotation) of axes is accomplished by taking the dot product of the average evoked response vector and each eigenvector. Each average evoked response is then specified in terms of the rotated axes by 4 principal components, before or after varimax rotation. Critical band effects should be present in some, though not all, of these principal components. Each of the two groups (before and after varimax rotation) of four principal components from experiment sessions with the same stimulus parameters were pooled and the mean and standard error of the mean of the principal components at each tone burst or noise carrier frequency were computed. Runs 18 to 22 from constant tone experiment sessions will be treated later.

The means of the two groups of principal components from four constand noise experiment sessions are shown in figures 39 to 46. Each point on a plot shows the mean ±1 standard error. The control 1 points show the principal component values calculated from average evoked responses to the masking noise, 150 msec after its onset. Generally the control 1 point was close to zero, indicating the absence of an evoked response during the absence of a tone burst. The control 2 points show the principal component amplitudes calculated from the average evoked responses to unmasked tone bursts. This principal component was usually significantly different from zero, indicating that the particular segment of the evoked response was different from zero during the evoked response to an unmasked tone burst.

It should be evident from figures 40, 44 and 45 that critical band effects are present in some segments, but from figures 39, 43 and 46 not all segments of the average evoked responses. The procedure used on all of the plots for quantifying the critical band effect is shown in figure 40. A baseline is drawn, by eye, through the portion of the masking curve which appears to represent unmasked responses. The peak of the masking curve was then selected. The actual peak didn't always occur at the center frequency of the abscissa and some manual curve smoothing was required. A line was drawn midway between the baseline and peak of the masking curve, parallel to the baseline, which was usually parallel to the abscissa, and the frequencies at which this line intersected the masking curve were noted. The lower frequency is designated f_L and the upper frequency f_H. The difference, $f_H - f_L$, is the width of the masking curve. The one-half peak amplitude width of the masking curve was

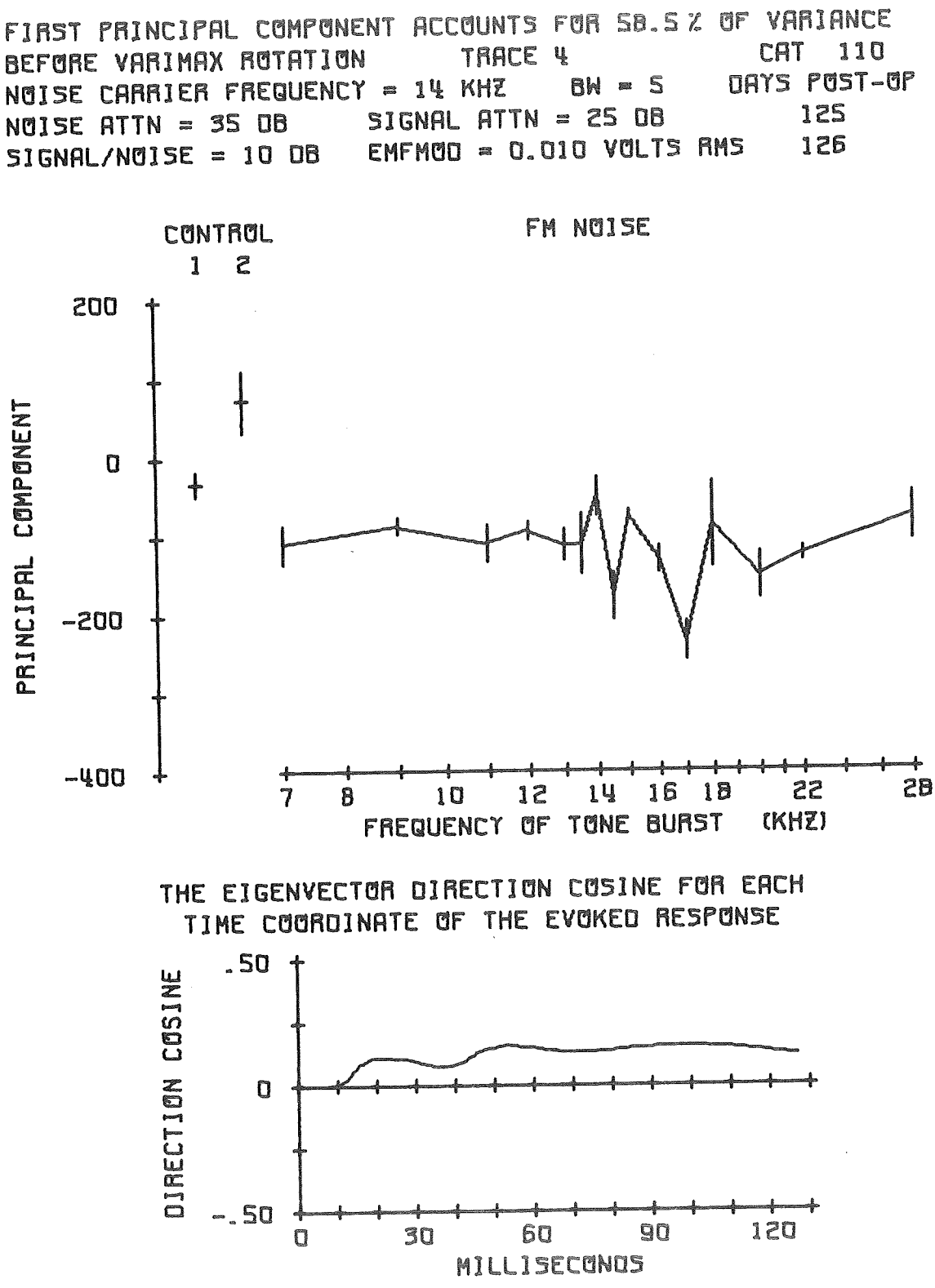

Fig. 39. Masking curve from constant noise experiment sessions.

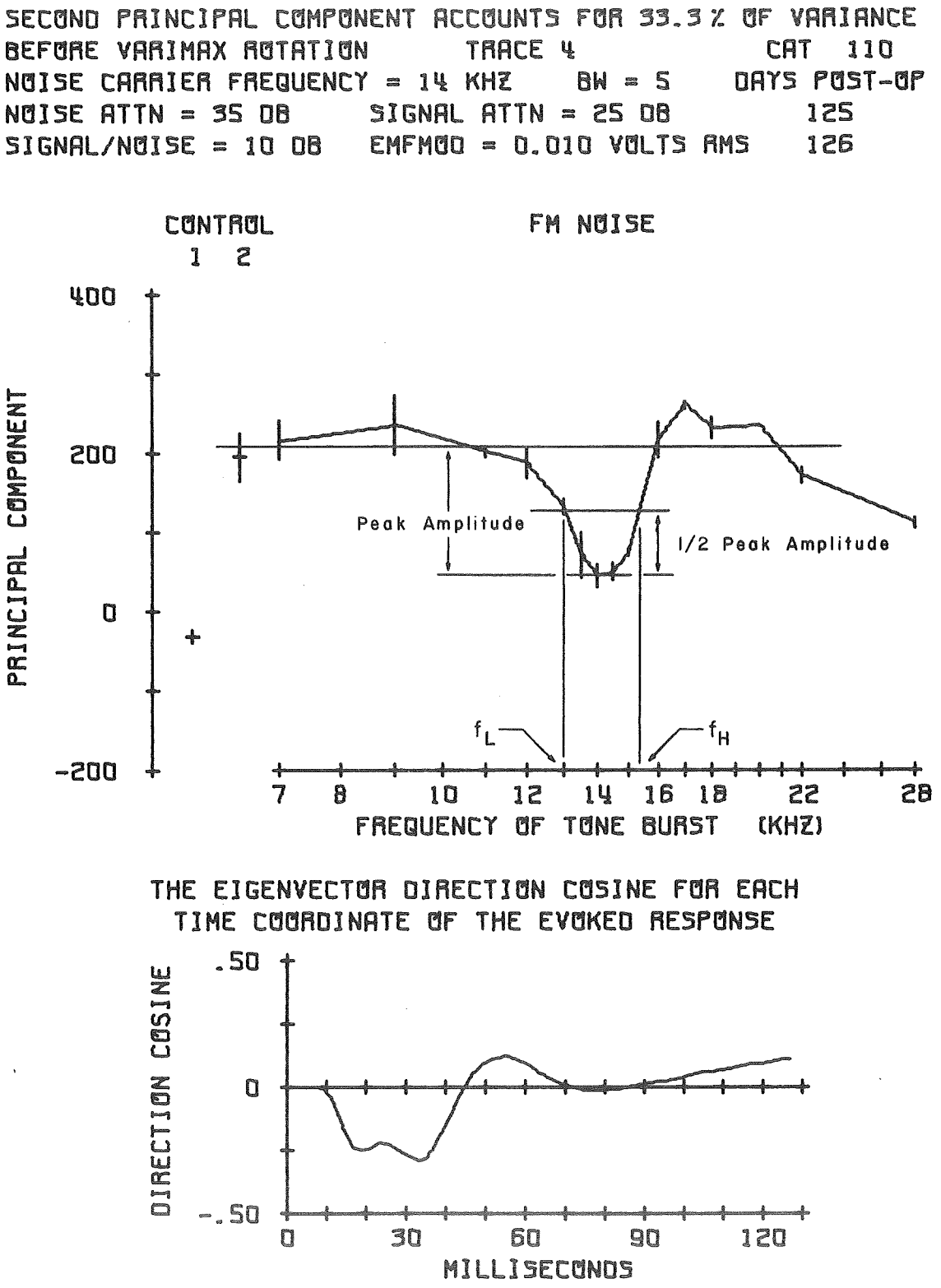

Fig. 40. Masking curve from constant noise experiment sessions.

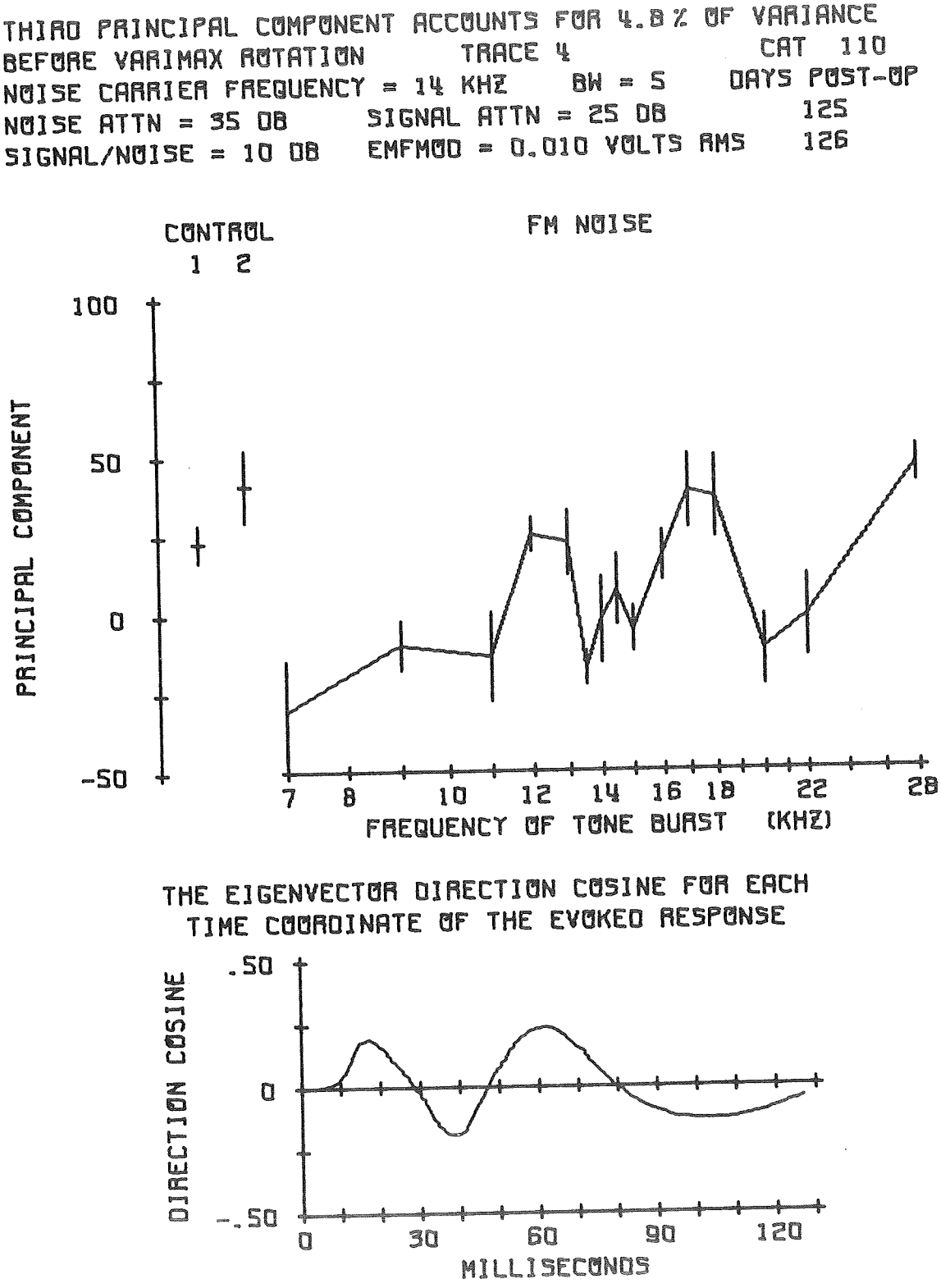

Fig. 41. Masking curve from constant noise experiment sessions.

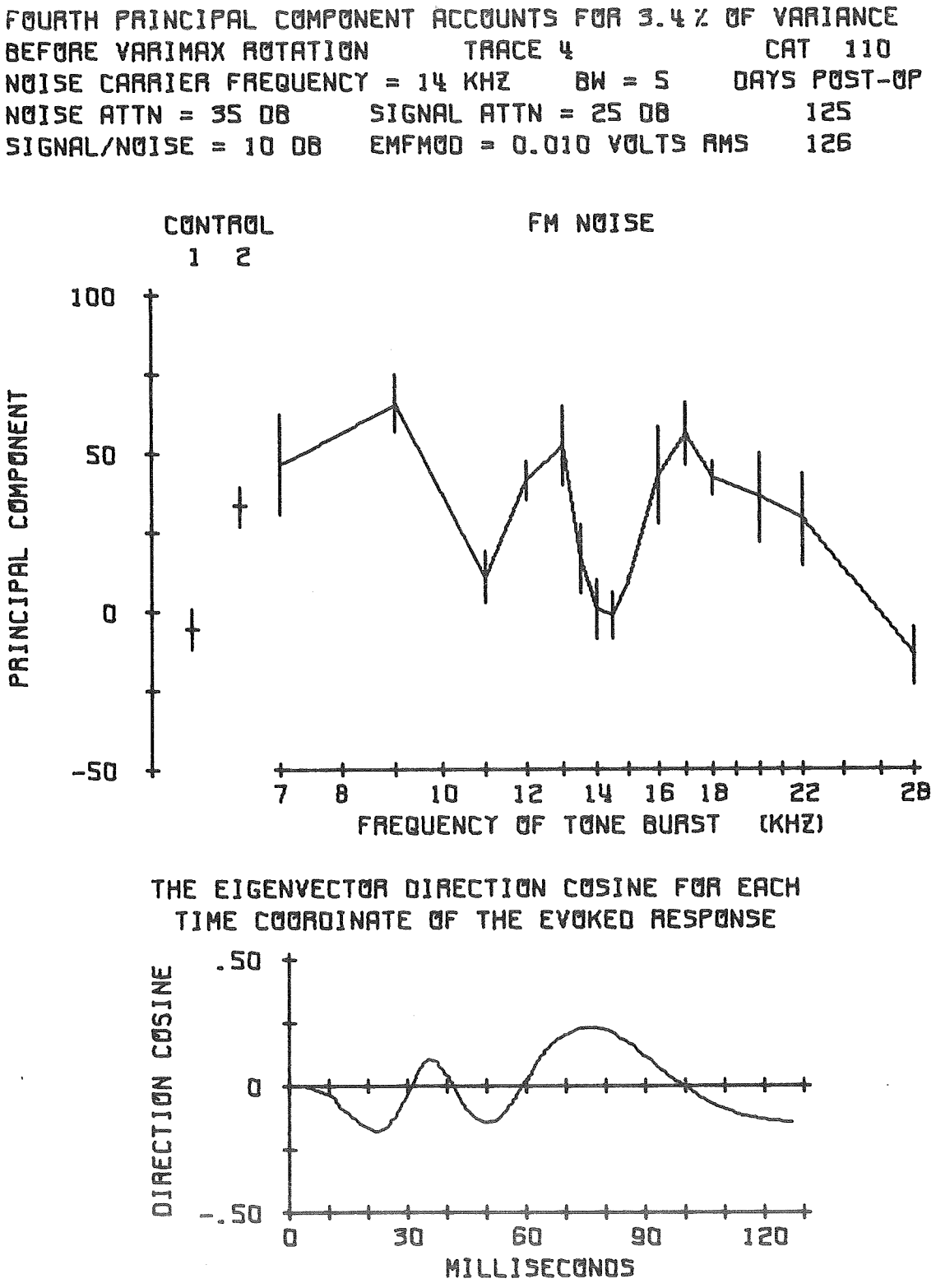

Fig. 42. Masking curve from constant noise experiment sessions.

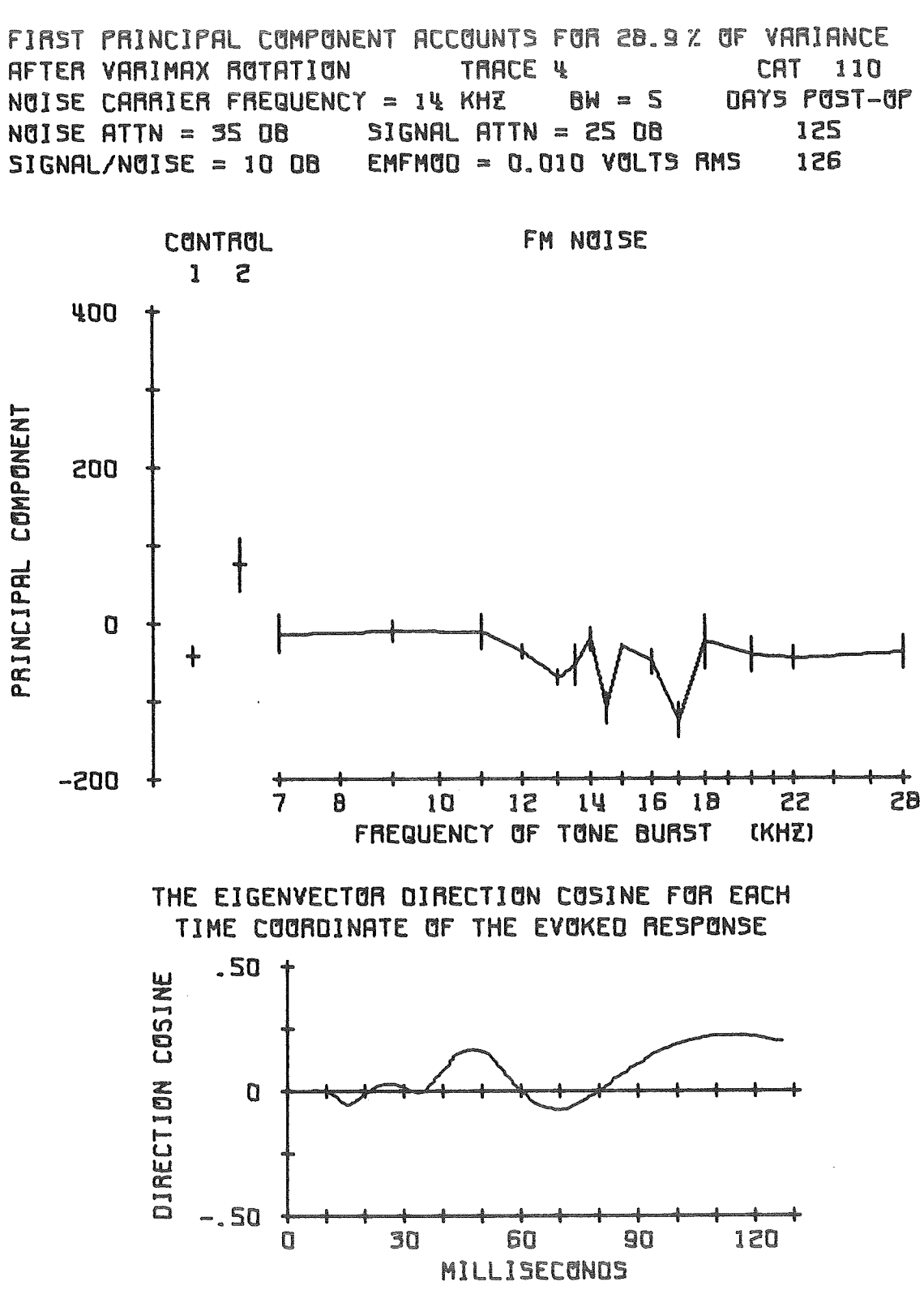

Fig. 43. Masking curve from constant noise experiment sessions.

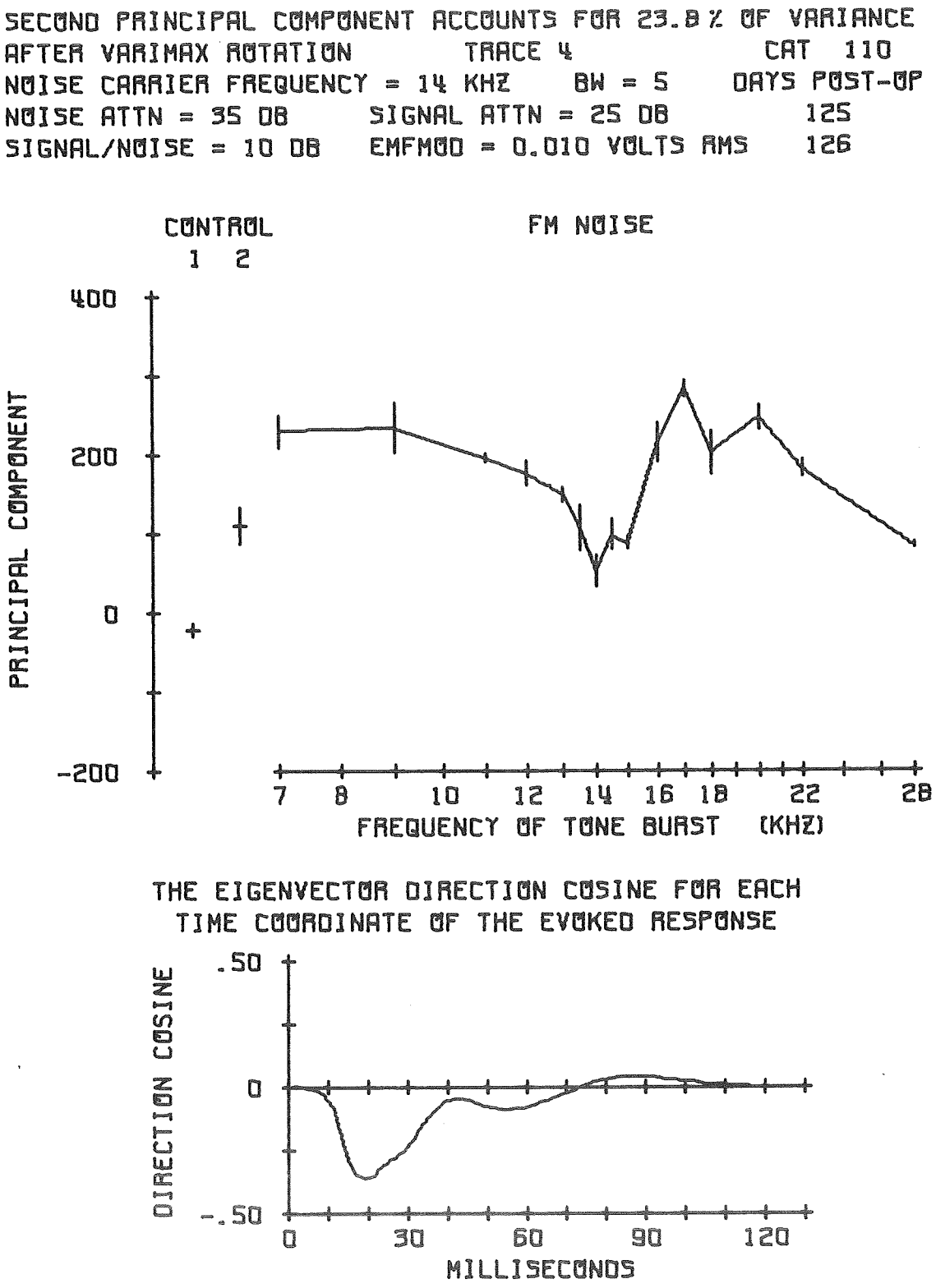

Fig. 44. Masking curve from constant noise experiment sessions.

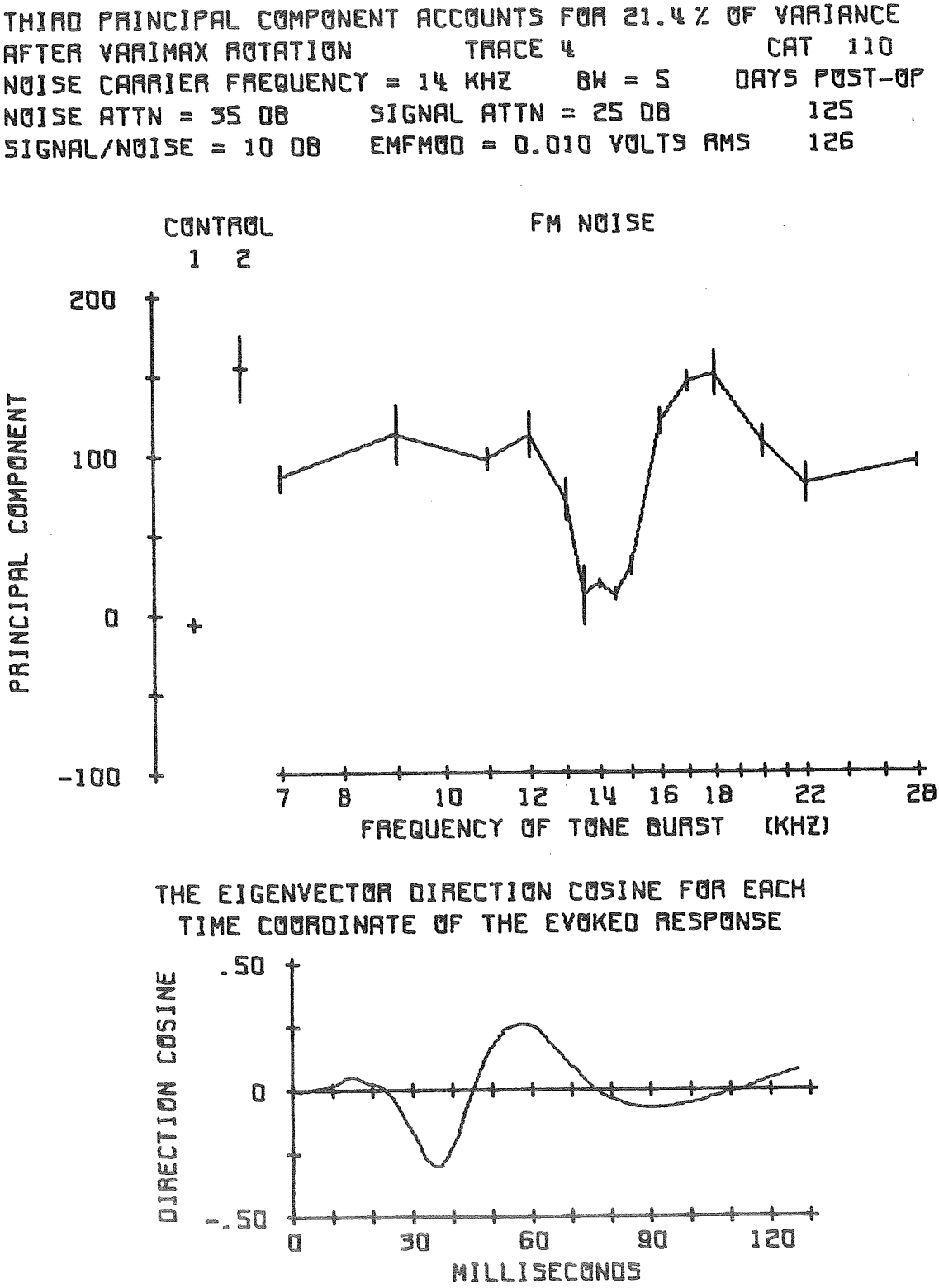

Fig. 45. Masking curve from constant noise experiment sessions.

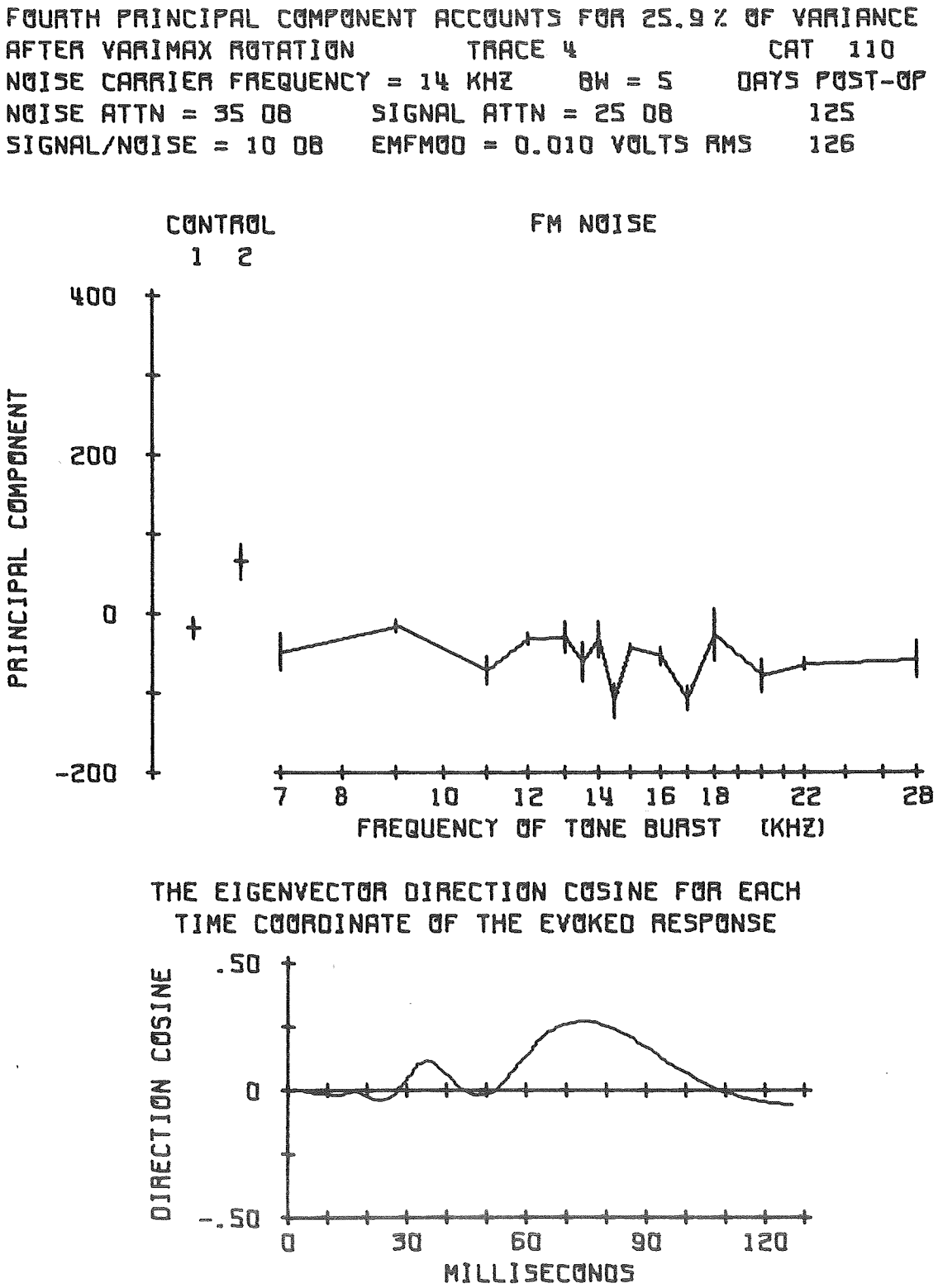

Fig. 46. Masking curve from constant noise experiment sessions.

used because it was operationally the easiest to define and should be proportional (approximately) to any other defined width on the masking curve. Some plots, such as in figure 42, showed what might be considered a critical band effect, but a baseline was not evident and, despite the normal control runs, such a plot would be considered abnormal. The masking curve in figure 44 would not be considered normal because the principal components for the control 2 runs were about equal to those in the masked region of the masking curve. If the control 1 and control 2 runs showed normal values, the masking curve was usually considered normal.

The frequency limits, f_L and f_H, of the masking curves for the constant noise experiment sessions are shown in table 9. All of the masking curves for the second principal component before varimax rotation, 2B, were considered normal. This principal component reflects activity in the 12 to 40 msec region of the average evoked response, which covers the ER_1 and ER_2 evoked response components. The two small peaks in this eigenvector at 17 and 35 msec (figure 40) may correspond to physiologic evoked response components at these same latencies; shown in table 4 for a t_r = 2.5 msec (the rise time of the tones used in constant noise experiment sessions).

The varimax rotation of the first four eigenvectors from the constant noise experiment sessions appears to separate what might be considered the ER_1 and ER_2 components. Both of the 2A and 3A principal components have masking curves which show critical band effects. It can be seen in table 9, however, that many of these masking curves were not considered normal. The wider 1/2 amplitude width of the masking curves

Table 9. Frequency limits of masking curves for constant noise experiment sessions. The lower, f_L, and upper, f_H, frequencies at the 1/2 peak amplitude points of the principal component versus tone frequency curve are shown in KHz for the first, second and third principal components after varimax rotation, 1 A, 2 A and 3 A, respectively, and the second principal component before varimax rotation, 2 B. The experiment sessions are listed in the Days Post-op column. The noise parameters, BW, EMFMOD and 6 dB bandwidth, are listed in their respective columns. The signal-to-noise ratio and the tone sound level in dB re animal threshold, are shown in the S/N and SL columns, respectively. The center frequency of the masking noise was 14 KHz. The average difference, $f_H - f_L$, is shown below each set of data from experiment sessions having the same noise bandwidth. An * indicates that the masking curve is normal, judging from the values of the control 1 and control 2 runs.

Days Post-op	BW	EMFMOD	6 dB bw	S/N	SL	Principal Component 1 A		2 B		2 A		3 A	
						f_L	f_H	f_L	f_H	f_L	f_H	f_L	f_H
171-176	10	0.01	130	10	50			* 13.1	15.4	13.2	15.2	13.2	15.1
171-176	10	0.01	130	0	50	12.1	16.5	* 13.4	15.5	13.2	15.7	13.8	14.4
						4.40		2.20		2.25		1.75	
149-155	7	0.01	200	10	50			* 12.8	14.9	13.1	14.6	* 13.3	14.7
149-155	7	0.01	200	0	50	12.0	17.0	* 12.8	14.9	12.6	14.8	* 13.7	14.6
						5.00		2.10		1.85		1.15	
125-126	5	0.01	250	10	50			* 13.0	15.2	13.2	15.2	* 13.1	15.2
142-147	5	0.01	250	10	50	12.1	17.1	* 13.1	14.9	13.1	14.9	* 13.6	14.8
118-122	5	0.01	250	0	50	12.5	18.0	* 12.9	15.1	* 13.2	14.9	* 13.5	15.1
142-147	5	0.01	250	0	50	12.6	17.3	* 13.1	14.9	13.0	14.9	* 13.6	14.8
						5.06		2.00		1.85		1.53	
178-184	10	0.05	425	0	50			* 12.1	15.8	* 12.2	15.6		
								3.70		3.40			
188-191	7	0.05	1.0K	0	30	12.1	15.9	* 11.9	16.0	11.8	15.9	13.5	15.5
						3.80		4.10		4.10		2.00	
178-184	10	0.10	1.4K	0	50			* 12.5	16.1	* 12.8	15.2		
								3.60		2.40			
125-126	5	0.10	1.8K	10	50			* 12.8	15.4	11.9	15.4	* 13.1	15.2
118-122	5	0.10	1.8K	0	50			* 12.0	15.5	* 12.2	15.7	* 12.1	15.0
								3.05		3.50		2.50	
188-191	7	0.10	2.1K	0	30	12.0	15.5	* 11.8	16.4	11.8	16.3		
						3.50		4.60		4.50			

for 2A than for 3A may indicate a greater sensitivity to masking noise present in the earliest parts of the average evoked response; a finding which would be in conformity with those of Teas and Kiang (53). There is a tendency for the measured width of the masking curve to increase as the bandwidth of the masking noise increases. The bandwidths of the masking noise were below the theoretical critical bandwidth, equation 13b, and this observation contradicts the invariance in the width of the masking curve for subcritical bandwidth noise, expressed by Greenwood (8, 14). This might be explained by the fact that the bandwidth of the masking noise within the skirts of the spectrum probably exceeded the critical bandwidth and was contributing to the evoked response masking. This possibility is supported by signal-to-noise data to be discussed below.

The first eigenvector, after varimax rotation, (1A) has a small peak in the region of ER_3 and a larger component over the latest portion of the 128 msec average evoked response. The width of the masking curves for principal component 1A decrease with an increase in masking noise bandwidth, but are always wider than the noise bandwidth. None of these masking curves were considered normal. The plots for principal components not listed in table 9 seldom, if ever, showed any critical band effect.

Figures 47 to 53 demonstrate typical masking curves (principal component versus noise center frequency) from constant tone experiment data. The widths of the masking curves were obtained by the same procedure shown in figure 40, and are presented in tables 10, 11 and 12. The general criteria used on the previous masking curves were applied to these masking curves. The means and standard errors for each column

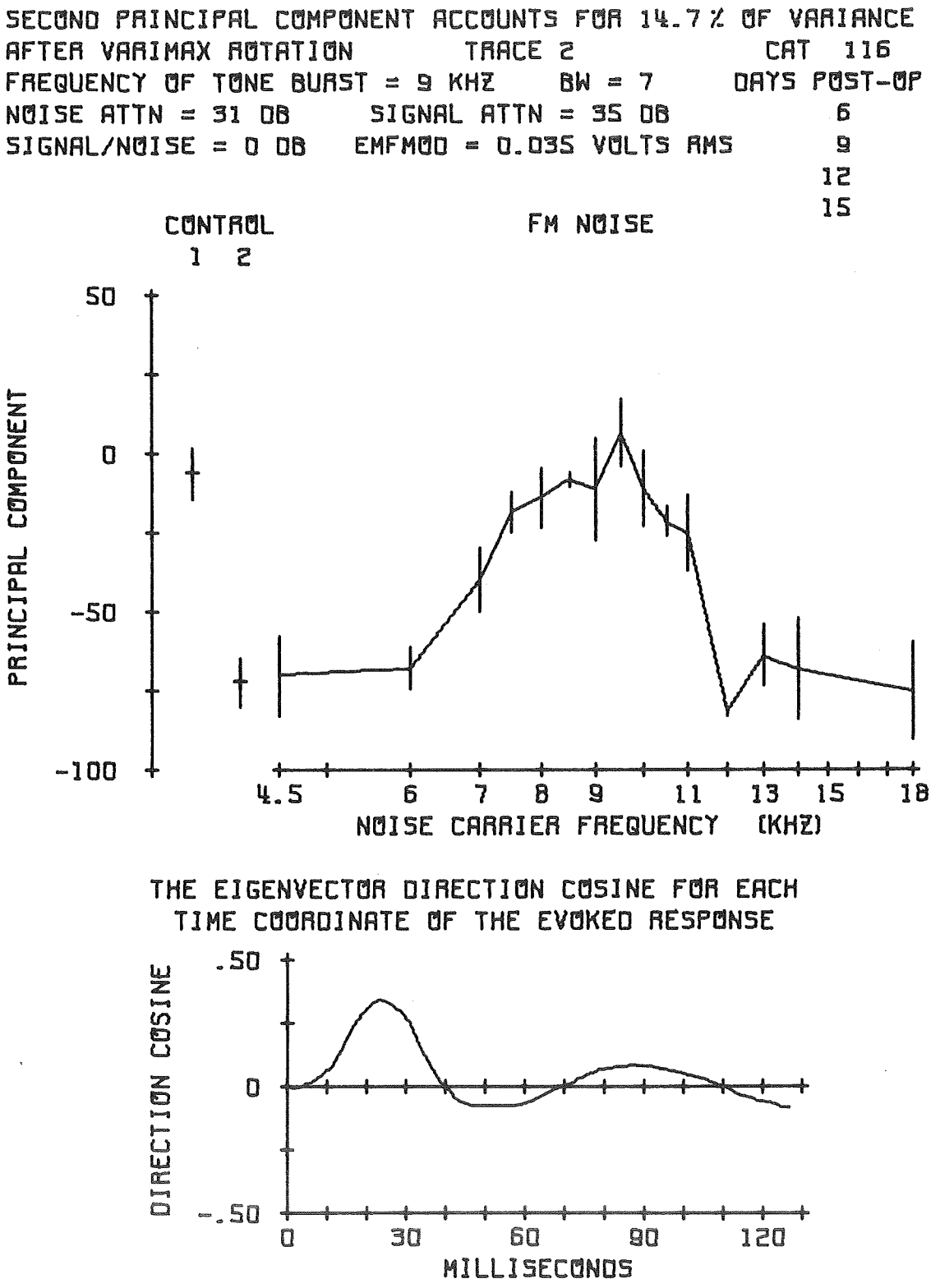

Fig. 47. Masking curve from constant tone experiment sessions.

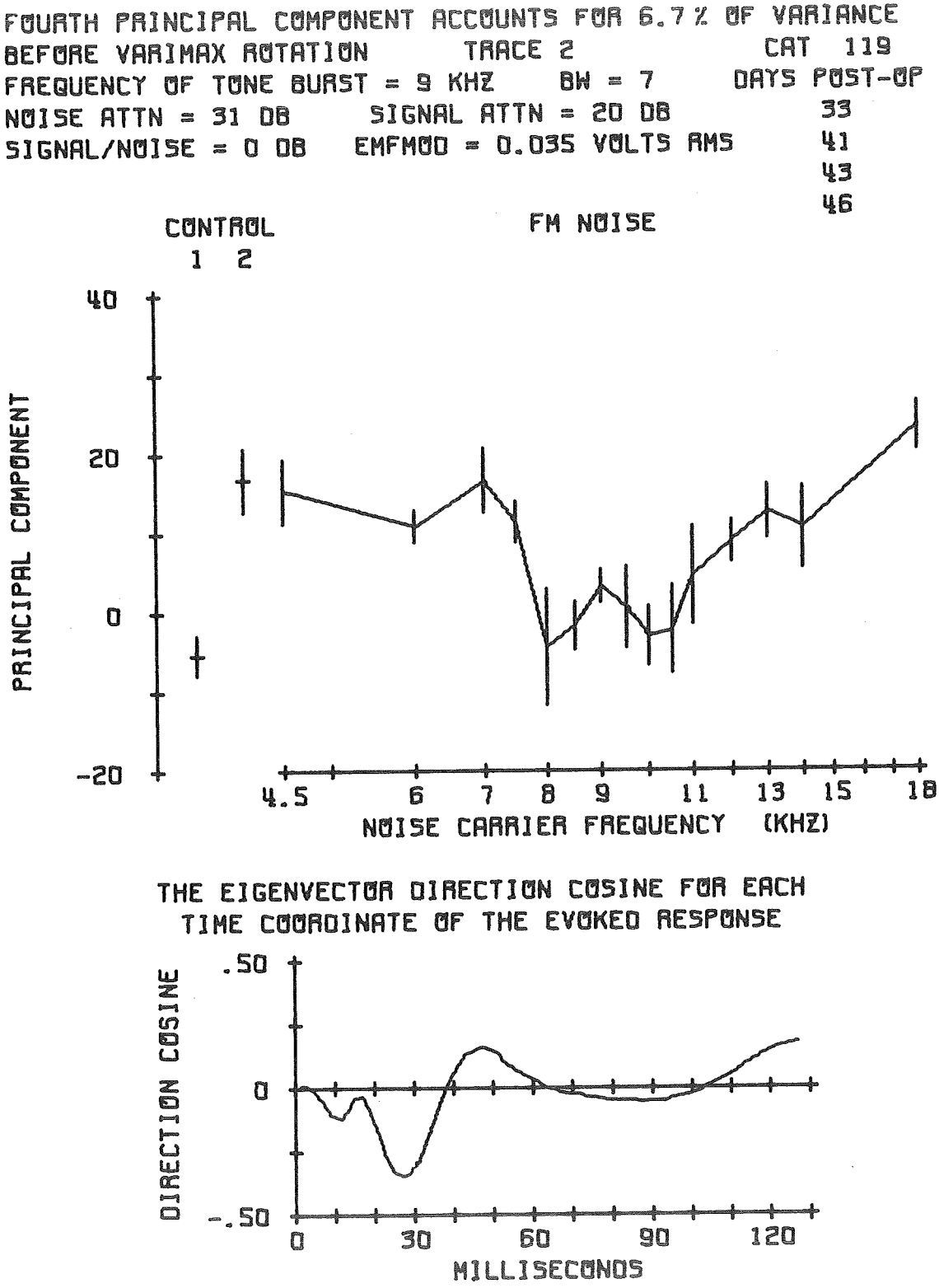

Fig. 48. Masking curve from constant tone experiment sessions.

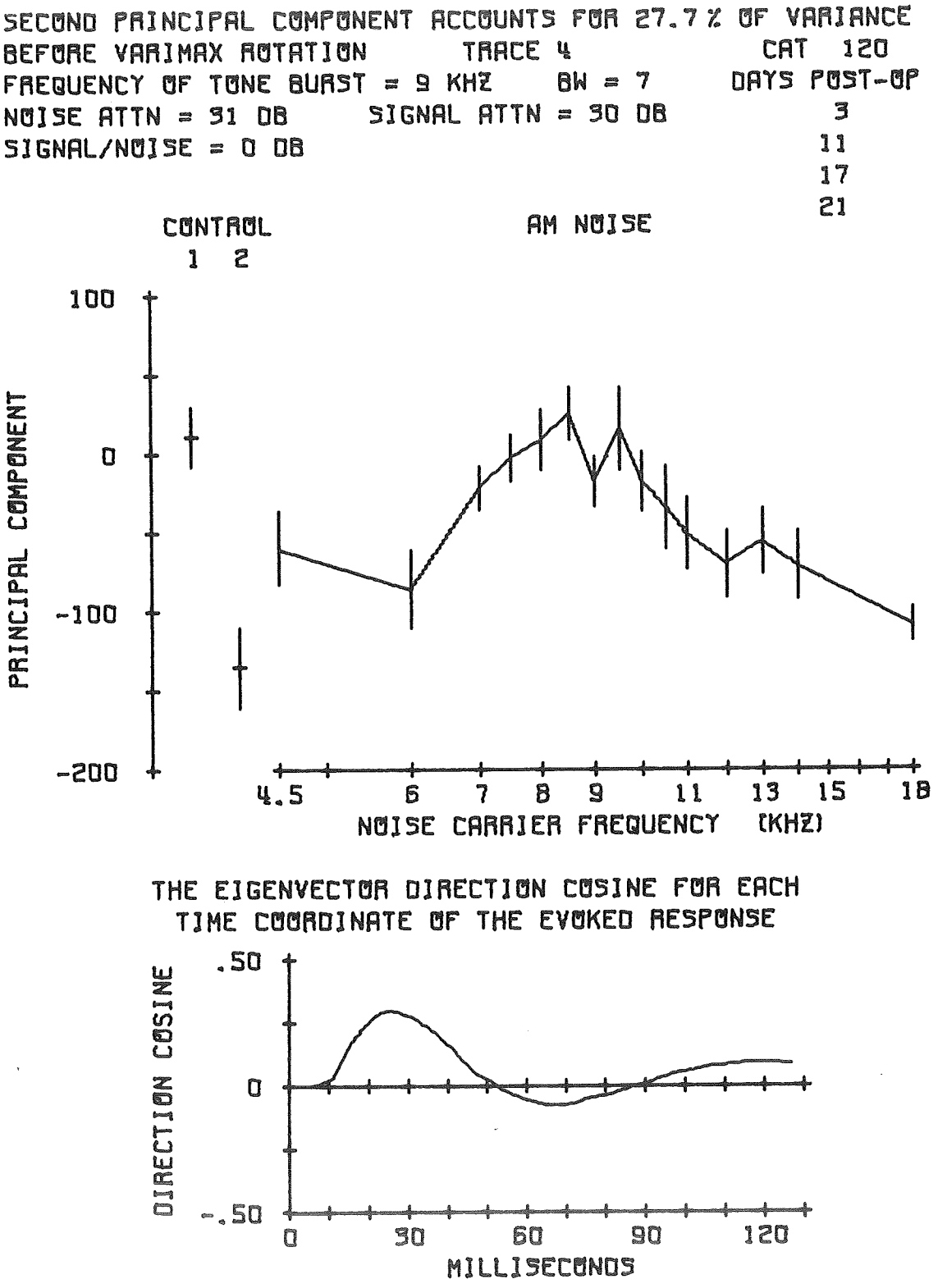

Fig. 49. Masking curve from constant tone experiment sessions.

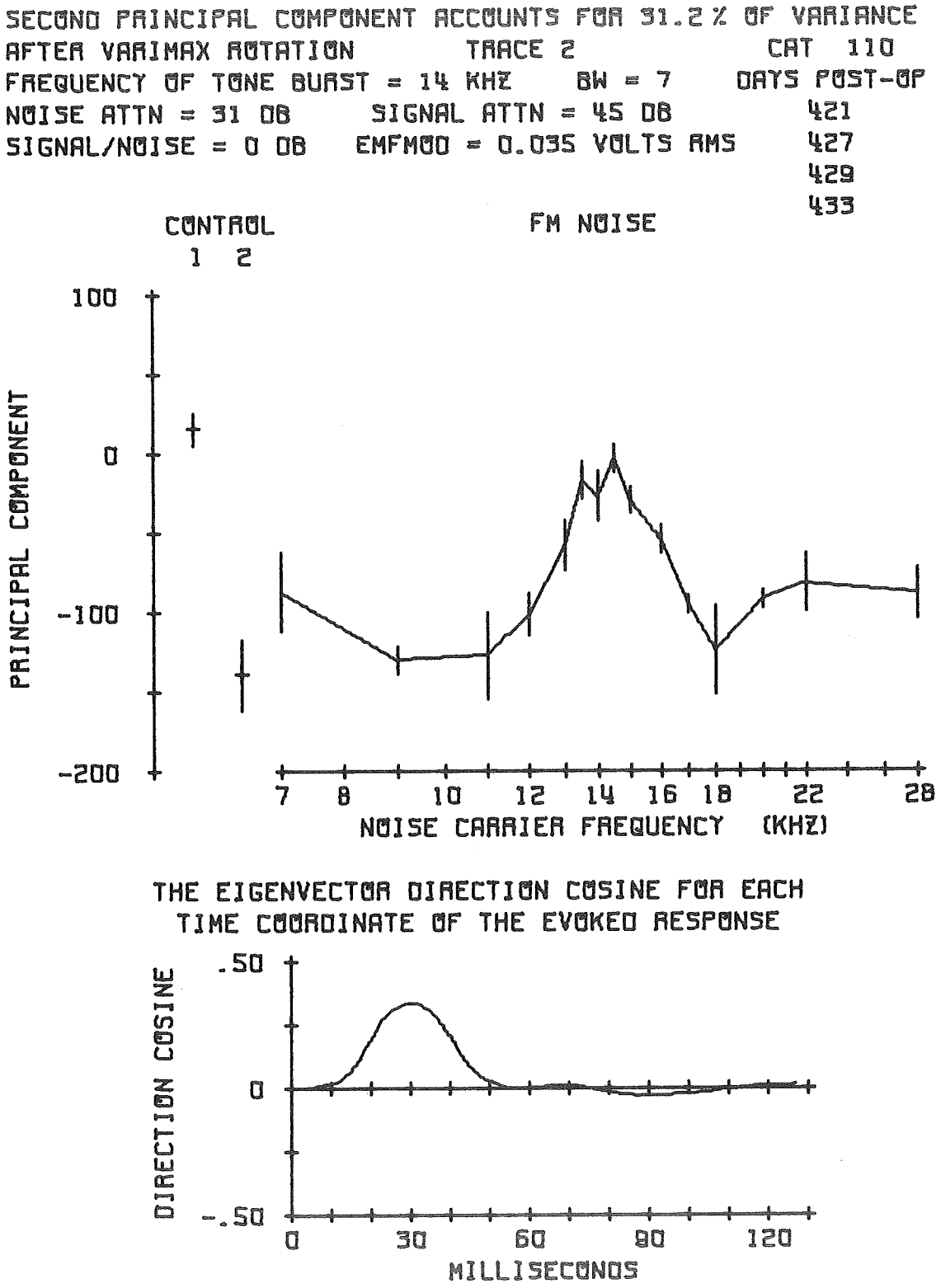

Fig. 50. Masking curve from constant tone experiment sessions.

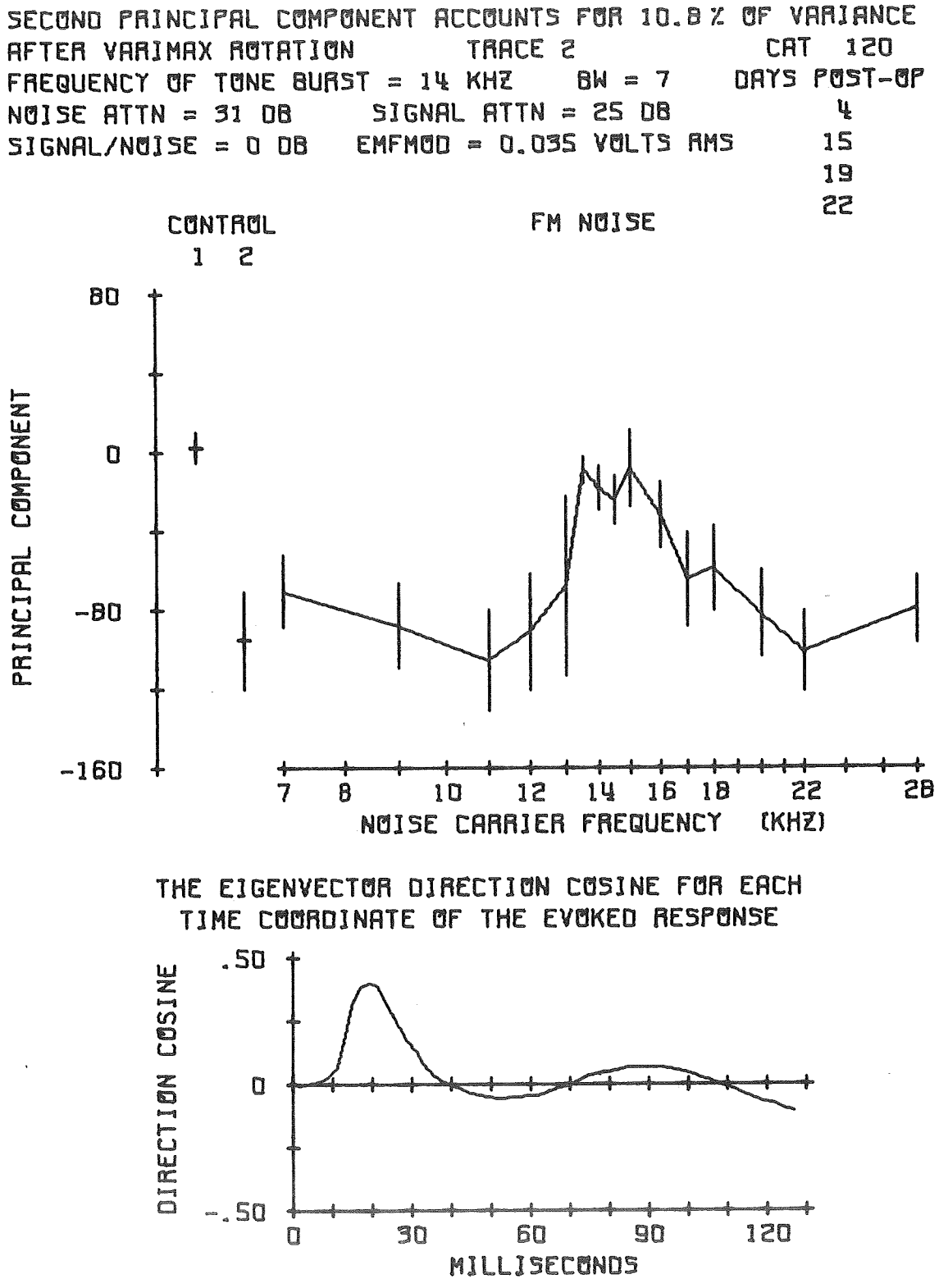

Fig. 51. Masking curve from constant tone experiment sessions.

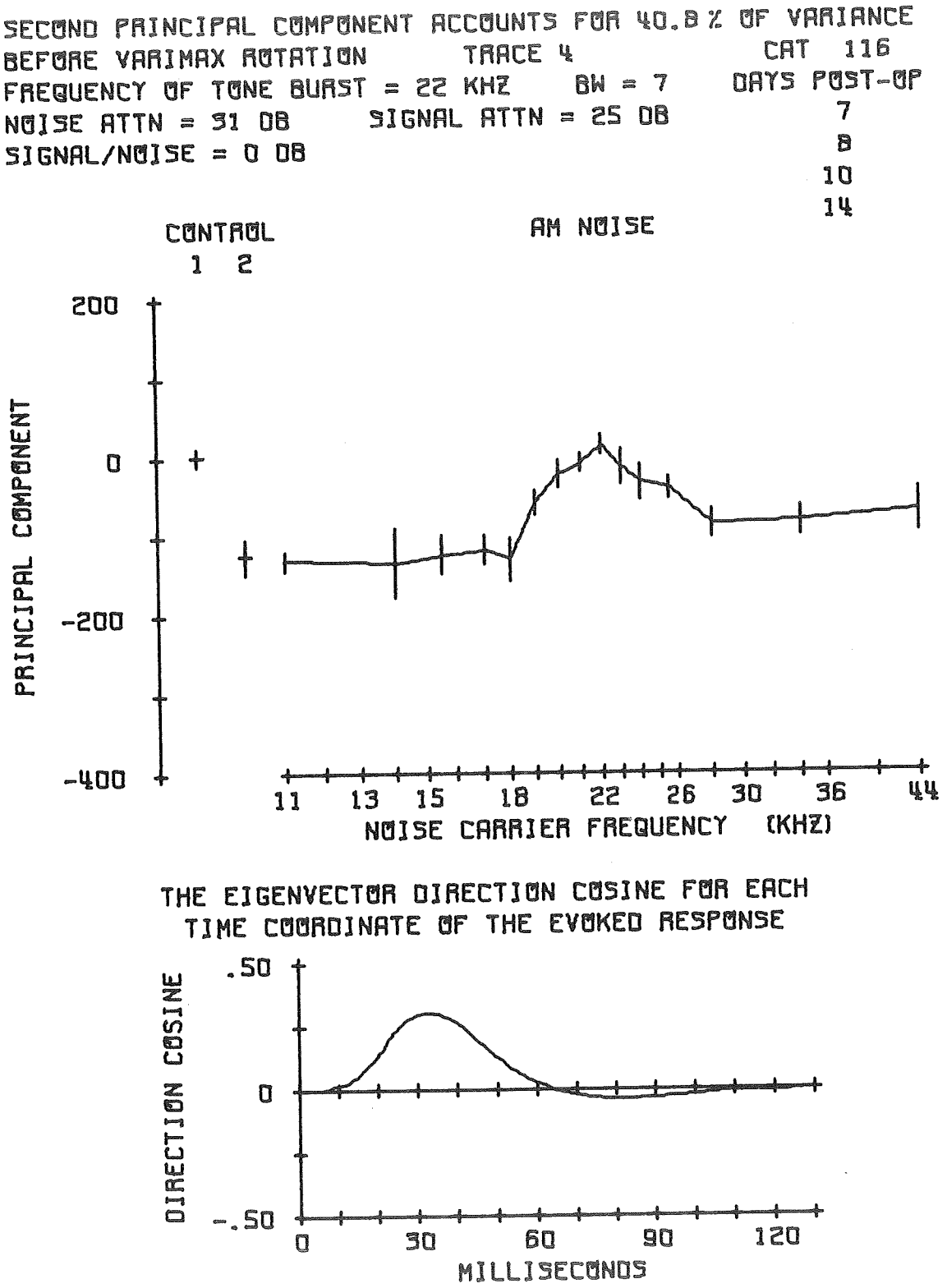

Fig. 52. Masking curve from constant tone experiment sessions.

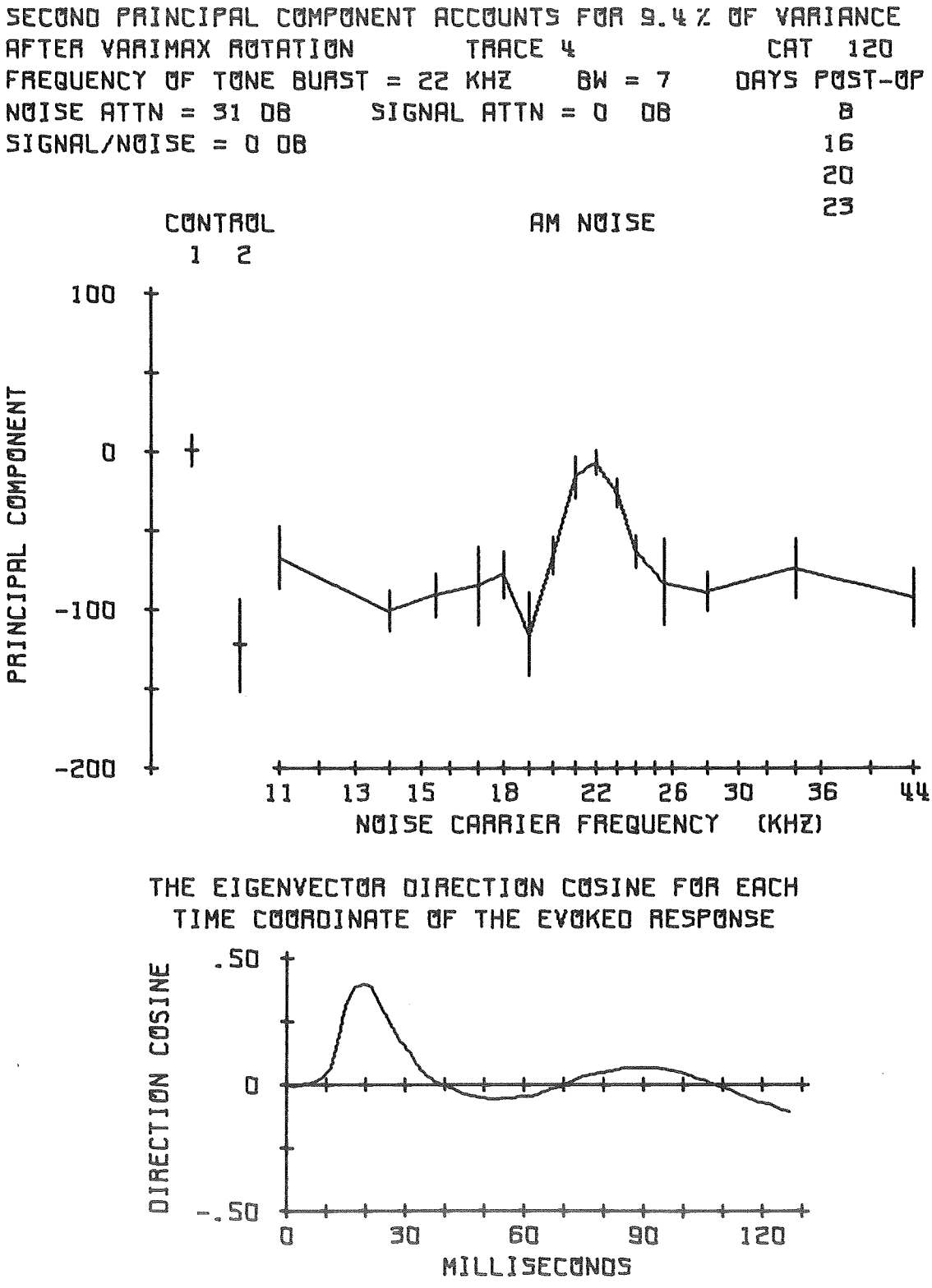

Fig. 53. Masking curve from constant tone experiment sessions.

Table 10. Frequency limits of masking curves from constant tone experiment sessions. The lower, f_L, and upper, f_H, frequencies at the 1/2 peak amplitude points of the principal component versus noise carrier frequency curve, and the difference, $f_H - f_L$, are shown in KHz for each type of noise. The mean of the difference, $f_H - f_L$, for the two noise types is listed in the Avg. column. The mean and standard error of the mean of the data in each column is shown below each set of data. The principal component number, before (B) or after (A) varimax rotation, is shown for each cat (see table 5 for grouping). An * indicates that the masking curve is normal, judging from the values of the control 1 and control 2 runs. Measurements from abnormal curves are not included in the column means. The data are from 14 KHz tone experiment sessions.

Cat	P.C.	Noise Type FM f_L	FM f_H	FM f_H-f_L	AM f_L	AM f_H	AM f_H-f_L	Avg.
110	1 B	* 12.1	16.1	4.0	* 12.1	17.1	5.0	4.50
116	1 B	* 11.5	17.1	5.6	* 11.3	17.7	6.4	6.00
119	1 B	13.7	14.2	0.5				
120	1 B	* 13.2	15.0	1.8	* 13.5	15.4	1.9	1.80
mean		12.26	16.06	3.8	12.30	16.73	4.43	4.12
S.E.		.48	.61	1.1	.64	.69	1.33	.78
110	1 A	* 10.2	16.0	5.8	* 12.1	16.9	4.8	5.30
116	1 A	* 11.5	15.4	3.9	11.1	17.1	6.0	4.95
119	1 A	13.8	14.2	0.4				
120	4 A	13.2	15.0	1.8	13.6	15.2	1.6	1.70
mean		10.85	15.70	4.85				4.83
S.E.								.55
110	4 A	* 11.5	17.0	5.5	* 11.4	17.4	6.0	5.75
116	4 A	* 12.0	15.9	3.9	12.1	17.3	5.2	4.55
119	2 A	13.7	14.1	0.4				
120	1 A	* 13.2	14.9	1.7	* 13.5	15.5	2.0	1.85
mean		12.23	15.93	3.70	12.45	16.45	4.0	3.82
S.E.		.50	.61	1.10				.88

Table 11. Frequency limits of masking curves from constant tone experiment sessions. The lower, f_L, and upper, f_H, frequencies at the 1/2 peak amplitude points of the principal component versus noise carrier frequency curve, and the difference, $f_H - f_L$, are shown in KHz for each type of noise. The mean of the difference, $f_H - f_L$, for the two noise types is listed in the Avg. column. The mean and standard error of the mean of the data in each column is shown below each set of data. The principal component number before varimax rotation (B) is shown for each cat. The tone frequency for each set of data is shown in the f_o column. An * indicates that the masking curve is normal, judging from the values of the control 1 and control 2 runs. Measurements from abnormal curves are not included in the column means.

f_o KHz	Cat	P.C.	Noise Type: FM f_L	FM f_H	FM f_H-f_L	AM f_L	AM f_H	AM f_H-f_L	Avg.
9	110	2 B	* 7.5	10.0	2.5	* 7.0	10.0	3.1	2.80
	116	2 B	* 7.4	10.0	2.6	* 7.4	9.8	2.4	2.50
	119	4 B	* 7.8	11.0	3.2				
	120	2 B	* 6.6	11.1	4.5	* 7.1	10.2	3.1	3.80
	mean		7.32	10.52	3.20	7.17	10.03	2.87	3.06
	S.E.		.26	.30	.46	.12	.12	.23	.27
14	110	2 B	* 13.1	16.0	2.9	* 13.1	16.0	2.9	2.90
	116	2 B	13.0	16.1	3.1	* 13.0	14.8	1.8	2.45
	119	4 B	* 12.0	16.0	4.0	* 13.0	16.1	3.1	3.55
	120	2 B	* 13.2	16.1	2.9	* 12.0	15.0	3.0	2.95
	mean		12.77	16.03	3.27	12.78	15.48	2.70	2.94
	S.E.		.38	.34	.37	.26	.34	.30	.24
22	110	2 B	* 21.0	24.5	3.5	* 20.3	23.3	3.0	3.25
	116	2 B	* 20.2	25.1	4.9	* 19.1	25.5	6.4	5.65
	119	4 B	* 20.0	24.8	4.8				
	120	2 B	21.2	22.9	1.7	* 20.6	22.8	2.2	1.95
	mean		20.40	24.80	4.40	20.00	23.87	3.87	4.13
	S.E.		.30	.17	.45	.46	.83	1.29	.62

Table 12. Frequency limits of masking curves from constant tone experiment sessions. The lower, f_L, and upper, f_H, frequencies at the 1/2 peak amplitude points of the principal component versus noise carrier frequency curve, and the difference, $f_H - f_L$, are shown in KHz for each type of noise. The mean of the difference, $f_H - f_L$, for the two noise types is listed in the Avg. column. The mean and standard error of the mean of the data in each column is shown below each set of data. The principal component number after varimax rotation (A), is shown for each cat. The tone frequency for each set of data is shown in the f_o column. An * indicates that the masking curve is normal, judging from the values of the control 1 and control 2 runs. Measurements from abnormal curves are not included in the column means.

f_o KHz	Cat	P.C.	Noise Type: FM f_L	FM f_H	FM f_H-f_L	AM f_L	AM f_H	AM f_H-f_L	Avg.
9	110	2 A	* 7.3	10.1	2.8	* 7.2	10.1	2.9	2.85
	116	2 A	* 7.1	11.1	4.0	* 7.3	10.8	3.5	3.75
	119	4 A	* 8.5	10.1	1.6				
	120	2 A	* 6.6	10.1	3.5	* 7.0	11.0	4.0	3.75
	mean		7.37	10.35	2.98	7.17	10.63	3.47	3.19
	S.E.		.40	.25	.52	.09	.27	.32	.32
14	110	2 A	* 13.1	15.8	2.7	* 12.9	16.1	3.2	2.95
	116	2 A	* 12.5	16.2	3.7	* 12.7	16.2	3.5	3.60
	119	4 A	12.5	15.2	2.7	13.2	14.7	1.5	2.10
	120	2 A	* 13.2	16.1	2.9	* 11.7	15.1	3.4	3.15
	mean		12.93	16.03	3.10	12.43	15.80	3.37	3.23
	S.E.		.22	.12	.30	.37	.35	.09	.15
22	110	2 A	* 20.7	24.5	3.8	* 20.1	23.8	3.7	3.75
	116	2 A	* 20.5	24.2	3.7	* 18.6	24.0	5.6	4.65
	119	4 A	* 21.1	22.7	1.6	20.5	23.6	3.1	2.35
	120	2 A	* 21.1	24.4	3.3	* 20.5	23.5	3.0	3.15
	mean		20.85	23.95	3.10	19.73	23.77	4.10	3.53
	S.E.		.15	.42	.51	.58	.14	.78	.45

of data include only the data from normal masking curves. The means and standard errors in the Avg. column were obtained from all of the $f_H - f_L$ values for normal masking curves. The masking curve data shown in table 10 are from experiment sessions using only 14 KHz tones. The masking curves for cats 110, 116 and 120 were usually normal, but there was a large variance. Most of the principal components at 9 and 22 KHz, unlike those at 14 KHz, failed to demonstrate consistant critical band effects. It should be noted that for constant tone experiments the latencies of the evoked response components (and hence the latencies of the principal components) are longer than for constant noise experiments because of the longer tone burst time (table 3).

The first principal component before varimax rotation, 1B, has a latency range which spanned those of principal components 1A and 4A. But unlike the 1B component in the constant noise experiments; it does not span the earlier latencies. The average width of the 1B masking curve is 4.12 KHz. The 1A principal component for cats 110 to 119 and the 4A component for cat 120 show masking curves of similar width, 4.83 KHz, but most of the masking curves were considered abnormal. These components were derived from parts of the evoked response at latencies greater than 90 msec. The last set of data in table 10 is derived from eigenvectors which have latencies in the region of 50 to 80 milliseconds. An examination of the sign of the principal components for unmasked tones and the sign of the eigenvector direction cosines reveals that these eigenvectors are similar to the evoked response component ER_3. There is considerable variability in the widths of the masking curves measured, but most curves were considered normal.

Two conclusions can be stated for the data in table 10: 1) the late portion (50 - 128 msec) of the evoked response shows a weak critical band effect; and 2) there is no obvious difference between the results obtained with the two types of noise, AM and FM.

The data from masking curves for the second principal component, cats 110, 116 and 120, and the fourth principal component, cat 119, before varimax rotation are shown in table 11. The data from the corresponding principal components after varimax rotation are shown in table 12. The second eigenvector for cat 110 is practically unchanged by varimax rotation. For cats 116 to 120, the latencies are slightly smaller in range and earlier in time coordinates of the evoked response after varimax rotation. It is not possible to state here which evoked response component is reflected in these eigenvectors, but the most likely one appears to be ER_1. The third eigenvectors after varimax rotation for cats 116 and 120 and before varimax rotation for cat 119, would then be in a latency position corresponding to ER_2. The polarities of the eigenvectors and their corresponding principal components for unmasked tone burst evoked responses is such that the proper polarities of the average evoked response components, positive for both ER_1 and ER_2, results from both assumptions. Most of the masking curves corresponding to the data in these two tables were considered normal. The average width of the masking curves from experiment sessions using 14 KHz tones were 2.94 and 3.23 KHz for tables 11 and 12, respectively, which is reasonably close to the average width of 3.17 KHz found for the constant noise experiment sessions (principal component 2B). The theoretical critical bandwidth, from equation 13b, at a frequency of 14 KHz is 3.14 KHz. It would appear, then, that the early portion of the average

evoked response displays a critical band effect which, in terms of bandwidth, confirms Greenwood's predictions. The theoretical critical bandwidths for frequencies of 9 KHz and 22 KHz are 2.05 KHz and 4.88 KHz, respectively. The average widths of the masking curves for 9 KHz and 22 KHz tones fail to agree with these values or, indeed, to be significantly different from the average bandwidth measured at 14 KHz, in view of the large variances present. The standard errors increase with frequency, so that the variance in the data does not appear disproportionately large at 22 KHz. There doesn't appear to be any bias imposed on the measured bandwidths by either the lower, f_L, or upper, f_H, frequency limits of the masking curve. The AM and FM noise produce about the same results.

There appears to be one of two possible conclusions from the data in tables 11 and 12: 1) the early portion of the average evoked response shows a critical band effect which confirms the bandwidths predicted by equation 13b, but the large variance in the data at 9 and 22 KHz precludes a confirmation; or 2) the various segments of the average evoked response display critical band effects which are manifestations of more finely tuned critical band phenomena at lower centers, and the apparent confirmation of equation 13b for a frequency of 14 KHz was a coincidence resulting from the choice of noise bandwidths. These two alternatives are examined in the Discussion section.

The principal component masking curves corresponding to the amplitude measurement masking curves plotted in figures 21 to 32 are shown in figures 54 to 61. These curves show the means and standard errors of the second principal component before and after varimax rotation for cats 110 and 116 from constant tone experiment sessions which were

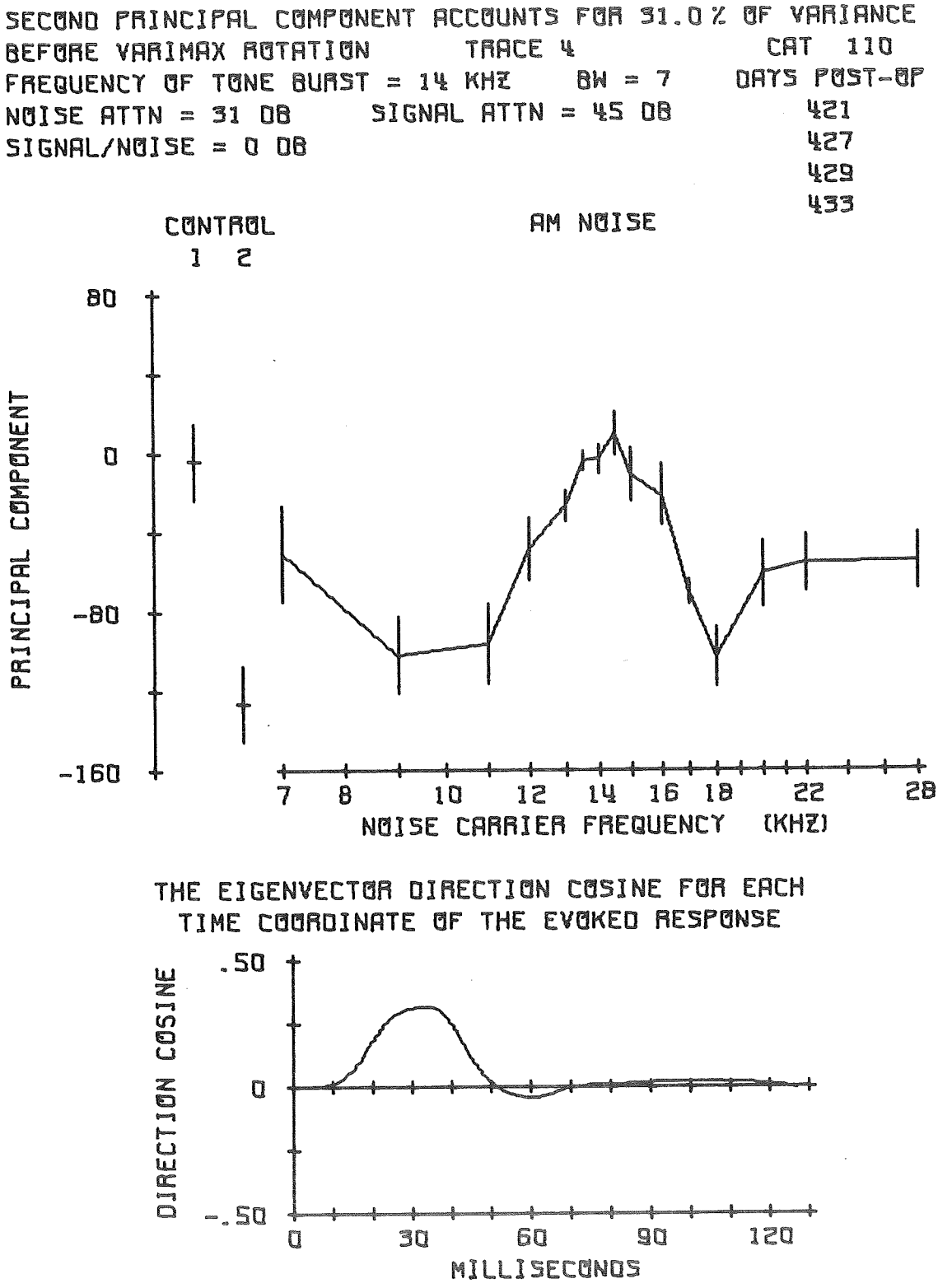

Fig. 54. Masking curve 2B; for AM noise at 14 KHz. Mean ±1 standard error.

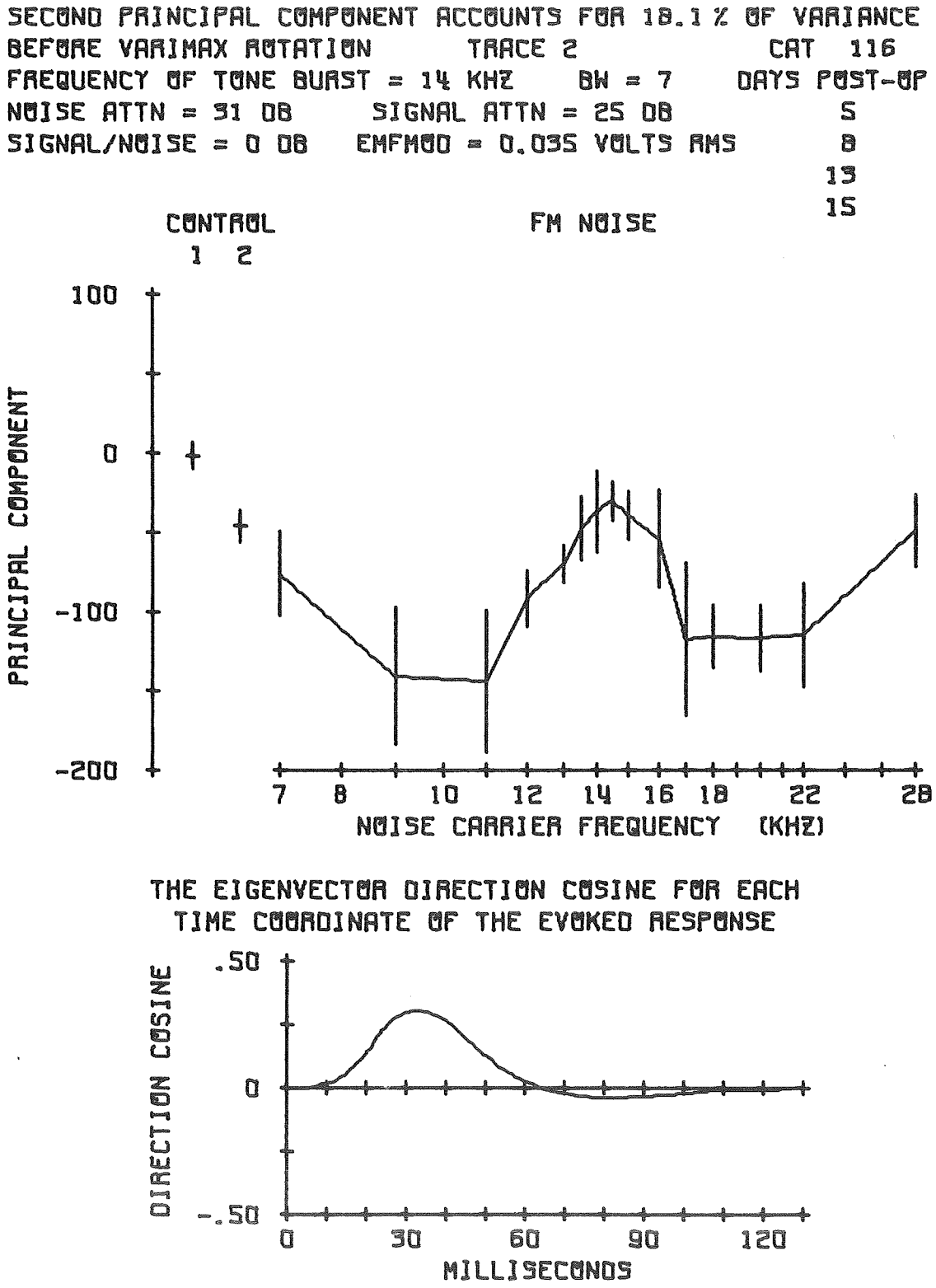

Fig. 55. Masking curve 2B, for FM noise at 14 KHz. Mean ±1 standard error.

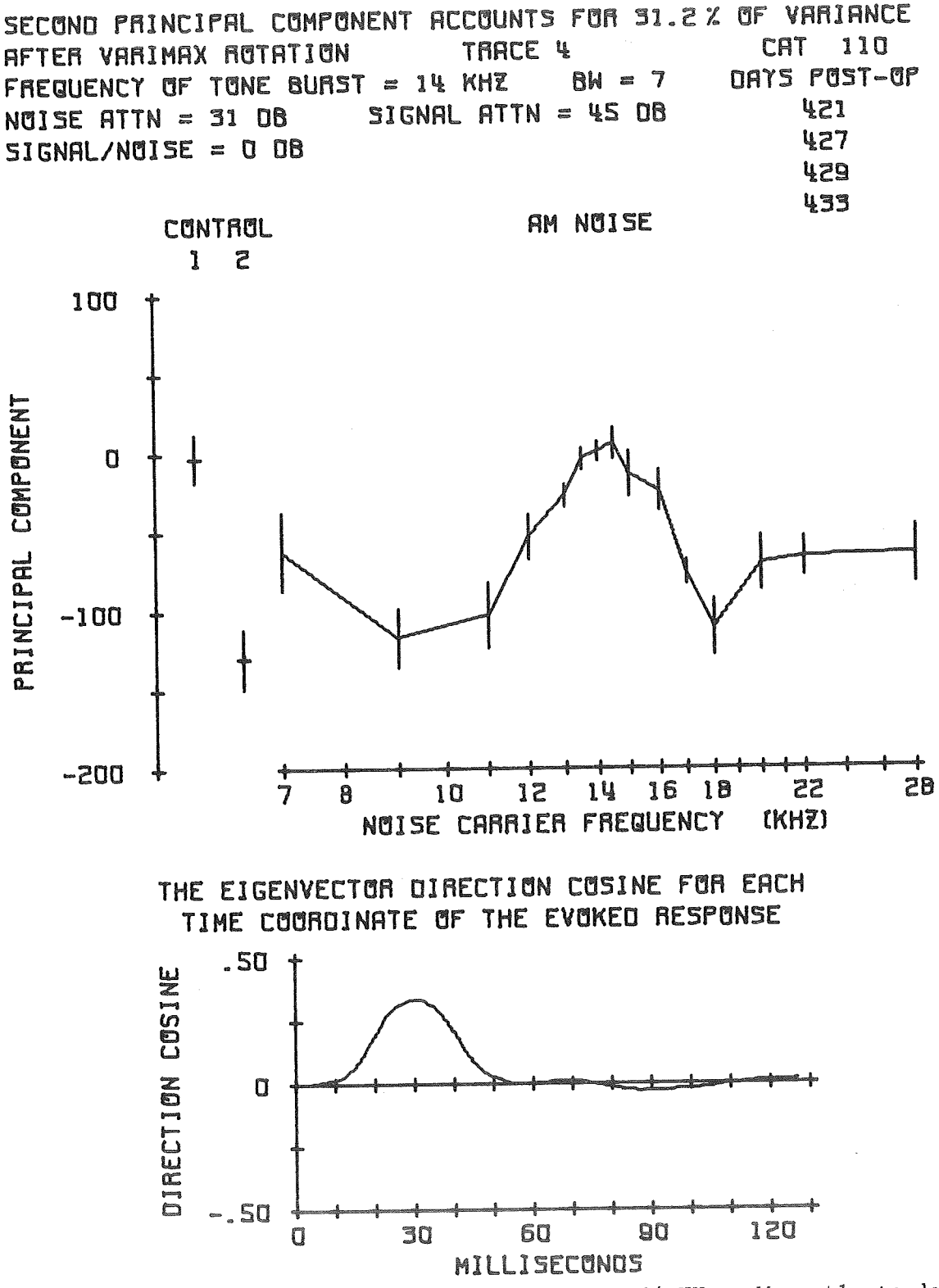

Fig. 56. Masking curve 2A, for AM noise at 14 KHz. Mean ±1 standard error.

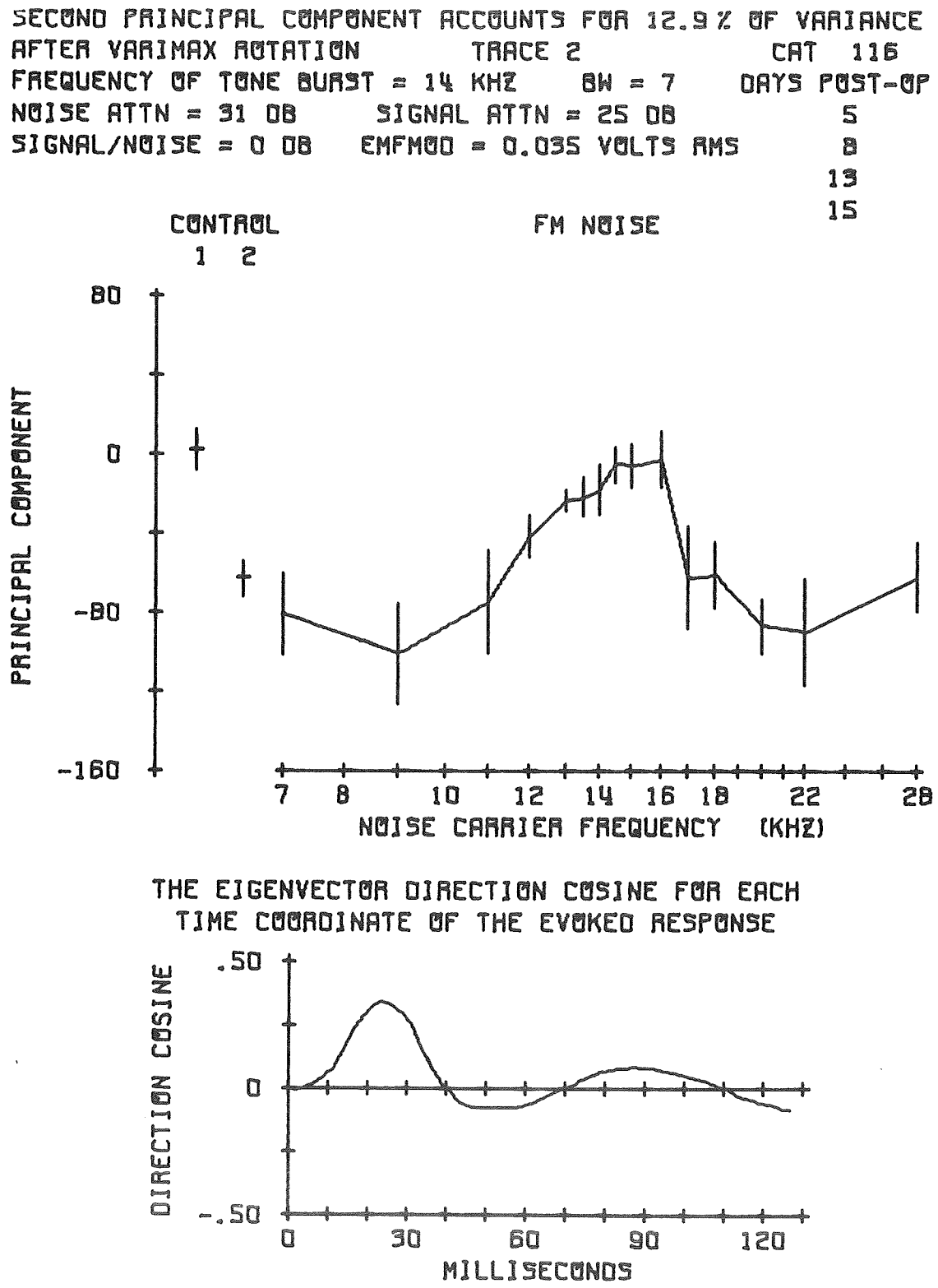

Fig. 57. Masking curve 2A, for FM noise at 14 KHz. Mean ±1 standard error.

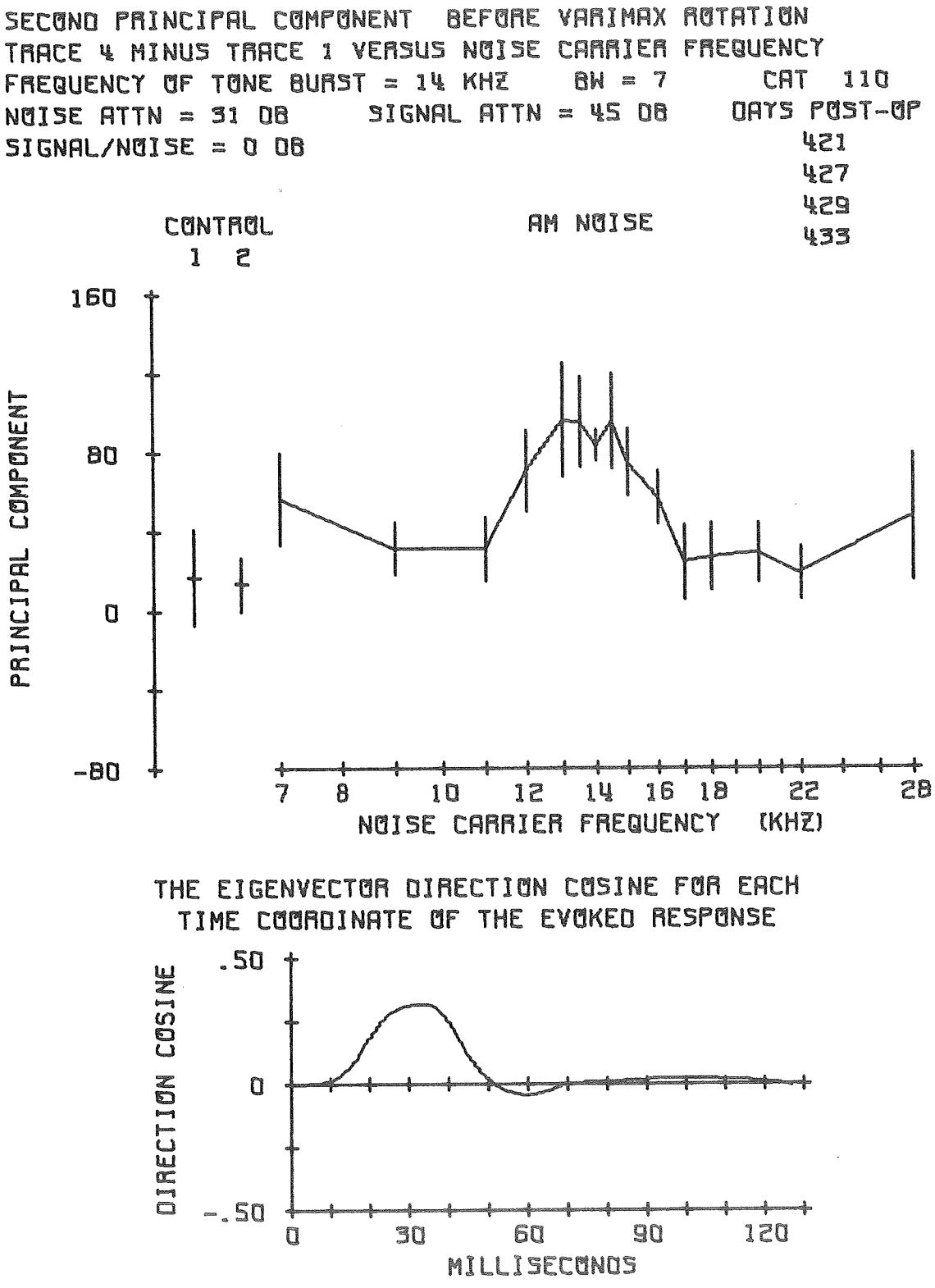

Fig. 58. Masking curve 2B difference, for AM noise at 14 KHz. Mean ±1 standard error.

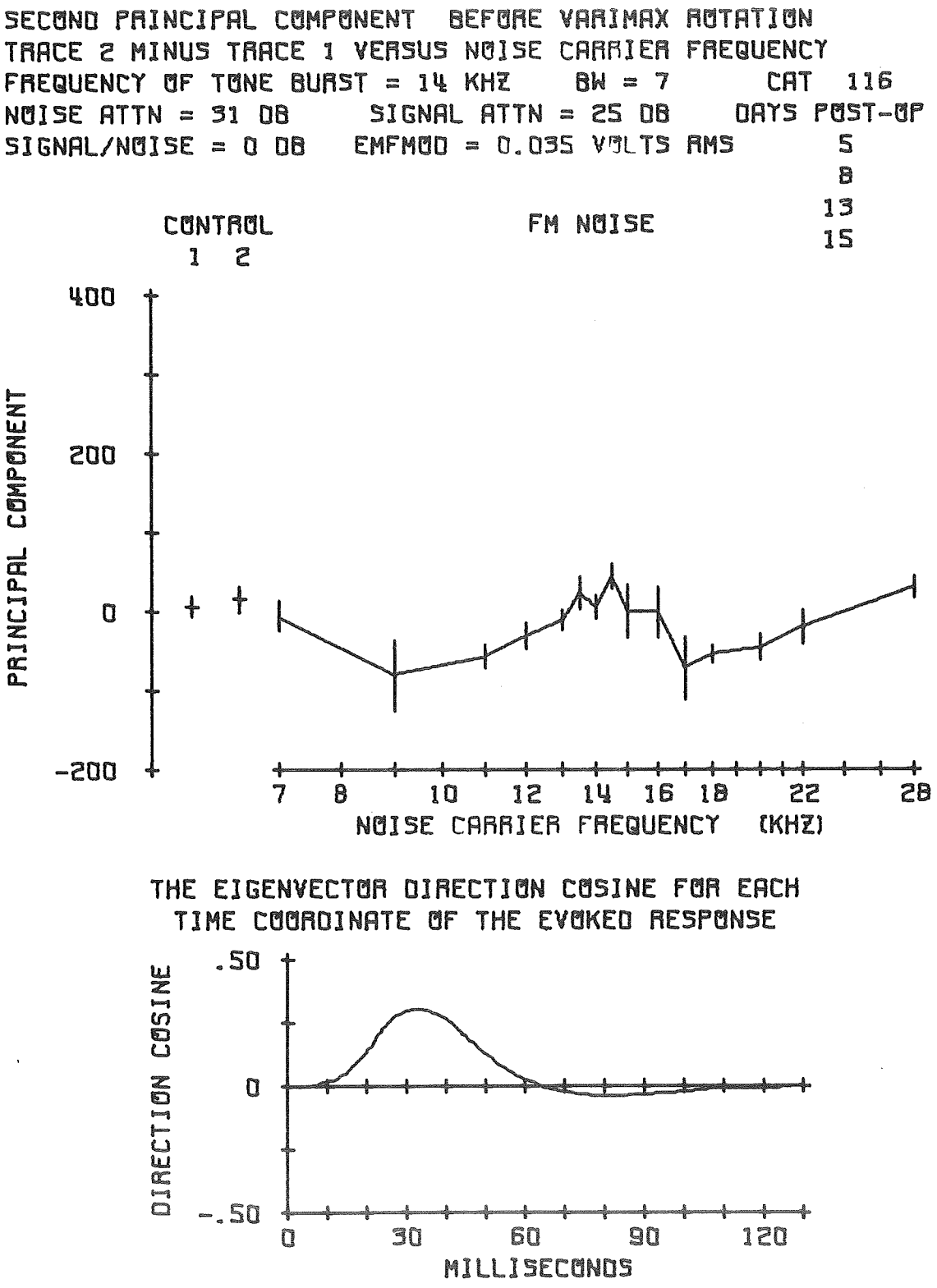

Fig. 59. Masking curve 2B difference, for FM noise at 14 KHz. Mean ±1 standard error.

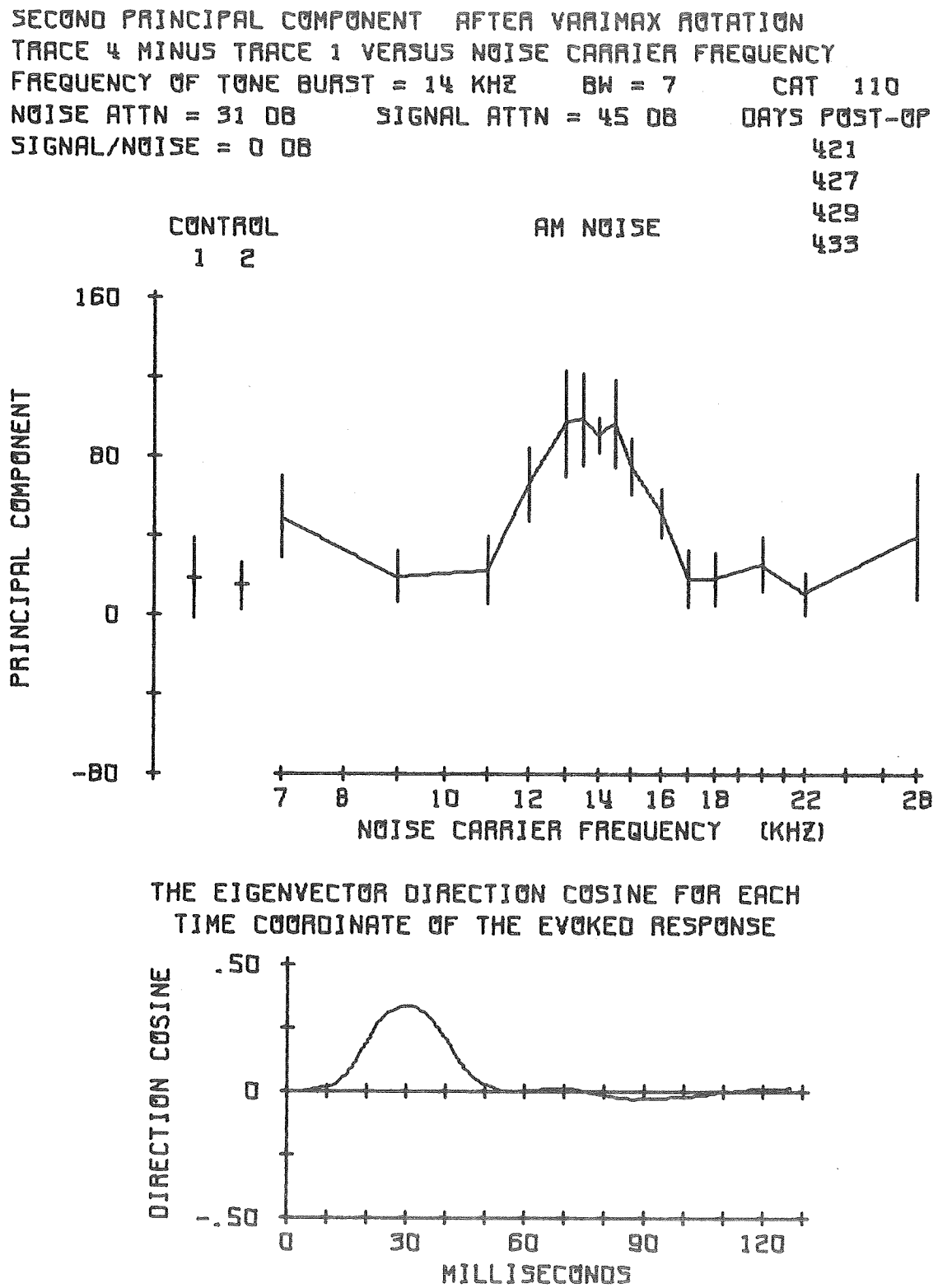

Fig. 60. Masking curve 2B difference, for AM noise at 14 KHz. Mean ±1 standard error.

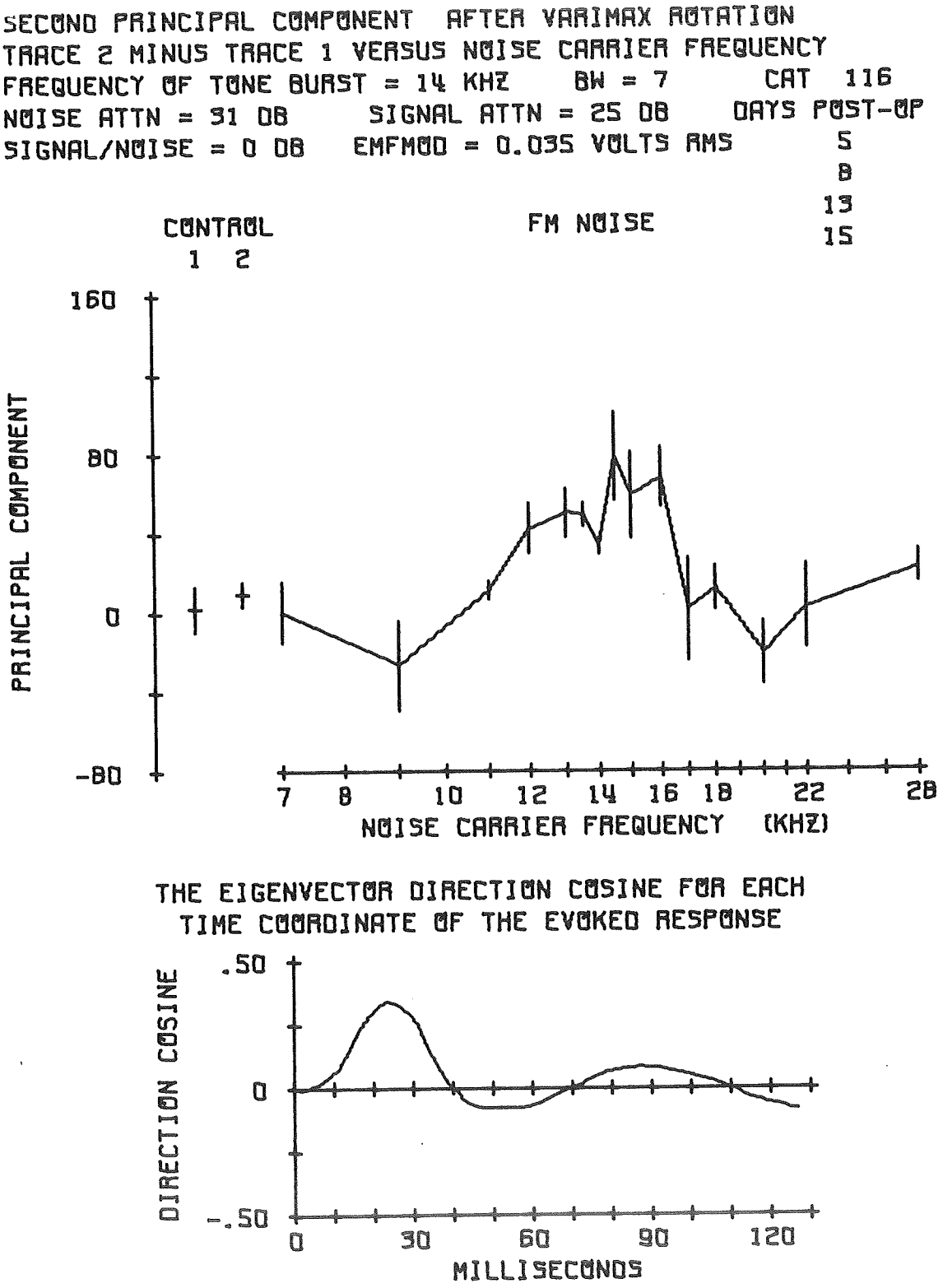

Fig. 61. Masking curve 2B difference, for FM noise at 14 KHz. Mean ±1 standard error.

conducted using a tone frequency of 14 KHz. Figures 54 to 57 show the means and standard errors of the principal components for evoked responses to tones presented in a noise background, trace 2 or 4. Figures 58 to 61 show the means and standard errors of the differences between principal components for trace 1 (average evoked response to unmasked tone) and either trace 2 or 4 in the same run. The logarithm of the ratio of unmasked and masked evoked responses could not be plotted because some of the principal components had negative values. A visual comparison of the masking curves in figures 21 to 32 with the corresponding curves in figures 54 to 61 reveals no substantial improvement was made in the masking curves by using principal components. The differences which are present are quantified in tables 13 and 14.

It can be seen from tables 11 and 12 that the measured widths of the masking curves from the 2A and 2B principal components were about the same, and hence these two principal components are treated together in table 13. It is interesting to note that the peaks of 2A eigenvectors for cats 110 and 116 are located at 30 and 25 msec, respectively, which are the latencies of the peak amplitude measurements used initially for these cats (see page 66). Table 13 shows the upper and lower frequencies and their difference at the one-half peak amplitude points on the masking curves from figures 54 to 61. Table 14 shows the corresponding frequency and bandwidth measurements for masking curves from figures 21 to 32.

The widths of the masking curves from the principal components (mean and S.E. in the Avg. col. of table 13) for plot types T_{24} (2.98 ± 0.20 KHz) and T_{24}-T_1 (3.32 ± 0.29 KHz) are both within one standard error of the theoretical critical bandwidth at 14 KHz (3.14 KHz;

Table 13. Frequency limits of masking curves from constant tone experiment sessions with cats 110 and 116. The lower, f_L, and upper, f_H, frequencies at the 1/2 peak amplitude points of the principal component versus noise carrier frequency curve, and the difference, $f_H - f_L$, are shown in KHz for each type of noise. The mean difference, $f_H - f_L$, for the two noise types is listed in the Avg. column. The mean and standard error of the data in each column is shown below each set of data. The mean and standard error of the $(f_H - f_L)$s is shown in the Avg. column. The masking curves for the second principal component, before and after varimax rotation, were plotted two ways: 1) principal component of masked response, trace 2 or 4, T_{24}, and 2) difference between principal components for unmasked and masked responses, T_{24}-T_1. The data are from 14 KHz tone experiment sessions.

Cat	PC	Plot	Noise Type: FM f_L	FM f_H	FM f_H-f_L	AM f_L	AM f_H	AM f_H-f_L	Avg.
110	2B	T_{24}	13.1	16.0	2.9	13.1	16.0	2.9	2.90
116	2B		13.0	16.1	3.1	13.0	14.8	1.8	2.45
110	2A		13.1	15.8	2.7	12.9	16.1	3.2	2.95
116	2A		12.5	16.2	3.7	12.7	16.2	3.5	3.60
mean			12.92	16.02	3.10	12.92	15.78	2.85	2.98
S.E.			0.14	0.09	0.22	0.27	0.33	0.37	0.20
110	2B	T_{24}-T_1	12.5	15.5	3.0	11.9	15.5	3.6	3.30
116	2B		13.0	16.1	3.1	13.0	14.8	1.8	2.45
110	2A		12.5	15.4	2.9	11.8	15.5	3.7	3.30
116	2A		11.9	16.2	4.3	12.1	16.3	4.2	4.25
mean			12.47	15.80	3.32	12.20	15.52	3.32	3.32
S.E.			0.22	0.20	0.33	0.27	0.31	0.28	0.29

Table 14. Frequency limits of masking curves from manual amplitude measurements of average evoked responses. The lower, f_L, and upper, f_H, frequencies at the 1/2 peak amplitude points of the evoked response amplitude versus noise carrier frequency curve, and the difference $f_H - f_L$, are shown in KHz for each type of noise. The mean difference, $f_H - f_L$, for the two noise types is listed in the Avg. column. The mean and standard error of the mean of the data in each column is shown for two types of evoked response measurements: peak amplitude, PA, and peak-to-peak amplitude, PP, each plotted three ways: 1) measurement of masked response, T_{24}, 2) difference between unmasked and masked response, T_1-T_{24}, and 3) the logarithms of the ratio of unmasked and masked responses, T_1/T_{24}. The data are from 14 KHz tone experiment sessions.

Cat	Plot	Noise Type: FM f_L	FM f_H	FM f_H-f_L	AM f_L	AM f_H	AM f_H-f_L	Avg.
110 PA	T_{24}	12.8	16.1	3.3	12.2	16.5	4.3	3.80
116 PA		11.9	16.6	4.7	12.1	16.8	4.7	4.70
110 PP		12.7	16.4	3.7	12.5	16.1	3.6	3.65
116 PP		11.9	16.6	4.7	12.4	16.7	4.3	4.50
mean		12.32	16.42	4.10	12.30	16.52	4.22	4.16
S.E.		0.25	0.12	0.35	0.09	0.15	0.23	0.20
110 PA	T_1-T_{24}	12.6	15.7	3.1	12.1	15.6	3.5	3.30
116 PA		12.3	16.1	3.8	12.5	14.9	2.4	3.10
110 PP		12.3	16.1	3.8	12.2	15.7	3.5	3.65
116 PP		11.8	16.5	4.7	12.5	16.1	3.6	4.15
mean		12.25	16.10	3.85	12.32	15.58	3.25	3.55
S.E.		0.16	0.16	0.33	0.10	0.25	0.28	0.23
110 PA	T_1/T_{24}	13.1	14.9	1.8	12.9	15.5	2.6	2.20
116 PA		13.8	16.3	2.5	12.7	14.9	2.2	2.35
110 PP		13.2	14.7	1.5	12.5	16.1	3.6	2.55
116 PP		11.9	16.1	4.2	12.5	15.9	3.4	3.80
mean		13.00	15.50	2.50	12.65	15.60	2.95	2.72
S.E.		0.40	0.41	0.60	0.10	0.26	0.33	0.33

from equation 13b). The widths of the masking curves from manual amplitude measurements of average evoked responses, table 14, for plot types T_{24} (4.16 ± 0.20 KHz), T_1-T_{24} (3.55 ± 0.23 KHz), and T_1/T_{24} (2.72 ± 0.20 KHz) are not within one standard error of each other or of the theoretical critical bandwidth. There does not appear to be any consistent differences in the standard errors of the bandwidths between table 13 and table 14, between noise types, or between plot types. The first observation confirms the compatability of conventional average evoked response measuring techniques with the principal component analysis. The second observation indicates that the structure of the masking noise (AM or FM) is of little importance in determining the critical bandwidth.

The third observation was very unexpected for the following reason. The variance in the bandwidth measurement is caused, in part, by the variance in the average evoked responses. The stimulus paradigm was structured to allow the accumulation of the average evoked responses to tone bursts presented with and without a noise background, over the same time span. It was reasoned that the state of the animal fluctuates during any given run. However, the average state of the animal should be the same for each trace in a run, since the masked and unmasked tone bursts, (present alternately in the paradigm), were usually separated by less than 2 seconds, i.e. the state of the animal should not change systematically between tone burst presentations. It was expected that the state of the animal and the average evoked response would fluctuate more between runs (both within and between experiment sessions) than between the traces in the same run. Measurements of the degree of masking made by comparing masked and unmasked traces within a run, rather than between runs, should have produced a more stable assessment of the critical bandwidth.

Table 15 shows the standard errors at various frequencies as obtained from the masking curves in figures 62 to 67. This table demonstrates the differences in the variability of the average evoked responses as the tone burst characteristics are changes. The SPL of the tones and the rise times of the tone burst onset are: 52 dB and 2.5 msec for DPO: 178-184; 32 dB and 2.5 msec for DPO: 188-191; 32 dB and 10 msec for DPO:421-433. It can be seen from figures 62 to 67 that the average evoked responses are larger for louder tones and/or faster rise times while the variance of the average evoked responses are generally smaller. Comparison of the variances of the principal components and of differences between principal components in table 15 reveals no consistent differences.

Table 16 shows the standard errors of principal components and of differences between principal components from some of the constant tone experiments. The 9 KHz variances are generally smaller than those at other frequencies. On the other hand the variances are about the same for the principal components and their within run differences.

It should be obvious from tables 15 and 16 that the between run variation was not appreciably greater than the within run variation in the average evoked responses. Although both variances may be considered large, it appears that the behavioral state of the animals can be considered as relatively stable throughout the experiments.

The cortical auditory system appears to possess a considerable amount of variability in the processing of peripheral neural events, apart from that caused by the behavioral state of the animal. The average evoked response to tone bursts with slow onset (Gaussian shaped

Table 15. Standard errors of the principal components and of differences between principal components. The differences were obtained by subtracting the principal components of trace 1 from the corresponding principal components of traces 2, 3 and 4 in the same run. The tone or noise center frequency, whichever was changed during the experiment, are shown in the fq column. The means of the principal components and their differences can be seen in figures 62 to 67.

Days Post-op	fq KHz	Standard Error of the Principal Components from Trace 1	2	3	4	Standard Error of the Differences between Trace 1 and Trace 2	3	4
178-184	9.0	12.9	10.0	10.1	12.8	14.5	8.4	16.4
	11.0	4.0	19.2	7.2	25.5	17.4	7.8	24.8
	13.5	8.0	12.1	14.9	9.8	19.4	13.3	11.7
	14.0	10.2	13.1	10.8	11.2	18.5	9.7	12.1
	14.5	19.7	9.5	13.0	15.4	18.2	8.0	28.0
	17.0	9.6	32.3	13.2	31.4	28.0	12.5	26.3
	22.0	11.2	5.0	10.5	4.1	12.3	17.2	13.0
188-191	9.0	25.9	43.0	33.4	41.6	54.5	10.5	41.7
	11.0	19.6	15.0	24.7	18.3	32.4	15.3	3.4
	13.5	31.1	25.4	20.7	22.8	27.7	35.0	17.5
	14.0	24.3	5.1	32.9	10.7	21.4	12.0	14.1
	14.5	14.8	9.7	16.3	16.5	20.6	8.8	23.6
	17.0	19.3	51.8	14.9	46.3	63.4	7.2	52.5
	22.0	35.4	18.7	22.5	32.2	18.0	14.9	18.1
421-433	9.0	10.7	8.7	16.8	19.8	15.0	16.2	13.6
	11.0	28.8	24.8	30.0	20.3	36.2	34.4	16.2
	13.5	19.0	13.1	28.2	5.2	12.4	30.6	23.2
	14.0	15.4	16.4	27.8	7.6	8.5	23.0	8.0
	14.5	26.1	8.3	16.6	11.2	27.0	9.7	24.4
	17.0	16.1	9.2	20.0	6.4	23.0	7.1	19.1
	22.0	19.7	19.4	36.1	14.4	18.4	35.8	13.7

Table 16. Standard errors of principal components, and differences between principal components. The differences were obtained by subtracting the principal components of trace 1 and from the corresponding principal components of traces 2, 3, and 4 in the same run. Data from four experiment sessions were used to compute means and standard errors. The standard errors for the principal components are shown for each trace. The standard error for the difference in principal components between trace 1 and traces 2, 3, and 4 are shown in the last three columns. The tone and noise carrier (center) frequencies are shown in the f_o and f_n columns, respectively. PC is the principal component number, before (B) or after (A) varimax rotation. Data from two of the fifteen noise carrier frequencies for each tone frequency are shown. Constant tone experiment sessions.

Cat	PC	f_o KHz	f_n	Standard Error of the Principal Components from Trace 1	2	3	4	Standard Error of the Differences between trace 1 and Trace 2	3	4
110	2B	9	6	17.9	8.9	7.8	7.2	18.2	17.6	11.8
			12	6.8	22.3	11.5	11.9	17.4	17.9	17.1
	2A		6	16.9	8.2	8.2	8.8	16.4	17.1	10.3
			12	6.0	19.9	10.9	11.6	14.1	16.1	16.0
116	2B		6	10.8	12.6	18.0	9.0	25.0	11.5	12.1
			12	14.1	9.1	16.6	18.7	5.7	19.7	16.2
	2A		6	12.0	6.8	20.0	5.6	10.2	15.3	9.8
			12	6.2	1.4	11.9	3.8	7.7	9.4	7.5
110	2B	14	11	28.8	24.8	30.0	20.3	36.2	34.4	16.2
			17	16.1	9.2	20.0	6.4	23.0	7.1	19.1
	2A		11	28.9	27.5	29.4	21.2	36.4	33.3	16.9
			17	14.4	6.1	17.4	8.2	33.3	9.8	14.7
116	2B		11	29.5	44.6	30.3	24.0	15.3	14.3	10.3
			17	17.2	48.5	9.8	15.1	40.3	9.3	18.4
	2A		11	23.3	26.4	15.4	10.3	5.5	9.6	17.2
			17	14.5	17.6	20.8	19.5	26.6	11.9	26.8
110	2B	22	19	22.9	17.4	26.3	27.7	17.2	5.5	6.0
			25.5	22.8	29.4	23.5	27.1	15.6	9.3	23.0
	2A		19	22.4	14.2	19.9	24.7	10.1	5.6	6.1
			25.5	20.6	28.8	21.6	25.4	15.2	10.5	17.3
116	2B		19	19.7	25.3	25.7	15.5	6.0	22.0	12.8
			25.5	26.6	36.9	24.2	14.2	30.4	18.1	25.2
	2A		19	14.9	15.0	9.2	9.0	9.5	15.7	10.8
			25.5	18.0	25.3	4.0	13.8	29.0	20.2	22.8

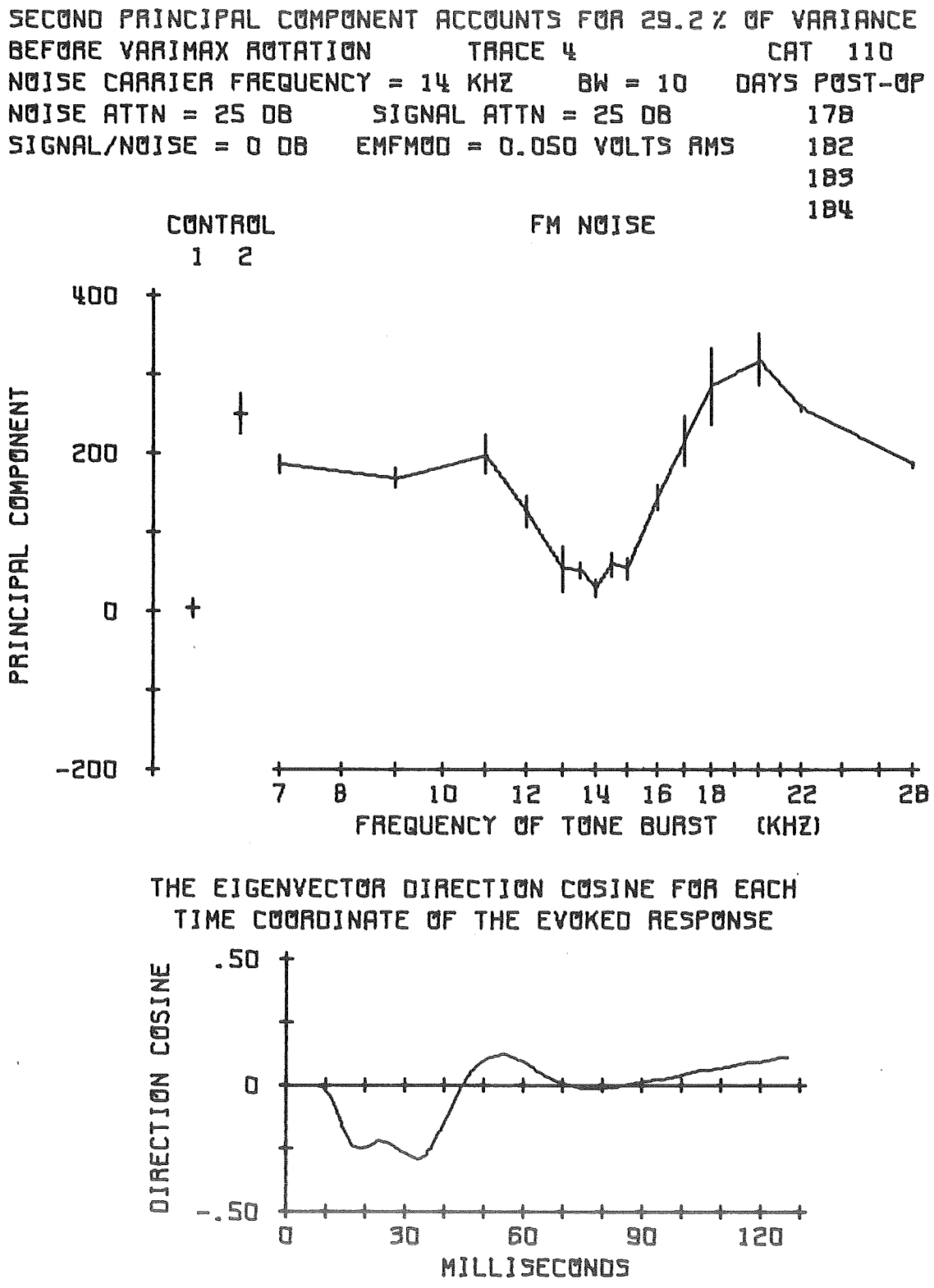

Fig. 62. Masking curve, 2B, tone at 50 dB SL, rise time of 2.5 msec.

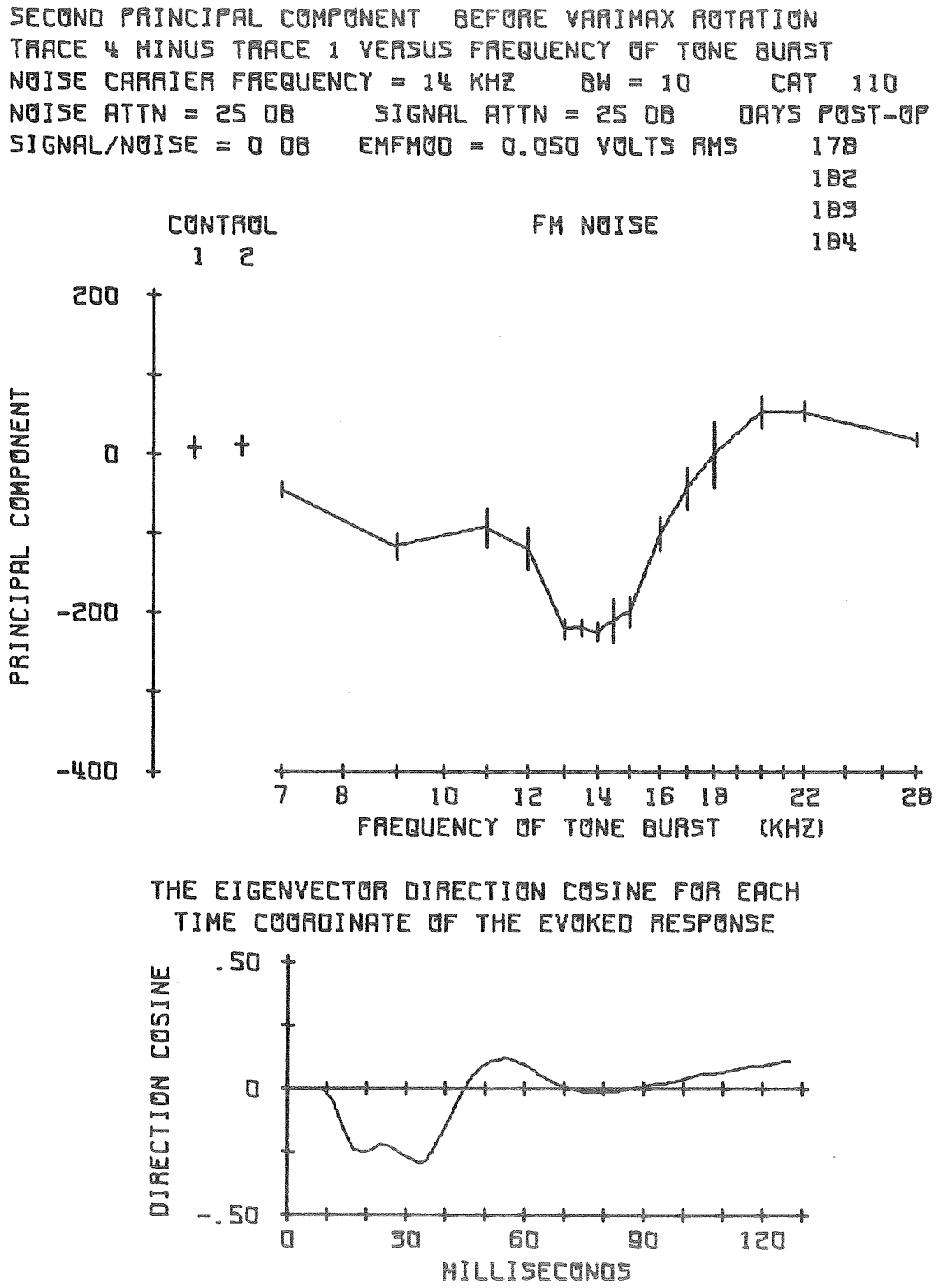

Fig. 63. Masking curve, 2B difference, tone at 50 dB SL, rise time 2.5 msec.

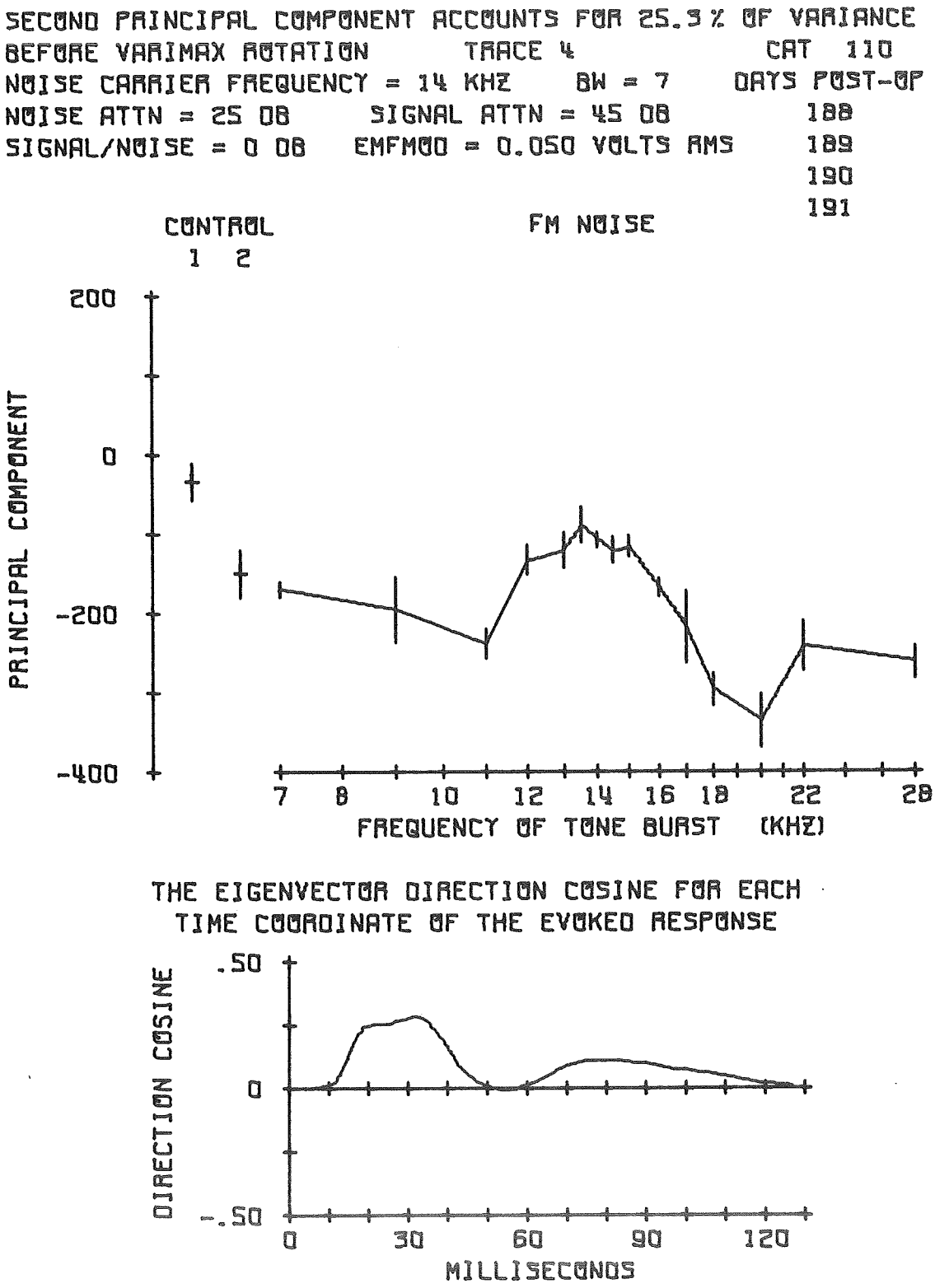

Fig. 64. Masking curve, 2B, tone at 30 dB SL; rise time = 2.5 msec.

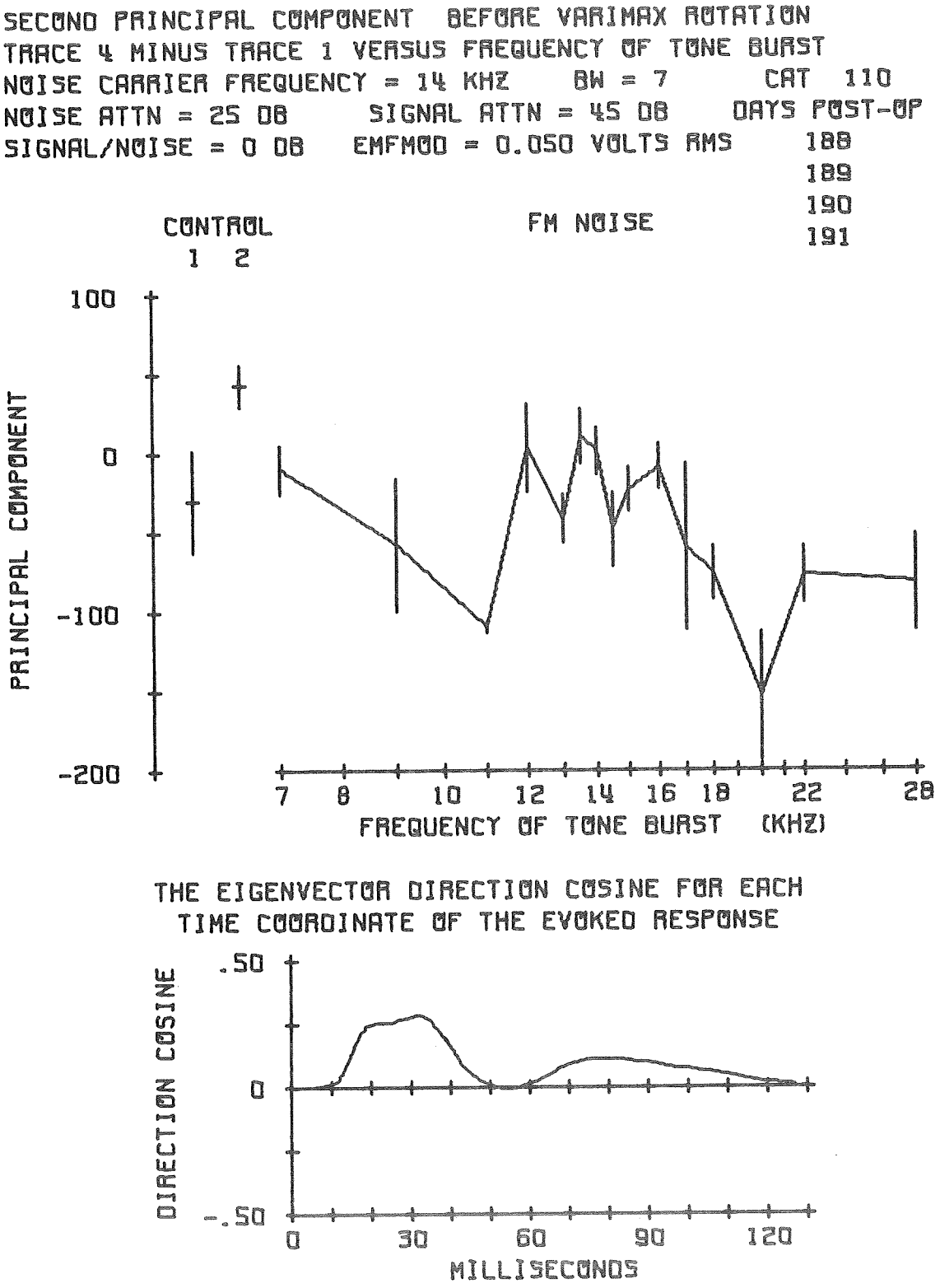

Fig. 65. Masking curve, 2B difference, tone at 30 dB SL, rise time = 2.5 msec.

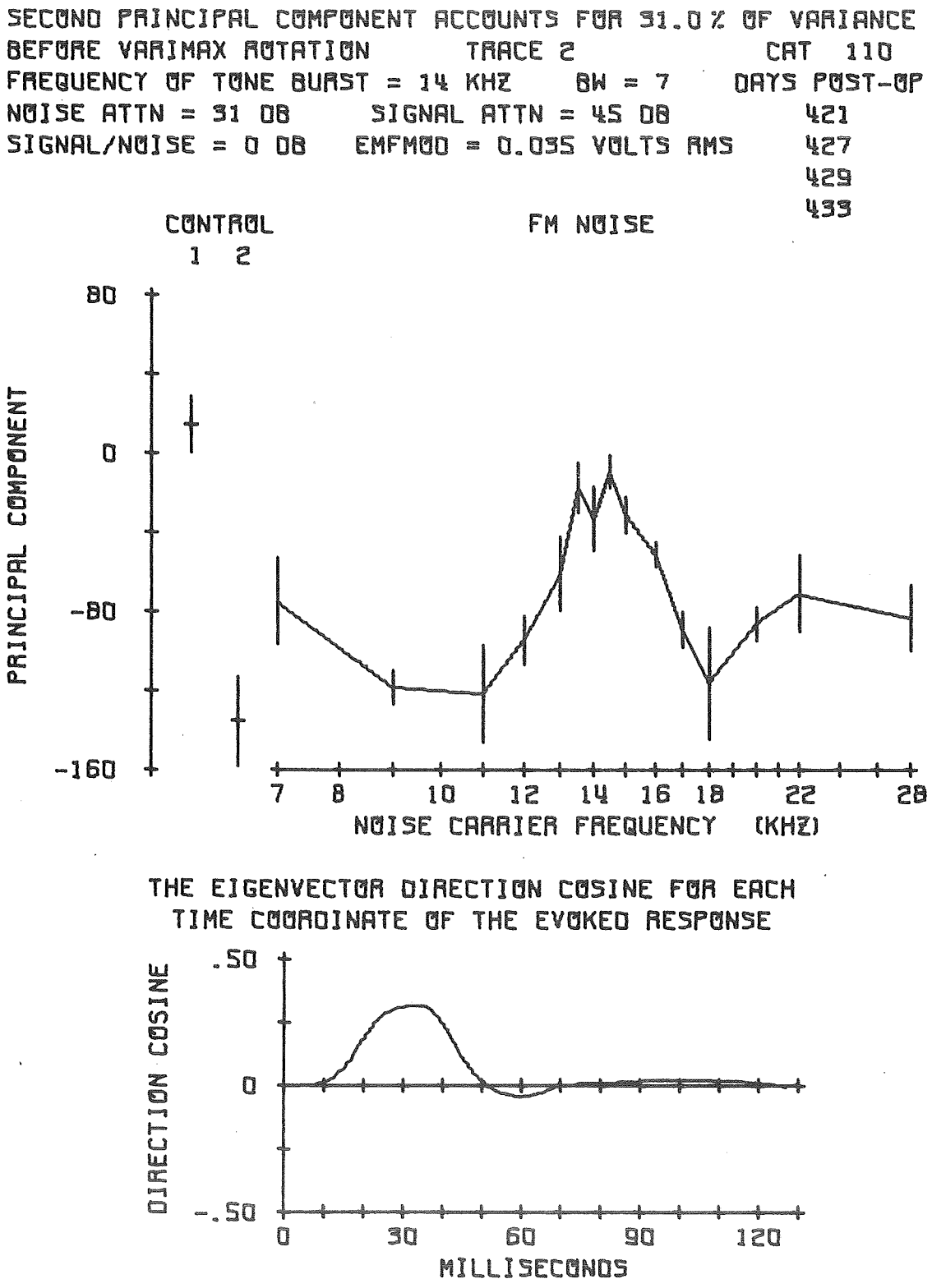

Fig. 66. Masking curve, 2B, tone at 30 dB SL rise time = 10 msec.

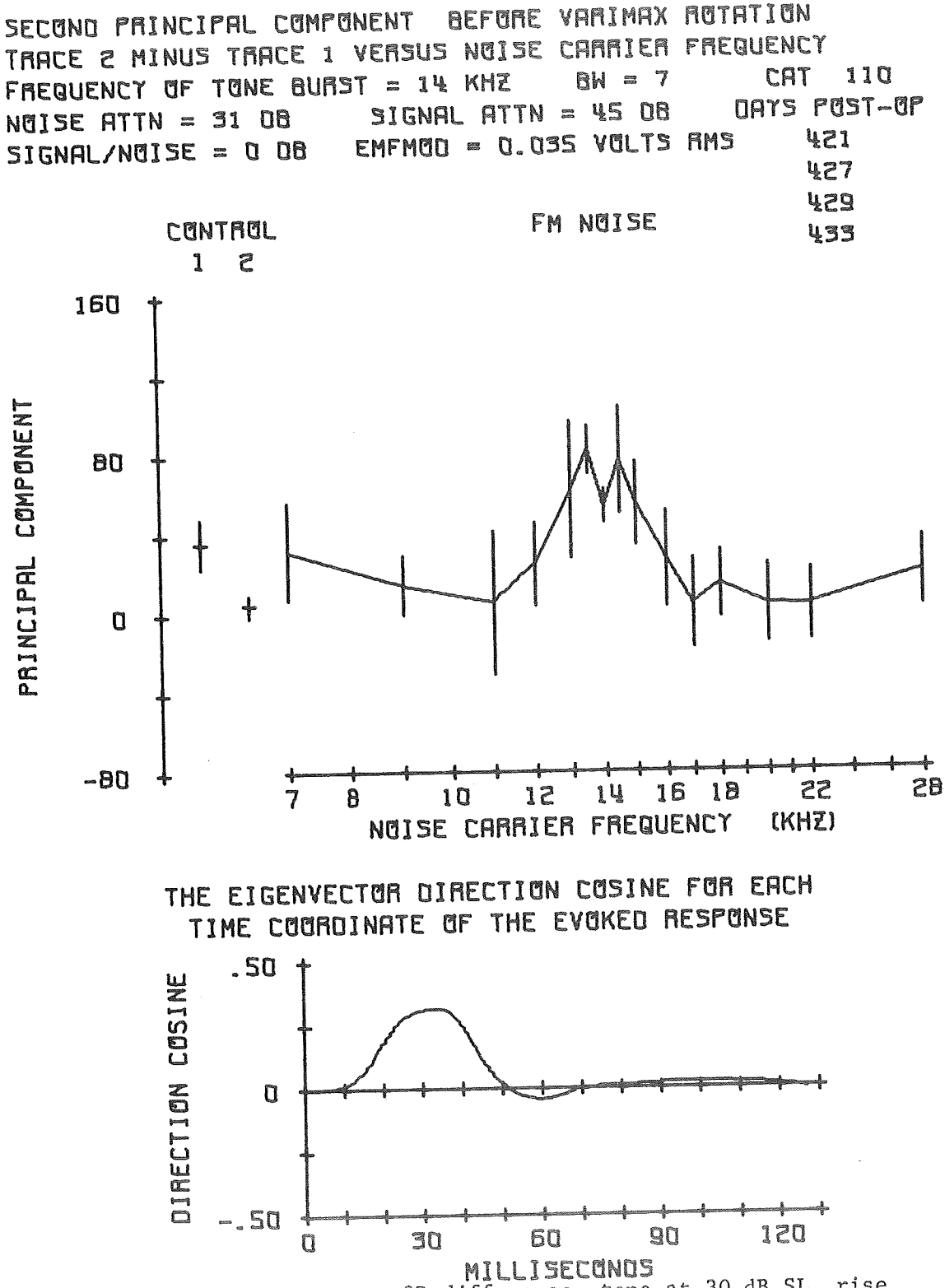

Fig. 67. Masking curve, 2B difference, tone at 30 dB SL, rise time = 10 msec.

and long rise time) and relatively low sound level (30 dB re: animal threshold) are particularly labile. Because it appears to make little difference, the results have been stated in terms of the amplitudes of traces 2 and 4, rather than in terms of differences between traces.

The results which have been presented have demonstrated the changes in the average evoked response which occur concomitantly with changes in the relative frequencies of a tone and a narrow band masking noise. These changes can be compared with the changes which occur in the average evoked response as the intensity of the tone burst or the level of a masking noise, relative to the level of the tone, are varied. The last five runs of each constant tone experiment session were conducted in order to observe these changes. During the first seventeen runs, except the control 1 run, the SPL of the tone burst was set to 30 dB above the animals threshold, defined in table 1. The signal (tone)-to-noise ratio was 0 dB, and the noise center frequency was varied. An FM noise was presented with the second tone burst and an AM noise with the fourth tone burst in the run stimulus paradigm. During the last five runs the center frequency of the FM noise was set equal to the tone frequency and the level of the noise was varied, resulting in signal-to-noise ratios of 20, 10, 5, 0 and −10 dB for runs 18 to 22, respectively. During these runs, the fourth tone burst of the run stimulus paradigm was presented without a noise background at SPLs of 20, 10, 5, 0 and −10 dB relative to the animal's threshold, i.e. the tone level was reduced by 10, 20, 25, 30, and 40 dB, respectively, from its level for the first three tone bursts in the paradigm.

Figures 68 to 73 show the results from the tone intensity and signal-to-noise runs for the six eigenvectors listed in table 5 for

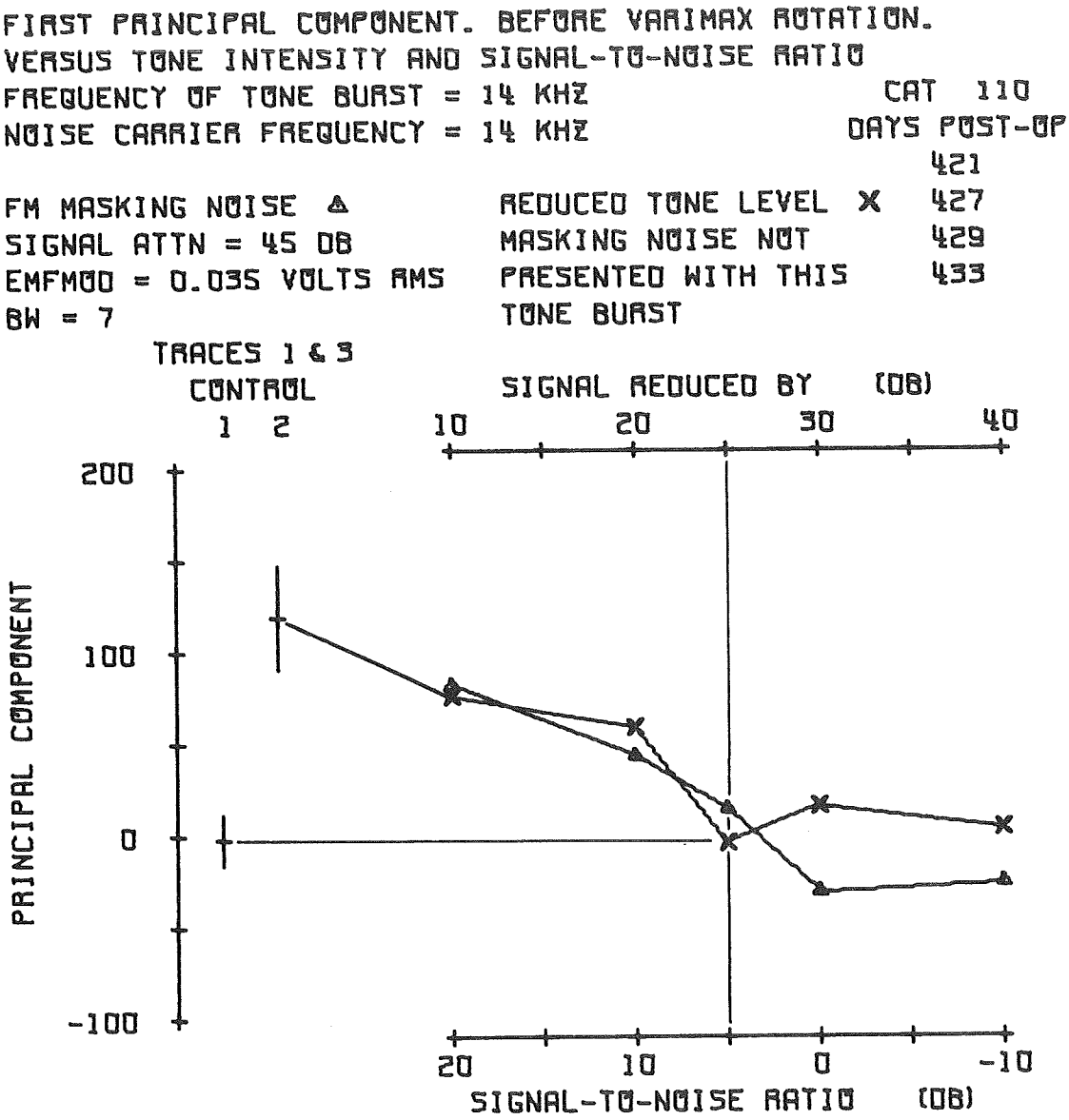

Fig. 68. Principal component 1B versus tone intensity and signal-to-noise ratio for cat 110.

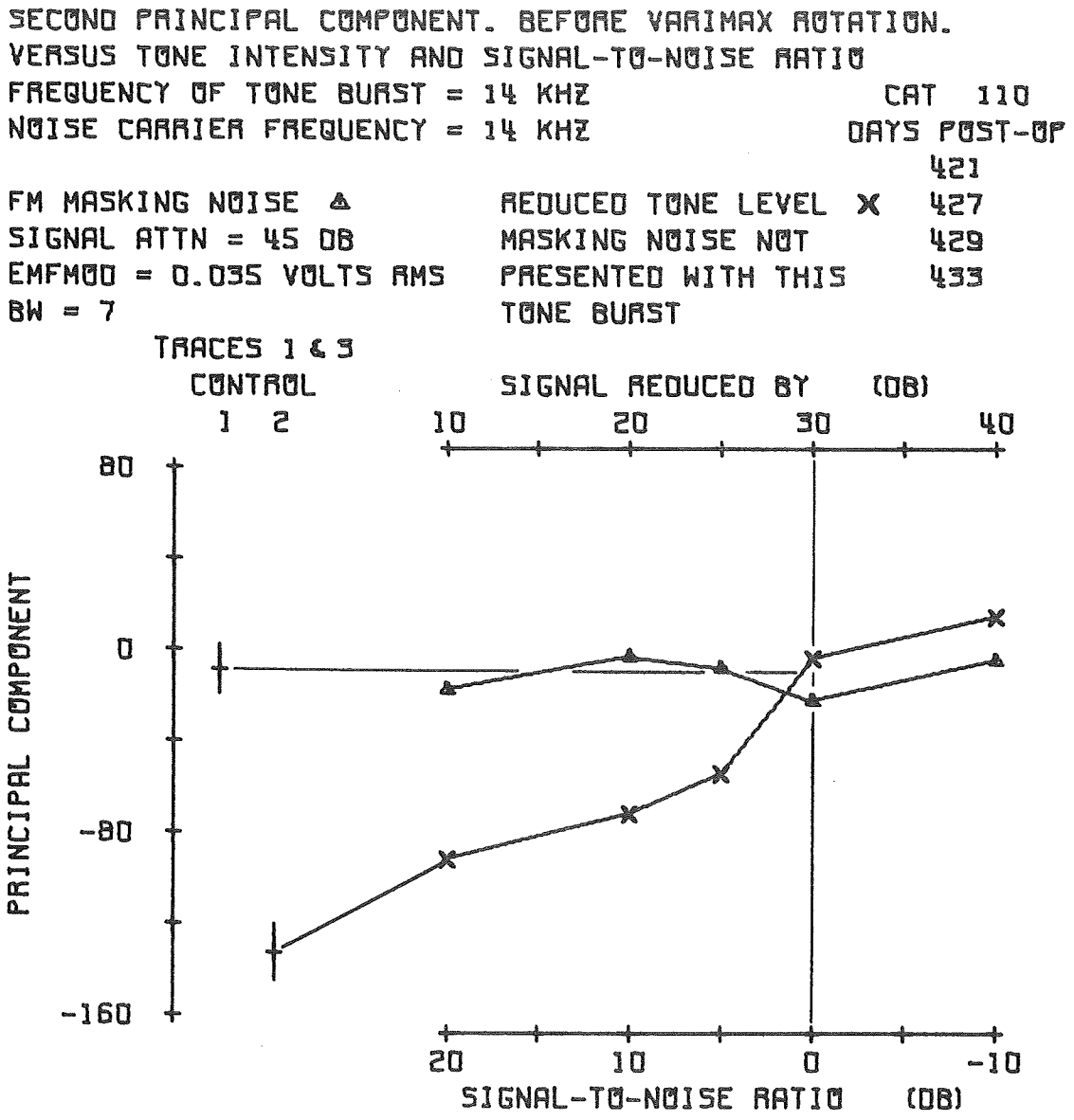

Fig. 69. Principal component 2B versus tone intensity and signal-to-noise ratio for cat 110.

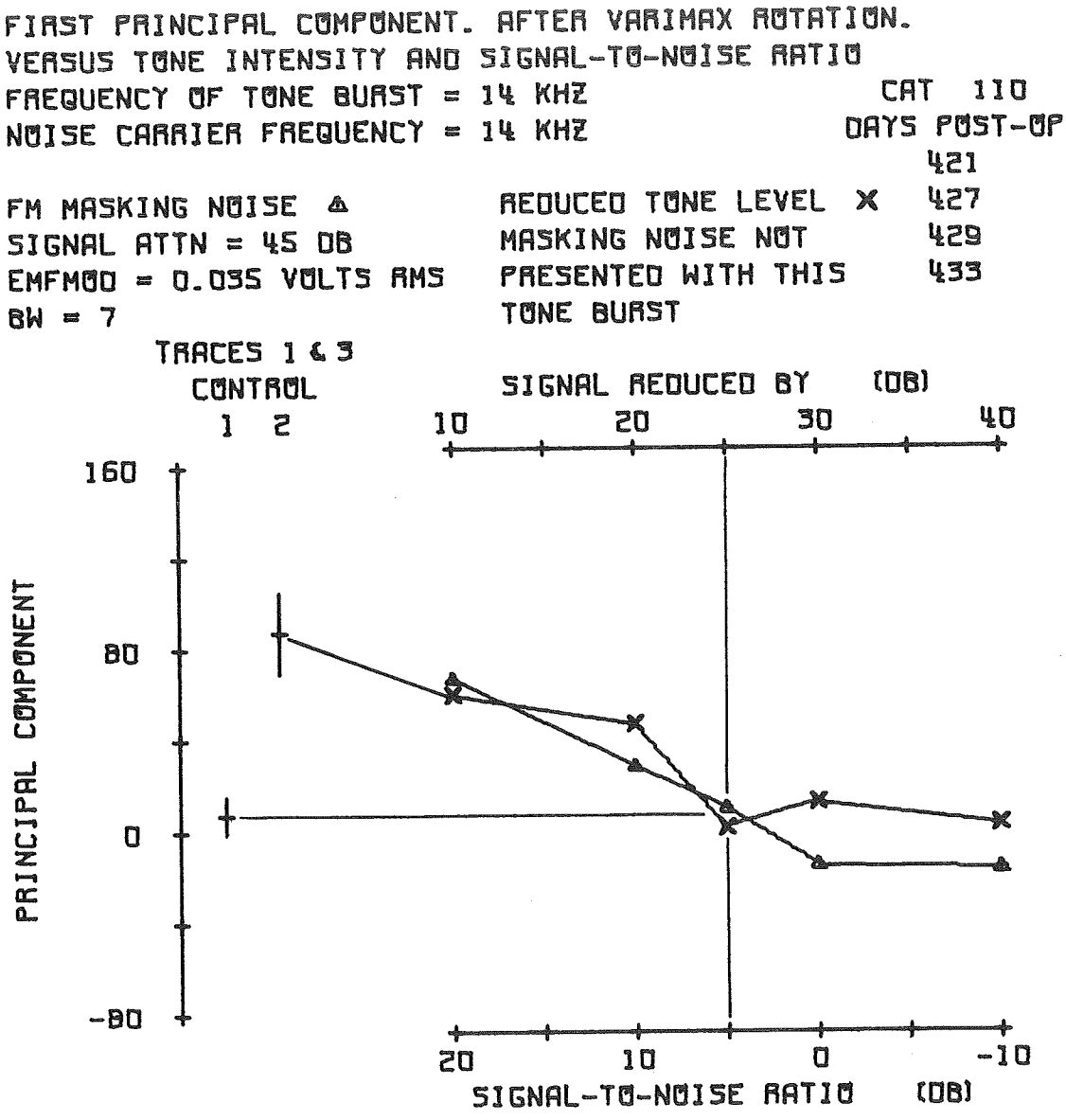

Fig. 70. Principal component 1A versus tone intensity and signal-to-noise ratio for cat 110.

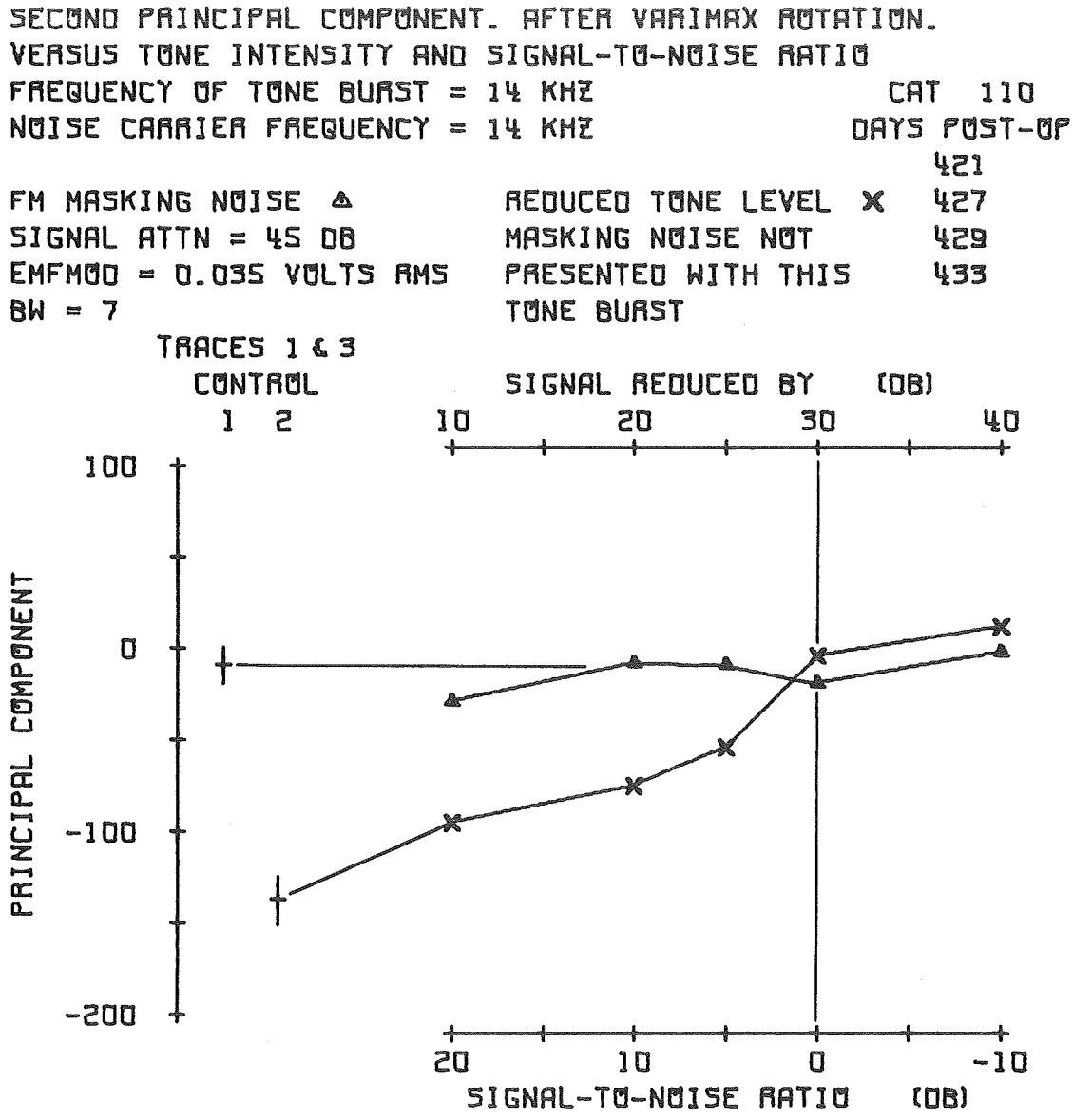

Fig. 71. Principal component 2A versus tone intensity and signal-to-noise ratio for cat 110.

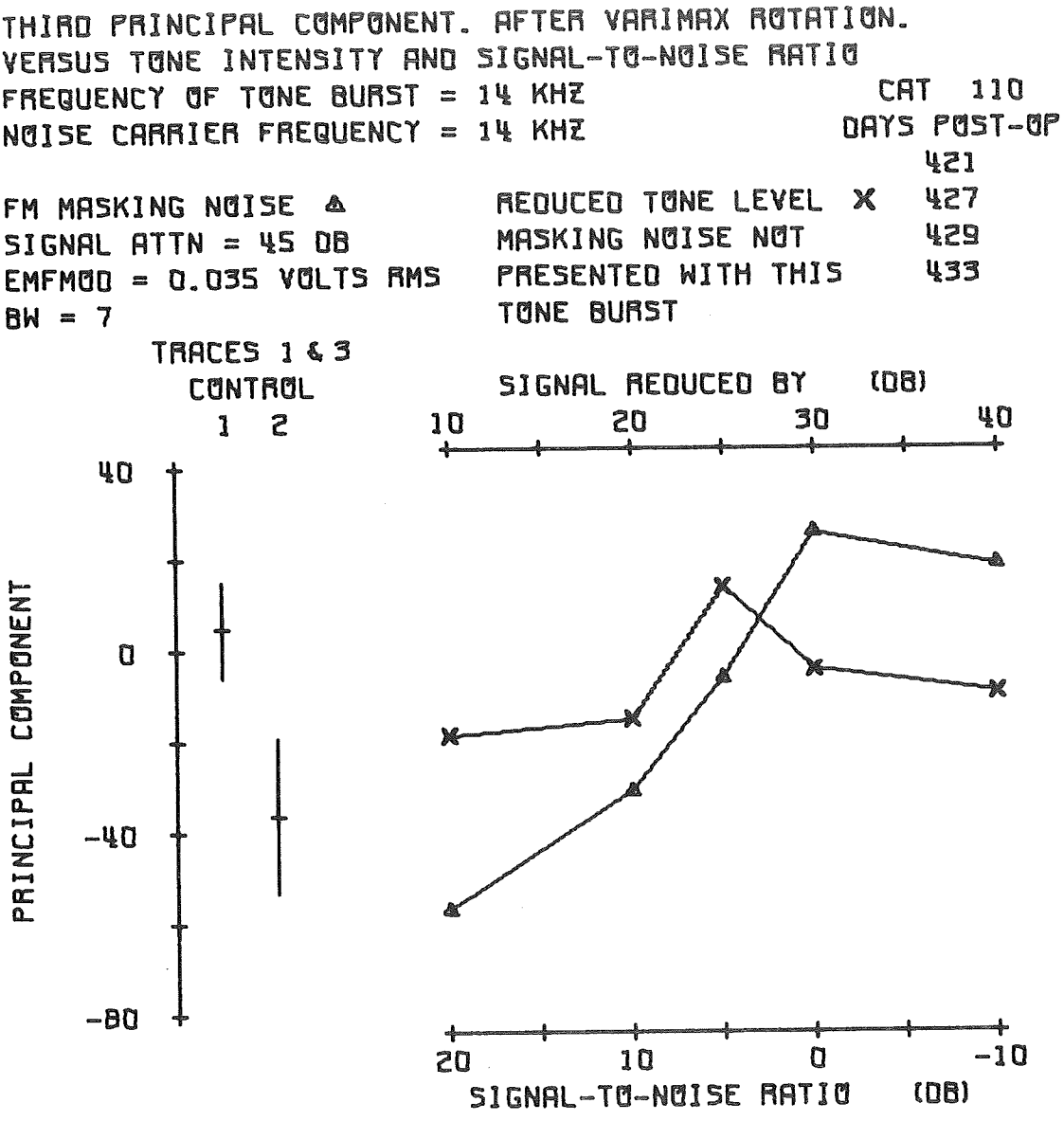

Fig. 72. Principal component 3A versus tone intensity and signal-to-noise ratio for cat 110.

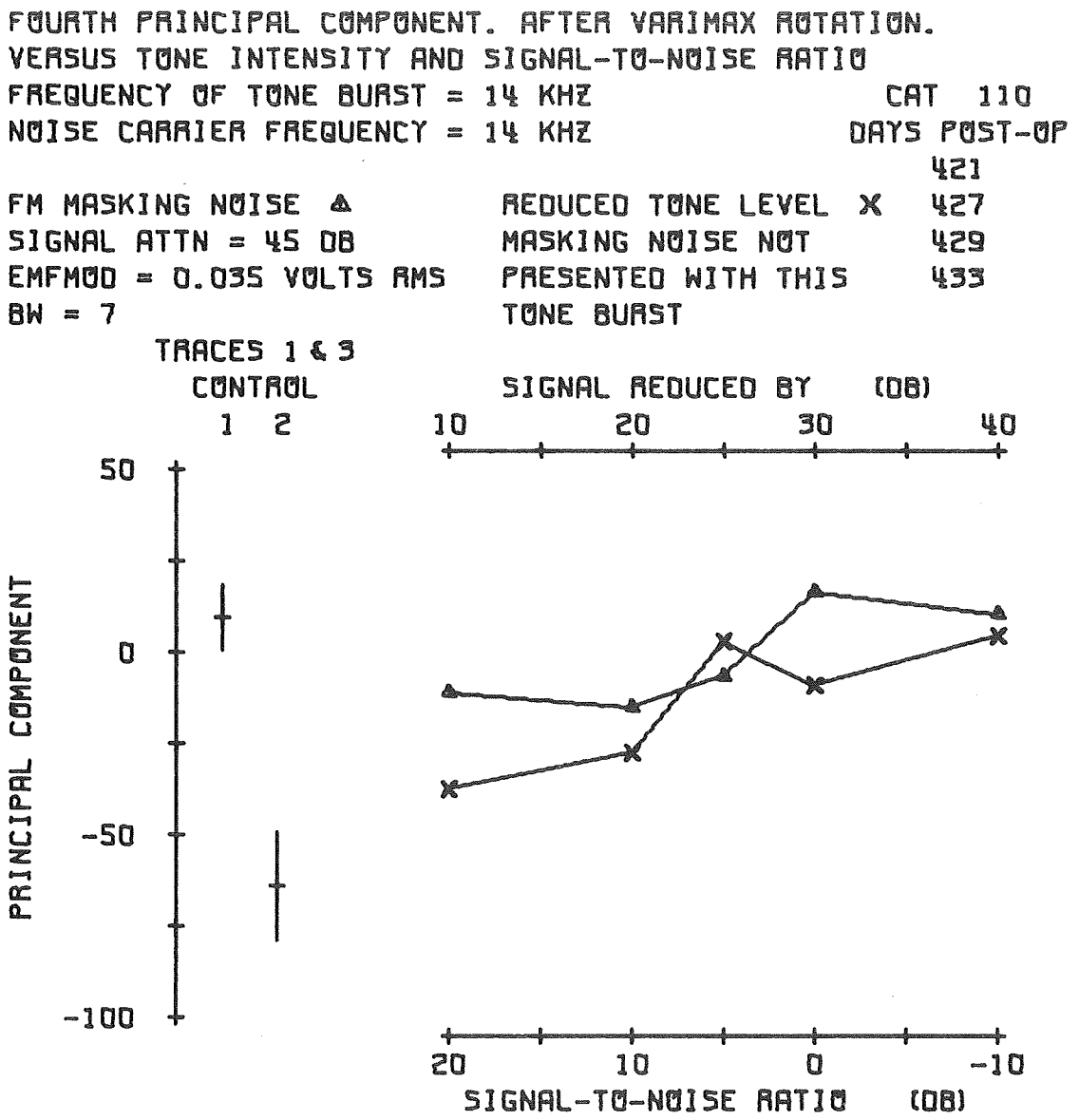

Fig. 73. Principal component 4A versus tone intensity and signal-to-noise ratio for cat 110.

cat 110. The principal component values for the control 1 and 2 runs were obtained from the average of traces 1 and 3. For control 2, the same stimulus (tone without noise) was used for all four traces. A line can be constructed between the control 2 principal component mean and the trace 4 principal component, "X" in the figures, at the abscissa coordinate "signal reduced by 10 dB". The limiting condition for the signal-to-noise would be an infinite ratio, i.e. tone without noise. For signal-to-noise ratios greater than 30 dB this condition should be approximated, since the noise intensity would be below the animal's threshold. Hence, as the tone intensity is reduced and as the signal-to-noise ratio is reduced (by increasing the noise level) the trace 2 and 4 principal components should change from their value for control 2 to their value for control 1, which should be close to zero.

Figure 68 shows this to be approximately true for the first principal component before varimax rotation. A tone which is reduced by 25 dB should still be 5 dB above threshold. This plot would indicate the threshold was 5 dB above what it was stated to be in table 1. However, the first eigenvector before varimax rotation has a latency range of 50 to 128 msec, and the late components are not reliable indicators of the stimulus level (see page 31 of the Introduction).

Figure 69 shows the plots for the second eigenvector before varimax rotation. The behavior of the trace 4 principal component is similar to that seen in figure 68. The threshold for this principal component is close to that stated in table 1. The behavior of the trace 2 principal component shows an interesting phenomenon. At signal-to-noise ratios up to 20 dB (noise only 10 dB above threshold) the masking is essentially complete. This behavior is characteristic of

ER_1 (page 31). The latency range for this eigenvector (19 to 43 msec) and the positive polarity of its principal component support the claim that the second eigenvectors before and after varimax rotation (these correspond to the fourth eigenvectors for cat 119) represent the ER_1 evoked response component. It can be seen in figure 71, that the 2A principal components behave in the same manner as the 2B components in figure 69. The latency ranges for these two eigenvectors are almost identical.

Figure 70 shows the principal component plots for the first principal component, after varimax rotation. This principal component is computed from the late (90 to 128 msec) portion of the average evoked response. Its behavior is similar to the 1B principal component. The third principal component after varimax rotation is shown plotted in figure 72 and behaves similarly to the 1A principal component. From table 5 it can be seen that the 3A eigenvector for cat 110 was not grouped with the corresponding eigenvectors from the other cats. A plot for the 3A principal component from cat 120 is shown in figure 74. Both figures 72 and 74 show that the behavior of this principal component, like evoked response component ER_2, is erratic. The 4A principal components for cat 110, figure 73, and cat 116, figure 75, display behavior similar to that described for evoked response component ER_3.

The behavior described for the principal components from evoked responses of cat 110 appears consistently in the other cats for the corresponding eigenvectors in each group (row blocks of table 5). As was found for the masking curves, the tone intensity and signal-to-noise ratio data for cat 119 showed the greatest variability in the

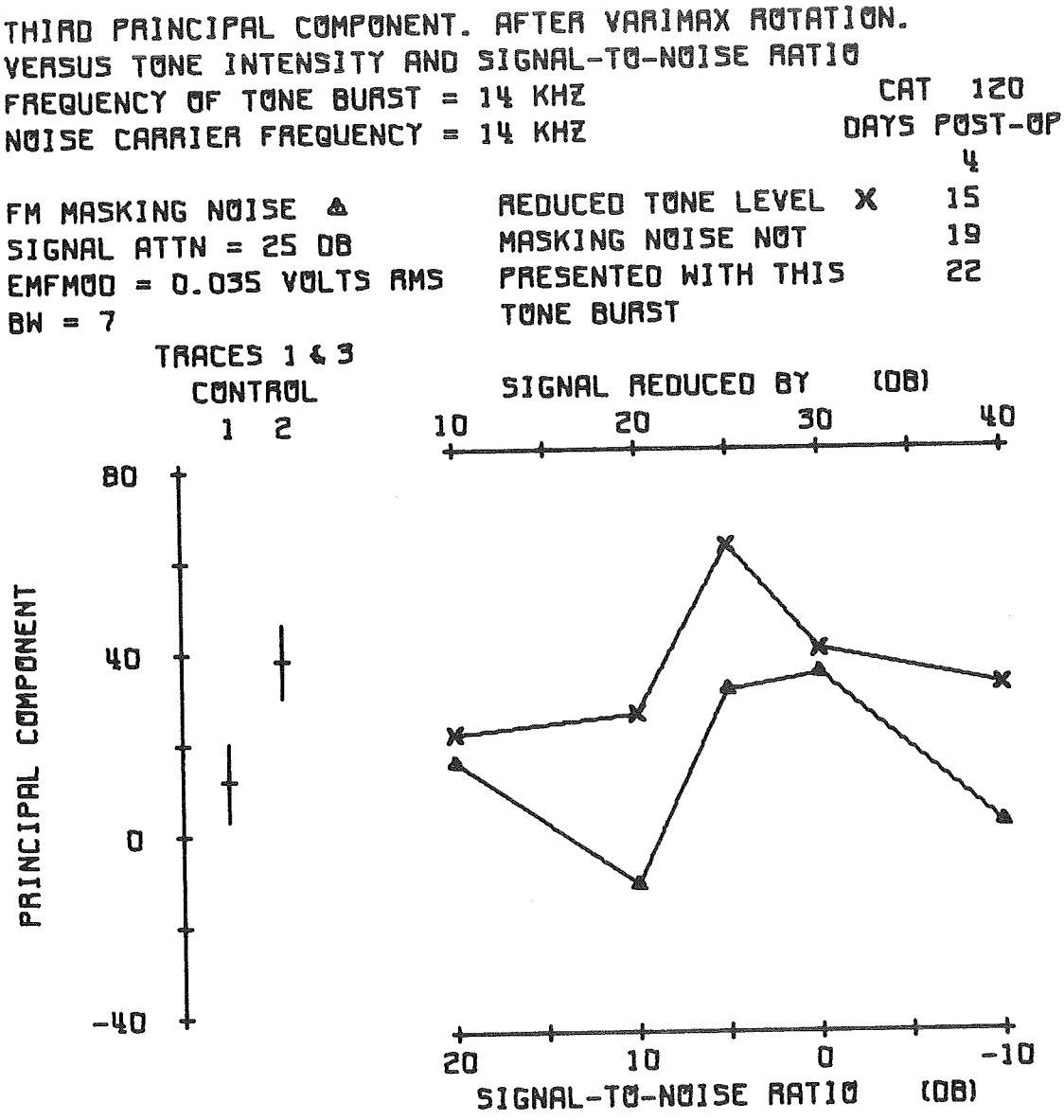

Fig. 74. Principal component 3A versus tone intensity and signal-to-noise ratio for cat 120.

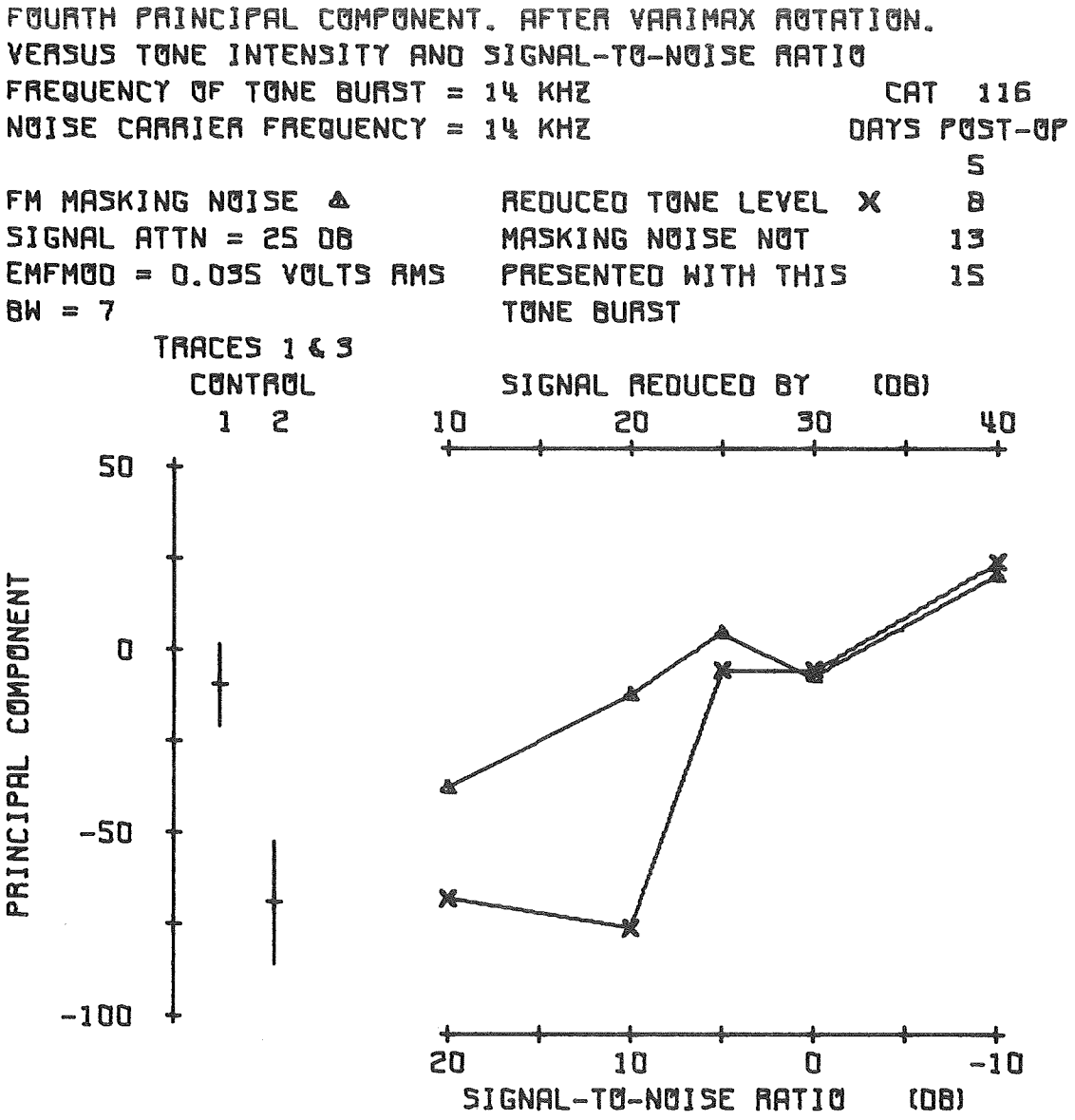

Fig. 75. Principal component 4A versus tone intensity and signal-to-noise ratio for cat 116.

plots but displayed no behavior which would contradict the above evidence for matching the 2A and 2B eigenvectors with ER_1, the 3A eigenvector with ER_2, and the 4A eigenvector with ER_3.* The very late (90-128 msec) component might be called ER_4 and would be matched with the 1A* eigenvector.

*These eigenvectors refer to cats 110 and 116. The corresponding eigenvectors (row blocks in table 5) for cats 119 and 120 are implied in making the comparisons.

DISCUSSION

Evoked potential correlates of the critical band have been observed in the cat at three center frequencies, 9, 14 and 22 KHz, using various structures of narrow band masking noise. The relative frequencies of the tone and noise were varied, one being varied over a 2 octave range centered about the other, which was fixed. The selection of center frequencies was governed, in part, by the frequency response of the sound system (Appendix F). The animal thresholds were such that only moderate intensity sounds were used (usually less than 80 dB re 0.0002 dyne/cm^2). During constant noise experiment sessions, the noise center frequency was held constant while the tone frequency was varied between runs. Only a 14 KHz center frequency was used because it was not possible, at the time, to measure the bandwidth of the noise. For this reason, the bandwidth of the FM noise was not changed systematically, as in Greenwood's experiments. It became apparent that Greenwood's method would not have worked here, because a very small amount of noise power in the critical band would have been sufficient to mask those components of the evoked response which were found to be the most sensitive to critical band masking. The measured noise spectra had Gaussian shapes and despite the large decrement in noise power near the 6 dB point in the spectrum, the decrement at frequencies in the region of the tails of the curve was small. It is the noise power in this region which would prohibit using Greenwood's method and which indeed probably contributed to the variability in the masking curve bandwidths which were measured in the present study.

Some studies of single unit response patterns to tonal stimuli have demonstrated the presence of neurons which were responsive to changes in frequency of tone, as opposed to changes in tone intensity (38, 39). On the basis of these observations it was decided to test for any differences in the masking effectiveness of AM and FM noise. The results of these experiments indicate that AM and FM masking noise produce equivalent masking results. It should be noted, however, that the average evoked response measured here is to a tone burst onset, and hence would not necessarily reflect activity in the units which are responsive only to frequency change. Masking of the average evoked response to swept tones using AM and FM noise may shed more light on this.

The average evoked response to 10 msec Gaussian onset tone bursts shows the ER_1, ER_2 and ER_3 evoked response components to clicks from cats described by Teas and Kiang (53). There are, however, several differences between the average evoked responses to the two types of stimuli. The evoked responses to the clicks are larger, the evoked response components are clearly separated and occur at shorter latencies. As the rise time of a tone burst is increased, the latencies of the evoked response components become longer and the amplitude of the evoked response becomes smaller. The ER_1 component shifts in latency more than ER_2 and these two components merge to the extent that they are not seen as separate components in many of the average evoked responses. These difficulties in measuring the evoked response are compounded by the presence of a masking noise and the apparent lability of the average evoked response to physiologic variables within the central nervous system. The fact that the variability in the average evoked response was not

much greater between runs (within and between experiment sessions) than within runs, indicates that the state of the animal was relatively constant. The variability seen within runs makes such an assessment difficult. It appears that the stability of the average evoked response could have been improved in two ways: 1) the intensity of the tone bursts could have been increased, and 2) the rise time of the tone burst could have been made shorter. Increasing the intensity of the tone would have increased the possibility of causing distortion in the sound system or of raising the level of any existing harmonics in the sound stimulus, which were down by at least 40 dB, above the animal's threshold. Decreasing the rise time of the tone burst would have made its spectrum considerably wider. A rise time of 10 msec (Gaussian shaped onset) results in a 6 dB bandwidth of less than 115 Hertz, while a 2.5 msec rise time would result in a spectrum four times as wide, thus diminishing the resolution available in measuring the critical bandwidth. It may be productive to use an experimental procedure similar to Zwicker's (6), where the threshold of a narrow band noise centered geometrically between two equally intense masking tones is measured as the separation of the tone frequencies is increased. Inasmuch as the AM and FM noise produced equivalent amounts of masking, these experiments could be performed using only very narrow band FM noise.

Many of the problems associated with measuring the amplitudes of the average evoked response components by hand are solved by subjecting the evoked response data to a principal component analysis. Each of the principal components quantifies a restricted segment of the average evoked response from which it is computed. The particular segment being

quantified is defined by the eigenvector associated with the principal component. It is not possible to see all of the evoked response components, ER_1, ER_2 and ER_3, in every average evoked response. However, the eigenvectors are determined by many average evoked responses measured under all of the experiment conditions and hence form templates for the various evoked response components. The eigenvectors reflect latency shifts within the evoked response data and thus can provide a more stable method of analyzing the average evoked response than the manual amplitude measurements which require separate judgments for each trace to be analyzed.

It should be noted that the number of (independent) eigenvectors which are meaningful is determined by the number of evoked response components which are made to vary independently. If the particular set of stimuli fails to elicit differential behavior by the different evoked response components, the entire evoked response will tend to act as a unitary phenomenon. It should be obvious from the data reported by Teas and Kiang (53) and the corresponding principal component data reported here, that the primary evoked cortical response is multidimensional.

The dimensionality of the average evoked response space is equal to the number of orthogonal coordinates (eigenvectors) required to span the space, i.e. the number of principal components required to specify the evoked responses to some selected degree of completeness. The dimensionality of the evoked response space, for the data reported here, is four. The first four principal components accounted for between 88 and 96 percent of the variance in the data. The eigenvectors were similar in shape between different sets, which were computed from different

cats or experiment sessions. The third and fourth eigenvectors, before varimax rotation, were usually not similar between eigenvector sets, but accounted for a relatively small amount of the information about the data.

It should be appreciated that the principal component analysis performs a linear decomposition of the average evoked response into a set of wave forms (the direction cosines of the eigenvector). These eigenvectors become, effectively, the evoked response components when multiplied by the particular principal components for an average evoked response. It has been shown here that these computed evoked response components display the correct polarity, latency, and behavior to, indeed, represent physiological components such as ER_1, ER_2 and ER_3. Two arguments can be presented against this interpretation: 1) under some stimulus conditions such as complete masking or the absence of the tone burst, the principal component computed for an evoked response is small, but of opposite polarity to the principal component calculated for a normal average evoked response, and 2) the linear decomposition of a waveform which is derived from a "complex" neuronal generator does not seem, a priori, to be physiologically realistic. Examination of the average evoked responses where masking is complete, or where the tone burst is not presented, reveals that, owing to background activity in the EEG, the baseline of the average evoked response shifts. This results in an occasional sign reversal in the principal component. Measuring the amplitude of the evoked response from the computed baseline would also result in evoked response components which occasionally show sign reversals. Hence the sign reversal is merely a manifestation of

CNS noise. The evidence against the second argument is not as simple because the actual mechanism for generating the evoked response is not completely known. However, two observations support a linear mechanism for the average evoked response: 1) Donchin and Lindsley (69) demonstrated that the average evoked response to a pair of perceived visual stimuli, spaced closely in time was equal to the linear sum of the average evoked responses to the stimuli presented separately; and 2) it was observed in experiments done previous to those reported here*, that the evoked response to a click plus a tone burst was equal to the linear sum of the evoked responses to the click and tone burst presented separately. In addition to these observations is the model by Towe (51) which supports a linear mechanism for at least some aspects of the evoked cortical response.

The principal components have been related to the various segments of the average evoked cortical potentials. Now the relation of these potentials to the critical band is discussed. As expected from the results of Teas and Kiang (53), the later portion of the evoked response (ER_2 and ER_3) did not demonstrate a close dependency upon the stimulus parameters. The earliest portion of the evoked response (ER_1) as represented by the second principal component for cats 110, 116 and 120 and by the fourth principal component for cat 119, displayed the greatest sensitivity to the sound stimulus conditions. There does not appear to be a simple explanation for the conformation of Greenwood's prediction of the critical bandwidth (equation 13b) at 14 KHz, but not at 9 and

*Cat 104, 7/29/66, run pairs 43 and 44. A click was presented 2 msec after the start of onset of a 10 msec rise time, 2 KHz tone burst.

22 KHz. If the measured bandwidth at 9 KHz had been smaller, it is possible that equation 13b could have been modified to conform to the measured bandwidths at the three frequencies. Since this is not possible with the present data, one or both of two areas for explanation may be appropriate. The first is concerned with the role of the primary auditory cortex in signal processing and the second concerns the manner in which the critical bandwidths were measured here.

The role of the primary auditory cortex in signal processing, as discussed here, follows more complete reviews of this topic presented elsewhere (70-72). A listener can describe four basic qualities of a sound: 1) loudness (intensity); 2) pitch (frequency); 3) location in space; and 4) temporal attributes such as duration or loudness and pitch fluctuations. The earliest theories of hearing were concerned primarily with the first two qualities, loudness and pitch. Of the two general theories of hearing, the volley and place theories of frequency-intensity analysis, the place theory seems to have gained the support of much of the early physiologic experiments (55, 73, 74). According to the place theory, the inner ear performs a spectral analysis of the incoming sound, different auditory nerve fibers being stimulated by the different frequencies. Intensity is supposedly reflected by the rate of firing of the neurons. This type of frequency-intensity analysis is presumably performed at the auditory cortex, with the lower auditory centers serving only as relay stations. The early theories of hearing are reviewed, by Whitfield (75), in the perspective of more recent investigation.

The experiments which demonstrated tonotopic organization within the auditory cortex were designed to investigate primarily the afferent

connections. The animals studied were under barbiturate anesthesia, and much of the complex behavior of the cortical auditory system was thus suppressed. More recent studies using either light anesthetic or no anesthetic have demonstrated some tonotopic organization of the auditory cortex, perhaps reflecting afferent influence, but that the frequency tuning at any location or between adjacent locations does not appear to be sufficient for the degree frequency discrimination which is observed from psychophysical experiments (17, 20, 39, 41, 56). Microelectrode studies indicate that within a column of tissue normal to the surface the neurons tend to possess similar characteristic frequencies (17, 42, 56), but that characteristic frequencies of adjacent columns can differ greatly.

Behavioral deficits which result from cortical ablation indicate that the function of auditory cortex may be related to analyzing the spatial and temporal properties of the sound stimulus (70, 71, 76, 77, 78). Supporting this are microelectrode studies showing the presence of units which respond only to novel stimuli such as clicks, noise or frequency modulated tone, or to sounds from sources having preferred locations relative to the animal's head (38, 39, 72, 79). It is still possible that some of the behavioral deficits occurred because the cortical ablation removed the influence of centrifugal activity from lower auditory centers which may be responsible for integrating temporal and spatial information (80). Summarizing (72), although the primary auditory cortex possesses some tonotopic organization, it appears unlikely that it is sufficient for performing frequency discrimination, or that frequency analysis is performed at this level.

Frequency may be a characteristic of the peripheral stimulus which, after processing at lower centers, has only a secondary importance at the primary auditory cortex. If this is truly the situation, then the earliest positive component of the average evoked response, which presumably heralds the arrival of a peripheral stimulus (81), may be a blurred reflection of more finely tuned frequency dependent events at lower centers. This would not account, specifically, for observing the theoretical critical bandwidth at one frequency but not at the other two frequencies, but is a very likely cause for much of the observed variability in the bandwidth measurements.

Although the lack of well defined tonotopic organization in the auditory cortex is certainly one possible cause for the failure to observe the predicted critical bandwidth at two of the three frequencies tested, an even more likely cause is the method employed in making the bandwidth measurements on the masking curves. One of the major disadvantages to the manual measurements made on average evoked response records is the inherent subjectivity. The principal component analysis provides an objective quantification of the average evoked response and frees the measurements from many chances for human error. How ironic it is; that after all of the sophisticated computer processing involved in the principal component analysis, the width of the masking curve is still measured with a ruler and a pencil.

Although it cannot be proven at the present time, it is probably safe to claim that subjecting the masking curves to a computer automated system of analysis would greatly improve the reliability of the measured bandwidths and might even result in a verification of equation 13b. The

most direct approach might be to make a least square fit of a standard curve, such as a Gaussian curve, to the masking curve and measure the bandwidth of this curve at either the 3 or 6 dB points. A second approach is a stepwise discriminant analysis (82) which can be applied directly to the evoked response, although its application to the principal components is probably preferred. This technique finds the linear combination of the minimum number of variables which maximizes the difference between two groups of data. It would be necessary to have a method of classifying a set of responses into masked and unmasked in order to set the proper boundaries for classifying future evoked responses. A third possible approach is the polynomial discriminant method described by Specht (83) for classifying vectorcardiograms. A linear or non-linear decision surface is created around clusters of points in an n-space using a set of training data. A Bayes strategy (84) is then used to classify future points added to the space. The set of unmasked principal components, all four after varimax rotation, would probably serve as the training data. Techniques similar to the polynomial discriminant method are used in computer recognition of a speaker's voice (85, 86). These represent only a few of the possible techniques, and almost any such analysis seems very likely to improve the bandwidth measurements associated with the critical band masking effects. Such improvements would not preclude the desirability of extending these experiments with improved stimulus conditions.

Although many of the masking curves for the later evoked response components were not classified as normal, some critical band effects were evident. It is likely that the analysis of these later components,

when combined with the analysis of ER_1 using one of the multivariate analysis techniques just described, will provide a better estimate of the masking bandwidth. If ER_1 reflects only the registration of afferent input to the primary auditory cortex, it might be postulated that ER_2 and ER_3 reflect various segments in the chain of events between sensory stimulation and stimulus recognition. Such a speculation receives support from experiments by Ruchkin and John (81) showing the existence of a positive component in the evoked response to visual stimuli, which followed an earlier positive component and had a latency of about 35 msec (ER_2?). This second component was shown to be dependent upon the animal's interpretation of the stimulus. If the animal recognized the conditioned stimulus, a 10 Hz flicker, and performed the learned response or if the learned response was performed to a novel, but similar, stimulus, i.e. the animal generalized, the second component in the evoked response was quite evident. If the animal failed to perform the learned response, i.e. failed to recognize or generalize, this second response component was absent or greatly attenuated.

It will be recalled that the critical bandwidth measurements were made from either sensory observations by a human listener, or on the basis of an animal's behavioral performance. The critical bandwidth measurements made here required no perception on the part of the experiment subject*. If the stimulus could be made to have meaning to the

*The response here were to tone burst onsets. The short term power spectrum is broader for this onset than for a tone which is at a study state level. What effect this has on the difference between results of average evoked response experiments and human listening experiments is difficult to assess.

SUMMARY AND CONCLUSIONS

1. Average evoked potentials were measured using chronically implanted epidural electrodes, located over the primary auditory cortex of awake cats. Critical band effects are evident from changes in the various segments of the average evoked response to tone bursts, imposed by narrow bandwidth masking noise.

2. A principal component analysis was applied to the average evoked responses, using the data variance-covariance matrix for initial (EIGEN) rotation. This analysis uses a linear decomposition of the average evoked response to provide an objective and parsimonious representation of the available information in terms of a few (4) orthogonal vectors which effectively span the average evoked response data space. The eigenvectors are the coordinate axes of the principal components. A varimax rotation was performed (VARMX) on the first four eigenvectors.

3. Several of the eigenvectors were found to be consistent between eigenvector sets, computed from different data, and between experiment sessions within the same set, as indicated by waveshape and variance measurements. The waveforms corresponding to the eigenvectors were found to be similar to the conventionally defined average evoked response components on the basis of polarity, latency, and corresponding principal component changes concomitant with changes in the stimulus parameters. The eigenvectors aid in determining where, within the evoked response, masking effects may be observed.

4. Principal components were plotted as a function of noise center frequency or tone frequency (masking curves). The plots showed a critical band effect which was most consistent for the principal component corresponding to the earliest evoked response component, defined as ER_1 by Teas and Kiang (53).
5. The 6 dB bandwidths of the masking curves confirmed Greenwood's (8) prediction at 14 KHz, equation 13b. The bandwidths measured at 9 and 22 KHz were not predicted by this equation, or, indeed, by any other simple equation. No difference was observed between bandwidths measured using AM and FM masking noise.
6. The principal component analysis, as used here, provided results which were compatible with, and only slightly more consistent than, results obtained from more conventional methods of measuring the average evoked response.
7. The failure of these results to show a functional relationship between masking curve bandwidth and frequency can be ascribed to both the inherent variability in the evoked response and the rather primitive methods used to analyze the principal component masking curves. The use of a more objective method to measure these bandwidths appears to be indicated.

APPENDIX A

Glossary of Terms

Term	Definition	Symbol
A1	see primary auditory cortex	
Auditory area I	see primary auditory cortex	
bel	the logarithm to the base 10 of the ratio of two powers, bel = Log P/P_o where P_o is a reference power	
BW	the symbol used in these experiments and computer programs to designate one of ten positions of a switch on the sample-and-hold and low-pass filter circuit of the noise generator	
CAT	computer of average transients, a trademark of Technical Measurements Corp.	
decibel	one-tenth of a bel. dB = 10 Log P/P_o where P_o is a reference power, dB = 10 Log I/I_o where I_o is a reference intensity, dB = 20 Log_{10} p/p_o where p_o is a reference rms pressure and $I = p^2/R$ where R is specific acoustic impedance	dB
difference limen	the differential threshold or just noticeable difference (JND), the minimum detectable change in intensity at constant frequency or the minimum detectable change in frequency at constant intensity	DL
EMFMOD	the symbol used in these experiments and computer programs to denote the rms voltage of the modulating voltage at the input of the voltage-controlled-frequency oscillator	
frequency	the number of cycles of a repetitive waveform in a unit of time, usually expressed as cycles per second, cps, or Hertz, Hz	cps or Hz
Hertz	one Hertz is equivalent to one cycle per second	Hz

I	intensity in watts/cm^2	
I_o	standard reference acoustic intensity = 10^{-16} watt/cm^2	
intensity	the power transferred across a unit area, usually expressed in watts/cm^2	I
intensity level	the intensity, relative to the standard reference acoustic intensity, expressed in decibles, dB = 10 Log_{10} I/I_o; numerically equal to SPL	IL
kilo-	thousand	K
level	the magnitude of a quantity relative to a reference quantity expressed in decibels	
loudness	the relative sensation of loudness of a sound compared to a sound of 40 phons	sone
loudness level	the intensity level of 1 KHz tone which has the same loudness	phon
masking	raising the sensation threshold for one stimulus by presenting a second stimulus	
mel	the unit of measure on a pitch scale	
phon	the unit of measure on the loudness level scale and numerically equal to the intensity level, in dB, of a 1 KHz tone	
pitch	the subjective quality primarily connected with frequency, the relative sensation of pitch of a sound compared to a 1 KHz tone of 40 phons which is arbitrarily designated as being 1000 mels	mels
Primary auditory cortex	Auditory area I (A1) - the only cortical auditory response area which is known to receive essential projections from the medial geniculate and generally considered (18) to lie posterior and vertical to the	

	suprasylvian sulcus, dorsal to the anterior ectosylvian sulcus and anterior to the posterior ectosylvian sulcus in cat.	
rms	root-mean-square, the effective value of voltage, current, pressure, etc for producing power, found by taking the square of the instantaneous values of a waveform, averaging them, and taking the square root of the average	
SL	sensation level, dB above threshold	
SPL	sound pressure level referred to the standard acoustic reference sound pressure, 0.0002 dyne/cm^2	
sone	the unit of measure on the loudness scale such that a 1 KHz tone having a loudness level of 40 phons has a loudness of 1 sone. A sound which gives the sensation of being twice as loud has a loudness of 2 sones, etc.	
sound pressure	the rms pressure of a sound, dyne/cm^2	p
sound pressure level	the sound pressure, relative to the standard reference acoustic sound pressure p_o = 0.0002 dyne/cm^2, expressed in decibels, dB = 20 Log p/p_o, numerically equal to IL	SPL
spectral density	the relative power contributed to the total power of a signal by each component frequency of the signal	
spectrogram	a plot of the spectrum	
spectrum	the power or intensity contributed by each component frequency of a signal. Frequency spectrum refers to the amplitude of the voltage, current, sound pressure, etc contributed by each component frequency of a signal, and is usually normalized.	

standard acoustic reference	arbitrarily chosen standards for power and intensity. For power, $P_o = 10^{-13}$ watts. For intensity, $I_o = 10^{-16}$ watts/cm^2 which at STP results in a sound pressure of $p_o = 0.0002$ dyne/cm^2 and corresponds roughly to acute auditory threshold for a 1 KHz tone
trace	the plotted average evoked response

APPENDIX B

APPENDIX C

APPENDIX H

Appendix B discusses the circuitry used to gate the input channels of the CAT, and control the auditory stimuli.

Appendix C discusses the circuitry used to create the pseudo-random trigger pulses.

Appendix H discusses the switching circuitry used to modify the auditory stimuli.

In the interest of cost and space saving, these sections have been omitted from this publication.

Requests for information on these sections should be addressed to the author at:

Division of Otolaryngology
University of Maryland Hospital
Baltimore, Maryland 21201

APPENDIX D

Bandwidth of the Masking Noise

The masking noise is a sinusoidal carrier which is either frequency modulated or amplitude modulated by a random A.C. voltage having a Gaussian amplitude distribution and a spectrum which is flat from zero to one of 10 switch selectable cut-off frequencies. An Allison Lab model 655 silicon diode noise source, having a flat spectrum from 5 Hz to 30 KHz, provides the initial random A.C. voltage. The sample-and-hold circuit samples the output of the Allison noise source at one of 10 switch selectable rates, designated by the BW setting and shown in Table D1. The voltage samples are statistically independent because the sample rate is low compared to the bandwidth of the Allison noise source. For this reason, the sample-and-hold circuit output bandwidth extends from D.C. (0 Hz) to the cut-off frequency imposed by the sampling rate. The output of the sample-and-hold circuit is filtered by a four stage active low-pass filter with a switch selectable (BW) cut-off frequency which is matched to the sample rate such that the output power of the modulating noise source is independent of its bandwidth. The same modulating noise can be used for both types of modulation (87).

When AM noise is desired, the modulating noise is amplified by a D.C. power amplifier (Hewlett-Packard model 6823A Harrison voltage controlled power supply) which applies the noise waveform to the current coil of a Hall multiplier (F. W. Bell model HM-4051 Hall-Pak multiplier). The modulating noise source voltage can be applied directly to the input of the voltage controlled oscillator and adjusted (EMFMOD) to

Table D1. Sample rates and measured noise bandwidths. The setting of a 10 position switch which controls the sample rate of the sample-and-hold circuit and the cut-off frequency of the four stage active low-pass filter is designated BW. The sample rate in samples per second is shown for each BW. The bandwidths in Hz at the 6 dB points of the noise amplitude spectra are shown for AM noise and for FM noise at several EMFMOD values. EMFMOD is the rms voltage at the input to the voltage controlled oscillator (FM modulator). The sensitivity of the voltage controlled oscillator is 7 KHz/volt at the input. The noise spectra were measured at a 14 KHz center frequency using a Tektronix 3L5 spectrum analyzer and an averaging computer.

BW	1	2	3	4	5	6	7	8	9	10
Sample Rate	12.7	25.5	51	102	204	408	816	1632	3264	6528
6 dB Bandwidth										
AM Noise					170	360	720	1.32K	2.6K	4.4K
FM Noise										
EMFMOD										
0.01					250		200			130
0.035							720			
0.05					1.0K		1.05K			425
0.10					1.8K		2.1K			1.35K

produce an FM noise bandwidth which is equal to the AM noise bandwidth at the same BW setting.

The bandwidth of the masking noise was measured at the output of either the AM or FM noise source using a Tektronix 3L5 spectrum analyzer. The horizontal sweep voltage of the oscilloscope swept the center frequency of the spectral window of the spectrum analyzer through the noise spectrum. An average response computer was synchronized with the sweep of the spectrum analyzer, and was used to accumulate the average noise amplitude spectrum. This spectrum was plotted, using an X-Y plotter connected to the computer, and the 6 dB bandwidth was measured. These bandwidths are shown in table D1 for the AM noise at BW settings of 5 to 10 and for the FM noise at several EMFMODs for BW settings 5, 7 and 10.

The AM noise bandwidth is a monotonically increasing function of BW. At a given BW, the FM noise bandwidth is a monotonically increasing function of EMFMOD (for at least the BWs and EMFMODs considered here). However, at a given EMFMOD the bandwidth of the FM noise decreases as the BW is increased above a particular setting. For smaller values of EMFMOD, the bandwidth of the FM noise reaches a maximum at lower settings of BW. It should be appreciated that behavior of this sort makes bandwidth estimates of the FM noise from mathematical computations extremely difficult (59, 60), and sells a lot of spectrum analyzers.

APPENDIX E

Tone Burst Characteristics

The tone bursts used in these experiments have trapezoidal envelope-waveforms with Gaussian leading and trailing edges. The Gaussian shaped onset is preferable to a linear rise because it minimized spectral spreading. The rise (and fall) time of the tone burst is 2.5 msec for constant noise experiment sessions and 10 msec for constant tone experiment sessions. The Gaussian edges are synthesized from a ramp function (88) as shown in figure E1. The rise time of the tone burst is defined as the rise time of the ramp, t_r, from which its envelope is derived.

The bandwidth of a trapezoidal pulse of long duration and Gaussian edges is less than the bandwidth of the corresponding Gaussian pulse. The bandwidth of the Gaussian pulse is presented here because it is easier to compute than the short term power spectrum of the tone burst onset, and is only slightly wider. The time function of a normalized Gaussian pulse, shifted to peak at zero time (for simplicity in computing its Fourier transform) is

$$f_{(t)} = \exp[-(t/\tau)^2/2] \qquad \text{(E1)}$$

When $t = \tau$, the function is at 0.606 of its peak value. For the synthesized Gaussian onset, the magnitude of τ is 0.325 t_r, and is measured from the time at which the onset reaches maximum (t_r). The Fourier transform of the Gaussian pulse is also Gaussian and is given by

$$F(\omega) = \tau(2\pi)^{1/2}\exp[-(\omega\tau)^2/2] \qquad \text{(E2)}$$

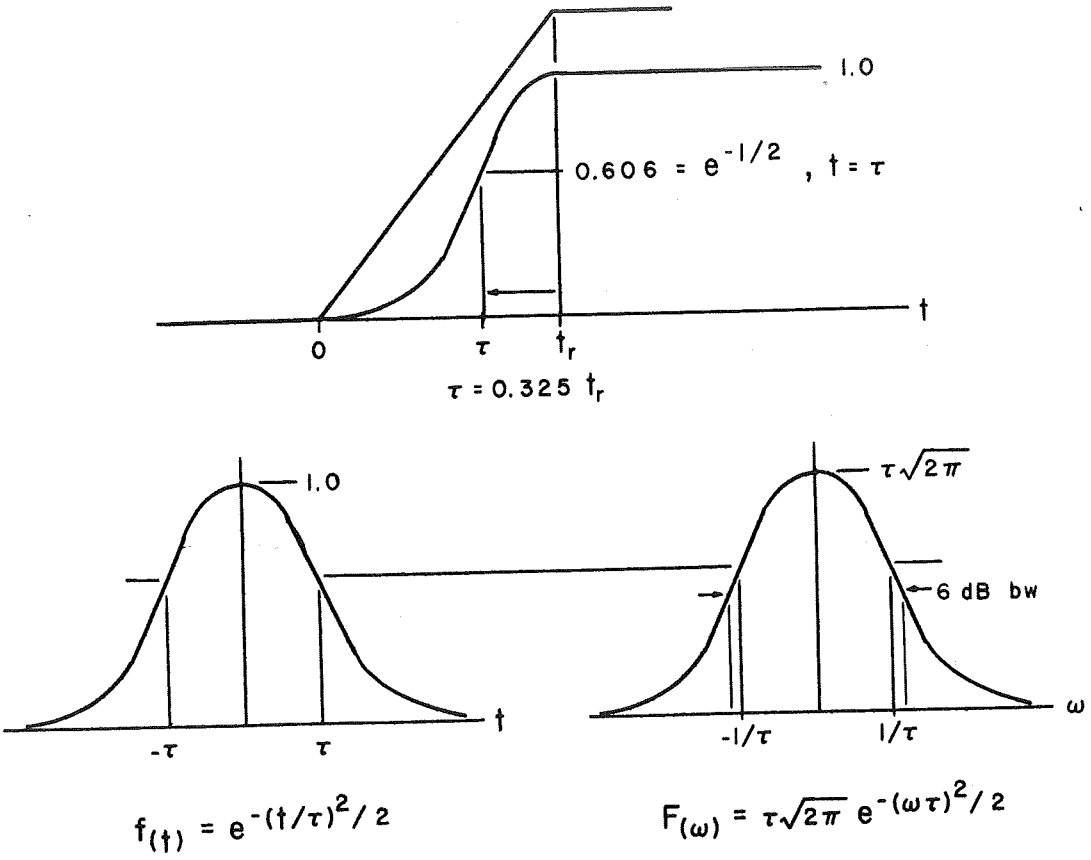

$$F_{(\omega)} = \tau\sqrt{2\pi}/2 \ , \quad (\tau\omega)^2/2 = 0.694$$

one-sided 6 dB bw = $\sqrt{1.388}/\tau$ rad/sec

total 6 dB bw = $0.375/\tau$ Hz

t_r msec	τ sec	6 dB bandwidth
2.5	0.81×10^{-3}	460 Hz
10.0	3.25×10^{-3}	115 Hz

Fig. E1. The onset envelope and spectrum of a tone burst.

$F_{(\omega)}$ is equal to 0.606 of its peak value when $\omega = 1/\tau$. What is desired, however, is the width of $F_{(\omega)}$ at its half amplitude (6 dB) value. The corresponding value of the exponent is 0.694, from which

$$\omega = (1.388)^{1/2}/\tau \qquad \text{radian/sec} \tag{E3}$$

$F_{(\omega)}$ is symetrical, and its bandwidth at the half amplitude level is double the magnitude of ω in equation E3. The total bandwidth in Hertz ($\omega = 2\pi f$) is then

$$6 \text{ dB bw} = 0.375/\tau \quad \text{Hz} \tag{E4}$$

where τ is in seconds. The computed bandwidths for the two rise times used in these experiments are shown at the bottom of figure E1. These bandwidths are slightly wider than the actual short term power spectra of the tone burst onsets.

The spectrum of a tone burst envelope-waveform is symetrical about zero frequency. When the envelope modulates a tone sinusoid, the spectrum is shifted along the frequency axis and is symetrical about the positive and negative frequencies of the tone (87).

APPENDIX F

Sound System Calibration

The frequency response of the sound stimulus system was measured under conditions which closely approximated the conditions which were present during the experiment sessions. A Bruel and Kjaer (B & K) model 2111 spectrum analyzer and 4133 one-half inch condensor microphone were used to measure the sound pressure level in free field. The microphone was placed on a stuffed pillow case, facing the Dukane Ionovac Duk 5 speaker, in about the same location as the animal's head would normally be, i.e. 60 cm from the speaker along its axis and 15 cm below this axis. The spectrum analyzer and other equipment were located external to the sound shielded room in order to maintain a sound field which was similar to that which would be present during an experiment. The bandwidth (3 dB) of the spectrum analyzer was 1/3 octave at each frequency tested. The tone oscillator output was set to 4.705 volts rms at 10 KHz (this reference was used during all of the experiments). A tone burst, 2.5 msec rise time, was generated at each 1/3 octave filter center frequency from 4 KHz to 31.5 KHz. The output of the spectrum analyzer was monitored with an oscilloscope. The height of the tone burst waveform was noted and a continuous tone of identical frequency as the tone burst was presented at the input of the spectrum analyzer, and adjusted to give the same amplitude on the oscilloscope as noted from the tone burst. This procedure was repeated at signal attenuator settings of 0, 25 and 45 dB, and the SPLs of the continuous tones (equivalent to the tone bursts) were read on the B & K meter and entered

on the plots in figure F1. It can be seen that the tone bursts delivered in free field by this system had SPLs which were within ± 5 dB of the SPL of a 14 KHz tone.

The narrow band noise equipment was essentially flat over the range of frequencies shown in figure F1, and used the same audio amplifier and speaker as the tone burst equipment.

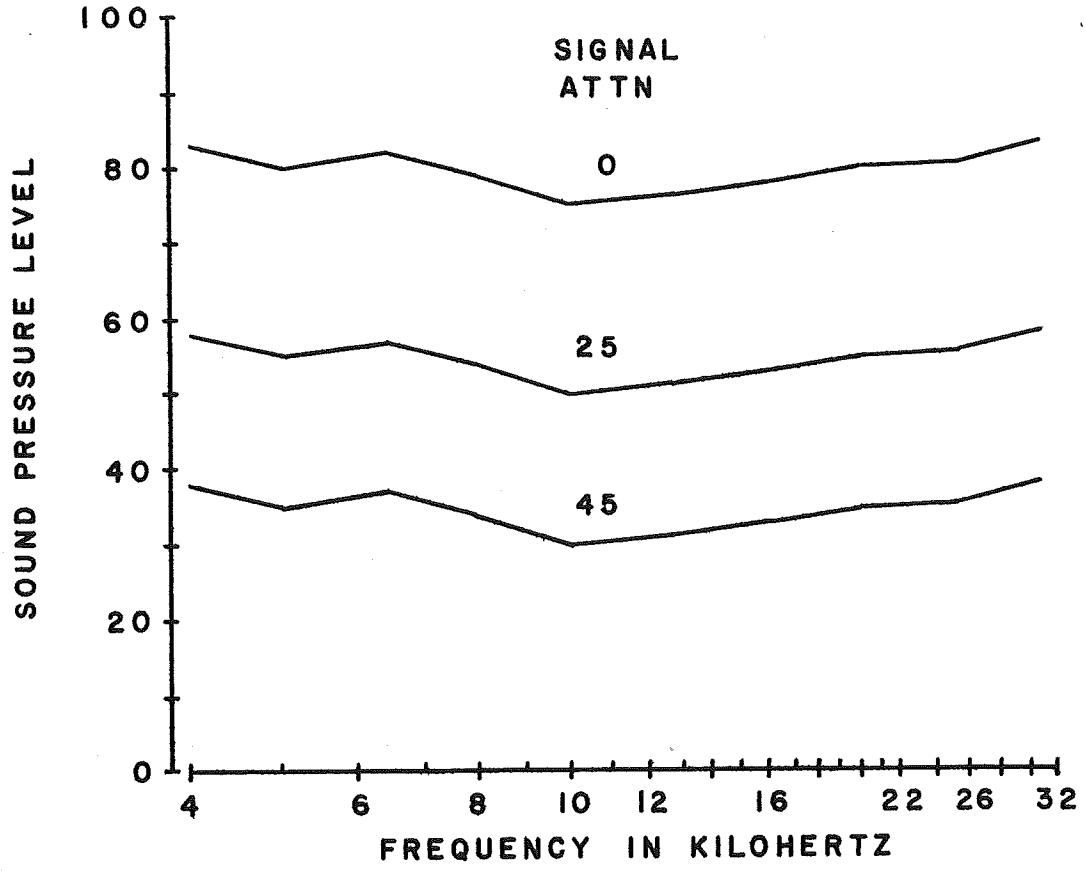

Fig. F1. Frequency response of the tone burst generator and audio system. The SPL measurements were made in free field using a B & K condensor microphone and audio spectrum analyzer.

APPENDIX G

Principal Component Analysis

The average evoked response can be considered as a vector in an n-space of large dimension, where n is the number of coordinates of the space; each coordinate corresponding to one of the n evenly spaced time points in the average evoked response. A principal component analysis provides an objective and compact method of describing the evoked response in terms of a few orthogonal vectors which effectively span the n-space. Before applying this technique to an entire evoked response, a brief introduction to principal component analysis is presented using the amplitudes at only two time points (23 and 39 msec) in the average evoked response.

A typical average evoked response is shown in the upper right corner of figure G1. The ordinate is the amplitude in microvolts of the average evoked response at each time point along the abscissa. The amplitudes of this average evoked response at 23 and 39 milliseconds are represented by the positions along the abscissa and ordinate, respectively, of a single point in the scattergram. Thus, each point in the scattergram represents the amplitudes of one (namely the j th) average evoked response at the two time points used (the i th and k th; where, in the present example, i = 23 and k = 39). The position of the j th point along the abscissa is the value of the j th observation of the variable x_i, and the corresponding position along the ordinate is the value of the j th observation of the variable x_k. The mean of the

x_{ij} = Amplitude of the jth Evoked Response at the ith Millisecond

$$\bar{X}_i = \sum_{j=1}^{N} x_{ij}/N$$

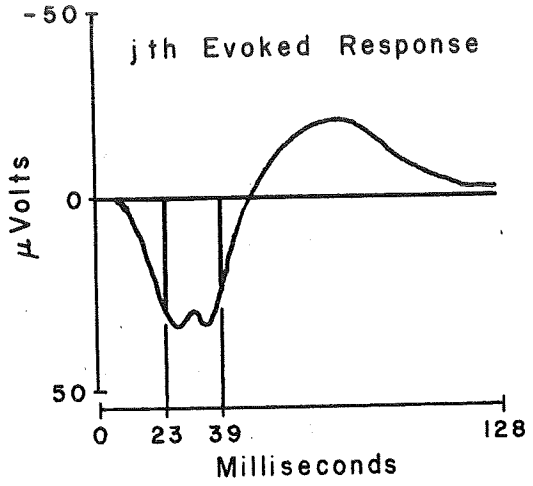

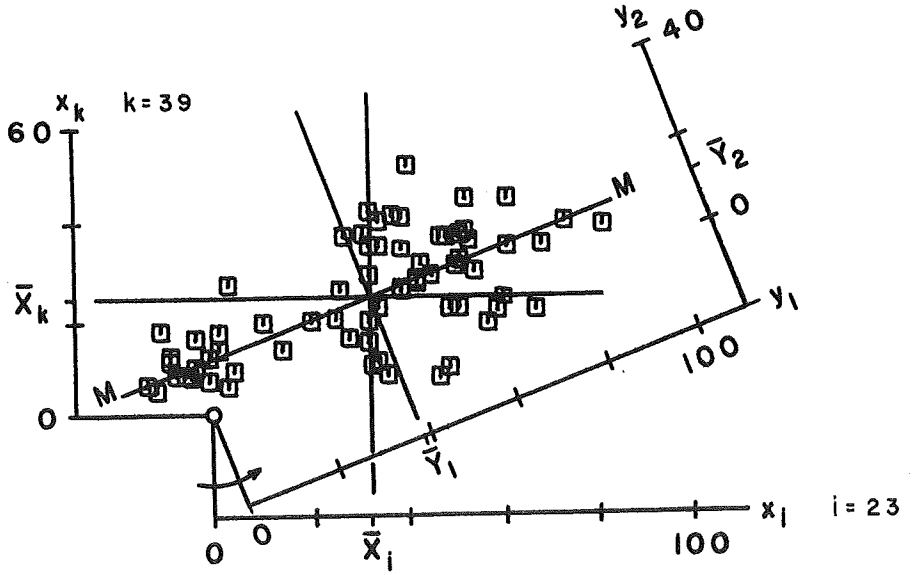

$$y_{1j} = (0.9352)x_{23j} + (0.3541)x_{39j}$$

$$y_{2j} = (-0.3541)x_{23j} + (0.9352)x_{39j}$$

VARIABLE	MEAN	VARIANCE	% VARIANCE	COVARIANCE
x_{23}	31	590	79.6	194
x_{39}	25	151	20.4	
y_1	38	663	89.5	0
y_2	12	78	10.5	

Fig. G1. A principal component analysis in a 2-space.

variable x_i is

$$\bar{X}_i = \sum_{j=1}^{N} x_{ij}/N \tag{G1}$$

where N is the number of data points (number of average evoked responses represented in the scattergram) and j references a particular data point (the j th data point, or the j th average evoked response). The unbiased estimate of the variance of the variable x_i is

$$R_{ii} = \sum_{j=1}^{N} (\bar{X}_i - x_{ij})^2/(N-1), \tag{G2}$$

and the standard deviation is

$$s_i = R_{ii}^{1/2} \tag{G3}$$

The unbiased estimate of the covariance of variables x_i and x_k is

$$R_{ik} = R_{ki} = \sum_{j=1}^{N} (\bar{X}_i - x_{ij})(\bar{X}_k - x_{kj})/(N-1), \tag{G4}$$

and the coefficient of linear correlation is

$$\rho_{ik} = \rho_{ki} = R_{ik}/s_i s_k. \tag{G5}$$

If x_{ij} and x_{kj} were uncorrelated, the probability that the j th data point was greater or less than both variable means would equal the probability that it was greater than one mean and less than the other. Knowing the value of one variable would be of no value in predicting the corresponding value of the other variable. The probability of $(\bar{X}_i - x_{ij})(\bar{X}_k - x_{kj})$ being greater than zero would be the same as the probability that it was less than zero and the mean value of this product, averaged over the N points, would then be zero. However, it can be seen from figure G1 that the data points are clustered about the line

MM, and as the value of x_{ij} increases, the corresponding value of x_{kj} tends to increase. Hence, some of the information about the location of the j th data point obtained from x_{ij} is repeated by x_{kj}. Specifying the average evoked response in terms of its principal components provides a parsimonious representation of the data by reducing this redundancy. To see how this is achieved, let the data points in figure G1 be defined in terms of two new variables, y_1 and y_2 which are measured along the axes y_1 and y_2, respectively. This new set of coordinate axes has several important properties: 1) it is obtained by a linear transformation (rotation) of the previous coordinate axes

$$\begin{bmatrix} y_{1j} \\ y_{2j} \end{bmatrix} = \begin{bmatrix} \cos\alpha & \sin\alpha \\ -\sin\alpha & \cos\alpha \end{bmatrix} \begin{bmatrix} x_{ij} \\ x_{kj} \end{bmatrix} \qquad (G6)$$

where α is the angle of rotation; 2) the maximum spread of the data (maximum variance) lies parallel to one of the axes (designated y_1); and 3) the covariance of y_{1j} and y_{2j} is zero. Because of these properties, the variables y_1 and y_2 are called principal components. The principal component with the largest variance (eigenvalue) is designated as the first principal component. The principal components are thus ranked by the size of their eigenvalues, with the first principal component containing the greatest portion of the information (variance) from the data, the second principal component having the greatest portion of the residual information, and so on for the remaining principal components. It can be seen from figure G1 that one of the x variables could account for 79.5% of the variance whereas the first principal component accounts for 89.5% of the variance.

In specifying the evoked responses in terms of their principal components it is necessary to know the transformation between the evoked response coordinates and the principal component coordinates. A geometric interpretation of this transformation is shown in figure G2. As noted in equation G6, the transformation is a rotation of the coordinates about the origin. The j th data point (located at point J in figure G2) can be expressed in terms of the evoked response coordinates, x_i and x_k, or in terms of the principal component coordinates y_1 and y_2. The equations shown in figure G2 apply to all of the data points; hence the subscript j can be omitted;

$$\begin{bmatrix} x_i \\ x_k \end{bmatrix} = \begin{bmatrix} \cos \alpha & -\sin \alpha \\ \sin \alpha & \cos \alpha \end{bmatrix} \begin{bmatrix} y_1 \\ y_2 \end{bmatrix} \tag{G7}$$

or in general matrix notation

$$[X] = [A][Y] \tag{G7a}$$

where each row of [A] is a set of component loading terms and each column of [A] is an eigenvector.* Equation G7a expresses the relation between the data variables and the principal components originally proposed by Hotelling (63). The sin α terms can be replaced by cos β terms, where β is the complementary angle of α. The i th amplitude

*As shown below, an eigenvector is a unit vector in an n-space along which a principal component is measured. The direction cosines of the m th eigenvector with respect to the n coordinates of the evoked response are the terms contained in the m th column of [A]. This set of direction cosines should, perhaps, be called an eigenfunction, but will be referred to as an eigenvector since this is the terminology commonly used.

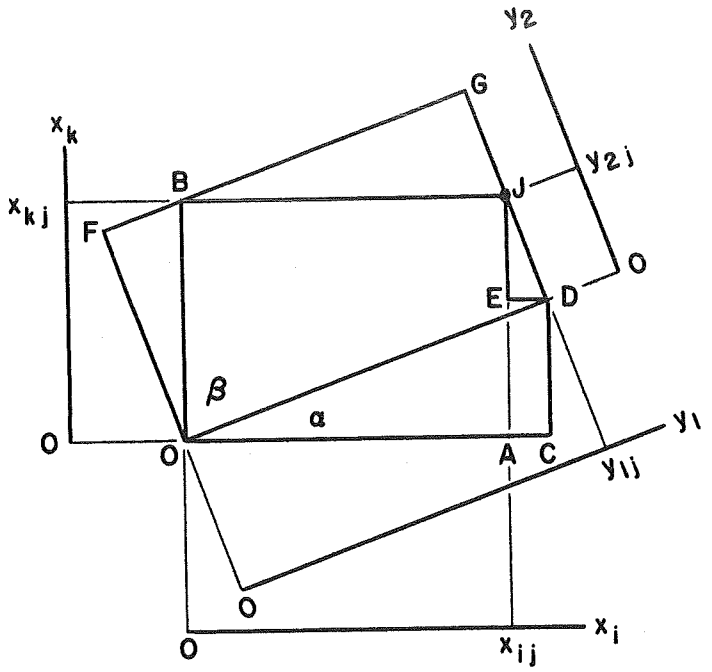

$$x_{ij} = OA = OC - AC = (\cos\alpha)y_{1j} + (-\sin\alpha)y_{2j}$$

$$x_{kj} = OB = AE + EJ = (\sin\alpha)y_{1j} + (\cos\alpha)y_{2j}$$

$$\begin{bmatrix} x_{ij} \\ x_{kj} \end{bmatrix} = \begin{bmatrix} \cos\alpha & -\sin\alpha \\ \sin\alpha & \cos\alpha \end{bmatrix} \begin{bmatrix} y_{1j} \\ y_{2j} \end{bmatrix} \qquad (G7)$$

$$y_{1j} = FG = BG + FB = (\cos\alpha)x_{ij} + (\sin\alpha)x_{kj}$$

$$y_{2j} = DJ = -JG + DG = (-\sin\alpha)x_{ij} + (\cos\alpha)x_{kj}$$

$$\begin{bmatrix} y_{1j} \\ y_{2j} \end{bmatrix} = \begin{bmatrix} \cos\alpha & \sin\alpha \\ -\sin\alpha & \cos\alpha \end{bmatrix} \begin{bmatrix} x_{ij} \\ x_{kj} \end{bmatrix} \qquad (G6)$$

Fig. G2. A geometric interpretation of the transformation from the evoked response (x) variables to the principal component (y) variables. The data point at J can be expressed in terms of either the evoked response variables or the principal components. The origin of both sets of coordinates is at 0, and the distance from the origin to any data point, or between any two data points, is unchanged by the transformation.

of the j th evoked response is thus

$$x_{ij} = \sum_{m=1}^{n} a_{im} y_{mj} \tag{G8}$$

where the n a_{im} terms are the cosines of the angles between the i th evoked response amplitude axis and the n principal component axes*, called the component loadings.

The lower set of equations in figure G2 is used to compute the principal components from the evoked response amplitudes. Omitting the subscript j

$$\begin{bmatrix} y_1 \\ y_2 \end{bmatrix} = \begin{bmatrix} \cos\alpha & \cos\beta \\ -\cos\beta & \cos\alpha \end{bmatrix} \begin{bmatrix} x_i \\ x_k \end{bmatrix} \tag{G9}$$

where the sin α terms have been replaced by the cos β terms. Note that the rows of the transformation matrix in equation G7 are the columns of the transformation matrix in equation G9. Thus, in general matrix notation

$$[Y] = [A]^T[X] \tag{G9a}$$

where $[A]^T$ is the transpose of $[A]$. The m th principal component, computed from the j th evoked response is

$$y_{mj} = \sum_{i=1}^{n} a_{mi} x_{ij} = A_m \cdot X_j \tag{G10}$$

where a_{mi}, i = 1, n is the m th eigenvector, A_m. A more concise definition of the y_{mj} is that it is the dot product of the m th eigenvector

*For the axes in figure G2 the a_i terms would be;

$a_{i1} = \cos\alpha$, $a_{12} = -\cos\beta$ and the a_k terms would be;

$a_{k1} = \cos\beta$, $a_{k2} = \cos\alpha$

and the j th evoked response vector, which is a data vector in an n-space (64); the n coordinates of the space corresponding to the amplitudes of the evoked response at n successive time points.* Geometrically, the m th eigenvector is the unit vector, along which the m th principal components are measured for the N evoked responses. The requirement of unit length for the eigenvector can be demonstrated by considering the distance between points in the n-space of the data. The distance from the origin to any data point or between any two data points in figure G2 is the same whether they are measured in terms of the evoked response coordinates or the principal components. The same applies to data points in an n-space. The square of the distance from the origin to any point J in an n-space is

$$D^2(J) = \sum_{i=1}^{n} x_{ij}^2 = \sum_{m=1}^{n} y_{mj}^2 \qquad \text{(G11)}$$

Substituting equation G8 in equation G11

$$\sum_{m=1}^{n} y_{mj}^2 = \sum_{i=1}^{n} \left[\sum_{m=1}^{n} a_{im} y_{mj} \right]^2 \qquad \text{(G12)}$$

The right side of equation G12 can be written to give

$$\sum_{m=1}^{n} y_{mj}^{\ 2} = \sum_{i=1}^{n} \sum_{p=1}^{n} \sum_{m=1}^{n} a_{ip} a_{im} y_{pj} y_{mj} \qquad \text{(G13)}$$

Equation G13 hold if, and only if,

$$\sum_{i=1}^{n} a_{ip} a_{im} = \delta_{pm} \qquad \text{(G14)}$$

*A vector from O to J in figure G2 would be the j th data vector in a 2-space.

where δ_{pm} is the Kronecker delta which is equal to unity when p = m, and equal to zero otherwise. Thus

$$\sum_{i=1}^{n} a_{im}^{2} = 1 \tag{G15}$$

and the length of the eigenvector is unity.

Summarizing the previous discussion; a set of variables, x_{ij}, i = 1, n, some of which are correlated can be expressed by a set of n uncorrelated principal components, y_{mj}, m = 1, n, by means of a suitable linear transformation, $[A]^T$. Figure G3 shows the matricies which are used in a principal component analysis. The figure shows the data matrix, [X], being computed from the product of the transformation matrix [A] and the principal component matrix [Y]. The analysis of the evoked responses requires that the principal component matrix be computed from the product of the data (evoked response) matrix and the transformation matrix $[A]^T$. From equation G14

$$[A]^T[A] = [I] \tag{G16}$$

where [I] is the identity matrix (unities in the diagonal and zero elsewhere). Hence

$$[A]^T[X] = [Y] \tag{G9a}$$

The unbiased estimate of the eigenvalue (variance) of the m th principal component is

$$\lambda_m = \sum_{j=1}^{N} (\bar{Y}_m - y_{mj})^2/(N-1) \tag{G17}$$

The expression for the unbiased estimate of the covariance of the principal components is

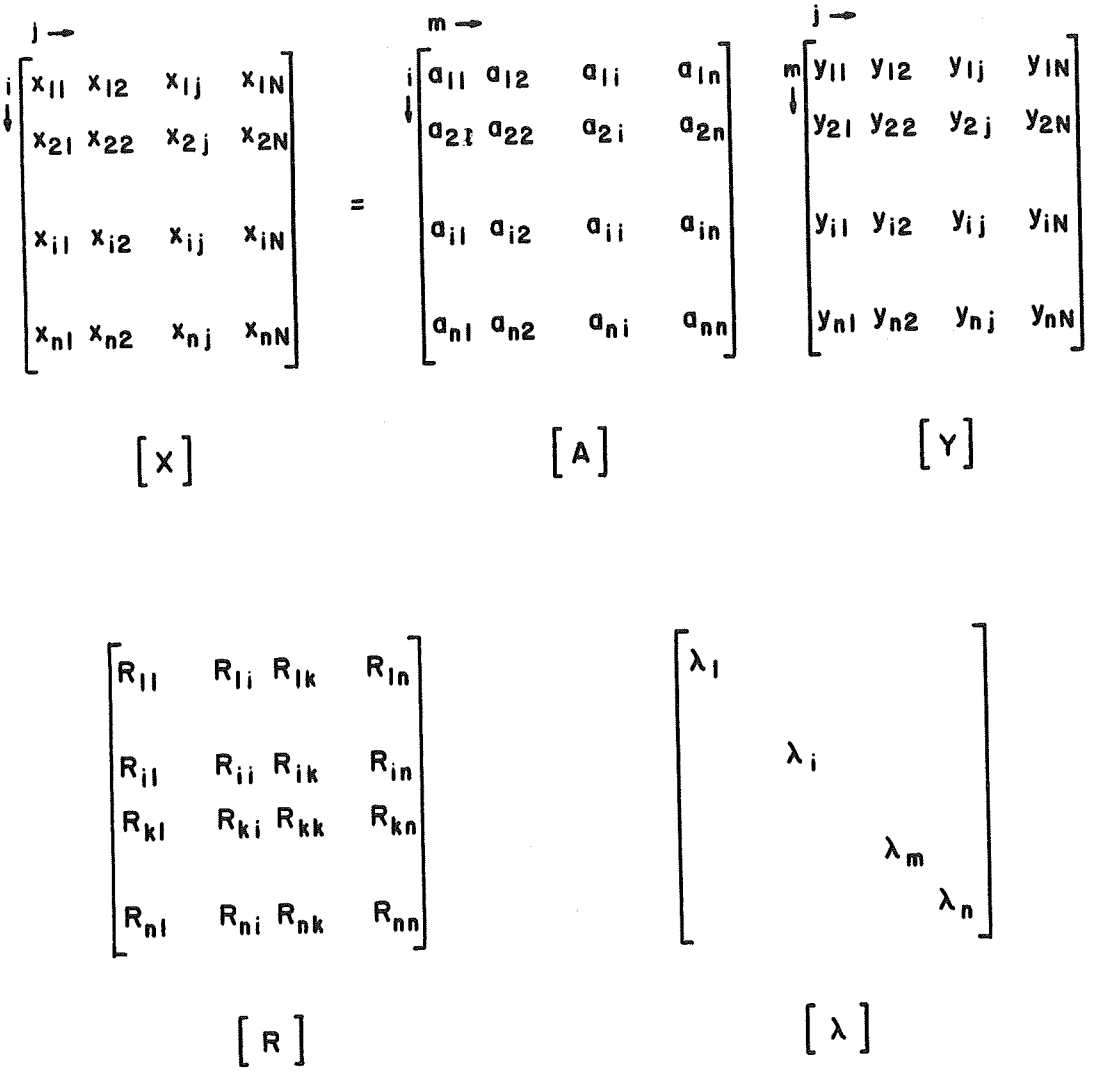

Fig. G3. The matricies used in a principal component analysis. The j th column of [X] contains the n amplitudes of the j th evoked response. [A] is the transformation matrix; rows are the component loadings and columns are the eigenvectors. The j th column of [Y] contains the set of n principal components for the j th evoked response. [R] is the variance-covariance matrix of the N evoked responses ($R_{ik} = R_{ki}$). [λ] is the eigenvalue (variance) matrix of the N sets of principal components. The covariances (off-diagonal elements) of the eigenvalue matrix are zero.

$$\lambda_{pm} = \sum_{j=1}^{N} (\bar{Y}_p - y_{pj})(\bar{Y}_m - y_{mj})\delta_{pm}/(N-1) \qquad (G18)$$

The covariances of the data can be expressed in terms of eigenvalues as follows. Start with

$$R_{ik} = \sum_{j=1}^{N} (\bar{X}_i - x_{ij})(\bar{X}_k - x_{kj})/(N-1) \qquad (G3)$$

Substitute equation G8 into equation G3

$$R_{ik} = \sum_{j=1}^{N} \sum_{m=1}^{n} a_{im} a_{km} (\bar{Y}_m - y_{mj})^2/(N-1) \qquad (G19)$$

Substituting equation G18 into equation G19 gives

$$R_{ik} = \sum_{m=1}^{n} a_{im} a_{km} \lambda_m \qquad (G20)$$

from which

$$R_{ii} = \sum_{m=1}^{n} a_{im}^2 \lambda_m \qquad (G21)$$

The total variance is

$$R_T = \sum_{i=1}^{n} R_{ii} = \sum_{m=1}^{n} \lambda_m \qquad (G22)$$

The contribution of the m th principal component to the total variance is given by the m th eigenvalue, λ_m. By definition of the principal components the first principal component is the one which makes the largest contribution to the total variance. The first step in computing the transformation matrix to be used in the analysis is to compute the terms of the first eigenvector, a_{i1}, i = 1, n, so as to maximize

$$S_1 = \sum_{i=1}^{n} a_{i1}^2 \lambda_1 \qquad (G23)$$

under the conditions of equation G20, where S_1 is the contribution of

the first principal component to the total variance (since from equation G15, $\sum_{i=1}^{n} a_{i1}^2 = 1$). The number of constraints imposed on this operation is only $n(n+1)/2$, because $R_{ik} = R_{ki}$. The method of Lagrange multipliers (89) is used to maximize a function of n variables (equation G23) which are related by a number of conditions (equation G20).

Let

$$2T = S_1 - \sum_{i=1}^{n} \sum_{k=1}^{n} \mu_{ik} R_{ik} \tag{G24}$$

where μ_{ik} are the Lagrange multipliers.

Substituting equations G20 and G23 into equation G24

$$2T = \sum_{i=1}^{n} a_{i1}^2 \lambda_1 - \sum_{i=1}^{n} \sum_{k=1}^{n} \sum_{m=1}^{n} \mu_{ik} a_{im} a_{km} \lambda_m \tag{G25}$$

Setting the first partial derivative of T with respect to any one of the n a_{i1} terms equal to zero and dividing through by 2

$$\frac{\partial T}{\partial a_{i1}} = \lambda_1 a_{i1} - \sum_{k=1}^{n} \mu_{ik} a_{k1} \lambda_1 = 0 \tag{G26}$$

from which

$$a_{i1} = \sum_{k=1}^{n} \mu_{ik} a_{k1} \tag{G27}$$

and

$$a_{ki} = \sum_{i=1}^{n} \mu_{ik} a_{i1} \tag{G27a}$$

Setting the first partial derivative of T with respect to any other $a_{im} (m \neq 1)$ equal to zero

$$\frac{\partial T}{\partial a_{im}} = - \sum_{k=1}^{n} \mu_{ik} a_{km} \lambda_m = 0 \tag{G28}$$

and combining equations G26 and G28

$$\frac{\partial T}{\partial a_{im}} = \delta_{lm}\lambda_m a_{il} - \sum_{k=1}^{n} \mu_{ik} a_{km}\lambda_m = 0 \qquad \text{(G29)}$$

Multiply equation G29 by $\sum_{i=1}^{n} a_{il}$

$$\delta_{lm}\lambda_m \sum_{i=1}^{n} a_{il}^2 - \sum_{k=1}^{n} a_{km}\lambda_m \sum_{i=1}^{n} \mu_{ik} a_{il} = 0 \qquad \text{(G30)}$$

Substituting equations G23 and G27a into equation G30

$$\delta_{lm}\lambda_m S_l / {}_l - \sum_{k=1}^{n} a_{km}\lambda_m a_{kl} = 0 \qquad \text{(G31)}$$

and multiplying by $\sum_{m=1}^{n} a_{im}$

$$\sum_{m=1}^{n} \delta_{lm}\lambda_m a_{im} S_l/\lambda_l - \sum_{k=1}^{n} a_{ki} \sum_{m=1}^{n} a_{im} a_{km}\lambda_m = 0 \qquad \text{(G32)}$$

Substituting equation G20 into equation G32 and carry out the summation over m

$$a_{il} S_l - \sum_{k=1}^{n} a_{ki} R_{ik} = 0 \qquad i=1,2,\ldots n \qquad \text{(G33)}$$

The equations G33 can be written out, dropping the subscript on S, since it can take on any of n values:

$$\begin{aligned}
&a_{11}(R_{11}-S) + a_{21}R_{12} + \ldots + a_{n1}R_{1n} = 0 \\
&a_{11}R_{21} + a_{21}(R_{22}-S) + \ldots + a_{n1}R_{2n} = 0 \\
&\quad\vdots \qquad\qquad\qquad\qquad\qquad\qquad \vdots \\
&a_{11}R_{n1} + \ldots\ldots\ldots\ldots + a_{n1}(R_{nn}-S) = 0
\end{aligned}$$

If the solution of the equations G33 is non-trivial, the determinant of the coefficients of the n a_{il} terms must be zero

$$\begin{vmatrix} (R_{11}-S) & R_{12} & \cdots & R_{1n} \\ R_{21} & (R_{22}-S) & \cdots & R_{2n} \\ \vdots & & & \vdots \\ R_{n1} & \cdots & \cdots & (R_{nn}-S) \end{vmatrix} = 0 \qquad \text{(G34)}$$

Expanding this determinant leads to an n-order polynomial in S which is called the characteristic equation. The n roots of this polynomial are the n eigenvalues. Substituting the largest eigenvalue, S_1, into equation G33 under the conditions of equation G14 permits the determination of the first eigenvector (a_{i1}, i = 1, 2, $\cdots$, n). Substituting the second largest root, S_2, into equation G33 under the conditions of equation G14 permits the determination of the second eigenvector; and similarly for the remaining eigenvectors.

The above procedure serves to establish a mathematical method for computing the transformation matrix (of eigenvectors) which is necessary for transforming evoked response variables into principal components. Because the variance-covariance matrix from these evoked response data is a real symmetric matrix of large size (64 x 64), the eigenvector computations are performed on a large computer (IBM360/44) using an IBM scientific subroutine (EIGEN) which employs the Jacobi method of determining the characteristic roots (66). This involves a series of elementary orthogonal transformations which reduce the off-diagonal elements of [R] to near zero. The product of all of these elementary transformations is a set of eigenvectors which, after sorting by value of the corresponding eigenvalues, is the transformation matrix $[A]^T$.

The principal component analysis derived here is based on the diagonalization of the variance-covariance matrix. An alternative is to diagonalize the matrix of correlation coefficients (44) or reduced correlation matrix (64). This has the effect of normalizing the original variables, thus giving each equal weight in determining the orientation of the eigenvectors. For instance, using the correlation matrix from the data in figure G1 results in an angle of rotation of 45 degrees instead of 20 degrees, since the normalized variable x_k has the same weight as x_i. This situation is particularly useful when the original variables are measures of different parameters, such as a set of psychological tests, or if evoked responses from different parts of the nervous system (between which signal strengths vary) are being pooled for analysis (44). In the present data, the evoked responses from each cat are all measured by the same electrode and the time points which have the larger voltage amplitudes are generally considered the important parts of the average evoked response. Using the variance-covariance matrix tends to give these variables (time points) more influence on the eigenvector orientation than those time points where the average evoked response amplitude is usually near zero. Implicit in this argument is the assumption that the time points with the larger voltage amplitudes will also have the larger variances. If a set of stimuli were presented which caused no variation in a particular large amplitude component in the evoked response, the cosine of the angles between the corresponding time coordinates and any of the more important eigenvectors would be small.

If the full benefit of a principal component analysis is to be derived, the number of principal components used to specify an evoked response must be less than the number of original variables (64 in the data analyzed here). The question is then, how many principal components should be retained for subsequent analysis of the data. Several approaches to testing the statistical significance of each successive eigenvalue have been reviewed (64, 65) with Harman expressing a distinction between statistical significance and "practical significance". The latter is applied here in the following manner. The first four principal components always accounted for more than 85 % of the variance in the evoked response data. The fourth principal component always accounted for more than 3.5 % of the variance while the fifth principal component usually accounted for less than 3 % of the variance. Since it was not known whether the eigenvectors were unique to a particular set of data, an initial principal component analysis was performed for each experiment session (68 average evoked responses) separately. Comparison of eigenvectors from 25 sessions with one cat revealed that the eigenvectors for the first two principal components are fairly similar between sessions. A third eigenvector, obtained for either the third or fourth principal component, was also present in most of the results. On the basis of similarity of the first four eigenvectors between separate analyses and the large portion of the information (variance) they absorbed, the evoked response data for each cat from experimental sessions which had similar auditory stimulus parameters were pooled and a principal component analysis performed,

with the first four principal components being retained for subsequent analysis.

The first four eigenvectors obtained by diagonalizing the variance-covariance matrix for one of the 25 experiment sessions analyzed separately are shown in figure C4 under the column heading, "Before varimax rotation." The varimax rotation is discussed below. The ordinates for the eigenvectors have no units since they indicate the cosine of the angle between the eigenvector and each of the n (n=64) time coordinates, the n a_{mi} terms. All of the average evoked responses from this experiment session were pooled to form the mean of the average evoked responses which is shown below the eigenvectors. The ordinate is in microvolts with positive at the active electrode being plotted downward. The abscissae for the eigenvectors and the average evoked response are identical and show the 64 time coordinates measured in milliseconds from the start of the evoked response.* The principal component number indicates which principal component is measured along each eigenvector. The m th eigenvector is largest over those time coordinates in the evoked response which make the greatest contribution to the m th principal component. The percent of the variance of the first four principal components accounted for by each principal component is shown with each eigenvector. The first four principal components for this particular experiment session accounted for 93.6 % of the variance of all 64 principal components.

*These plots could be shown as 64 separate points corresponding to 1, 3, 5 ... 127 milliseconds since this is the manner in which the average evoked responses and the eigenvectors are represented in the digital computer.

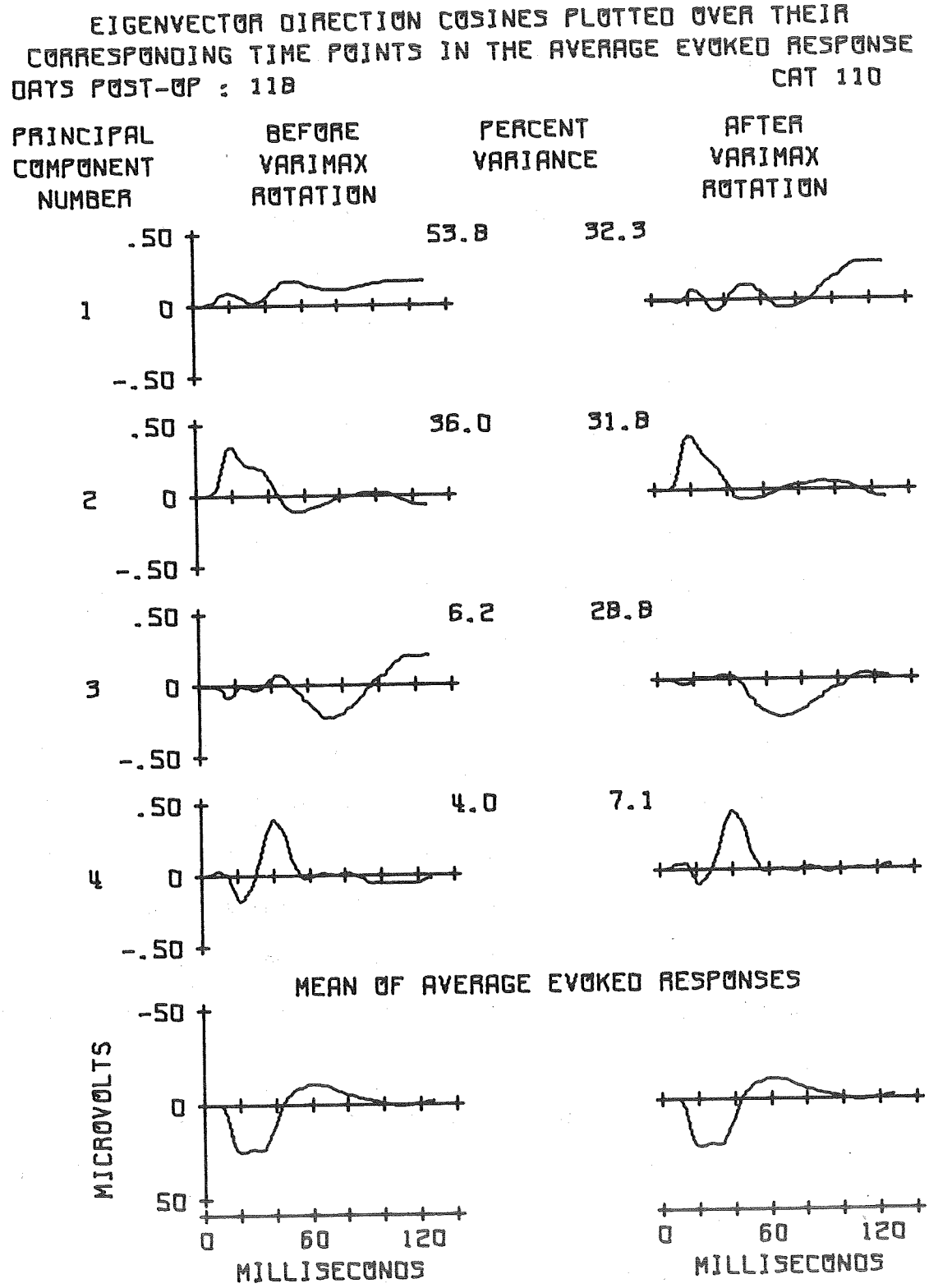

Fig. G4. The first 4 eigenvectors from one experimental session.

The principal component analysis of the evoked response data discussed up to this point has provided several results: 1) an estimate of the number of orthogonal coordinates (eigenvectors) required to span the data space (defined by the 64 time coordinates), four eigenvectors being considered sufficient for these data; 2) a set of eigenvectors with a unique orientation that minimizes the covariance between principal components and compresses most of the variance (information) into the first principal component, most of the residual variance into the second principal component, and so on for the remaining principal components. The first result, finding 4 eigenvectors sufficient to define an average evoked response, seems reasonable in light of work done by Teas and Kiang (53) showing the evoked response to be made up of 3 qualitatively determined evoked response components (their work is discussed in the Introduction of this dissertation). However, there is no reason to expect that the unique orientation of the eigenvectors from the second result is the most desirable and the selection of a different orientation will be discussed. A more complete treatment, replete with historical perspective, is contained in chapter 14 of Harman (64), and the original paper on the particular method of selecting a new eigenvector orientation (the varimax criterion) by Kaiser (67).

In seeking a criterion for reorienting the eigenvectors a primary consideration is to maintain a scheme which preserves the objectivity inherent in the previous part of the analysis. One such scheme is to simplify the structure of the transformation matrix [A]. The simplest interpretation of an eigenvector occurs when the direction cosines are

The net result of a principal component analysis is two sets of 4 eigenvectors, each of which objectively decomposes the average evoked response into weighted sets of time coordinates. It is not possible to predict which, if any, of these decompositions is physiologically meaningful. This question can only be answered by applying the principal component analysis to an appropriate set of experimental data.

BIBLIOGRAPHY

1. Fletcher. H. Reviews of Modern Physics 14:47, 1940.

2. Shower, E. G. and R. Biddulph. J. Acous. Soc. Am. 3:275, 1931.

3. Hawkins, Jr., J. E., and S. S. Stevens. J. Acous. Soc. Am. 22:6, 1950.

4. Zwicker, E., G. Flottorp and S. S. Stevens. J. Acous. Soc. Am. 29:548, 1957.

5. Zwicker, E. Acustica 2:125, 1952.

6. Zwicker, E. Acustica 4:415, 1954.

7. Gassler, G. Acustica 4:408, 1954.

8. Greenwood, D. D. J. Acous. Soc. Am. 33:1344, 1961.

9. vonBekesy, G. Experiments in Hearing. New York:McGraw-Hill Book Co. Inc., 1960.

10. vonBekesy, G. J. Acous. Soc. Am. 20:227, 1948.

11. Schuknecht, H. F. In: Neural Mechanisms of the Auditory and Vestibular Systems, edited by G. L. Rasmussen and W. F. Windle. Springfield, Ill.:Thomas, 1960.

12. Watson, C. S. J. Acous. Soc. Am. 35:167, 1963.

13. Elliot, D. N., L. Stein and M. J. Harrison, J. Acous. Soc. Am. 32:380, 1960.

14. Greenwood, D. D. J. Acous. Soc. Am. 33:484, 1961.

15. Hamilton, P. M. J. Acous. Soc. Am. 29:506, 1957.

16. Scharf, B. Special Report-Critical Bands. Laboratory of Sensory Communications, Syracuse Univ., Syracuse, N. Y., 1966.

17. Hind, J. E. In: Neural Mechanisms of the Auditory and Vestibular Systems, edited by G. L. Rasmussen and W. F. Windle. Springfield, Ill.:Thomas, 1960.

18. Woolsey, C. N. In: Neural Mechanisms of the Auditory and Vestibular Systems, edited by G. L. Rasmussen and W. F. Windle. Springfield, Ill.:Thomas, 1960.

19. Mulligan, B. E., M. J. Mulligan and J. F. Stonecypher. J. Acous. Soc. Am. 41:7, 1967.

20. Katsuki, Y. Prog. in Brain Res. 21:71, 1966.

21. Galambos, R. and H. Davis, J. Neurophysiol. 6:39, 1943.

22. Kiang, N. Y-s. Acta. Oto-Laryngol. 59:186, 1965.

23. Kiang, N. Y-s., T. Watanabe, E. Thomas, and F. Clark. Discharge Patterns of Single Fibers in Cat's Auditory Nerve. Cambridge:The M.I.T. Press, 1965.

24. Kiang, N. Y-s., M. B. Sachs and W. T. Peake. J. Acous. Soc. Am. 42:1341, 1967.

25. Rupert, A., G. Moushegian and R. Galambos. J. Neurophysiol. 26: 449, 1963.

26. Sachs, M. B., N. Y-s. Kiang, J. Acous. Soc. Am. 43:1120, 1968.

27. Greenwood, D. D. and N. Maruyama. J. Neurophysiol. 28:863, 1965.

28. Pfeiffer, R. R. Exp. Brain Res. 1:220, 1966.

29. Rose, J., R. Galambos and J. R. Hughes. The Johns Jopkins Hosp. Bul. 104:211, 1959.

30. Rose, J., R. Galambos and J. R. Hughes. J. Neurophysiol. 23:211, 1960.

31. Galambos, R., J. Schwartzkopff and A. Rupert. Am. J. Physiol. 197:527, 1959.

32. Hilali, S. and I. C. Whitfield, J. Physiol. 122:158, 1953.

33. Erulkar, S. Proc. Roy. Soc. Lon., series B. 150:336, 1959.

34. Rose, J., D. D. Greenwood, J. M. Goldberg, and J. E. Hind. J. Neurophysiol. 26:294, 1963.

35. Thurlow, W. R., N. B. Gross, E. H. Kemp, and K. Lowy. J. Neurophysiol. 14:289, 1951.

36. Gross, N. B. and W. R. Thurlow. J. Neurophysiol. 14:409, 1951.

37. Galambos, R. J. Neurophysiol. 15:381, 1952.

38. Bogdanski, D. F. and R. Galambos. In: Neural Mechanisms of the Auditory and Vestibular Systems, edited by G. L. Rasmussen and W. F. Windle. Springfield, Ill.:Thomas, 1960.

39. Evans, E. and I. C. Whitfield. J. Physiol. 171:476, 1964.

40. Gerstein, G. L. and N. Y-s. Kiang. Exp. Neurol. 10:1, 1964.

41. Goldstein, Jr., M. H., J. Hall, and B. O. Butterfield. J. Acous. Soc. Am. 43:444, 1968.

42. Conishi, S. and Y. Katsuki. Japan J. Physiol. 15:342, 1965.

43. Bourbon, W. T., T. R. Evans and B. H. Deatherage. J. Acous. Soc. Am. 43:56, 1968.

44. John, E. R., D. S. Ruchkin and J. Villegas. Ann. N. Y. Acad. Sc. 112:362, 1964.

45. Fox, S. S. and R. J. Norman. Science 159:1257, 1968.

46. Clare, M. H. and G. H. Bishop. Am. J. Psychiat. 111:818, 1955.

47. Fox, S. S. and J. H. O'Brien. Science 147:888, 1965.

48. Frost, Jr., J. and A. Gol. Exp. Neurol. 14:506, 1966.

49. Gerstein, G. G. EEG Jour. Suppl. 20:68, 1961.

50. Gerstein, G. G. and N. Y-s. Kiang. Exp. Neurol. 10:1, 1964.

51. Towe, A. L. Exp. Neurol. 15:113, 1966.

52. Towe, A. L., H. D. Patton and T. T. Kennedy. Exp. Neurol. 10:325, 1964.

53. Teas, D. C. and N. Y-s. Kiang. Exp. Neurol. 10:91, 1964.

54. Tunturi, A. R. Am. J. Physiol. 184:321, 1956.

55. Hind, J. E. J. Neurophysiol. 16:475, 1953.

56. Abeles, M., R. L. Daly, M. H. Goldstein, Jr. and J. S. McIntosh. J. Acous. Soc. Am. 44:362, 1968.

57. Ruchkin, D. S. IEEE Trans. Bio-Med. Eng. BME-12:87, 1965.

58. Ritter, W., H. G. Vaughn, Jr., L. D. Costa. EEG Jour. 25:550, 1968.

59. Abramson, N. IEEE Trans. Comm. Sys. CS-11:407, 1963.

60. Middleton, D. Tech. Report AF-9, The Johns Hopkins University Radiation Laboratory, Baltimore, Md., 1955.

61. Glaser, E. M. and C. M. Suter. J. Acous. Soc. Am. 41:1586, 1967.

62. Donchin, E. IEEE Trans. Bio-Med. Eng. BME-13:131, 1966.

63. Hotelling, H. J. Ed. Psychol. 24:417, 498, 1933.

64. Harman, H. H. Modern Factor Analysis. Chicago: Univ. Chicago Press, 1967.

65. Seal, H. L. Multivariate Statistical Analysis for Biologists. London:Methuen, 1964.

66. Greenstadt, J. In:Mathematical Methods for Digital Computers, edited by A. Ralston and H. Wilf. New York:J. Wiley & Sons, 1960.

67. Kaiser, H. F. Psychometrika 23:187, 1958.

68. Watanabe, S. In:Trans. of the Fourth Prague Conf. on Information Theory, Statistical Decision Functions and Random Processes (1965). Prague:Czech. Acad. Sc., 1967.

69. Donchin, E. and D. B. Lindsley. EEG Jour. 19:325, 1965.

70. Neff, W. D. In:Neural Mechanisms of the Auditory and Vestibular Systems, edited by G. L. Rasmussen and W. F. Windle, Springfield, Ill.:Thomas, 1960.

71. Diamond, I. T.: In:Contributions to Sensory Physiology, Vol. 2, edited by W. D. Neff. New York:Academic Press, 1967.

72. Evans, E. F. In:Hearing Mechanisms in Vertebrates, edited by A. V. S. DeReuck and J. Knight. Boston:Little Brown, 1968.

73. Woolsey, C. N. and E. M. Walzl. Bull. Johns Hopkins Hosp. 71:315, 1942.

74. Tunturi, A. R. Am. J. Physiol. 162:489, 1950.

75. Whitfield, I. C. The Auditory Pathway. Baltimore:Williams & Wilkens, 1967.

76. Goldberg, J. M. and W. D. Neff. J. Neurophysiol. 24:119, 1961.

77. Diamond, I. T., J. M. Goldberg, and W. D. Neff. J. Neurophysiol. 25:223, 1962.

78. Masterson, R. B. and I. T. Diamond. J. Neurophysiol. 27:15, 1964.

79. Hall, J. L., II and M. H. Goldstein, Jr. Jour. Acous. Soc. Am. 43:456, 1968.

80. Whitfield, I. C. In:Hearing Mechanisms in Vertebrates, edited by A. V. S. DeReuck and J. Knight. Boston:Little Brown, 1968.

81. Ruchkin, D. S. and E. R. John. Science 153:209, 1966.

82. Donchin, E. and L. Cohen. EEG Jour. 22:537, 1967.

83. Specht, D. F., J. E. Mangelsdorf and J. G. Toole. Biomed. Sc. Inst. 4:132, 1968.

84. Mood, A. M. and F. A. Graybill. Introduction to the Theory of Statistics. New York:McGraw-Hill, 1963.

85. Luck, J. E. Jour. Acous. Soc. Am. 46 (1), 1969. In press.

86. Beakley, G. and F. B. Tuteur. Jour. Acous. Soc. Am. 46 (1), 1969. In press.

87. Glaser, E. M. Proc. of the 20th Ann. Conf. on Eng. in Medicine and Biology, 1967.

88. Glaser, E. M. Jour. Acous. Soc. Am. 36:1288, 1964.

89. Korn, G. A. and T. M. Korn. Mathematical Handbook for Scientists and Engineers. New York:McGraw-Hill, 1961.